INFORMATION TO USERS

This manuscript has been reproduced from the microfilm master. UMI films the text directly from the original or copy submitted. Thus, some thesis and dissertation copies are in typewriter face, while others may be from any type of computer printer.

The quality of this reproduction is dependent upon the quality of the copy submitted. Broken or indistinct print, colored or poor quality illustrations and photographs, print bleedthrough, substandard margins, and improper alignment can adversely affect reproduction.

In the unlikely event that the author did not send UMI a complete manuscript and there are missing pages, these will be noted. Also, if unauthorized copyright material had to be removed, a note will indicate the deletion.

Oversize materials (e.g., maps, drawings, charts) are reproduced by sectioning the original, beginning at the upper left-hand corner and continuing from left to right in equal sections with small overlaps. Each original is also photographed in one exposure and is included in reduced form at the back of the book.

Photographs included in the original manuscript have been reproduced xerographically in this copy. Higher quality 6" x 9" black and white photographic prints are available for any photographs or illustrations appearing in this copy for an additional charge. Contact UMI directly to order.

UMI

UMI Number: 9721275

Copyright 1997 by
Werner, Carl Edward

UMI Microform 9721275
Copyright 1997, by UMI Company. All rights reserved.

UMI
300 North Zeeb Road
Ann Arbor, MI 48103

ABSTRACT

COUNTERPULSATION CARDIAC ASSIST DEVICE CONTROLLER DETECTION FILTER SIMULATION AND CANINE EXPERIMENTS

by
Carl Edward Werner

Electronic control systems for counterpulsation Cardiac Assist Devices (CADs) are an essential part of cardiac assistance. Synchronization of the counterpulsation CAD controller with the cardiac cycle is critical to the efficacy of the CAD. The robustness of counterpulsation CAD controllers varies with the ability of the CAD controller to properly trigger on aortic pressure (Pa) and electrocardiogram (ECG) signals for sinusoid rhythms, non-sinusoid rhythms and non-ideal signals resulting from surgical intervention. An analog-to-digital converter and digital-to-analog converter based CAD controller development platform was devised on a 33Mhz PC-AT.

Counterpulsation Pa systolic rise and dicrotic notch detectors were demonstrated with a 15cc pediatric Intraaortic Balloon (IAB) and 50cc Extraaortic Counterpulsation Device (EACD) CADs using mongrel canine experimental models in which biological variation due to changing heart rate and arrhythmia as well as surgical interference due to mechanical ventilation, electrocautery, signal attenuation and random noise was present. The robust Pa triggering algorithm was based on a derivative comparator "riding clipper" algorithm for the Pa-based controller.

In order to empirically determine the robustness of the Pa triggering algorithms, a simulation platform, Pa trace model, and Pa trace artifact and physiological variation models were devised. Each set of simulation experiments utilized a different Pa trace artifact or physiological variation model to determine the capability of the Pa trigger algorithm to withstand the effects of the Pa detection impediments while maintaining 100% accuracy of the dicrotic notch detection. Multiple simulation experiments were conducted in which the same nominally adjusted interference was increased to benchmark the immunity threshold of the dicrotic notch detector. Biological variation and deviations in Pa artifacts due to clinical conditions experienced in

cardiothoracic surgery were investigated. Pa triggering was unhindered by biological variation of a Pa trace with a 3 mmHg dicrotic notch deflection along with a Pa trace with no dicrotic notch deflection present. Pa triggering was unhindered by heart rate variability ranging from 60 to 80 bpm due to respiration. Pa triggering was unhindered by clinical conditions including 40 mmHg changes in the Pa baseline modeling mechanical ventilation, aortic trace attenuation modeling variations in pressure transducer positioning and blood coagulation on the pressure catheter tip ranging from 100% to 200% of the Pa trace amplitude every four seconds, uniformly distributed noise with a mean of 0.5mmHg and standard deviation of 0.289mmHg and Gaussian distributed noise with a zero mean and standard deviation of 0.6mmHg. The results of the simulation experiments performed quantified the robustness of the Pa detection algorithm.

Development of a fault tolerant counterpulsation CAD control system required the development of a robust ECG triggering algorithm to operate in tandem with the Pa triggering algorithm. An ECG detector was developed to provide robust control for a range of ECG traces due to biological variation and signal interference. The ECG R-wave detection algorithm is based on a modified version of the Washington University QRS-complex DD/1 algorithm (Detection and Delineation 1) which uses the associated AZTEC (Amplitude Zero Threshold Epic Coding) preprocessing algorithm and provides accurate ECG-based CAD control R-wave detection for 96.56% of the R-waves stored within the MIT/BIH ECG Arrhythmia database with a maximum detection delay of 8 milliseconds.

Further IAB experiments performed with mongrel canine experimental models demonstrated that the systolic time interval to heart rate relationship existing in humans (essential to human patient CAD control inflation prediction) is not prevalent in canine mongrels particularly when treated with beta-blockers.

In order to execute both Pa and ECG C software detection algorithms for a fault tolerant counterpulsation CAD controller, investigation into the communications throughput of a quad-

transputer board was performed. Development of streamlined communication primitives led to a

communication processor utilization of 8.3%, deemed efficient enough for fault tolerant

multiprocessor CAD control implementation.

COUNTERPULSATION CARDIAC ASSIST DEVICE CONTROLLER
DETECTION FILTER SIMULATION AND CANINE EXPERIMENTS

by
Carl Edward Werner

A Dissertation
Submitted to the Faculty of
New Jersey Institute of Technology
in Partial Fulfillment of the Requirements for the Degree of
Doctor of Philosophy

Department of Electrical and Computer Engineering

January 1997

Copyright © 1997 by Carl Edward Werner
ALL RIGHTS RESERVED

APPROVAL PAGE

COUNTERPULSATION CARDIAC ASSIST DEVICE CONTROLLER DETECTION FILTER SIMULATION AND CANINE EXPERIMENTS

Carl Edward Werner

_____   _____

Dr. Stanley Reisman, Dissertation Advisor   Date
Professor of Electrical and Computer Engineering, NJIT

_____   _____

Dr. Nirwan Ansari, Committee Member   Date
Associate Professor of Electrical and Computer Engineering, NJIT

_____   _____

Dr. John Carpinelli, Committee Member   Date
Associate Professor of Electrical and Computer Engineering, NJIT

_____   _____

Dr. Peter Engler, Committee Member   Date
Associate Professor of Electrical and Computer Engineering, NJIT

_____   _____

Dr. Michael Lacker, Committee Member   Date
Professor of Mathematics, NJIT

BIOGRAPHICAL SKETCH

Author: Carl Edward Werner

Degree: Doctor of Philosophy in Electrical Engineering

Date: January 1997

Undergraduate and Graduate Education:

- Doctor of Philosophy in Electrical Engineering
  New Jersey Institute of Technology, Newark, NJ, USA 1997

- Master of Science in Electrical Engineering
  New Jersey Institute of Technology, Newark, NJ, USA 1989

- Bachelor of Science in Electrical Engineering
  New Jersey Institute of Technology, Newark, NJ, USA 1988

Major: Electrical Engineering

This dissertation is dedicated to my wife, Karin L. Williams Esq., who with her devotion and encouragement I was able to achieve my Doctoral Degree.

v

ACKNOWLEDGEMENT

The author wishes to acknowledge Dr. Stanley Reisman, my Dissertation Advisor for exceptional advice throughout my education at New Jersey Institute of Technology. His academic and personal leadership was demonstrated through his firm beliefs, caring words and moral support time after time.

I would also like to thank Dr. Ansari, Dr. Carpinelli, Dr. Engler and Dr. Lacker for serving as members of my dissertation committee.

NJIT, Cornell University Medical College, New Jersey American Heart Association, and Bellcore (Bell Communications Research, Morristown, New Jersey) must be thanked for their support of this dissertation research through research and teaching assistantships, Cornell's use of facilities, AHA research grants, Bellcore's tuition sponsorship.

Again, I would like to thank my wife for all her love and devotion.

o

TABLE OF CONTENTS

LIST OF TABLES

x

LIST OF FIGURES

xi

xix

1. Introduction and Literature Survey

Each year approximately 500,000 people in the United States die from heart attacks(1). This places heart disease as the number one cause of natural death in the U.S. In addition to heart attack, congestive heart failure occurs in 400,000 Americans per year resulting in approximately 30,000 deaths per year due to this disease(1). In an effort to treat the ill effects of heart disease, work in circulatory support research attempts to prolong life for patients with heart disease and attempts to maintain the best possible quality of life.

Circulatory support systems provide assistance for movement of the blood through artificial means (e.g., external pump) or by modifying the impedance of an artery to increase blood flow. An example of decreasing the resistance of an artery is an intraaortic balloon deflation which increases aortic cross-sectional area and thus decreases aortic resistance(1). Circulation is essential for the body to meet its own metabolic needs, including those of the heart tissue.

Circulatory systems provide circulation or circulatory assistance when the heart cannot function at all (e.g., during cardiac arrest) and when the heart is not healthy enough to maintain minimal circulation. A third type of situation for circulatory support occurs when the body is under forces greatly exceeding that of gravity and thus the normal capability of the heart is not enough to maintain normal circulation (e.g., a pilot in a military aircraft makes an aerial maneuver)(1). In the first two cases, cardiac disease conditions exist which warrant the intervention of circulatory assistance.

Circulatory assistance can provide various combinations of four major physiological benefits(1). The first benefit is to increase overall aortic flow Qa. This increase in circulatory output can be defined as an increase in the total positive blood flow [the rate at which a variable physical quantity (the blood within the aorta) changes in position in a motion toward the systemic system] in the aorta. The second benefit is to redirect the available aortic blood flow to various parts of the body. Most importantly, additional blood should be provided to the heart and the brain. The third benefit is to decrease the demand of necessary blood flow needed by the heart. This can be accomplished by decreasing either the left ventricle's loading volume prior to contraction or the volume after contraction. The fourth benefit of circulatory assistance of the heart is to increase the amount of blood returned to the heart by applying external pressure to the veins. Individual or combinations of circulatory assistance benefits are utilized by the cardiac physician in an attempt to remedy the specific pathology of the patient.

Subjects needing circulatory assistance range from a patient with a failing left ventricle to a pilot avoiding an enemy aircraft(1). Due to the wide range of needs for circulatory assistance, the techniques and their corresponding cardiac assist devices (CADs) vary considerably in method of assistance. The types of circulatory support systems may be classified by the degrees of invasive procedures that must be performed on the body(1). The three major categories of invasion are systems that require cardiothoracic intervention to surgically implant the CADs, systems that require entry to a vessel through the skin, and systems that assist circulation without any surgical intervention to the body as seen in Figure 1-1 (1). A second level for classification is based on the methodology of motivating blood flow or changing vascular impedance(1). The five different methods include pressing of the heart, moving the blood through hydraulic means, timed displacement of volume within blood vessels by balloons placed in major blood vessels, compressing different sections of the body, thus constricting the blood vessels (refer to Figure 1-2) and pressurizing the cardiothoracic cavity using the lungs.
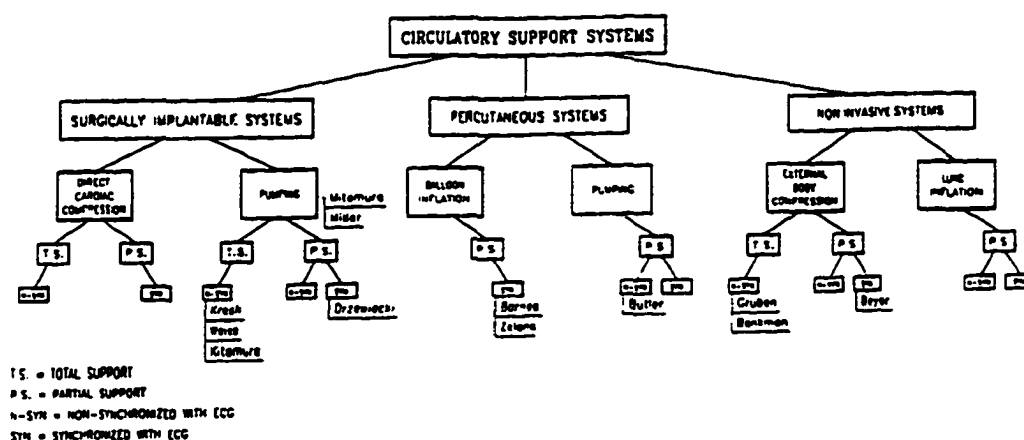
Figure 1-1. Classifications of Circulatory Support Systems (1)

The third level of categorizing circulatory assistance is based on the contribution made to the circulation of the blood(1). The two further classifications in this level include those which completely maintain circulation and those that assist circulation.

Blood moved solely by externally generated hydraulic processes completely maintain circulation. In this case the heart is not involved at all. Two examples include cardiopulmonary resuscitation, in which the heart is compressed by repeatedly pressing on the outer chest, and surgical implantation of an artificial mechanized heart(1).

Partial support of circulation requires that the circulatory assistance performs a fraction of the work by moving the blood through unnatural applied forces. Circulatory assistance may be provided, for
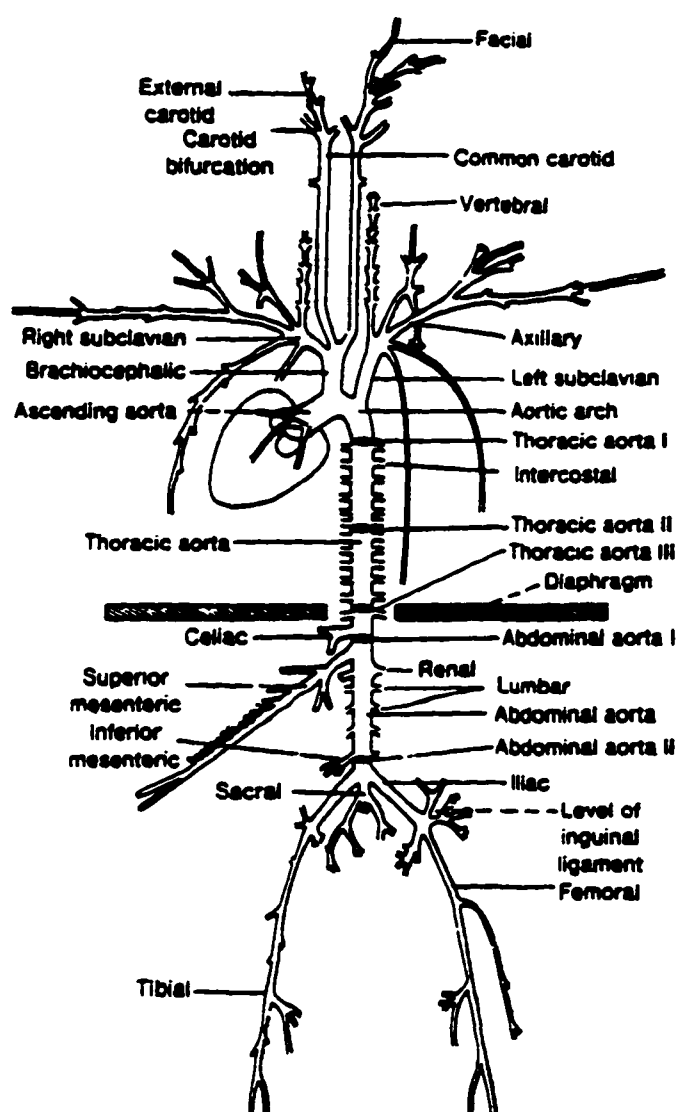
Figure 1-2. Major Branches of the Arterial Tree(6)

example, by chest compression and intra-aortic balloon pumping (as seen in Figure 1-3 and Figure 1-4)(1). These circulatory assist systems require synchronization with the cardiac cycle. Typical cardiac cycle timing signals utilized for control include the electrocardiogram, left ventricular pressure and aortic pressure as seen in Figure 1-5 (1). The most prevalent synchronization technique is "counterpulsation". Counterpulsation attempts to increase diastolic aortic pressure and decrease systolic aortic pressure as seen in Figure 1-6. Proper timing with the heart is essential to the efficacy of the partial support circulatory systems so as to provide augmented assistance and ensure particularly that the normal pumping action of the heart is not hindered as seen in Figure 1-7.
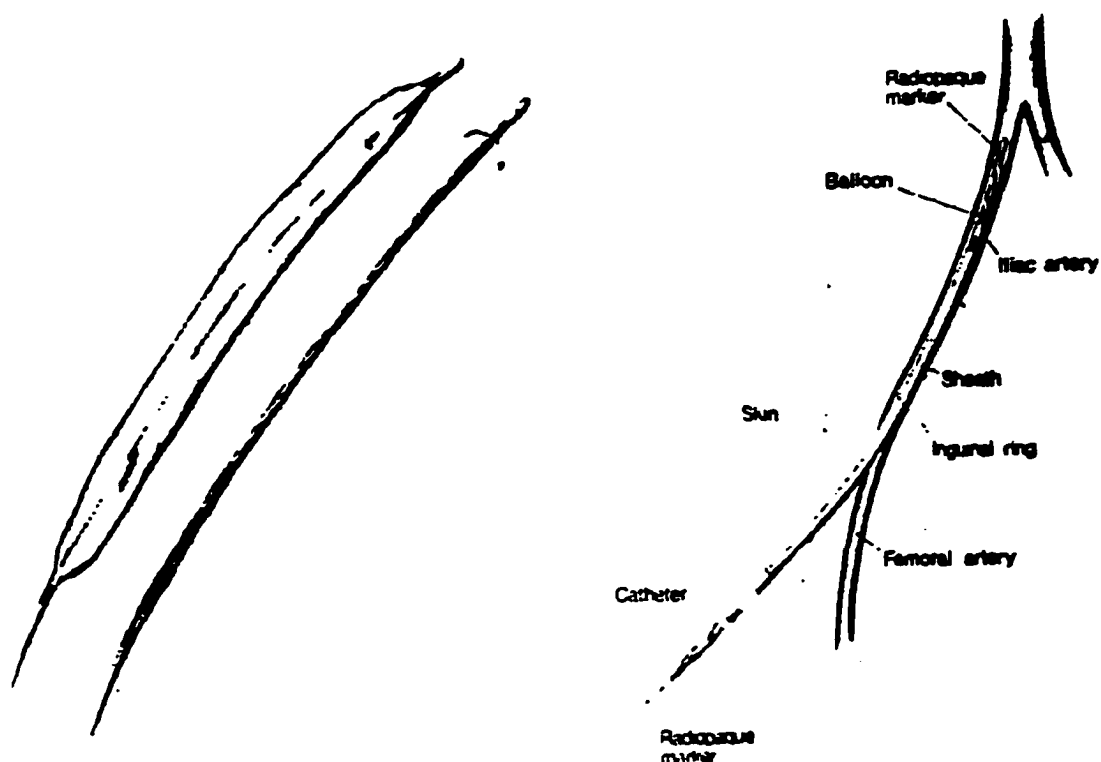
Figure 1-3. The Percutaneous Intraaortic Balloon(4)
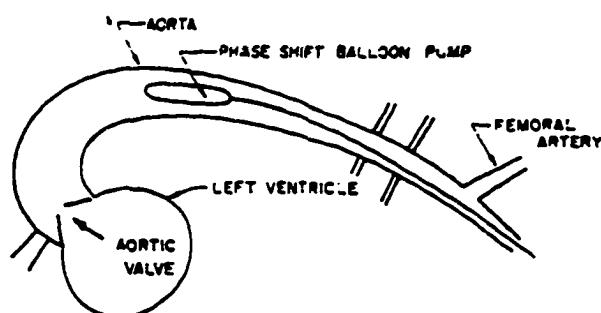
Figure 1-4. Final Positioning of the Percutaneous Intraaortic Balloon (5)

1.1 Cardiac Assist Systems and Cardiac Assist Devices (CADs)

Cardiac assistance is provided by medical equipment with three main system components: (1) CAD electronic controller, (2) CAD pneumatic driver, and (3) gas (Helium) driven CAD.

Cardiac Assistance is provided hemodynamically with Cardiac Assist Devices (CAD). The Intraaortic Balloon (IAB), the most clinically utilized Cardiac Assist Device, is a long thin catheter assembly with a cylindrical balloon chamber which can be inflated and deflated. The catheter is a
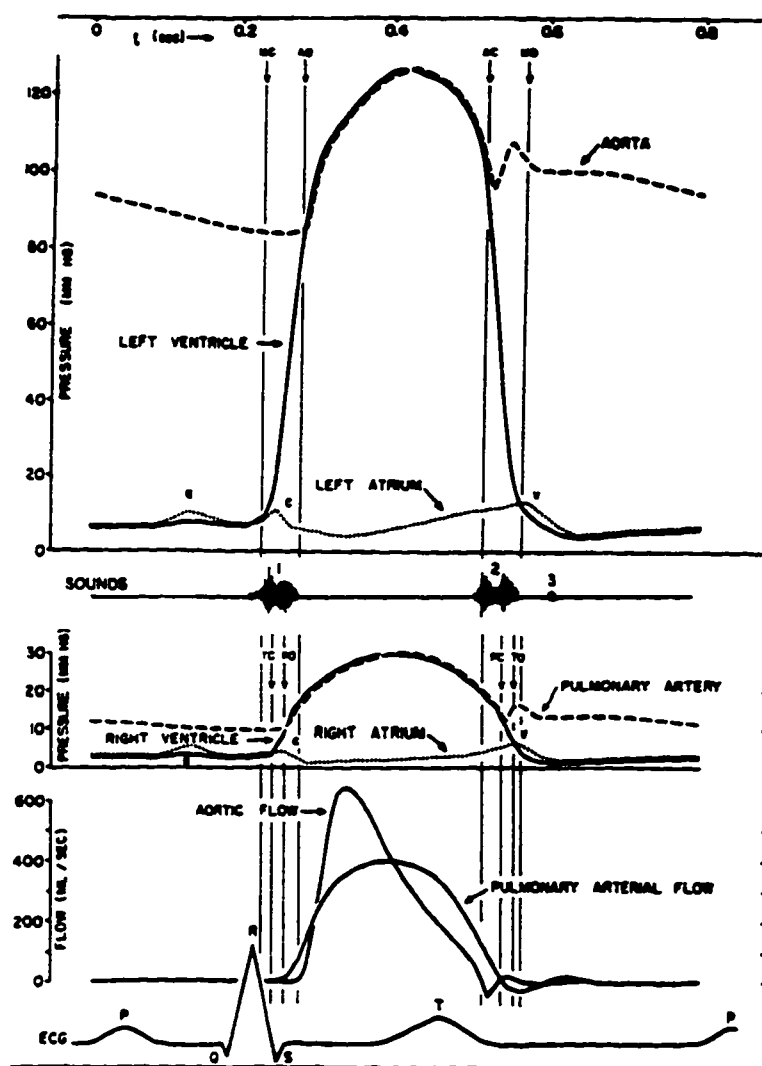
Figure 1-5. Events in the Cardiac Cycle in Man(6)

long thin semi-rigid tube which typically gains access to the arterial system via the femoral artery and is inserted until it reaches the ascending aorta. The IAB utilizes the finite capacity of the aorta and inflates with a counter pulsating rhythm to assist circulation by displacing the blood within the aorta once the aortic valve has closed. It is extremely important that the IAB is deflated before systole begins so as to not obstruct the normal circulation of the heart's contraction.

The second CAD to be investigated was the Extra-aortic Counterpulsation Device (EACD). The EACD is a Left Ventricle Assist Device (LVAD). (LVADs are not typically utilized for clinical Cardiac Assistance because of the necessity to make an anastomosis (a surgical connection of aorta and the opening of the LVAD) incision within the descending aorta including the trauma of open thoracic surgery.) The EACD to be utilized consisted of a disc-shaped anastomosed blood
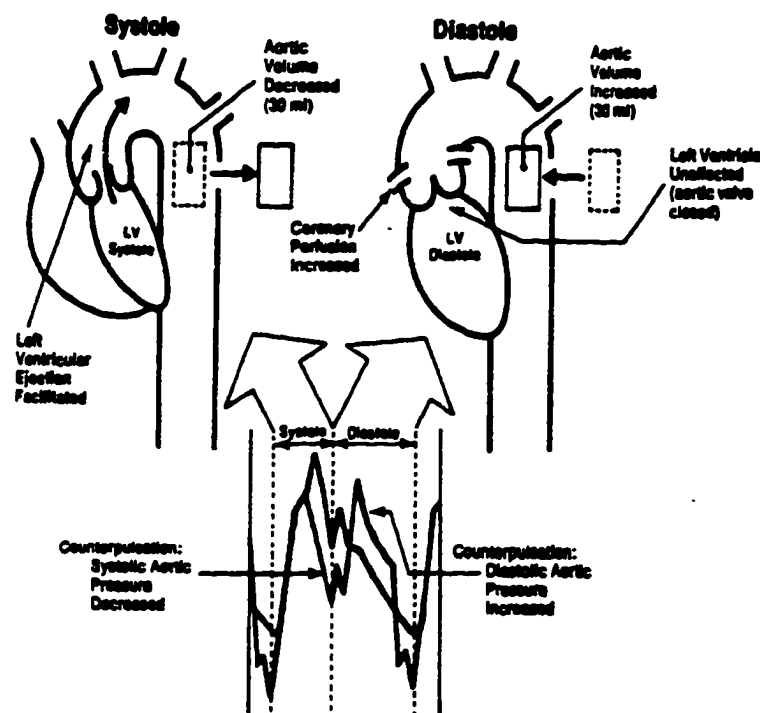
Figure 1-6. Physiology of Counter Pulsation(5)

congruous polyurethane chamber with a membrane in the middle that could be displaced to either side of the "disc" shaped chamber as seen in Figure 1-8. The EACD has a short surgical tube connected to each side (i.e. compartment) of the EACD's disc-shaped safety chamber. The tube to be sutured to an incision (i.e., anastomosed) in the descending aorta has surgically compatible fabric attached. The second tube is connected to the driving gas source/vacuum of the pneumatic system. Assistance is provided when the membrane is displaced (i.e., pressurized with Helium gas) from one side of the ventricle chamber to the other side expelling the fluid (blood) contents. The EACD assistance performs piston-cylinder type action by evacuating the fluid during systole and then displacing fluid contents back into the aorta during diastole. The combination of the disc shaped "safety" chamber and central membrane mechanically prevents any over augmentation by limiting the displaced volume. This is similar to the finite volume displacement that can be imparted to the aorta with a intraaortic balloon which is limited by the maximum inflation of the balloon. The EACD utilized in this research had a maximum displacement of 50cc, while the maximum displacement of the intraaortic balloons were two different sizes, 15 cc for a pediatric balloon and 30cc for an adult balloon. The size of the balloon utilized depended on the anatomy of the canine experimental model.
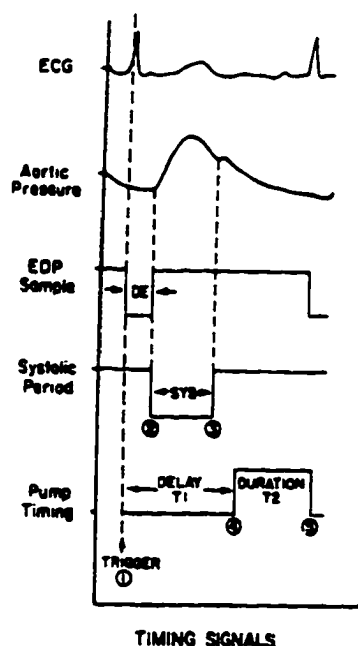
TIMING SIGNALS

FIG. 2. Timing signals. Critical timing points are shown for the pump controller. Point (1) is an ECG trigger. Point (2) is the beginning of systole. Point (3) is the end of the systole. The pump was inflated from point (4) to point (5).
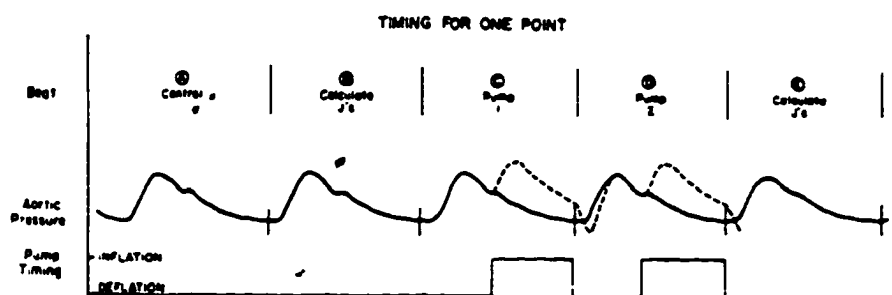
Figure 1-7. Critical Timing Signals are shown in Figure 1-7A (top) and Resulting Augmentation of the IABP is shown in Figure 1-7B (bottom)(7)

The IAB and EACD CADs are inflated/deflated by the helium gas of the pneumatic system. The pneumatic system is controlled by the CAD electronic controller, the most complicated component of any counter pulsating cardiac assist system. The CAD controller must receive biological signals from the patient and determine when to inflate and deflate the CAD through the use of the CAD pneumatic system. Current cardiac assist device controllers do not have the capability to follow changes in heart rate due to abnormal variations in rate or drastic changes due to arrhythmia.

Maximum Fluid
Displacement 50cc
(i.e., 50cc Chamber
volume)

Pneumatic Driving
Gas From Cardiac
Assist Controller

Resulting Hydraulic
Cardiac Assistance

Displaced Membrane
Converts Pneumatic
Pressure and Vacuum
into Aortic Pressure
Augmentation during
Diastole and Reduced
Ventricular Afterload
during Systole

Surgical Tube Anas-
tomosed to Aorta
utilizing Surgically
Compatible Fabric
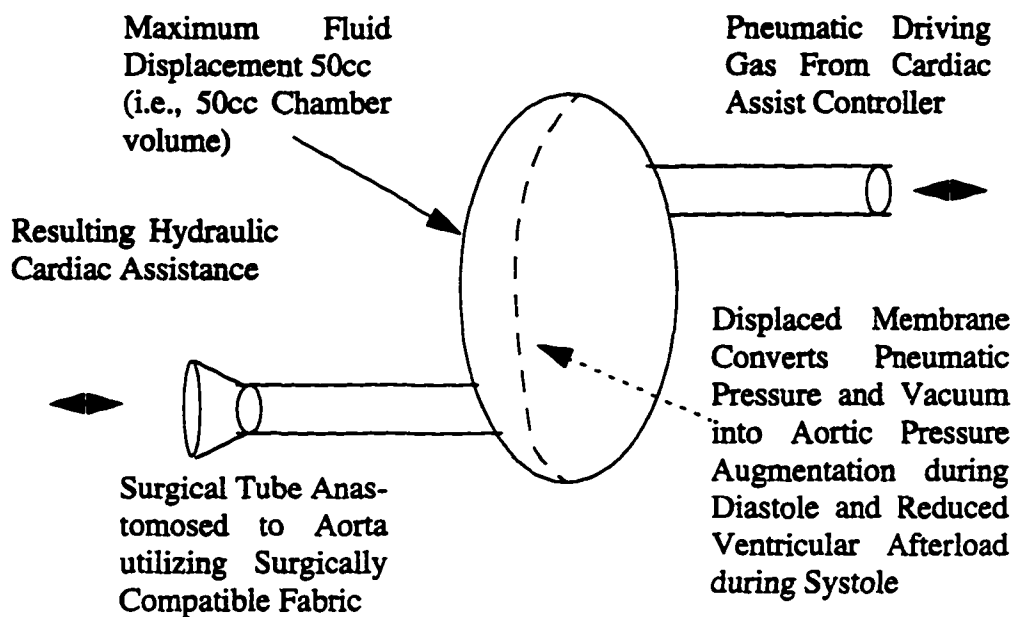
Figure 1-8. Illustration of Extraaortic Counterpulsation Device (EACD)

Cardiac Assist Devices (CADs) are used for selected patients awaiting open heart surgery and those recovering from cardiothoracic surgery. The two major circulatory benefits obtained from cardiac assistance are increased cardiac output and increased coronary blood flow(11). The increase in flow provides an elevated oxygen supply to the systemic system. Several devices can provide cardiac assistance. All categories of cardiac assist devices have their own optimum timing criteria e.g., inflation/deflation. The optimum timing attempts to maximize the hemodynamic benefits to the patient. The focus of this dissertation centers on counterpulsation cardiac assist devices. Both the IABP and EACD are utilized as counterpulsation devices.

Counterpulsation is based on two fundamental hemodynamic principles. The cardiac assist device timing is synchronized with the cardiac cycle and the cardiac assist device timing works 180 degrees out of phase with the heart. In counterpulsation the cardiac assist device assists circulation during diastole and attempts to reduce root aortic impedance during systole (to assist by providing a reduced load on the heart and, particularly, to not obstruct the normal contraction of the heart). Cardiac assist devices improve hemodynamics in the following three ways; by increasing cardiac output (Qa, i.e., aortic flow), by increasing the blood flow within the coronary arteries (i.e., Qc) and by increasing the overall blood flow to the systemic system(8). The additional benefits to the heart include a decrease in the volume of blood remaining in the left ventricle after a contraction and a decrease in the aortic resistance (Zin) and a decrease in the diastolic pressure just prior to systole (i.e., end diastolic pressure or EDP)(8). The resulting effort of the heart is reduced and may be

observed nominally in two ways(8). The computed average of the Pa during systole (i.e., mean systolic pressure or MSP) is reduced and the value of the Pa at the end of systole (i.e., end diastolic pressure or EDP) is reduced(11). By decreasing the MSP and EDP the amount of work the heart is performing is reduced and thus the myocardial oxygen consumption (MVO_2) is reduced(11). The final result is that the hemodynamic power output W_{LV} of the patient is increased and the work the patient's heart must perform decreases(9).

Due to the increased mean arterial diastolic pressure (MDP, measured over a single diastole as compared with the unassisted diastole), the amount of oxygen available in the coronary arteries (i.e., myocardial perfusion) increases. This effect is particularly pronounced because the majority of myocardial perfusion occurs during diastole when the heart is not contracting. An increase in the absorption of oxygen by the tissue of the heart improves the ability of the left ventricle to contract. IABP are commonly utilized on patients in which, due to a limited amount of blood reaching an area of the heart, a portion of the heart's tissue has stopped functioning (i.e., an infarct). If cardiac assistance is utilized quickly after the infarct (an area of dead tissue caused by insufficient blood supply(9)) occurs, the increase in blood flow within the coronary arteries helps prevent the size of the nonfunctioning tissue from increasing (i.e., limits the infarct)(11).

In conclusion, cardiac assist devices are generally utilized in the clinical treatment of ischemia of the heart (a localized ischemia resulting from a mechanical obstruction of the blood supply to cardiac tissue within the heart (9)). CADs are required when the utilization of pharmacological means demonstrates to be insufficient(11).

The IABP is the most clinically utilized cardiac assist device used to treat ischemic conditions of the heart(17). As with any counterpulsation device, the IABP provides dual phase assistance to help reduce required cardiac work during systole and increase systemic oxygen supply during diastole. As compared with other cardiac assist devices, the IABP provides a feature that is most desirable in a clinical setting, percutaneous insertion through the femoral artery. This alleviates the necessity for open chest cardiothoracic surgical intervention. However, the IABP cannot provide aortic pressure augmentation that rivals that of some LVADs. The IABP utilizes the concept of the finite volume of the aorta. In the deflated state during systole, ideally, the IABP takes zero volume. In an instant of time just after systole (e.g., at the dicrotic notch of the aortic pressure), the hemodynamic motivational force, can be modelled after the following principles as seen in Equation 1-1.

$$\text{Aortic Pressure (Pa)} = \text{Volume of Aortic Fluid} / \text{Aortic Capacity} \qquad \text{(1-1)}$$

Once the balloon inflates, the aortic capacity is decreased, increasing the aortic pressure as seen in Equation 1-2 assuming the aortic volume stays constant.

$$\text{Increased Pa} = \text{Volume of Aortic Fluid} / \text{Decreased Aortic Capacity} \qquad (1\text{-}2)$$

Just after the end of systole, the IABP ideally increases its volume to full capacity to increase the antegrade flow of the blood toward the systemic system. The IABP works on the principle of volume displacement assuming the aorta has a somewhat finite volume. The IABP efficacy is limited by the size and compliance of the aorta.

The IABP diameter is also limited by the diameter of the aorta. In contract, the LVAD displace a greater volume by providing an additional capacity to the aorta. The additional capacity allows the displacement to be greater during diastole. The larger displacement of blood allows the EACD to provide superior hemodynamic benefits (27). In an instant of time just after systole the aortic pressure, the hemodynamic motivational force, can be modelled after the following principles as seen in Equation 1-3.

$$\text{Aortic Pressure (Pa)} = \text{Volume of Aortic Fluid} / \text{Aortic Capacity} \qquad (1\text{-}3)$$

Once the EACD inflates, the volume of aortic fluid is increased, increasing the aortic pressure as seen in Equation 1-4 assuming the aortic capacity stays constant.

$$\text{Increased Pa} = \text{Increased Volume of Aortic Fluid} / \text{Aortic Capacity} \qquad (1\text{-}4)$$

The increase in volume to capacity ratio (e.g. (100cc + 50cc) / 100cc = 1.5) of the EACD in Equation 1-4 is superior to the volume to capacity ratio (e.g., 100cc / (100cc -15cc) =1.18) in for IABP in Equation 1-2. Thus the EACD provides superior pressure augmentation. In addition to the basic difference in volume to capacity ratio, the EACD does not obstruct the aorta and thus does not increase the internal impedance of the aorta(27).

The LVAD utilized in this dissertation was the EACD. The EACD is an experimental device and not a clinical device because of the delicate surgery that is needed to anastomose the surgically compatible fabric to the ascending aorta. This experimental procedure of anastomosing the EACD would be an exceptionally dangerous clinical procedure due to the delicate nature of the aortic tissue and the fact that the aorta is the most centralized (with the highest pressure), and thus the most essential arterial branch to sustaining life. For experimental verification reasons the EACD was utilized in this dissertation to demonstrate the flexibility of the cardiac detection filters to operate for two cardiac assist devices

In order for any counterpulsation device to operate optimally, timing with the cardiac cycle is essential. The IABP and EACD cardiac assist devices are no exceptions to the complications of timing (27). In cardiothoracic clinical settings, typical timing signals available to detect and track events in the cardiac cycle include ECG as well as aortic pressure (Pa). The timing of these cardiac assist devices to the cardiac cycle is essential to maximize their benefits as well as eliminating potential injury to the patient. The timing of the IABP is particularly critical because of its positioning within the aorta. Inflation of the IAB during systole may hinder the normal pumping action of the heart through obstruction of the aorta. Improper timing of the EACD can lead to increased afterload of the heart, yet the timing is less critical because the device cannot physically obstruct the normal path of blood within the aorta. Improper timing of the cardiac assist device can hinder the normal functioning of the heart and diminish the welfare of the patient. For this reason, in particular with the clinically utilized IABP, a certified technician is present for the entire duration of its use, which can span several days. Synchronization with the cardiac cycle is critical to the optimization and non-harmful functioning of counterpulsation devices. The focus of this dissertation research investigates detections filters both with canine mongrel experimental models and simulated experiments to ensure invented robust aortic pressure and ECG detection filters provide critical timing signals for proper operation of the cardiac assist device controller and thus the cardiac assist device.

1.2   CAD Research Literature Review

The focus for the dissertation research was to perform investigations towards developing a multiprocessor based fault tolerant cardiac assist device controller that would optimize hemodynamic benefits on a beat to beat basis for various counterpulsation cardiac assist devices. Research in this area requires a literature review which spans several distinct areas of research including ECG and Pa real-time control detection[1], counterpulsation cardiac assist device timing (for e.g., IABP and EACD), and systolic time interval (STI) prediction for adaptive inflation during arrhythmias. (An estimate of the STI can be used to predict the onset of diastole and thus a prediction for inflation timing.)

---

1. There is a distinction between real-time detection and real-time control detection. Real-time detection implies that the signal is processed as fast as it is received and delay is acceptable in the detection e.g. a 1 second delay in an ECG monitor. In contrast, real-time control detection implies detection the signal is processed as fast as it is received and delay is not acceptable in the detection e.g. typically a 10-20 millisecond delay in an ECG CAD control trigger signal.

The scope of the research would involve the proper detection of strategic events within the cardiac cycle for two different signals that are typically available in a clinical setting, namely, ECG and aortic pressure. The detection filters were to be designed to be robust in order to detect with high accuracy during disturbances such as 60Hz noise, electrocautery, variations between patients, variation in heart rate and baseline Pa due to respiration, variations due to sensor attenuation/ amplification, heart rate variability due to respiration and forms of arrhythmia, e.g., premature ventricular contraction (PVC).

1.2.1   Criteria for Optimal Control e.g. Timing Criteria

Reliable detection of the important heart cycle events provide the foundation to optimize cardiac assist device (CAD) control. (Investigations into CAD research has led to the criteria for optimal timing of the counterpulsation cardiac assist device(4)(10)(11).) For example, if the counterpulsation cardiac assist device is an intra-aortic balloon (IAB), optimal control of a CAD requires the IAB to provide pressure augmentation within the ascending aorta just as the aortic valve closes. The aortic valve closing creates the dicrotic notch within the Pa wave. The IAB should deflate in order to align the lowest point in the Pa droop exactly at the start of isovolumetric systole to minimize end diastolic pressure and thus root aortic impedance. In other words, the heart should pump into the lowest possible Pa, to decrease the work requirements of the heart.

Optimal timing for the LVAD utilized in this dissertation research, the EACD, is similar to the that of the IABP. Previous investigation demonstrates that deflation timing is less critical to the efficacy of the EACD because it does not obstruct the aorta during contraction because it is anastomosed externally to the aorta(27).

Clinical conditions may dictate slight variations in timing, however, for IABP control the fundamentals of timing dictate certain criteria. The efficacy of IABP counterpulsation is dependent upon physiological factors. However, efficacy of the IABP timing (i.e., phase relationship with the cardiac cycle) is the major factor which determines the improvement of cardiovascular factors via IABP(12)(13).

Inflation is timed to occur at the end of heart's contraction at the end of systole (optimal inflation). IABP inflation should create an augmentation in Pa starting just at the dicrotic notch.

Deflation is timed to occur just before the start of the hearts contraction, i.e., just before the start of systole (optimal deflation). The IABP should deflate just prior to diastole so as to not interfere with

the earlier stages of contraction and to create a minimized root aortic impedance pressure for the heart to pump into(7)(14). The optimal deflation prevents retrograde flow and fill. The hemodynamic benefits are maximized with optimal timing. The benefits include maximized systemic perfusion, coronary perfusion and minimized LV afterload.

The search for optimal inflation and deflation timing of the IABP for a periodic heart rate occurs through the use of the developed feedback control algorithm. Inflation of the cardiac assist device occurs exactly at the dicrotic notch. The initial pumping interval (period of IAB inflation) is short and slowly increases until the low pressure point in the droop of the augmentation occurs just as the systolic rise in the pressure occurs.

If the sinusoidal rhythms of the heart remain constant, once reliable detection and tracking of the cardiac cycle is determined, inflation and deflation of the cardiac assist device remains periodic to provide optimal augmentation.

Previous studies implemented CAD controllers to determine optimal inflation and deflation for a patient with a sinusoid heart rate(7). The optimum timing was established on a subject by subject basis by using the R-wave as the sole timing trigger signal. The controller also accepted aortic pressure (Pa), aortic flow (Qa), coronary artery flow, (Qc) and ventricular pressure (Pv). The hemodynamic signals were used as criteria for optimal IABP efficacy. The optimal inflation and deflation times relative to the R-wave timing reference were derived by the controller by systematically ranging around a typical timing of systolic delay and diastolic period (i.e., deflation/ inflation intervals) pair. Optimization data was collected during the ranging period. The optimal timing was derived by determining a weighted optimization of the mean coronary artery flow, left ventricular stroke work, end diastolic aortic pressure, cardiac output, and tension time index. This algorithm could derive the optimal timing for a patient with a fixed heart rate. However, deriving the optimal timing weighting parameters for this constant heart rate involved experimentally ranging around the optimal timing. The systematic ranging would not be clinically viable due to its potential harm to the patient. Additionally, quick variations in heart rate would make the optimization invalid. The algorithm was also solely dependent on detection of the R-wave to establish timing.

1.2.2   Commercial CAD Products

Commercial IABP controllers work using a single cardiac signal (typically the ECG R-wave) to establish timing for every new cardiac cycle. During systole the IAB is deflated. During diastole the

IAB is inflated.(11). The timing may be established with the cardiac cycle utilizing the occurrence of the ECG R-wave or systolic rise in aortic pressure. A certified IABP technician selects timing (i.e., inflation and deflation relative to the cardiac signal). The technician also observes the timing relative to the cardiac cycle. In the event the timing appears to be slipping due to changes in heart rate, manual adjustments are made to the inflation and deflation times. Changes in heart rate affect the phasing of the balloon inflation and deflation relative to the heart cycle. The commercial IABP follows ideal timing for periodic sinusoid rhythms. Optimization only occurs during sinusoid rhythms of the heart rate. Changes in heart rate must be compensated for manually by the technician, which requires time and reduces the overall optimization of the IABP circulatory assistance.

1.2.3   Hemodynamic Benefits of the IABP

The IABP has been shown to improve circulation. As was stated previously, the optimal criteria for counterpulsation is well established, particularly for the IABP. However, optimal criteria assumes that the heart has a sinusoid rhythm. Hemodynamic IABP effects are dependent upon timing relative to the diastolic phase. Microprocessor-based controllers are implemented and commercially available. The IABP provides optimal inflation and deflation times through manual control. Most IABPs work in a semiautomatic fashion, an initial inflation/deflation cycle is started by the IABP controller(11). Adjustments are performed by the certified IABP technician. Experiments demonstrate increases in diastolic aortic pressure, aortic flow and coronary flow. Demonstration of the hemodynamic benefits are illustrated by changes in aortic flow, coronary flow, and end diastolic pressure(7). Reduced end diastolic pressure reduces ventricular afterload. The reduced amount of blood within the ventricle reduces the aortic resistance. The overall benefit of the IABP is that the work demand on the left ventricle is reduced (Wlv) and the heart receives more blood flow (Qc), and thus more oxygen to aid in contraction (i.e., left ventricular work)(7)(15).

The IABP is typically used for patients with myocardial infarction(16). The health of patients with myocardial infarction improves because the IABP increases the LV myocardial oxygen supply/consumption ratio (S/C)(19). The heart of the patient is working less and the heart is receiving a raised blood supply through the coronary arteries during diastole. Therefore, the oxygen supply has been raised and the demand has decreased.

1.2.4 Limitations of Commercial CAD Products

Current cardiac assist device controllers do not have the capability to follow changes in heart rate due to abnormal variations in rate or drastic changes due to arrhythmia(11). Brief intervals of an elevated or lowered heart rate will cause incorrect timing relative to the cardiac cycle. The improper phasing will reduce the optimization of the IABP timing(11). The hemodynamic benefits of the IABP are based on proper timing, thus improper timing will reduce the benefits. The major concern of improper timing is inflation during systole. This type of improper timing can hinder the normal pumping action of the heart and potentially hurt the patient. This improper inflation will add resistance to the aortic root impedance and increase the loading on the normal functioning of the LV. An added load during systole may lead to diminishing CAD returns. For this reason the commercially available IABP will cease inflation until the heart reaches a suitable stable constant heart rate for a sequence of (arrhythmic) abnormal heart beats.

The basis for this dissertation research is that computer control (based on Pa detection) can address the changes in heart rate due to arrhythmia quicker than that of an IABP certified technician.

1.2.5 CAD Control Based on R-wave Timing

A second method of CAD control (see Section 1.2.1, reference(7) for first method) is based on the R-wave timing reference as the only hemodynamic signal(19). This method of control utilized Pa regression equations on a subject by subject basis. The regression equations would derive their optimization data by systematically migrating around a typical systolic delay and diastolic period (i.e., deflation/inflation intervals) pair derived from the regression equation below(19):

$$\text{(Inflation Delay Relative to R-wave)} \quad L = 0.4HR + 127(\text{msec}) \qquad \textbf{(1-5)}$$

$$\text{(Deflation Delay Relative to R-wave)} \quad H = 1.3HR + 373 \text{ (msec)} \qquad \textbf{(1-6)}$$

After several points of data were taken to maximize each of the regression weighting factors, the regression could estimate the optimal timing of inflation and deflation for a given heart rate. The algorithm would updating the weighting factors each beat. This was done in an attempt to sustain hemodynamic optimization. Adjusting to a different heart rate was possible but required time to recalculate weighting factors. Subsequently, the systolic delay and diastolic period timing were readjusted. As in the previous control algorithm(7), the ECG R-wave would be used as the sole timing signal to establish a reference point in the cycle. However, any shift in heart rate will cause the controller to have to recalculate optimization and during arrhythmias these regression equations

most likely become inaccurate. The optimal timing for an ectopic beat cannot be derived over a long period because of its sporadic nature.

Since the R-wave would occur just at the start of systole, the calculation on heart rate could not be performed until the next R-wave occurred and the rate for that beat could be established. This would prevent optimal timing for a single ectopic beat to be missed, particularly if a gross adjustment in the heart rate occurred and the HR regression equation was utilized as previously noted in Equation 1-5 and Equation 1-6 (19) to determine inflation and deflation timing.

For example, a PVC would cause the heart rate to change drastically for that single beat. Prediction of the inflation timing would be invalid because of the variation in heart rate for the upcoming beat. Also deflation timing was not treated on a beat by beat basis since the R-wave was the only physiological signal available for detection. The two control algorithms based on R-wave detection noted previously were incapable of triggering on signals other than the R-wave and thus incapable of determining the inflation and deflation timing on a beat-by-beat basis.

1.2.6   CAD Control Based on R-wave, P-wave and Pa Second Heart Sound

More recently investigators(11) utilized both ECG and Aortic Pressure signals. R-wave, atrial P-wave and Pa dicrotic notch detectors were used to measure the STI (R-wave to dicrotic notch) in real-time. This allows for inflation to be performed prior to the S2 (second heart sound) and allows the IABP controller to adjust the end timing of IAB inflation (i.e., start of deflation) for arrhythmias. The P-wave was detected using the signal from a pacing catheter located in the atria. Detection of the P-wave enabled the P-R interval average to be derived. The detection of the P-wave along with the estimated interval between P-wave and the R-wave provided information early enough to allow the IAB to be deflated as to not obstruct the normal contraction of the heart. The atrial P-wave provided a critical timing reference that allowed the controller to deflate in the event of an arrhythmia. However, P-wave detection is very complex(39)(40). The ability to detect the P-wave in this study was dependent upon atrial cardiograms from a pacing catheter inserted into the right atrium. This P-wave information is usually unavailable in an operating room environment. Only surface ECGs are typically available.

P-waves within routine surface electrocardiograms are typically very difficult to detect. In an experimental setting, typically high resolution and low noise electrocardiograms are required to reliably detect P-waves from a multi-lead surface ECG(38). However, in this investigation (11), as well as the previous two R-wave triggered CAD controller investigations, the timing signals

presented were ideal. In the specific case of the atrial P-wave detection, the ECG P-wave signal presented was artificially ideal as compared to a surface ECG prevalent within a clinical setting.

The research of this dissertation investigates reliable detection of cardiothoracic signals (Pa and ECG) typically available in a clinical environment with distortion normally present due to both noise artifacts and arrhythmia.

1.2.7 Assumptions of Previous Investigators

All previous investigators assumed the cardiac Pa and ECG signals are ideal and cardiac event timing is established and 100% reliable. However, if the heart rate changes due to normal variations in rate or to arrhythmia, or noise artifacts are presented to the triggering signals, then CAD control becomes considerably more complex. If the reference events are no longer reliable e.g. R-wave, systolic rise and dicrotic notch, then providing counterpulsation cardiac assistance is impossible. Tracking the heart cycle from non-ideal detection signals (e.g., arrhythmetic or noisy) requires a robust detection and control algorithm. The focus of the dissertation detection algorithms were to provide reliable detection during non-optimal conditions for detection.

1.2.8 Focus of this Dissertation

All previous investigators did not address the triggering of Pa and ECG during non-optimal condition. The underlying assumption for all previous research is that the signals can be detected with close to 100% accuracy and thus using the stringent criteria imposed on IAB timing, the optimal augmentation and thus hemodynamic benefits may be derived.

This dissertation addresses the research of triggering and control conditions in which aortic pressure and ECG signals are non-optimal. The non-optimal conditions include biological variation in signal characteristics, quickly changing heart rate, arrhythmia, ectopic beats (i.e., non-sinusoid rhythms), noise, and variation due to respiration. These non-optimal detection signals challenge the foundation for optimal control. The reliable detection of the cardiac signals including the aortic pressure systolic rise, aortic pressure dicrotic notch and the ECG R-wave are essential for optimizing control. In addition to addressing the nonoptimal signal conditions, the dissertation research focussed on solely digitally based filtering as to make the algorithm design applicable for a CAD implantable application.

1.3   Pa Detection

Investigators research into hemodynamic signal detection filtering for the purpose of delimiting the cardiac cycle was noted in (20). The signal used was ascending aortic blood flow. This detection algorithm was not used for real-time control but forms a basis for utilizing methods of analog filtering analysis techniques (e.g., transfer function) for a digital filter. Additionally, techniques in computer pattern recognition were utilized (e.g. looking for a sharp slope for the onset of systole within the aortic blood flow). The approach performed low pass filtering using a linear moving average filter as well as an algorithm for signal characteristic recognition. The moving average filter was modelled after the following set of equations:

(1-7)

$$g(\omega) = \sum_{j=-k}^{k} C_j e^{-i\omega j} \qquad i = \sqrt{-1}$$

(1-8)

$$\omega = 2\pi f\Delta \qquad f < \frac{1}{2}\Delta \qquad m = 2k+1$$

If all Cj's are equal and Cj = 1/m then Equation 1-7 may be expressed as:

(1-9)

$$g(\omega) = \frac{1}{m} \sum_{j=0}^{m-1} e^{(-i\omega)j}$$

(1-10)

$$|g(\omega)|^2 = \frac{1}{m}\left[\frac{1 - \cos m\omega}{1 - \cos \omega}\right]$$

If a wide sense stationary process with spectral density function $h_F(w)$ is passed through the filter in Equation 1-10, the resulting spectral density can be expressed as:

$$h_A(\omega) = |g(\omega)|^2 h_F(\omega)$$

The amplitude vs. frequency transfer function of the moving average filter (when normalized with respect to the sampling frequency) provide the typical low pass filter frequency roll off. Improvements in roll off occur as the number of points in the filter increases. The values of m between 9 and 15 have demonstrated the most beneficial results(20). (Other investigators utilized a five point moving average filter for computational efficiency(37).)

Once the sampled data is filtered using the low pass filter, the filtered data is presented to the signal characteristic recognition algorithms. These algorithms, developed to delineate systole and diastole in ascending aortic blood flow, were based on the following three criteria:

1. Aortic flow rapidly reaches its maximum

2. The aortic flow maximum declines rapidly to a negative value.

3. The aortic flow follows a relatively long period of virtually zero flow.

Utilizing a two point first derivative filter

$$A_{i'} = [A_{i+1} - A_i]/T \tag{1-12}$$

to establish maximum and minimum from slope changes, the algorithm can be implemented to detect the onset of systole and diastole within the ascending aortic blood flow.

Although detection on aortic flow delineation is not typically utilized for CAD control the research method listed(20) describes the basic detection philosophy for biomedical digital filters. However, the low pass filtering and detection filters used, a 9 or 15 point moving average filter and a two point derivative filter respectively, provide a reasonable method of performing their function on relatively smooth data but are extremely susceptible to noise.

More recently cardiac catheterization investigators (28) described methods to detect the onset (systolic rise) and end (dicrotic notch) of systole within aortic pressure. Both aortic pressure and ECG are entered into the on-line system that processes pressure data during catheterization. A two-point low pass filter is used to smooth the ECG and pressure data

$$V_i = (V_{i-1} + V_i)/2. \tag{1-13}$$

The digital filter of Equation 1-13 has a 3-db frequency of 0.25 of the f_s (sampling frequency).

The difference filter

$$dV_i = V_{i+1} - V_{i-1} \qquad \text{(1-14)}$$

is used to determine the average maximum of the positive slope of the ECG R-wave. The two thirds of the average maximum ECG R-wave derivative in turn is utilized to detect R-waves during a 300ms backward search of the data. The R-wave is used as a reference point for Pa processing.

The detection of the systolic rise is performed by determining the average maximum of the first derivative (with the difference filter in Equation 1-14) in the first five seconds of data and then using that threshold for detection by filtering shortly after the occurrence of the ECG R-wave. The exact location of the systolic rise is determined by finding the maximum of the second derivative. The second derivative of the Pa signal is provided by the difference equation:

$$d^2V_i = V_{i-6} + V_{i-5} - V_{i-2} - V_{i-1} - V_{i+2} - V_{i+3} + V_{i+5} + V_{i+6} \qquad \text{(1-15)}$$

The dicrotic notch is detected using a heart rate to systolic time interval relationship(29) to search in a 70ms selected time period centered around the target dicrotic notch with a second derivative filter that is more sensitive to the dicrotic notch, namely,

$$d^2V_i = V_{i-2} - V_{i-1} - V_i + V_{i+1} \qquad \text{(1-16)}$$

The dicrotic notch is specified at the peak of this second derivative function. However, if the first derivative is positive at this point, the detection point is adjusted backward sample by sample until the first derivative is not positive. The reason for this retrace is that at the exact end of systole, the slope of the Pa should still be negative (indicated by a zero or negative first derivative).

The previously listed algorithm for systolic rise and dicrotic notch aortic pressure detection may be utilized for CAD control if it is adapted to work for real-time control. The detection of the dicrotic notch in which the reverse search is employed could not be utilized for real-time control. Additionally, the dependence of the Pa search on the ECG will not work in a fault tolerant CAD in which control should be able to use both signals independently. Also, as in the case of the aortic flow detection algorithm, the low pass filtering and detection filters used a 2 point moving average filter, a two point first derivative and an eight and four point second derivative filter, respectively, to provide a reasonable method of performing their function on relatively smooth data but are extremely susceptible to noise. The susceptibility to high frequency noise would cause false positive detections.

1.4   ECG QRS-Complex Detection Review

This section addresses research toward robust detectors of the second signal (i.e., for the ECG R-wave) to be utilized in the cardiac assist device controller for timing. Since a fault tolerant system should be tolerant to noise, QRS detectors will be reviewed for characteristics that provide that high degree of noise immunity.

ECG R-wave (a.k.a. QRS-complex detection) is a requirement for counterpulsation CAD controllers. The functional necessity for R-wave detection for the CAD is to provide timing with the cardiac cycle. A secondary need for high-accuracy R-wave detection is that this signal is a safety which signals an immediate need for deflation (particularly for IAB) because it signals the onset of systole. A counterpulsation device should be "deflated" during systole to reduce ventricular afterload as well as not interfering with the normal pumping action of the heart. The criteria for real-time control applications is that there is little (e.g., 10-20 milliseconds) or no phase delay. Additionally, as noted earlier for Pa systolic rise and dicrotic notch detection, there can be no backward search. R-wave detection requires robust detection for arrhythmias and noise. The approach taken in the literature review was to first identify computationally efficient algorithms, secondly to identify the criteria that makes an ECG R-wave detection noise immune and lastly to find an algorithm that provides high accuracy during arrhythmia. The combination of the three criteria provided the optimal R-wave detection algorithm.

1.4.1   ECG QRS-Complex Detection

Previous investigators evaluated four different types of ECG QRS detectors(22) for noise immunity using the same test criteria. Three algorithms were based on amplitude and first derivative, Two algorithms were based on the first derivative only. Two algorithms were based on the first and second derivative and two algorithms were based on digital filters. In total, nine different algorithms were stress tested for noise immunity.

The signal utilized was a single-channel lead II. A "normal" synthesized (a healthy ECG digitized trace for one cardiac cycle copied and appended to itself multiple times) ECG was corrupted with five different types of synthesized noise. The noise types were:

1. Electromyographic interference,
2. 60Hz powerline interference,
3. Baseline drift due to respiration,

4. Abrupt baseline shift, and

5. Composite noise from all the previously listed simulated sources.

The results were tabulated in terms of percentage of QRS complexes detected, the number of false positives and the detection delay. In order to fully stress test the algorithms, the highest levels of interference were set to cause all algorithms to detect invalid QRS complexes (e.g., false positives). It was found that algorithms based on amplitude and slope had the highest performance for the EMG-corrupted ECG. A digital filter based algorithm performed the best for composite noise corrupted data.

The QRS detection algorithm termed AF2 that provided the best immunity to EMG-corrupted ECG was based on amplitude and the first derivative. The algorithm was based on an analog technique developed by Fraden and Neuman(23). A threshold is determined as a 40 percent of the peak value of the ECG amplitude:

$$\text{Amplitude Threshold} = 0.4 * \max [X(n)] \tag{1-17}$$

The data is then rectified:

$$YO(n) = X(n) \text{ if } X(n) >= 0 \tag{1-18}$$

$$YO(n) = -X(n) \text{ if } X(n) < 0 \tag{1-19}$$

The rectified ECG is then processed by a low level clipper

$$Y1(n) = YO(n) \text{ if } Y(0) >= \text{amplitude threshold} \tag{1-20}$$

$$Y1(n) = \text{amplitude threshold if } Y(n) < \text{amplitude threshold} \tag{1-21}$$

The first derivative is determined for the rectified signal

$$Y2(n) = Y(n+1) - Y1(n-1) \tag{1-22}$$

A QRS candidate is detected when the output of the derivative exceeds a fixed constant threshold:

$$Y2(n) > 0.7 \tag{1-23}$$

The digital filter, termed DF1, was most immune to composite noise. DF1 detected QRS complexes based on an algorithm developed by Engelese and Zeelenberg (24) as follows:

The ECG is passed through a notch filter differentiation with a 62.5 hz notch center frequency at 250 samples per second.

$$YO(n) = X(n) - X(n-4) \tag{1-24}$$

The output of that is then low pass filtered with the following equation.

$$Y1(0) = YO(n) + 4YO(n-1) + 6YO(n-2) + 4YO(n-3) + YO(n-4) \tag{1-25}$$

Two thresholds are used, one positive and one negative, but both equal in magnitude. The output of the low pass filter is scanned until a point with a value greater than the positive threshold is found. At that point $Y1(i) > 21.0$. The search region is started and will continue for 160 ms. During the 160 ms, any one of the following three conditions must occur for a QRS occurrence to be classified as a QRS complex.

Condition 1: If $Y1(i+j) < -21.0 \; 0 < j < 40$ (1-26)

Condition 2: If $Y1(i+j) < -21.0 \; 0 < j < 40$ and $Y1(1+k) > 21.0 \; j < k < 40$ (1-27)

Condition 3: If $Y1(i+j) < -21.0 \; 0 < j < 40$ and $Y1(1+k) > 21.0 \; j < k < 40$ and $Y1(i+j) < -21.0$ $k < l < 40$ (1-28)

If more than four crossings of the threshold occur (i.e., greater than Condition 3) either positive or negative, the QRS candidate is considered to be noise. At this point the QRS complex will have had too many positive and negative slopes within the 160ms window.

The first algorithm, termed AF2, utilizes an amplitude technique to ensure the QRS complex has sufficient amplitude to be deemed a perspective complex. In addition, areas in which no perspective QRS complex exists is converted into a flat line to prevent the derivative from improperly triggering on any noise. The derivative filter then ensures the derivative has a sharp enough positive slope to be detected as a QRS complex.

The second algorithm, termed DF1, utilizes a notch filter to remove frequencies around 60Hz. The resulting wave is then smoothed with a template matching "u" shaped filter to amplify any wave forms that rise within 8ms (i.e., two samples at 250 hz), typically a QRS complex. If the output of the smoothed template filter exceeds a certain threshold then criteria for detection within the next 160 ms includes a corresponding negative slope, or a negative slope and a positive slope or lastly a negative slope, a positive slope and a negative slope. This detection technique search for more than two slopes accounts for multi-peak QRS complexes.

The combination of all the requirements in the two previously mentioned algorithms led to the utilization DD/1 QRS-complex detection/delineation algorithm (26) which is part of the ARGUS/ 2H (ARrhythmia GUard System) algorithm. The results of the QRS DD1 detection/delineator utilized have demonstrated a greater than 98.3% MIT/BIH Arrhythmia Database(30) detection accuracy. The algorithm also has a robust noise immunity algorithm due to the vectorization of the signal. The robust noise immunity can be seen from the high detection accuracy within the noise riddled MIT/BIH arrhythmia database.

The DD/1 algorithm which provides the basis for the cardiac assist device real-time QRS detector algorithm in this dissertation, was developed on the following four principles:

1. QRS complexes originate and terminate to approximately the same ECG potential (i.e., same baseline potential),

2. QRS complexes have a certain minimum height,

3. QRS complexes have a certain minimum slope,

4. QRS complexes are greater than a minimum time duration and less than a maximum time duration.

These DD/1 principles provide not only immunity to noise but also provides a high degree of detection accuracy for detection during arrhythmia. The DD/1(26) (detection/delineation) QRS algorithm of the Arrhythmia Guard System (ARGUS) performs the same type of amplitude analysis the AF2 algorithm(23) does in that the amplitude is tested to ensure at least on QRS complex vector is greater than a certain absolute value. DD/1 additionally tests to ensure the validated QRS complex consists of a limited number of vectors both positive and negative as in the DF1 algorithm(24). The sum of the heights of the of a potential QRS-complex must sum close to zero to prevent the algorithm from triggering on a baseline shift as is also noted in DF1. The DD/1 algorithm also converts "unwanted" sections of the ECG to flat lines as does the AF2 algorithm.

DD/1 does not have a 62.5 hz notch filter as noted in DF1. This notch filter is in the form of a two point derivative filter. The two point derivative filter selectively filters out 60Hz noise; however, the filter make an algorithm more susceptible to high frequency noise that will be highly amplified by the derivative aspect of the notch filter. In addition, certain high frequency QRS complexes may be improperly attenuated.

This DF1 filter proves to be somewhat more sensitive to EMG noise. DD/1 can avoid triggering on EMG noise by ensuring a QRS complex has a certain width.

DD/1 provides a detection technique superior to the two previous algorithms in that it combines the most desirable features of both noise immune algorithms previously described with proven detection reliability with arrhythmias. DD/1 was developed as a QRS detector/delineator algorithm utilized for the detection and delineation of QRS complexes in patients with arrhythmias(26). DD/1 was also developed to be computationally efficient by utilizing preprocessed data that has been converted to lines and slopes (vectorized) using the AZTEC ECG preprocessing algorithm(25).

Amplitude-Zone-Time-Epoch-Coding (AZTEC) (25) is the preprocessing algorithm for the DD/1 (26) (detection/delineation) QRS algorithm of ARGUS/2H. AZTEC converts the 500hz sampled

digital representation of the data into a sequence of slopes and lines to be utilizes in the DD/1 algorithm to detect QRS complexes as seen in Figure 1-9.

A sequence of samples is converted to a line L if the samples all fall within a certain threshold value K of each other. For the data set $\{v_i\}[i=0$ to m] where v_{max} and v_{min} are the maximum values and minimum values respectively within $\{v_i\}[i=0$ to m].

If $v_{max}- v_{min} <= K$ for the set $\{v_i\}[i=0$ to n-1] and $v_{max}- v_{min} > K$ for the set $\{v_i\}[i=0$ to n] then the set $\{v_i\}[i=0$ to n-1] is considered a line $L = 1/2(v_{max}+ v_{min})$ for the samples [0 to n-1].

Any point within the data set $\{v_i\}[i=0$ to m] does not vary from the estimate by more than the K/2 (i.e., $|V(L) -v_i| <= K/2$).

In order to define the second type of vectorization, "the slope" the bounds (or endpoints) of the slope are defined. The two bound types are a "plateau" and an "extremum".

If L_i is the ith AZTEC line following a line L_0. The line L_i is a plateau if:

1. $t(L_i)>T$ (duration of four samples).
2. L_i is an extremum if $\{V(L_{i+1}) -V(L_i)\} \{V(L_i) -V(L_{i-1})\} <0$

Lines are converted to slopes if the following criteria is true:

1. A set of AZTEC lines $\{L_i\}[i=1$ to m-1] is a slope if no L_i is bound and L_0 and L_m are bounds.
2. The slope S is specified by its value $v(S) = v(L_m)-v(L_0)$, and its duration
3. $t(S) =$ summation $t(L_i)$ from $i=1$ to $i=m-1$.

This sequence of unbound lines indicates the several short lines are occurring quickly due to the quick change in ECG slope, typically due to a QRS complex. The AZTEC QRS complex preprocessing algorithm coverts the ECG into a ordered set of bounds and slopes.

The DD/1 detection/delineation algorithm uses the lines and slopes of the AZTEC preprocessing algorithm to accurately detect the QRS complexes bases on the following criteria.

1. A QRS complex consisting of slopes must have a minimum height compared to the moving average.
2. A QRS complex slopes must be of a certain minimum first derivative value.
3. A QRS complex must fall within minimum and maximum duration.
4. A QRS complex must consist of a set of slope vectors in which the sum of the vector heights is smaller than a certain minimum (near zero).

Fig. 1. ECG sampled at 500 samples per second (top) and resulting AZTEC representation (bottom) as reproduced by a digital plotter. The horizontal line at the upper left indicates 100 ms and the vertical line indicates one eighth of full scale, in this case 400 μV.

1	2	3	4	VECTOR #	1	2	3
3	-2	1	-2	VECTOR UNITS	-1	4	-3.5
3	1	2	0	VECTOR SUM	-1	3	- .5
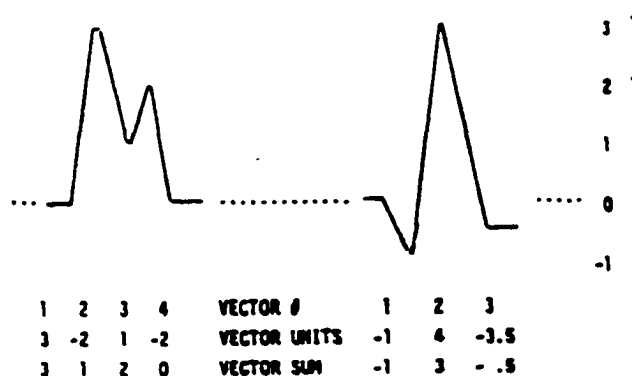
Figure 1. VECTOR SUM. Shown are AZTEC caricatures of two QRS complexes with artificial voltage ordinate to the right and dotted baseline. The left-hand QRS contains four vectors whose voltage values appear below; the left-to-right accumulating vector sum testifies that the QRS returns to baseline. The righthand QRS returns nearly to baseline with a vector sum = -0.5.

Figure 1-9. AZTEC Transformation is shown in Figure 1-9A (top)(25)and DD/1 QRS-Complex Vector Sum Calculation on AZTEC Data is shown in Figure 1-9B (bottom)(26)

The fourth criteria provides noise immunity to baseline shift because a single slope will not be detected as QRS complex. The fourth criteria also allows for dual peaked QRS complexes to be

detected, not typically accounted for in other QRS complex detectors.

AF2 demonstrated a susceptibility to ECG artifacts due to respiration, baseline shift and composite noise. When baseline shift was present, due to the threshold set by 40% of the maximum value of the data set, the baseline shift causes the threshold to be too high and certain QRS-complexes are not detected. It must also be noted that this algorithm is a post processing algorithm because of the need to determine the maximum data point for a threshold. The DD/1 algorithm is a real-time implementation which utilized a running average for a threshold.

DF1 demonstrated a false positive susceptibility due to severe electromyographic (EMG) noise. This is mainly due to the fact that EMG noise has broad frequency characteristics which overlap the frequency spectrum of the QRS complex. The DD/1 algorithm attempts to avoid false positives due to EMG noise by ensuring a minimum width for the set of QRS complex slopes. The DF1 algorithm does not ensure the QRS complex has a minimum width, DF1 only ensures the QRS complex is less than a maximum width. Ensuring the QRS-complex has a maximum width helps prevent the detection of EMG noise because the EMG noise typically consists of higher frequency components that the QRS-complex and thus the swings in slope endure for shorter period.

The DD/1 algorithm encompassed the basic techniques (amplitude/first derivative as well as the digital filter) utilized in the two most reliable algorithms for EMG and composite noise. In addition the algorithm has proven detection capability with cardiac arrhythmias. Since the S/N ratio of R-wave is very high, the DD/1 uses a primitive logical (using vectorized data) image processing technique, much like the human brain does to detect the QRS complex within an ECG trace.

1.5   Prediction of STI for Ectopic (Arrhythmetic) Beats

In order to optimally inflate during an ectopic beat, the control algorithm must predict the onset of the dicrotic notch in order to initiate the inflation signal prior to the dicrotic notch event. This is required because of the inherent delay between the pneumatic action of the CAD pump and the associated hemodynamic augmentation that is observed in the aortic pressure. For this reason, research into the heart rate to systolic time interval relationship is investigated.

1.5.1 Systolic Time Interval (STI) to Heart Rate (HR) Relationship in Man and Animal

A vast amount of research was performed documenting the inverse relationship between the STI and the heart rate(31)(32)(33)(34) in man. A regression equations for normal male patients is as follows (31):

$$STI \text{ (in seconds)} = .266 - 0.0021[HR(\text{in BPM})-73] \qquad (1-29)$$

Normal males typically demonstrate a correlation coefficient of -0.90 and a (p < 0.01). This high correlation can be observed in Figure 1-10. Patients with myocardial failure also demonstrate a correlation between STI and the heart rate in which the decrease in ejection time is significant. However, what can be observed from the data is that if the regression lines are slid vertically downward, an inverse linear relationship still exists between STI and the heart rate as seen in Figure 1-11.
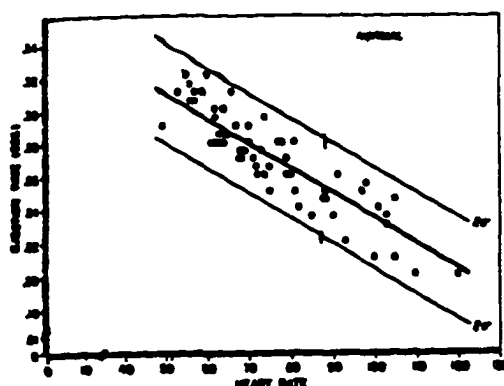
Figure 1-10. Relationship Between STI and Heart Rate in Normal Individuals(31)

Studies on animals' inverse relationship between the STI and the heart rate, in particular canine mongrels (35) and rabbits (36) demonstrate a nonlinear relationship. Experiments were conducted over a variety of experimental conditions to emulate cardiac and circulatory disease. The animal studies indicate that for a variety of experimental models (either canine mongrels or rabbits) taken as a whole, the correlation between the STI and HR is very rough as compared with the STI and HR relationship in humans. The research in this dissertation has taken this information into consideration. Since the experimental models utilized for the research were canine mongrels,
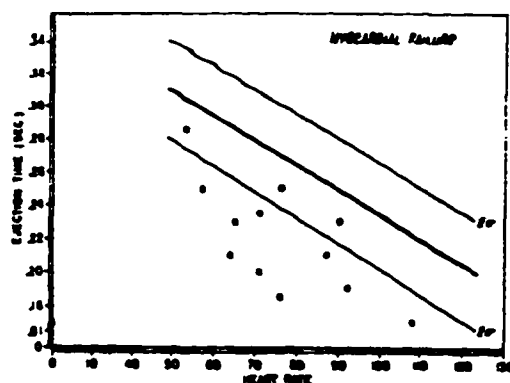
Figure 1-11. Relationship Between STI and Heart Rate in Myocardial Failure. The Regression Lines Shown are those for the Normal Group.(31)

studies were performed to demonstrate if for a single animal, a linear regression may be derived. In other words, although for a set of animals of the same type, there is a scattering of plotted points in the relation between STI and HR as seen in Figure 1-12. The correlation coefficient for the STI vs. 1/HR data in Figure 1-12 is a mere 0.62. However, experiments were performed to determine if a regression equation could be estimated for a single mongrel canine experimental model.

Coefficients of the regression equation would then be derived during CAD assistance from two or more data points including both STI and HR values.
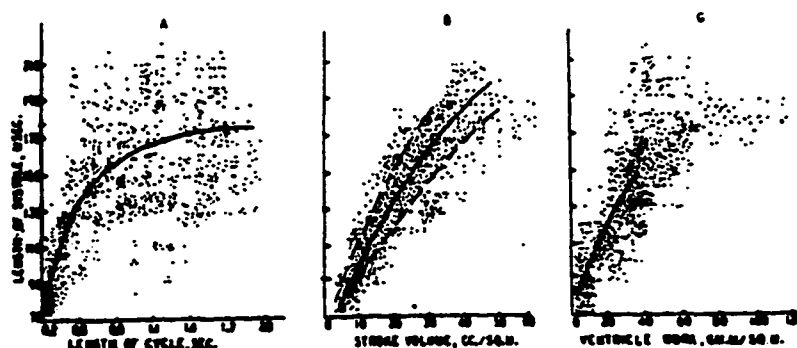
Figure 1-12. Relationship Between Lengths of Systole and Cycle Lengths of Dog Pulses (Left Graph) (35)

It is apparent in man that for both healthy and unhealthy patients (i.e., those with myocardial disease) there exists an inverse relationship between STI and HR. However if the data is intermixed, as in the animal experiments of the same type of animal, the data may be somewhat uncorrelated. For this reason, research into the heart rate to systolic time interval relationship is investigated for canine mongrels on a per experimental model basis. This will focus the study of the regression

equation to a health or unhealthy animal. The focus will be on unhealthy experimental models (animals with surgically impaired hearts modelling that of myocardial disease e.g. by occluding the coronary arteries).

1.6   Challenges of Fault Tolerant Cardiac Assist Device Research

In order to advance the optimization of augmentation provided by CAD detection and CAD control for applications of non-sinusoid rhythms (arrhythmetic rhythms) and the applications of implantable CADs, fault tolerant detection algorithms and control algorithms must be devised. These CAD detection and control algorithms were used to establish timing with the cardiac cycle and react to (inflate/deflate) cardiac assist devices. The signals (Pa and ECG) presented shall be non ideal in presentation and cardiac state.

This section describes briefly the each area of research investigated toward the development of a fault tolerant CAD counterpulsation controller to be utilized to advance the optimization of CAD control as well as providing a robust control prototype for a implantable counterpulsation CAD.

1.6.1   Optimized CAD Control and Prediction of STI for Optimized CAD Inflation

Electronic CAD controllers are far superior to control provided by a certified IABP technician because a computer can make decisions in milliseconds where person may take a few seconds to a minute. Optimized cardiac assist device control requires knowing the phasing of the cardiac cycle. In order to optimize CAD inflation, the development of a STI prediction technique for mongrel canine experimental models (i.e., those animals used for experimental verification) was developed. The initial studies attempted to determine if a STI to HR regression equation (prevalent in humans both healthy and those demonstrating myocardial disease) exists on a per canine experimental model basis. Due to the uncorrelated results with the canine HR to STI regression equation, a different technique was developed utilizing the sinusoid model of the STI pressure trace. However, unusually shaped canine pressure systolic traces were encountered. In cases where the sinusoid estimate was calculated to be unreasonable, a dicrotic notch inflation trigger as well as an STI running average estimate was employed as an estimate for apparently long and short STI estimates respectively. This method proved to be reliable during canine ectopic beats.

1.6.2   ECG Detection

Implementation of an ECG detector that maintained a high accuracy of detection for a variety of impairments causing unusually shaped or distorted QRS-complexes due to arrhythmia and signal artifacts was desired. For this reason the ARGUS DD/1 QRS-complex detector/delineator was implemented. Slight variation were made to the DD/1 detection algorithm to provide more efficient execution and to prevent the algorithm from self destructing during run-away traces. These improvements include autoscaling and threshold damping to prevent a single large vector (non-QRS-complex artifact) from inflating the running average height threshold.

1.6.3   Pa Detection

The development of a robust systolic rise and dicrotic notch Pa detector was developed. Previous investigators provided methodology for Pa traces that were ideal. This investigation called for the algorithm to be tolerant to variations due to both aberrant heat beats (arrhythmias) and aberrations due to noise artifacts. A method utilizing set thresholds proved unreliable particularly during increases in random noise. The utilization of a derivative based riding clipper technique combined with a Butterworth LPF provided a computationally efficient and robust method to detect the dicrotic notch. The sensitivity of the algorithm ranges from a notch with no perturbation (just a change in slope) to a single dip notch perturbation buried in uniformly and Gaussian distributed noise.

1.6.4   Experimental Model Verification of ECG-based and Pa-based Controller

Multiple experiments utilizing canine experimental models were conducted to develop and verify the ECG and Pa detection algorithms as well as the control algorithms. The results demonstrate the CAD controller properly tracking the cardiac cycle during non-ideal conditions including arrhythmia and signal interference.

1.6.5   Multiprocessor Communications Verification

In order to verify that a multiple processor fault tolerant system was feasible, throughput experiments were conducted. The throughput experiments determined if the transport of Pa and ECG information, through a PC plug-in quad transputer card with four RISC processors, could be performed in an efficient manner. Utilization of the modified interface primitives demonstrated that

communication between the processors, necessary for a CAD fault tolerant multiprocessor implementation, required a reasonable fraction of the processing power. A CAD control protocol was developed to ensure enough information was present in the throughput experiment. The received ECG and Pa signals from the patient monitor and generated control signals to the CAD pneumatic driver were accounted for in the throughput experiments.

1.6.6 Simulation Verification of Pa Detection

In order to further verify and quantitatively assess the maximum tolerances of the Pa systolic rise and dicrotic notch detection algorithms, a simulation platform was developed. Artifacts model generators were developed that "modelled" those experienced while performing canine mongrel experiments in the cardiothoracic research laboratory. The experimental conditions imparted to the Pa were similar to those experienced in a cardiothoracic operating room within a hospital.

1.6.6.1   Simulation Platform

In order to perform the simulations, a simulation package had to be selected. Acclimation to the modeling elements in the simulation package was necessary to build and perform the various simulations. A method had to be devised to synchronize data communications between the modeling elements and detection algorithm. A method also had to be devised to display simulated Pa and respective CAD Pa triggering signals for visual inspection.

1.6.6.2   Pa Trace Model

The development of an aortic pressure model to run continuously in real-time to facilitate a visual method of stability verification with the use of a ECG/aortic pressure patient monitor was needed. In order to generate the aortic pressure (Pa) simulated waveform, an aortic pressure model along with a dicrotic notch models was needed. Once the individual models were developed, verification of the stability (long term simulation results) and integrity (ensure realistic and rationale results) of the models separately would be completed. Integration of the two models ensuring the stability and integrity of the arterial pressure wave was next.

1.6.6.3   Pa Trace Artifact and Physiological Variation Models

For verification of the Pa detection filters, creation of modeling filters to integrate undesirable Pa artifacts (into the Pa wave) was the last stage of development necessary to "challenge" the Pa detectors. The biological variation and deviations in Pa artifacts models due to clinical conditions experienced in cardiothoracic surgery was investigated. Pa biological variation was modelled with an Pa trace with and without a dicrotic notch deflection. The second biological variation model was caused by heart rate variability due to respiration. Artifact models included baseline wander variation due to artificial ventilation, transducer signal attenuation, uniformly distributed noise, and Gaussian distributed noise.

1.6.6.4   Experimental Strategy

Each set of simulation experiments utilized a different Pa trace artifact or physiological variation model to determined the capability of the Pa trigger algorithm to withstand the effects the Pa detection impediments while maintaining 100% accuracy of the dicrotic notch detection. Multiple simulation experiments were conducted in which the same nominally adjusted interference was increased to benchmark the immunity threshold of the dicrotic notch detector.The results of the simulation experiments performed were designed to quantify the robustness of the Pa detection algorithm.

1.6.7   Challenges of CAD Research

The tremendous challenges associated with Cardiac Assist Device Control research include the fact that all biological signals are inherently nonlinear and unique for each canine experimental model. Additionally, real-time control does not allow for any "looking back". Control decisions have to be made exactly at the time the cardiac cycle event has occurred. Post processing detection (i.e. detection slightly after the cardiac event has occurred) is not useful because optimal real-time counterpulsation requires the control algorithm to dynamically react to each cardiac cycle event as the event occurs. Additionally, real-time post event analysis or "learning" (e.g. during the same cardiac cycle before the next similar event occurs) for the CAD research conducted was also restricted by the processing power of the personal computer. All available processing power was utilized in the detection and control algorithm.

The control of a cardiac assist device using aortic pressure poses an additional complexity. Cardiac assistance proactively modifies aortic pressure through augmentation. Unlike control using the ECG signal, when using Pa as the control signal, the modified signal is the same signal control decisions must be derived from. This is a form of positive feedback which is inherently unstable.

An additional complexity and challenge with CAD filtering design is due to restrictions in the use of Infinite Impulse Response (IIR) digital low pass filtering e.g. Butterworth. In order to reduce the possibility of false triggering caused by noise, low pass filtering can be used as a front-end filter. Low pass filtering is very effective in aiding detection algorithms susceptible to noise thus providing a degree of noise immunity. The attenuation of unwanted noise results in more repeatable detection of a Pa wave. However, low pass filters (LPF) at the traditional break frequency most useful to Pa detection (e.g. 2 Hz for 120 bpm), will add excessive phase delay for real-time control. For example, in off-line Pa detection (i.e. not real-time control detection), the output of a 2 Hz 3dB break frequency 3rd order Butterworth digital LPF (derived using a bilinear transformation) results in a smoothed Pa wave. The resulting filtered Pa wave would have a 135 degree phase shift at 2 Hz resulting in a 188 ms phase delay (0.5 sec/cycle * 0.375 cycles) for that fundamental frequency. Again, phase delay is not tolerable in CAD real-time control applications. The CAD inflation interval may be as small as 200 ms, therefore a 188 ms phase delay would make real-time control unfeasible because detection would occur considerably after any respective cardiac event had occurred. Low pass filters utilized in real-time CAD applications must be designed with break frequencies greater than the most desirable break. This restriction diminishes the effectiveness of the low pass filter for noise reduction and further challenges detection algorithms to avoid false positive detections.

A second restriction on IIR filters (as well as FIR filters) is that as the order of the filter increases, the computational demand increases. For real-time control, computational power is limited thus limiting the order of the IIR and FIR filters (and limiting the filter's effectiveness).

Another complexity of CAD control development is the design of computationally efficient FIR derivative filters. These FIR filters are an essential component of CAD controller design because of the need to detect changes in biological signal slope and direction. However, the FIR derivative filters must be carefully designed because of their susceptibility to noise and the restrictions on LPF IIR filtering. For all these reasons, including restrictions on IIR LPF cutoff, FIR derivative filters noise susceptibility and limited computing resource for real-time control, cardiac assist device control is an extremely challenging field of research.

1.6.8 Strategy of the CAD Research

For the CAD controller to be implantable, digital filters should be used (as opposed to analog filters) in an attempt to provide all cardiac signal processing and control signal generation on a single integrated circuit (IC). Analog filters would require discrete analog components which would be considerably more bulky than their digital counterparts. Additionally, CAD implantable devices require the most robust form of detection and control because the ideal implantable CAD would allow the patient complete mobility within and outside an area of cardiothoracic care e.g., a cardiothoracic critical care unit within a hospital.

In order to develop the previously mentioned areas of experimental and simulated CAD research as well as to demonstrate the results, an experimental model and simulated model research system was derived. The canine mongrel experimental system included a PC-based control system with A/DC and D/AC converter cards, a patient monitor to observe cardiac signals and their respective trigger signals, a pneumatic driver, an experimental operating area and a data recording system.

The simulated Pa model experimental system included a PC-based simulation platform with a software interface to C-based Pa detection code, models to generate aortic pressure and corresponding Pa artifact models, and a visual/printed method to record results. The experimental and simulated CAD development platforms provided the methods to develop and record the modelled CAD research.

The following chapters describe the details of this research along with the corresponding results.

o

2. CAD Aortic Pressure and ECG Detectors for Cardiac Cycle Events

The detection and control algorithm development required the biological signals to be generated, converted into digital format (for the all integer-based digital detection and control algorithms), processed and corresponding signals must be regenerated for visual analysis. For this reason the detection and control algorithm development station was synthesized from available laboratory equipment.

2.1 Detection and Control Algorithm Development System

In order to develop the detection and control algorithms, a algorithm development station had to be engineered. The system consisted of the FM (frequency modulation) recorder reel-to-reel tape drive. The Cornell University Medical College Canine Aortic Pressure (Pa) and Canine ECG Database was recorded on 8 track reel-to-reel tapes. The software development was performed on a 33Mhz 80386 PC-AT clone. The PC-AT was configured with an A/DC as well as 2 D/AC cards for digitizing a single analog signal and transmitting four analog signals, respectively. The patient monitor was used to perform visual analysis on the detection signals. A typical visual analysis would require both the original digitized signal and detection trigger signal to ensure the signal was properly detecting the respective events in the cardiac cycle. The algorithm development station is illustrated in the bottom third of Figure 2-1.

2.1.1 FM Recorder Reel-To-Reel Tape Drive

The Cornell University Medical College canine aortic pressure data base was recorded on four FM tapes (Scotch 10.5 inch reels, 0.5 inch magnetic tape) using a FM reel-to-reel tape recorder (Honeywell 5600). The tapes were cardiac signals recorded from approximately 40 various animal experiments on a variety of canine mongrel, sheep and pig experimental models under different experimental and pharmacological protocols as seen in Figure 2-2 and Figure 2-3. The recorded signals included root aortic pressure and ECG.

Figure 2-2 demonstrates five different Pa traces of normal (sinusoid) cardiac rhythms. Figure 2-2A illustrates a Suffolk sheep[1] Pa trace. (Note that the systolic rise does not have as pronounced a first derivative slope as the other four canine traces below.) Figure 2-2B illustrates a canine aortic pressure trace. Figure 2-2C illustrates a canine aortic pressure trace with a small amount of cardiac

---

1. An English breed of hornless sheep(9).
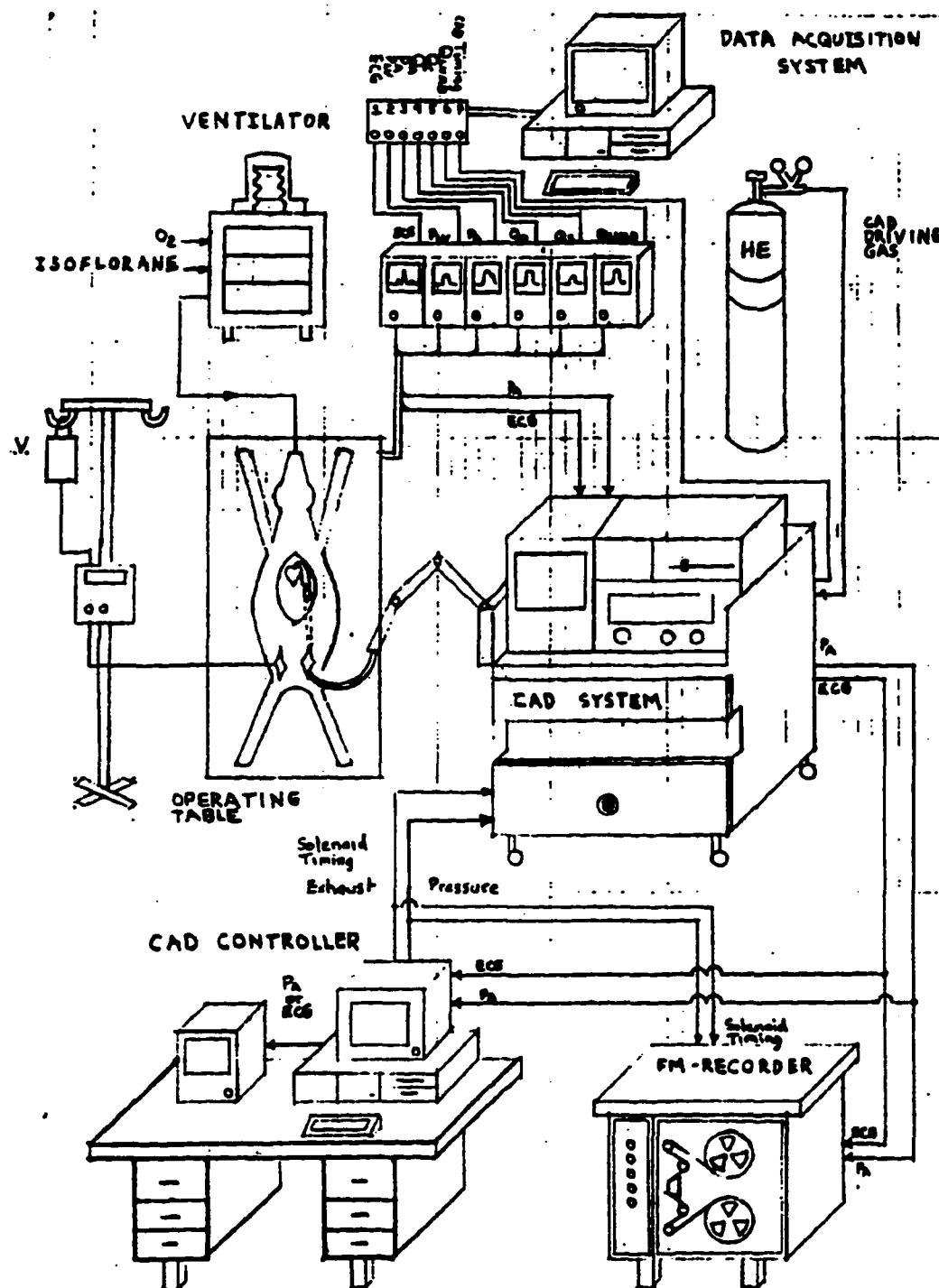
Figure 2-1. Experimental Pictorial

assistance (IABP) augmentation applied slightly after the dicrotic notch. Figure 2-2D illustrates a canine aortic pressure trace. Figure 2-2E demonstrates the type of aortic pressure canine mongrel trace in which detecting the dicrotic notch is very difficult due to the pressure "spur" half-way down the fall in systolic pressure.

Figure 2-3 demonstrates six different canine mongrel Pa traces, two of which demonstrate variation due to respiration and noise, and four which demonstrates arrhythmetic (non-sinusoid) cardiac rhythms. Figure 2-3A demonstrates aortic pressure variation due to artificial ventilation, the affect is particularly noticeable on the left where the trace speed was reduced. Figure 2-3B demonstrates a combination of mechanical ventilation and noise. Figure 2-3C illustrates arrhythmia presumably due to ventricular bigeminy. Figure 2-3D illustrates premature ventricular contraction (PVCs). Figure 2-3E illustrates tachycardia. Figure 2-3F illustrates a missed beat. Figure 2-2 and Figure 2-3 illustrate the considerable variation in Pa traces that challenge CAD Pa detection algorithms.

2.1.2   PC-AT Based Development System

The Pa or ECG signal (depending on the algorithm developed) from the FM reel-to-reel tape recorder was presented to an Analog-to-Digital Converter (A/DC) converter card (Scientific Solutions Labmaster Card) within the PC-AT (Datatech Enterprises Co., Ltd. DTK PEM 2501/3301 - 33Mhz 64 Kb Cache 80386/80387). A timer on the A/DC was configured to interrupt the PC-AT (Interrupt #0F) 500 times per second. An assembly level interrupt routing was implemented using Borland C++(45). Thus the analog signals were read into the PC-AT sample-by sample through a memory mapped register via an interrupt routine generated at 500 Hz.

2.1.3   Patient Monitor

Once the ECG or Pa data was processed by the detection algorithm, two signals were presented to the Datascope 870 monitor (as seen in Figure 2-4) via a dual interface Digital-to-Analog Converter (D/AC) (also within the Scientific Solutions Lab Master board). The signals generated during detection algorithm development depended on the different stages of development and test. The Patient Monitor (Dual Trace Datascope 870 monitor) received the signals on the inputs designated as "Pa" and "ECG". The designated inputs had no relation to the signals received except these signals are typically displayed on a cardiac patient monitor. Occasionally a second dual interface D/AC card (Keithley Metrabyte) was utilized to send and display data on a second patient monitor as seen in Figure 2-5. In order to test the finalized Pa or ECG detection algorithm, the two detection traces sent to the patient monitor were the preprocessed data (either Pa or ECG) and the detection algorithm trigger.
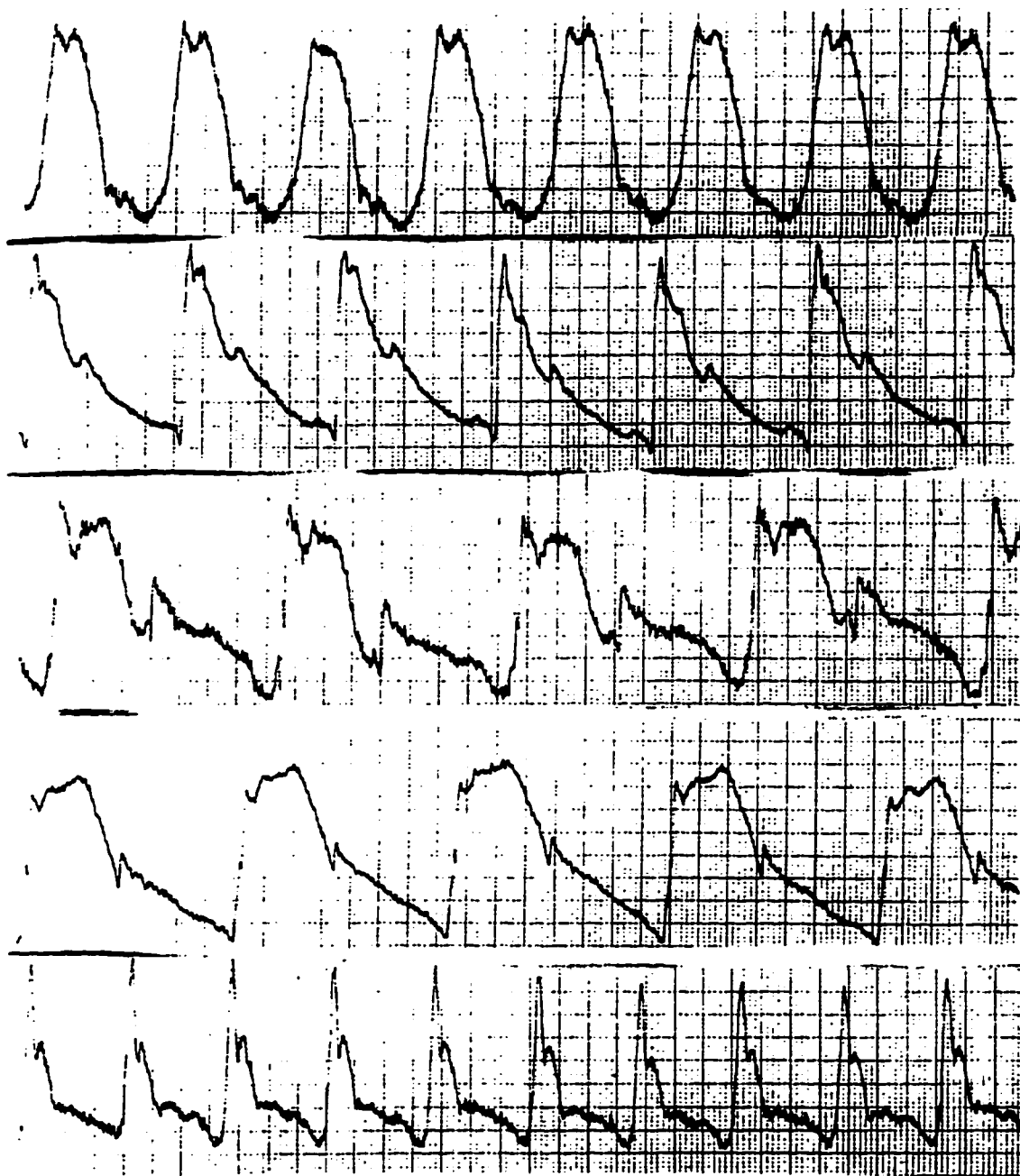
Figure 2-2. Canine Mongrel and Suffolk Sheep Experimental Model Pa Traces during Sinus Rhythms. Figure 2-2A (top trace) illustrated Pa of a Sheep. Figure 2-2B (2nd from top) illustrated Pa of a Canine. Figure 2-2C (3rd from top) illustrated Pa of a Canine with CAD Pa Augmentation. Figure 2-2D (4th from top) illustrated Pa of a Canine with Obvious Dicrotic Notch. Figure 2-2E (bottom trace) illustrated Pa of a Canine with a Dicrotic Notch that is Not Obvious.
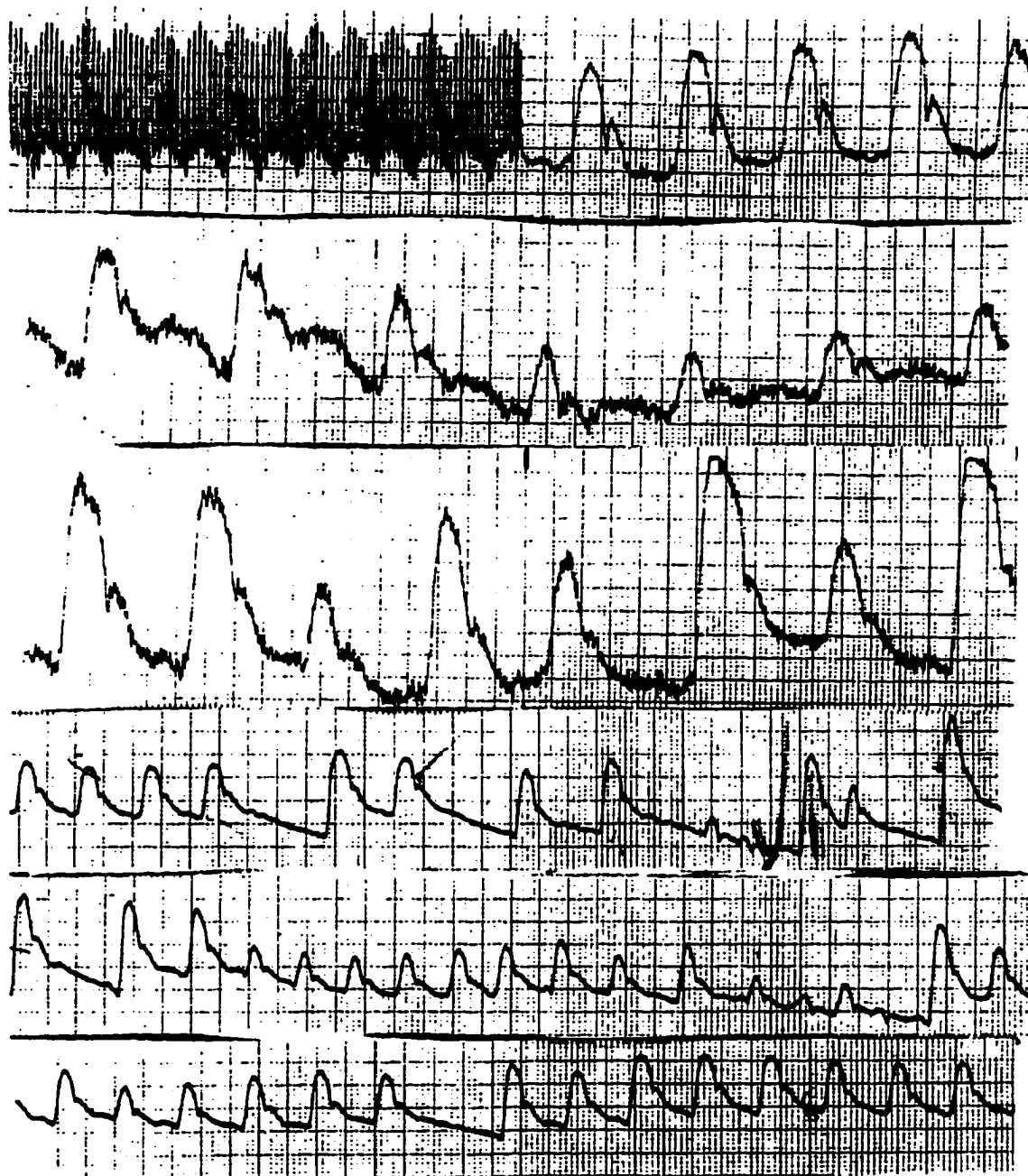
Figure 2-3. Canine Mongrel Experimental Model Pa during Signal Interference and Arrhythmia. Figure 2-3A (top trace) illustrated Pa Interference due to Mechanical Ventilation (MV). Figure 2-3B (2nd from top) illustrated Pa Interference due to MV and Cardiothoracic Surgery Noise. Figure 2-3C (3rd from top) illustrated Pa Interference and PVC Arrhythmia. Figure 2-3D (4th from top) illustrated Pa during Ventricular Bigeminy Arrhythmia. Figure 2-3E (5th from the top) illustrated Pa during Tachycardia Arrhythmia.Figure 2-3F (bottom trace) illustrated Pa during an Ectopic (missed beat) Arrhythmia.
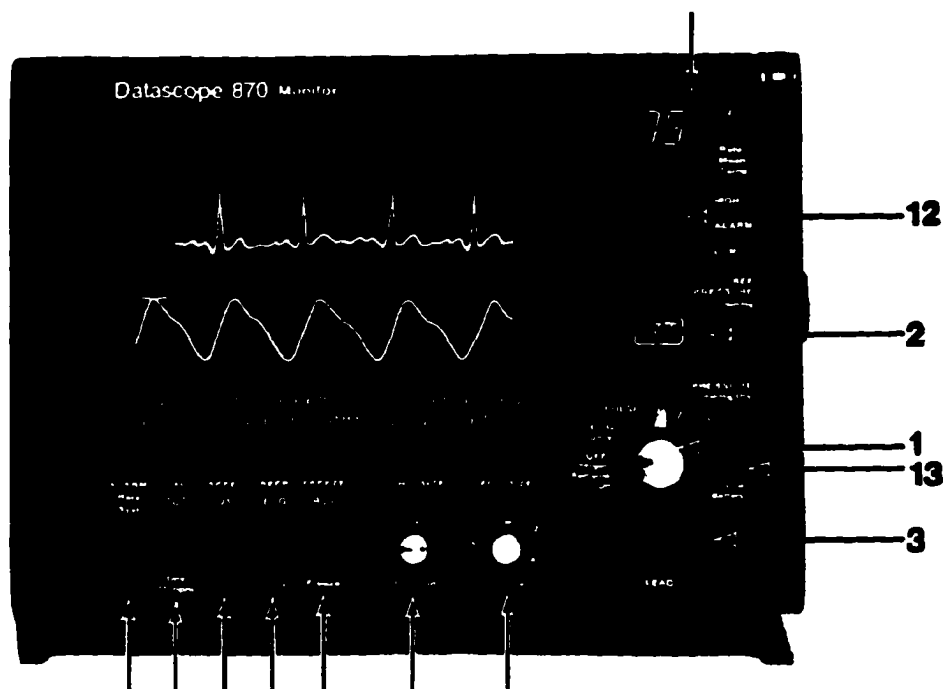
Figure 2-4. Datascope 870 Monitor Front Panel with ECG and Pa Trace(43)

PC-AT CAD Detection and
Control Development System
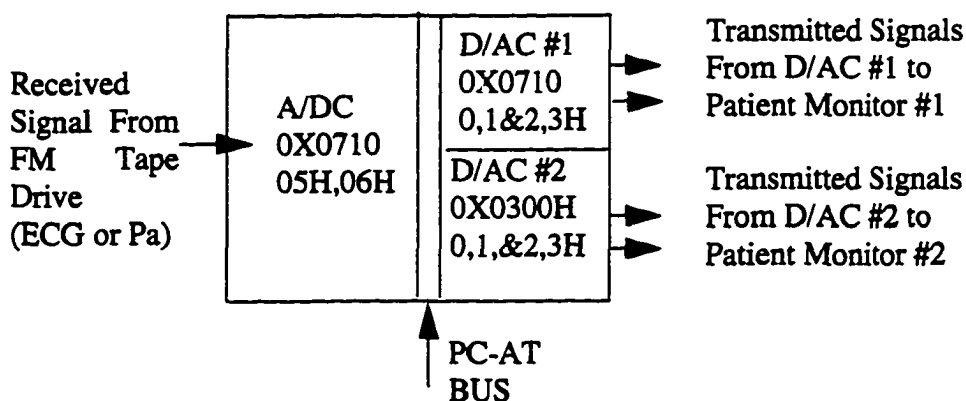
Figure 2-5. CAD Development Station Received and Transmitted Signals

2.2 Pa Systolic Rise and Dicrotic Notch Detection

The detection of the systolic rise and dicrotic notch within the aortic pressure was essential to properly timing events within the cardiac cycle. The rise in systolic pressure signals the onset of the systole in the cardiac cycle. The dicrotic notch within the aortic pressure signals the end of systole.

The systolic rise and dicrotic notch detection algorithm was developed to trigger on a wide variety of aortic pressure waves. The algorithm's complexity was limited by the real-time constraints placed on the CAD control application. Simple algorithms generally provide short computation time which allows complete processing between samples. The processing time between samples was 2 milliseconds (1 / 500 Hz = 2 milliseconds)[1].

The approach taken was to utilize algorithms typically employed for real-time ECG detection making variations when necessary for the differences between aortic pressure and ECG signals. A high level description of the algorithm starts with the reading in of the 12-bit data through the A/DC at 500hz. A running average of the sample values establishes a mean pressure to allow scaling of the wave. A running average of the absolute values of pressure minus the average is maintained to perform autoscaling of the wave. This autoscaling constantly maintains a systolic/ diastolic difference in pressure of approximately 200 centered around zero[2]. A 3 pole Butterworth 23.8Hz low pass filter is used to filter the incoming signal to remove unwanted high frequencies.

A cardiac cycle is identified by the detection of its diastolic pressure (trough), systolic pressure rise (first derivative peak) and systolic pressure (peak). A trough is established by following the pressure wave downward until a suspected lowest value is collected. The trough is then verified by establishing several sample values of higher pressure on the systolic rise. The systolic rise is determined by crossing a first derivative peak threshold. For this process the first derivative is calculated using a 5 point least squares polynomial fitting technique on the output of the 23 Hz filter. The employed derivative technique for Pa has been demonstrated to be reliable in several ECG QRS-complex detectors (41)(42). This threshold is determined by keeping a running average of the highest window integration value for the previous six cycles. Additional criteria for detecting the systolic rise include performing a comparison in value between the current first derivative window[3] and the ambient first derivative window filters[4].

---

1. For this real-time controller computational efficiency is essential, thus all calculations are done with double precision 32-bit integers. No real number are used because of there relatively longer processing time for numerical calculation.

2. Preprocessed autoscaled Pa data values are centered around zero and reduced to a systolic to diastolic amplitude difference of approximately 200 to minimize the chance of double precision integer (32-bit) overrun. In addition, Butterworth filters were utilized as opposed to Elliptical and Chebyshev filters because of stability problem with the latter low pass filters (LPFs) due to integer value overrun.

3. The first derivative window is a digital filter that sums the first derivative for ten consecutive samples of the Pa trace starting from the latest sample. This filter gives an approximation of the first derivative within the wave adjacent to the current sample.

The systolic peak is detected by following the pressure upward until a suspected highest value is found and verifying it with several pressure samples lower. Once the diastolic trough and systolic rise are verified the detection is transferred to the peak. Upon detection of a peak the initiation of a cycle is detected and established.

Once the heart rate (and corresponding cycle length) are known[1], detection of the dicrotic notch is initiated. For this process, the second, third and a combination of second and third derivative is calculated using a 5 point least squares polynomial fitting technique on the output of the 23 Hz filter. A cycle is identified by the detection of its systolic pressure rise (first derivative peak) and systolic pressure (peak). Once the cycle is verified by a systolic rise and peak, the dicrotic notch detection is activated. A proper detection interval is established to be half a cycle length after the detection of the peak. A pressure blanking window is established using a percentage of the trough and peak difference to prevent the dicrotic notch from being incorrectly determined by an unusual peak pattern (i.e. two horned peak). Once detection is past the pressure window a detection must pass the time blanking interval to prevent false detection on the systolic fall due to noise. After both blanking windows have satisfied the dicrotic notch may be detected. The detection criteria requires surpassing the second, third or second and third derivative threshold. The employed derivative technique for Pa detection has been demonstrated to be reliable in several ECG QRS-complex detectors (41)(42). For this process the first derivative is calculated using a 5 point least squares polynomial fitting technique on the output of the 23.8 hertz filter. After dicrotic notch detection occurs or the detection interval elapses, status is changed to look for the next cycle.[2]

In order to implement the Pa detection algorithm mentioned above, the following "C" function were developed in C language (44) using the Borland C++ compiler(45):

1. Interrupt Handling Routine

2. Definitions for Included Functions, Constants, Functions Declarations, Types, Enumerations Types, and Variables

3. Data Preprocessing Routine

---

4. The ambient first derivative window is a digital filter that sums the first derivative for ten samples that are spaced every third sample within the Pa trace starting from the latest sample. This filter gives an approximation of the overall first derivative value within the wave over a relatively long period thus providing a comparative baseline for the riding clipper algorithm which may be compared with the current first derivative window.

1. During the calculation of the heart rate and subsequently, statistics are accumulated for detection thresholds, timing windows and pressure windows.

2. Noise rejection has been added to prevent false triggering in the event of substantial deviations, oscillations and random noise in the pressure wave. Detection is suspended until the noise subsides.

4. Systolic Rise Detector

5. Dicrotic Notch Detector

6. Pa Running Statistics (e.g., Thresholds)

2.2.1   Interrupt Handling Routine

The interrupt handling routine required four different sub-functions to configure the A/DC to interrupt the PC-AT every 2 milliseconds and allow an interrupt handler read in the two bytes that made up the sample.

2.2.1.1   Initialize the Interrupt

The first sub-function initializes the interrupt on the PC-AT to be utilized by the A/DC card. This is accomplished by resetting the A/DC "done" flip flop by performing a read on the two memory mapped addresses to the 12-bit digital conversion to the analog input (i.e., 0X0710 + 5= 0X715, low byte; 0X0710 + 6 = 0X716, high byte). Interrupts are temporarily disabled on the PC-AT. The PC-AT 8259 interrupt chip is then enabled for interrupts. The old interrupt is then saved. The new interrupt handler is then installed. The sub-function to configure the A/DC interrupt generation is then executed (see Section 2.2.1.2). Interrupts are then disabled again and the immediate "interrupt" byte is moved into the byte register. Lastly, the A/DC done flip flop is reset. After this function is executed, the A/DC will be generating an interrupt every 2 milliseconds and the user specified interrupt handler reads in the data at that rate.

o

2.2.1.2   Configure A/DC Timer to Send Interrupts to the PC-AT

The second subfunction configured the timer within the A/DC to time out every two milliseconds. The timer subfunction set up counter 5 in the A/DC board[1]. The done (sample processed) flip flop was reset by reading the starting memory address of the board + 6 (i.e., 0X0710 + 6 = 0X716). The control byte is written to the board to address 0X0714 to disable auto-incrementing, external start conversions, and all interrupts. In addition, external start conversions are enabled after the counter is started and the gain is set equal to one. The data pointer is then set to point to the master mode register. The master mode register is then set for scaler control = binary coded division (BCD)

---

1. A hardware jumper was placed between pins 3 and 4 of connector J2. This connected the output of counter 5 with the external start conversation input. (The input rage is assumed to be -5 to +5 volts.) The board was I/O mapped to 0X710 hexadecimal.

enable increment, 8 bit bus, FOUT was turned on, divide by 16, source = F1, both comparators are disabled and time of day(TOD) is disabled. The data point is then set to the register of counter 5. Counter 5 is configured for no gating, counting rising edge of F5 (100Hz) disable special gate, reload for the load setting, count repetitively; BCD count down and active high time counter (TC) pulse. Loading counter 5 with 19 produces a 500 Hz output. Counter 5 must be loaded from the register assigned to counter 5. The counter is also armed (starts counting). Lastly, the control byte must be written to the A/DC board to start the conversion and specify the channel number of the A/ DC board (because multiple channel inputs signals are possible).

2.2.1.3   Interrupt Handler Routine

The Borland C++ compiler causes the PC-AT to utilize the user specified interrupt handler when the interrupt redirect is specified in an interrupt initialization procedure. The first step in the interrupt handler routine is to enable interrupts. A variable is initialized to ensure that all algorithm software is processed after the interrupt (i.e., the next interrupt does not occur before all the processing is completed for the current sample). The two byte A/DC information is read and converted into a 16 bit integer. Several D/AC write command statements are included to generate traces for different detection signals being diagnosed. Appropriate sizing is performed to scale the detection signals for the input range requirements of the Datascope 870 patient monitor as well as being large enough for visual inspection. Interrupts are then disabled. Lastly, an end of interrupt routine (EOI) command is sent to the interrupt controller.

2.2.1.4   Restore PC-AT Original Interrupt Routine

The original PC-AT interrupt routine is re-enabled after the Pa detection and control algorithm stops running in order to restore the PC-AT interrupt vectors back to their original state, and thus the state of the PC-AT.

2.2.2   Data Preprocessing Routine

The data preprocessing routine performed the following functions:

1. Maintain a sample number count
2. Maintain an updated history of non-filtered and filtered data
3. Calculate a moving average mean pressure

4. Calculate an autoscale divisor

5. Calculate the autoscaled data

6. Low pass filter the data using a Butterworth filter

7. Create first, second, and third derivatives

8. Create first, second, third and a combination of the second and current third derivative window filter using the respective derivatives

9. Create first, second, third and a combination of the second and ambient third derivative window using the respective derivatives

2.2.2.1   Sample Number and Data History

The sample number was maintained using a 32 bit unsigned long integer. At 500 Hz, this data structure would roll over in 4294967296 ($=2^{32}$) samples or 99.4 ($=4294967296/(43200000$ samples/day) days. This number is well within period of a single experiment both with canine experimental models and simulated models.

The data history was kept in traditional fashion in which the oldest sample was discarded and replaced with the more recent sample as seen in Equation 2-1 and Equation 2-2[1]. The variable holding the oldest value must be replaced first in sequence of data shift as to not write over any data needed in the shift. This would occur if the data was shifted starting with the more recent data values.

$$NewDataValue[t\text{-}i\text{-}1] = OldDataValue[t\text{-}i] \text{ for } i = n\text{-}1... 1 \qquad \text{(2-1)}$$

$$NewDataValue[t\text{-}0] = NewSampleValue \qquad \text{(2-2)}$$

2.2.2.2   Moving Average Mean Value and Autoscaling

In order to reduce the data value of the samples to their smallest possible absolute value, a moving average mean value was calculated. (Variable overrun was avoided in the butterworth filter utilizing this approach.) A moving average required a history of values to be stored. In order to reduce the computational time a ring buffer was constructed in software so only one value would have to be rewritten for each new sample. The moving average filter can be seen in Equation 2-3.

---

1.   The Pa data values were implemented in a circular array.

(2-3)

$$\text{MovingAvergeMeanValue}\,[t-0] \;=\; \frac{\displaystyle\sum_{i=0}^{n-1} \text{Sample}\,[t-i]}{n-1}$$

Autoscaling was accomplished by approximating the aortic pressure as a sinusoid signal. The autoscale divisor was created by averaging a full wave rectified signal to create a moving average full wave rectified mean value as seen in Equation 2-4[1]. Once again the historical data for this algorithm is stored within a ring buffer to reduce the use of CPU time.

(2-4)

$$\text{FullRectifiedMeanValue}\,[t-0] \;=\; \frac{\displaystyle\sum_{i=0}^{n-1} \text{Sample}\,[t-i]\;-\;\text{MeanValue}\,[t-i]\,]\,]}{n}$$

The autoscaled data is calculated as seen in Equation 2-5. The scaling factor was defined as appropriate for the display equipment within the experimental environment

(2-5)

$$\text{ScaledData} \;=\; (\text{Sample} - \text{Average})\,\frac{\text{DefinedScalingFactor}}{\text{FullRectifiedMeanValue}}$$

---

1. For the sake of brevity, the use of the term "moving average" shall be excluded from now on within this dissertation. However, it is inherent that all signals are a form of a "moving average" because of the constantly updated time domain in real-time control applications.

2.2.2.3 Butterworth Low Pass Filter

In order to more effectively smooth the data, a infinite impulse response (IIR) filter was chosen over a finite impulse response filter (FIR). A program was developed using the Bilinear Transformation Method equation (46). The bilinear transformation method provided a frequency response similar to the analog prototype used to create the digital counterpart. The design is relatively straightforward and may be programmed for quick prototype development(46).

The use of the Bilinear Transformation Method allowed quick creation of the Butterworth, Chebyshev and Elliptical filter digital coefficients from the analog prototype coefficients. Due to the limited size of the long integers within the software compiler and the fact that Chebyshev and Elliptical filters were less stable than the respective Butterworth counterparts, a Butterworth type filter was chosen for low pass filtering. The Bilinear transformation is accomplished by mathematically transforming the Laplace Transform analog representation as seen in Equation 2-6 to the Z-Transform digital representation as seen in Equation 2-7. Upon determining that a fourth order filter utilized too much CPU time, a third order Butterworth filter was selected. The group delay tolerance dictated the break frequency of the filter. A 23.8 Hz 3-db break frequency was determined to be tolerable with a group delay of less than 20 milliseconds and a linear phase response as seen in Figure 2-6, Figure 2-7 and Figure 2-8. The coefficients of analog low pass filter denominator polynomials can be seen in Figure 2-9. The bilinear transformation digital filter coefficients in terms of analog coefficients for a third order filter can be seen in Figure 2-10. The resulting Pa waveform after autoscaling and low pass filtering can be observed in Figure 2-11.

(2-6)

$$G(s) = \frac{A_0 + A_1 s + \ldots + A_k s^k}{B_0 + B_1 s + \ldots + B_k s^k}$$

$$H(z) = \frac{a_0 + a_1 z + \ldots + a_k z^k}{b_0 + b_1 z + \ldots + b_k z^k}$$

2.2.2.4 First, Second, and Third Derivative

In order to effectively detect timing events within the aortic pressure, derivatives of the Pa wave form has to be computed. The first derivative was calculated using a five point least squares polynomial fitting technique. Previous authors (28) utilized a two point differentiator as seen in Equation 2-8 and Figure 2-12A. The amplitude of three different differentiators in Figure 2-12 can be seen in Figure 2-13. The five point derivative based on a least squares polynomial fit is displayed in Equation 2-9. The five point derivative has an advantage over the two and three point filter in that there are two additional poles at $z = 0.25 + j0.968$ and $0.25 - j0.968$ that "low pass filter" the signal more than the other two filters. Some high frequency noise is attenuated because of the inherent smoothing characteristic of the polynomial fitting approach. This is especially important for high frequency noise that may be present in the Pa signal.

$$H_1(z) = (1/T)(1-z^{-1}) \qquad (2-8)$$

$$H_1(z) = (1/10)(2 + z^{-1}-z^{-3}-2z^{-4}) \qquad (2-9)$$

The 5 point derivative filter utilized (21) provided the building blocks for the second derivative noted in Equation 2-10 as well as the foundation for the third derivative filter. The third derivative filter was derived by multiplying the transfer function of the second derivative filter with a 3-point differentiator as illustrated in Equation 2-11 and Equation 2-12.

$$H_2(z) = (1/14)(2 - z^{-1}-2z^{-2}-z^{-3}+2z^{-4}) \qquad (2-10)$$
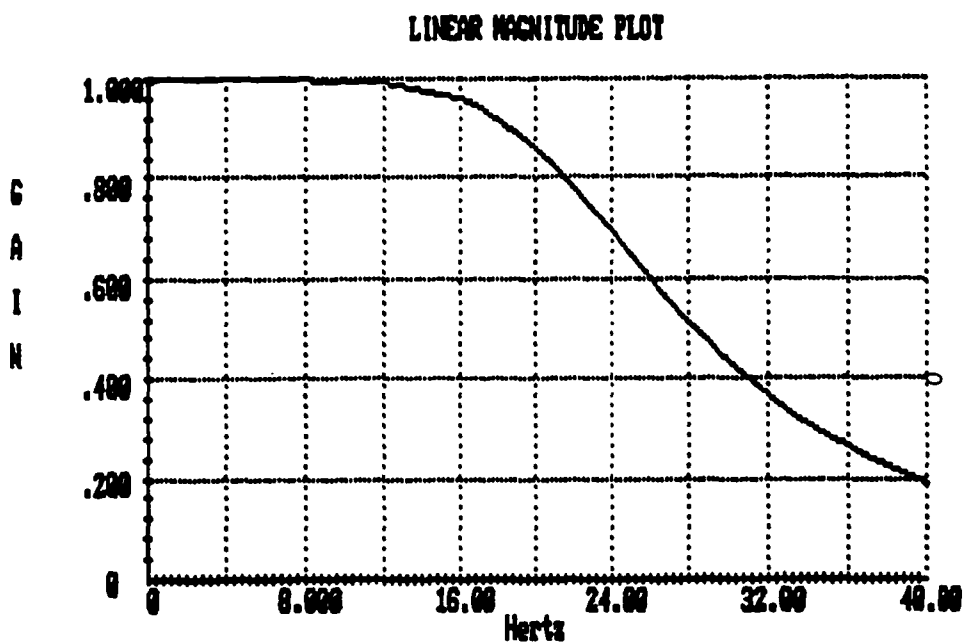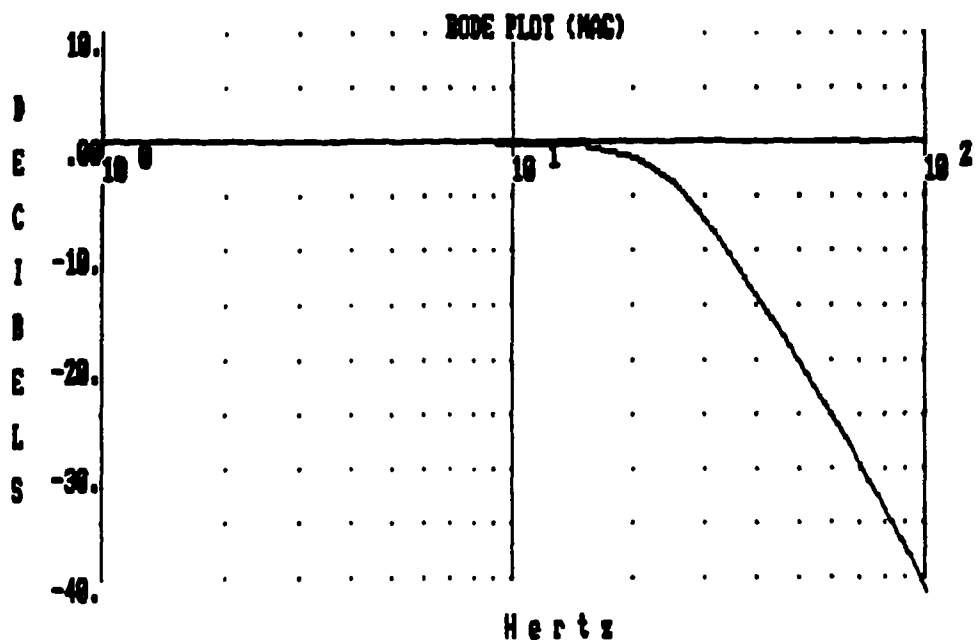
Figure 2-6. Pa Butterworth LPF Bode Magnitude Plot is illustrated in Figure 2-6A (top) and Linear Magnitude Plot is illustrated in Figure 2-6B (bottom).

$$H_3(z) = H_2(z)^* H_1(z) = [(1/14)(2 - z^{-1}-2z^{-2}-z^{-3}+2z^{-4})] [(1/2)(1 - z^{-2})] \tag{2-11}$$

$$H_3(z) = (1/28)(2 - z^{-1}-4z^{-2}-4z^{-4}+z^{-5}-2z^{-6}) \tag{2-12}$$
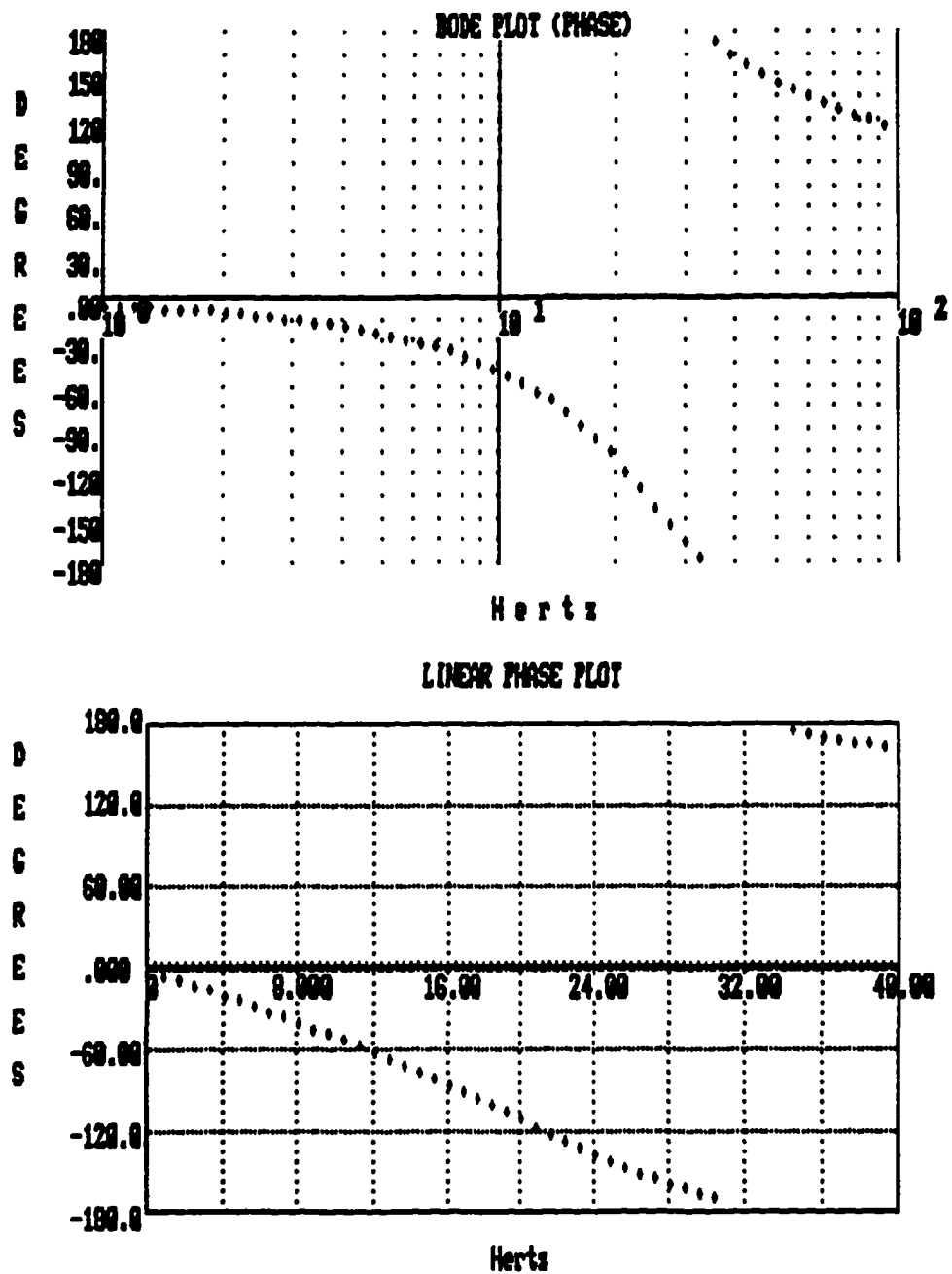
Figure 2-7. Pa Butterworth LPF Phase Bode Plot is illustrated in Figure 2-7A (top) and Linear Phase Plot is illustrated in Figure 2-7B (bottom).
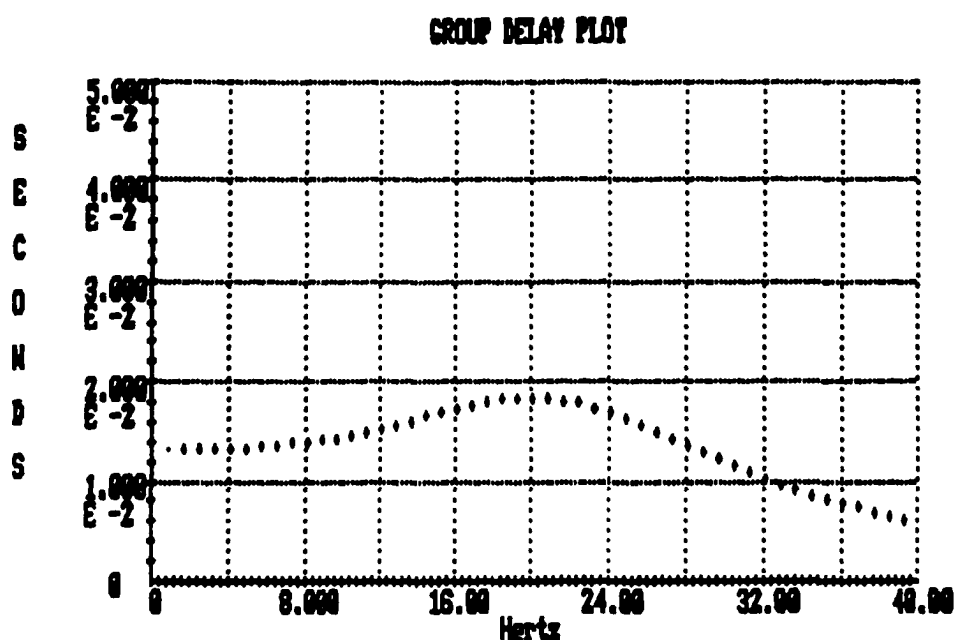
GROUP DELAY PLOT

Figure 2-8. Pa Butterworth LPF Group Delay Plot

2.2.2.5 Current Derivative Window and Ambient Derivative Window Methodology

Previous Pa and aortic flow detection investigators(20)(21)(28) each used an average maximum derivative threshold to determine the occurrence of the systolic rise and dicrotic notch. The average maximum first derivative was used for the detection of the systolic rise and the average maximum second derivative was used for the detection of the dicrotic notch. However, this method falters on a noisy or quickly attenuating signal because the threshold becomes inaccurate. For example, if the amplitude of the Pa signal were attenuated by 50%, the associated first derivative would decrease by 50% and if a 60% threshold were utilized, detection of the systolic rise would be missed. Detection of the Pa events is further complicated by noise, which is amplified by the derivative filters.

The approach in this dissertation utilizes the matched filter technique which provides the greatest signal to noise ratio of the output signal (51)[1]. ECG investigators (64) have previously utilized this

---

1. The matched filter is commonly used in radar where a signal is transmitted and the returning signal (with imposed noise) is processed with a matched filter to determine if the signal is present (e.g., detecting an object in the sky)(51).

Table 6-2

Coefficients of low-pass filter denominator polynomials. (Note: Coefficients are defined in accordance with equation 6-35.)

Order	B_0	B_1	B_2	B_3	B_4	B_5
			BUTTERWORTH			
1	1	1				
2	1	1.4142136	1			
3	1	2	2	1		
4	1	2.6131259	3.4142136	2.6131259	1	
5	1	3.2360680	5.2360680	5.2360680	3.2360680	1

			CHEBYSHEV 0.5 DB RIPPLE ($\epsilon^2 = 0.122084$)			
1	2.8627752	1				
2	1.5162026	1.4256245	1			
3	0.7156938	1.5348954	1.2529130	1		
4	0.3790506	1.0254553	1.7168662	1.1973856	1	
5	0.1789234	0.7525181	1.3095747	1.9373675	1.1724909	1

			CHEBYSHEV 1 DB RIPPLE ($\epsilon^2 = 0.2589254$)			
1	1.9652267	1				
2	1.1025103	1.0977343	1			
3	0.4913067	1.2384092	0.9883412	1		
4	0.2756276	0.7426194	1.4539248	0.9528114	1	
5	0.1228267	0.5805342	0.9743961	1.6888160	0.9368201	1

			CHEBYSHEV 2 DB RIPPLE ($\epsilon^2 = 0.5848932$)			
1	1.3075603	1				
2	0.8230604	0.8036164	1			
3	0.3268901	1.0221903	0.7378216	1		
4	0.2057651	0.5167981	1.2564819	0.7162150	1	
5	0.0817225	0.4593491	0.6934770	1.4995433	0.7064606	1

			CHEBYSHEV 3 DB RIPPLE ($\epsilon^2 = 0.9952623$)			
1	1.0023773	1				
2	0.7079478	0.6448996	1			
3	0.2505943	0.9283480	0.5972404	1		
4	0.1769869	0.4047879	1.1691176	0.5815799	1	
5	0.0626391	0.4079421	0.5488626	1.4149847	0.5744296	1

(These results were obtained from L.A. Weinberg, *Network Analysis and Synthesis*, McGraw-Hill, 1962, with permission of the author.)

Figure 2-9. Coefficients of Analog Low Pass Filter Denominator Polynomials Prototype(46)

approach for R-wave detection. The digitized Pa signal to be filtered is a combination of signal and noise as seen in Equation 2-13.

$$Pa_{sampled}[nT] = Pa_{WithoutNoise}[nT] + Noise[nT] \qquad (2\text{-}13)$$

The current derivative window is the output of the approximated matched filter. The impulse response of the matched filter is noted in Equation 2-14.

(3rd order).

A	$B_0 + B_1 C + B_2 C^2 + B_3 C^3$
a_0	$(A_0 + A_1 C + A_2 C^2 + A_3 C^3)/A$
a_1	$(3A_0 + A_1 C - A_2 C^2 - 3A_3 C^3)/A$
a_2	$(3A_0 - A_1 C - A_2 C^2 + 3A_3 C^3)/A$
a_3	$(A_0 - A_1 C + A_2 C^2 - A_3 C^3)/A$
b_1	$(3B_0 + B_1 C - B_2 C^2 - 3B_3 C^3)/A$
b_2	$(3B_0 - B_1 C - B_2 C^2 + 3B_3 C^3)/A$
b_3	$(B_0 - B_1 C + B_2 C^2 - B_3 C^3)/A$

Figure 2-10. Bilinear Transformation Digital Filter Coefficients in Terms of Analog Coefficients for a Third Order Filter(46)
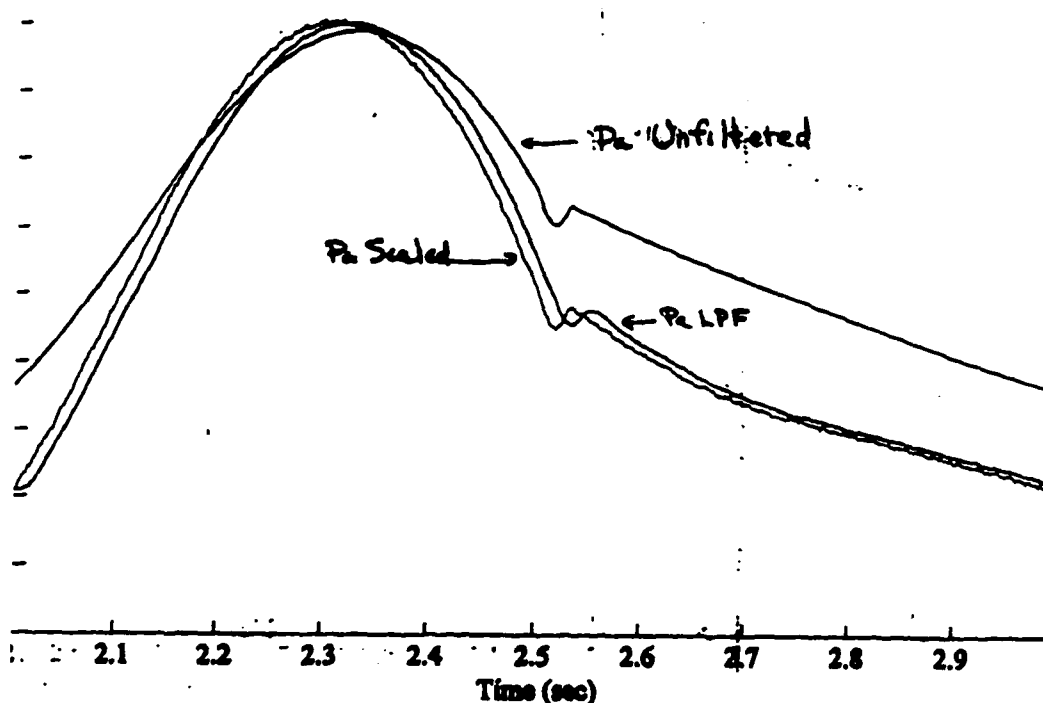
Figure 2-11. Pa Detection Filter Signals: The Unfiltered Pa Trace and the Resulting Autoscaled Pa Trace and the Low Pass Filtered (LPF)Trace

$$h(nT) = Pa_{event}(n_0 T - nT) \qquad (2\text{-}14)$$

The matched filter requires that:

1. The signal is known within a multiplying factor e.g. $h(nT) = \text{Constant} * x(nT)$

2. The noise is wide sense stationary (WSS)

WSS dictates that the following two assumptions are true:
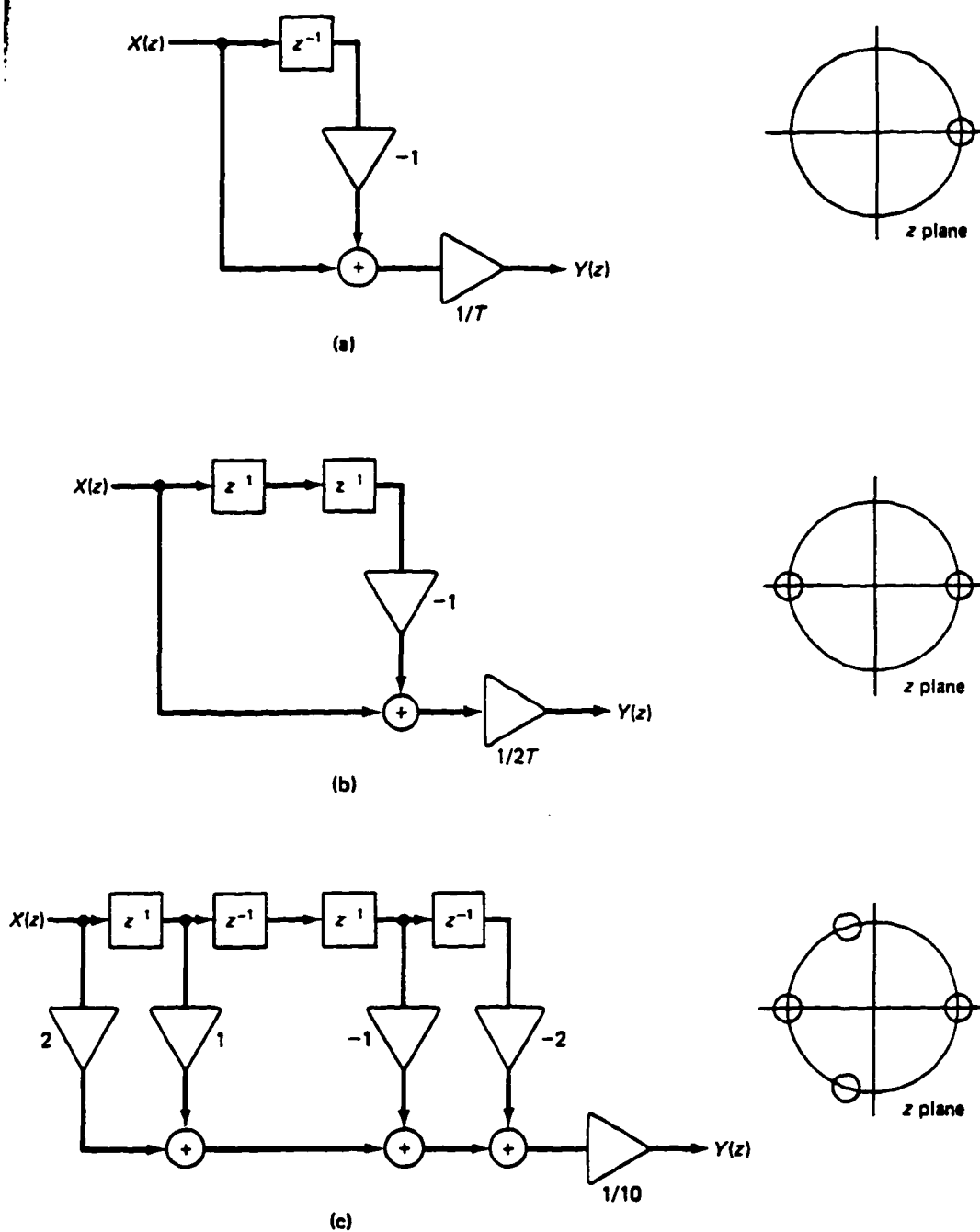
Figure 2-12. Block Diagrams and Pole-Zero Plots of Nonrecursive Digital Filters for Differentiation. Figure 2-12A (top) illustrates the 2-point Difference. Figure 2-12B (middle) illustrates the 3 point Difference. Figure 2-12C (bottom) illustrates the 5 point Polynomial Fit (47).

1. The mean is a function that is independent of time e.g., mean(t) = constant

2. The autocorrelation is a function of t_{delta} where $t_{delta} = t_1-t_2$ or $Rxx(t_1,t_2) = Rxx(t_{delta})$

It was presumed that these matched filter requirements were satisfied.
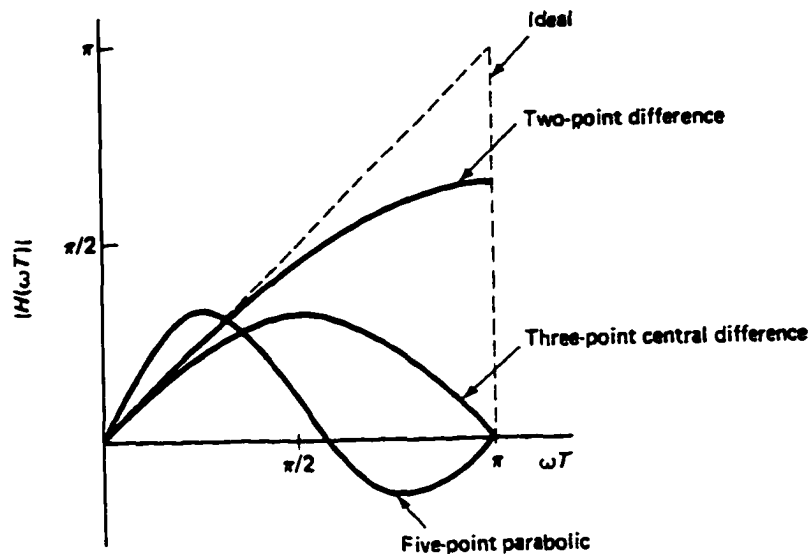
Figure 2-13. Amplitude Responses of Differentiators.For the 2-point and 3-point Difference Filters, and 5-point Parabolic Differentiator. The Sampling Period is set to One(47).

The current derivative window filter is the output of the matched filter (i.e., after a discrete time convolution is performed on the Pa signal with the impulse response of the Pa matched filter) as indicated in Equation 2-15.

$$\text{CurrentDerivativeWindow}[nT] = Pa[nT] \, {}^*Pa_{event}(n_0T - nT), \quad {}^* = \text{Convolution} \qquad (2\text{-}15)$$

The parameter selection of the matched filter (i.e., its length) for the current derivative window filter is dictated by the range of physiological variation and the limits of real-time computational power.

It is assumed that the physiological variations of the length of the systolic rise and dicrotic notch Pa events are as follows:

1. Systolic Rise Length Range = 10 - 40 milliseconds
2. Dicrotic Notch Length Range = 10 - 50 milliseconds

The length of the matched filter (i.e., polynomial derivative fit FIR filter) was set to the minimum length of the systolic rise and dicrotic notch (i.e., 10 msec = 5 samples at 500 Hz)

For example, the matched filter for the systolic rise has 5 filter taps (5 samples = 10 msec). The associated matched filter coefficients for detection of the systolic rise are the set [-2, -1, 0, 1, 2].

To perform the convolution to calculate the value of the current derivative window, the summed value of the matched filter impulse response operating on the Pa signal was required for a total of 10 consecutive samples (i.e., current derivative window length = 10 samples = 20 msec).

The minimum length of matched filter impulse response was utilized for computational efficiency.

The selection of the matched filters requires that the impulse response function resemble that of the of the Pa event to be detected. The Pa systolic rise is roughly a sharp positive slope. For that reason, a first derivative filter which approximates the curve noted in Equation 2-16, was selected.

$$y=x \tag{2-16}$$

To further justify this filter selection, previous authors (20)(21)(28) used this filter to detect the systolic rise using thresholding methods.

The shape of the dicrotic notch typically appears in two forms, a "U" shaped notch and a reversed "N" shaped dicrotic notch (i.e., if the letter "N" is reflected about the Y axis). In order to detect the dicrotic notch with the "U" shape, a second derivative filter, which approximates the curve noted in Equation 2-17, was selected.

$$y=x^2 -2 \tag{2-17}$$

To further justify this filter selection, previous authors (20)(21)(28) used this filter to detect the dicrotic notch using thresholding methods.

In order to detect the dicrotic notch with the reversed "N" shape, a third derivative filter, which approximates the curve noted in Equation 2-18, was selected.

$$y=x^3 - 5x \tag{2-18}$$

To further justify this filter selection, previous authors of ECG detection (41) used this filter to detect the QRS complex. In addition, the third derivative impulse response filter was derived from the first and second derivative filters used to detect the dicrotic notch using thresholding methods.

In summary, the ideal matched filter is not possible because the expected signal is not predictable. The Pa template of each heart beat differs from patient to patient and beat to beat. However, the use of derivative filters, previously used for Pa detection (in which a thresholding technique was employed), for matched filter impulse response functions, ensures that a strong signal will be generated. This is guaranteed even though the filter may not "perfectly match" the Pa event to be detected. This is demonstrated in the physiological case where there is no dicrotic notch deflection (i.e., no "U" or "N" shape), yet the current derivative window still creates a strong signal to noise ratio.

In addition to utilizing polynomial fit FIR derivative filters (previously used for threshold detection) as impulse functions for the matched filters, a second technique was used to compensate for the fact that the "ideal" Pa matched filter was not possible. The second technique employs what is referred to as the ambient derivative window. The ambient derivative window compensates for any unpredictable variations in the value of the current derivative window.

The determination of the ambient window length was dictated by two factors:

1. The output of the ambient derivative window is as recent as possible.

2. The ambient derivative window was phased delayed enough to ensure there was not a significant overlap in the output between the ambient derivative window and the current derivative window during detection.

A window length of 60 milliseconds (i.e., 10 total impulse response values staggered every third sample) was chosen for the ambient first derivative window. A window length of 120 milliseconds was chosen for the ambient second derivative and ambient third derivative windows (i.e., 10 total impulse response values staggered every sixth sample). The resulting waveforms for the current second derivative window and the ambient second derivative window can be seen in Figure 2-14.

Figure 2-14. Pa Detection Filter Signals: The Unfiltered Pa Trace and the Resulting Current Second Derivative Window Trace and the Ambient Second Derivative Window Trace

The ambient derivative window is identical to the current derivative window is terms of using the matched filter impulse function, however, the time window is longer to provide a more accurate value of the "ambient" strength of the respective derivative window signal.

The two signals, the current derivative window and ambient derivative window, are compared as a second detection scheme to compensate for any unexpected variations in the output of the derivative window filters. This is possible because the impulse response filters are not perfectly "matched" with the associated Pa event. The ambient derivative window is longer in time than the current derivative window. The ambient derivative window determines if the "overall" derivative window amplitude has been raised within the Pa wave. This detection comparison technique compensates for any rise in the current derivative windows not associated with the targeted Pa event to be detected.

An example of a rise in the current derivative windows (not associated with the targeted Pa event) would be if the Pa wave DC component experienced an upward climb. The first derivative values would be artificially higher based on the rise in the slope. A comparison of the current derivative window with the ambient derivative window compensates for the increased values. This technique is similar to a riding clipper in pulse circuits where detection "rides above the noise threshold".

In conclusion, the Pa detection algorithm uses the following methodology to provide robust detection of the systolic rise and dicrotic notch using the following three techniques:

1. Matched Filter
2. Oversampling of Pa Signal (500 Hz)
3. Digital Version of the "Riding Clipper" Analog Circuit

Oversampling of the Pa signal[1] (i.e., according to the Nyquist theorem) provides an opportunity to utilize the matched filter technique in real-time which provides the maximized signal to noise ratio for detection.

The digital filter version of the "riding clipper" analog circuit (i.e., comparing the current derivative window and ambient derivative window) as a means for detection provides a more updated derivative reference (or threshold) for detection. The riding clipper derivative detection method is superior to the threshold method calculated from previous beats particularly for non-ideal Pa signals

---

1. If the sampling frequency was reduced, the samples per event may be reduced to the point where a matched filter representation would not be practical. In the case of 100 Hz sampling, only a single point would represent a dicrotic notch of 10 milliseconds in length.

that change beat to beat. The combination of the matched filter, Pa oversampling and "riding clipper" techniques provide the foundation for a robust detection method for non-ideal Pa signals.

In the evaluation of filter parameter optimization, the filter parameter and the factors that effect those parameters were examined.

The filters with detection parameters can be categorized into the following types:

1. DC Removal Filter

2. Autoscaling

3. LPF

4. Derivative 1,2,3

5. Pattern Recognition Detection Logic

6. Current Derivative Window 1,2,3, 2&3

7. Ambient Derivative Window 1,2,3, 2&3

Optimization of parameters would require the determination of the effects of at least the factors within the three broad categories:

1. Real-time CAD Control Constraints

    1. Computational Efficiency

    2. Filter Phase Delay

    3. Variation in Augmentation to Pa Signal

2. Biological Variation

    1. Experimental Model to Experimental Model

    2. Heart Beat to Heart Beat

3. External Interference

    1. Mechanical Ventilation

    2. Electrocautery

    3. Signal Attenuation (e.g., Blood Coagulation)

    4. External Noise Sources (e.g., powerline interference)

The realization that the many of these factors cannot be empirically characterized, indicates that parameter optimization is close to impossible. The parameter values within this dissertation were selected based on their perceived optimization of robustness during a sequence of tests using the Cornell University Medical College Canine Mongrel Aortic Pressure Database. The utilization of the matched filter and current to ambient derivative window comparison filter (i.e., riding clipper) aided in the optimization of the detection for the following two reasons:

1. The matched filter maximized the signal to noise ratio

2. The current to ambient derivative window filter compared the signal against itself (with different time windows) in an attempt to compensate for any unanticipated effects of the Pa signal variation to the output of the derivative windows.

Furthermore, general qualitative comments can be made about the correlation between certain non-ideal Pa signal factors and certain filters. For example, the autoscaling algorithm compensates for signal attenuation. The damping parameters of the autoscaling filter dictate how quickly signal would be properly scaled during a quick change in amplitude. In general, the tuning range of any filter parameter for Pa detection provides a tradeoff, between quick response and stability of the filter. The research in this dissertation attempts to reach a compromise in filter parameters, to provide the broadest range of detection (i.e., robust detection). The Pa detection filter parameters were selected to allow the Pa detection algorithm to properly detect on a broad range of non-ideal Pa signals caused by a variety of factors.

2.2.2.6   Current Derivative Window Filter

In order to accurately detect the Pa systolic rise and dicrotic notch, more was needed than just the derivative of a single sample. In fact, ten samples were utilized and combined together to form the Current Derivative Window Filter for the first, second, third and a combination of the second and third derivatives. This was done by accumulating the value from ten consecutive samples for the first, second, and third derivatives as seen in Equation 2-19, Equation 2-20, and Equation 2-21. The ten samples typically encompass the duration of an entire Pa characteristic, e.g. a systolic rise and dicrotic notch. The combination of the second and third derivative consists of the second derivative and any negative contribution from the third derivative as seen in Equation 2-22. The third derivative is typically negative during the maximum deflection in the second derivative of the dicrotic notch.

(2-19)

$$CurrentFirstDerivativeWindow\,[t] = \frac{\sum_{i=0}^{n-1} FirstDerivative\,[t-i]}{(n-10)}$$

(2-20)

$$\text{CurrentSecondDerivativeWindow}\,[t] \;=\; \frac{\displaystyle\sum_{i=0}^{n-1} \text{SecondDerivative}\,[t-i]}{(n-10)}$$

(2-21)

$$\text{CurrentThirdDerivativeWindow}\,[t] \;=\; \frac{\displaystyle\sum_{i=0}^{n-1} \text{ThirdDerivative}\,[t-i]}{(n-10)}$$

(2-22)

$$\text{Curr2nd3rdDerivWindow}\,[t] \;=\; \frac{\displaystyle\sum_{i=0}^{n-1} \text{2ndDeriv}\,[t-i]}{(n-10)} \;+\; \left| \frac{\displaystyle\sum_{i=0}^{n-1} \text{3rdDeriv}\,[t-i]}{(n-10)} \right|$$

$$\text{If3rdDeriv} < 0$$

$$\text{Otherwise3rdDeriv} = 0$$

2.2.2.7 Ambient Derivative Window Filter

As a detection threshold for the systolic rise and dicrotic notch, the first, second, third and a combination of the second and ambient third derivative window using the respective derivatives must be derived. The ambient derivative window established a "noise floor" (equal to the average derivative amplitude calculated from evenly spaced samples of the derivative) as a detection

reference. Typically noise levels can vary considerably particularly in the Cornell University Medical College Canine Mongrel aortic pressure database. The increases in noise floor can lead to false positive triggers particularly due to the derivative implementation in this Pa detector in this dissertation. For that reason a "riding clipper" technique was employed to avoid false triggers by having the detection criterion ride above the noise floor. The ambient derivative window is a collection of derivative samples for a window considerably larger than an event that shall be triggered on, e.g., systolic rise and dicrotic notch. The ambient window filter was critical to the success of the detection filter. The equation for the first, second, third and a combination of the second and ambient third derivative window can be seen in Equation 2-23, Equation 2-24, Equation 2-25, and Equation 2-26. The spacing for the first derivative is every three samples and for all others the spacing is every six samples. For the ten sample window the spacing is 30 samples and 60 samples for the first derivative and all other derivatives, respectively. In contrast, the current derivative window filter utilized also for detection is 10 samples as seen in the previous section.

$$(2\text{-}23)$$

$$AmbientFirstDerivativeWindow\ [t]\ =\ \frac{\sum_{i=0}^{n-1} FirstDerivative\ [t-3i]}{(n-10)}$$

$$(2\text{-}24)$$

$$AmbientSecondDerivWindow\ [t]\ =\ \frac{\sum_{i=0}^{n-1} SecondDerivative\ [t-6i]}{(n-10)}$$

$$(2\text{-}25)$$

$$AmbientThirdDerivativeWindow\ [t]\ =\ \frac{\sum_{i=0}^{n-1} ThirdDerivative\ [t-6i]}{(n-10)}$$

$$\text{Ambient2nd3rdDerivWndw}\,[t] = \frac{\sum_{i=0}^{n-1} 2\text{ndDeriv}\,[t-6i]}{(n-10)} + \frac{\left|\sum_{i=0}^{n-1} 3\text{rdDeriv}\,[t-6i]\right|}{(n-10)}$$

$$\text{If3rdDeriv} < 0$$
$$\text{Otherwise3rdDeriv} = 0$$

2.2.3　Systolic Rise Detector

The Systolic Rise Detector routine performed the following functions to accurately detect the onset of systole within the Pa:

1. Collect Diastolic Pressure Just Prior To Systole

2. Detect the Systolic Rise

3. Accumulate Minimum Diastolic Pressure Value Average and Position History

4. Collect Maximum Systolic Pressure Just After Systolic Rise

5. Accumulate Systolic Pressure Value Average and Position History

6. Determine Average Difference Between Systolic and Diastolic Pressure

7. Accumulate Systolic Rise Position History

8. Determine Cardiac Cycle Length Average

9. Generate Error Condition if False Negative on Systolic Rise May Have Occurred

10. Attempt to Ensure False Positive Trigger Does Not Occur During Systole; i.e., Detect the Same Systolic Rise Twice

2.2.3.1　Diastolic Pressure

In order to maintain various statistics on diastolic pressure and timing, the position and pressure value is recorded for the current and past five cardiac cycles. The diastolic pressure is assumed to be the lowest Pa pressure value between the end dicrotic notch and the start of the systolic rise. The algorithm utilized is seen in Figure 2-15.
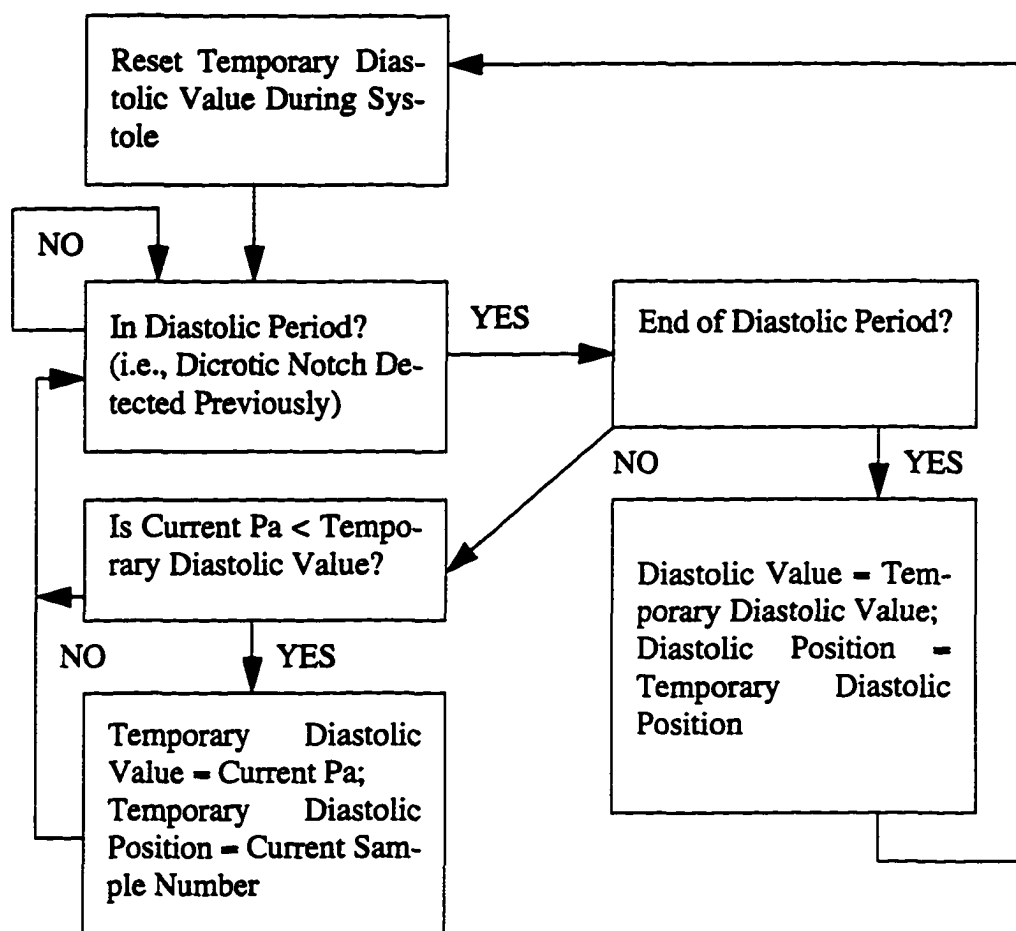
Figure 2-15. Algorithm to Determine Diastolic Pressure and Position

2.2.3.2 Detect Rise in Systolic Pressure

Detection of the systolic rise in Pa is one of the two events that must be detected in the cardiac cycle. Detection involves a two gate process as seen in Figure 2-16. The first gate ensures there is a transition in slope from positive to negative using two criteria, a current second derivative threshold and a comparison between the current second derivative threshold and the ambient derivative history. The first criterion compares the current second derivative window with an average of the largest current second derivative threshold for the last six cycles. The second criterion compares the current second derivative window with the ambient second derivative window history. The first gate ensures a strong second derivative window has occurred which is prevalent in the change in slope associated with the systolic pressure rise. Once the criterion for the first gate is met once, the

algorithm passes the detection criterion on to the second gate for every upcoming sample within a reasonable duration for the rise in systole.

The second gate ensures there is a substantial rise in first derivative window using two criteria, a current first derivative window average threshold and a comparison between the current first derivative threshold and the ambient first derivative window history. The first criterion compares the current first derivative window with a average of the largest current second derivative threshold for the last six cycles. The second criterion compares the current first derivative window with the ambient first derivative window history. The second gate ensures a strong first derivative window increase has occurred which is prevalent in the quick increase in Pa associated with the systolic pressure rise. The second gate also ensures there is a minimum height difference between diastolic pressure and the current sample as compared with the running average of the last six cardiac cycles of the difference in systolic and diastolic pressure.

2.2.3.3   Accumulate Statistics

Once the systolic pressure is detected, several statistics can be accumulated to improve detection accuracy. The diastolic pressure value and position[1] history is recorded. The systolic pressure value and position history is also recorded similarly to the algorithm depicted in Figure 2-15 except the less than sign is reversed. The average difference between the systolic and diastolic pressure is recorded for the last six cardiac cycles. A window criterion for the dicrotic notch pressure is determined. A minimum pressure and a maximum pressure is determined. The maximum pressure is determined to be 80% of the average difference between systolic pressure and diastolic pressure added to the diastolic pressure for the current cardiac cycle. The minimum pressure is determined to be 33% of the average difference between systolic pressure and diastolic pressure added to the diastolic pressure for the current cardiac cycle. This forms an amplitude window in which the dicrotic notch may be located.

The position of the systolic rise detection is recorded. The cycle length average is calculated from the position of the systolic rise detection. The position of the systolic rise is utilized for the cycle length average because it is the most reliable periodic detection characteristic due to the quick deflection in pressure and substantial amplitude change. The second reason the position of the

---

1.   Position refers to the sample number in which the associated event occurs i.e., position in time.

```
                    ┌─────────────────────┐
                    │ Start Search For Systol- │
                    │ ic Rise             │
                    └─────────────────────┘
```

Current Second Derivative Window > Average
Second Derivative Window Threshold?
&
Current Second Derivative Window > Ambient
Second Derivative Window * Multiplier?

Gate 1

NO   YES

Current First Derivative Window > Average First
Derivative Window Threshold?
&
Current First Derivative Window > Ambient First
Derivative Window * Multiplier?
&
Pa Difference Between Diastolic Pa and Current
Pa > Running Average Systolic Diastolic Pa Dif-
ference Threshold

Gate 2

NO   YES

Pa Systolic Rise Detected
- Update Statistics

Figure 2-16. Systolic Rise Detection Algorithm

systolic rise is utilized for the cycle length average is because of the accuracy of the characteristic.
Detection typically occurs on the rise in pressure itself which endures for only 10-20 milliseconds
creating an accuracy for that resolution. The accuracy and reliability make the systolic rise the best

candidate to calculate running average of the cycle length. The heart rate is calculated from the cycle length average.

Heart Rate (in bpm)= (60 sec per min *500 hz)/(Cycle Length Ave in samples) (2-27)

In addition to collecting statistics, the detection of the systolic rise updates a variable which provides a reference for a time window for the search for the current first derivative window peak utilized to calculate the current first derivative window average threshold noted in Section 2.2.3.2.

2.2.3.4 False Negative and False Positive Error Detection for Cycle Length Average

In the event a systolic rise is detected (e.g., due to an impulse of noise) in which the previous systolic rise has occurred within unreasonable limits, the cycle length averages are not modified. The boundaries for a reasonable detection include a heart rate of 40 bpm to a heart rate of 250 bpm. The associated cycle length average values are 758 samples and 121 samples respectively. If the time between the previous systolic rise detection and the current systolic rise detection is less than 121 samples (i.e., 242 milliseconds) typically a false positive has occurred (an illegitimate detection). If the time between the previous systolic rise detection and the current systolic rise detection is greater than 758 samples (i.e., 1516 milliseconds) typically a false negative has occurred (a missed detection). During development these error messages provided very useful information for fine tuning the Pa systolic rise detection algorithm. This type of error detection is essential to ensure the cycle length average is not corrupted. The cycle length average is utilized throughout the Pa detector.

o

2.2.4 Dicrotic Notch Detector

The Dicrotic Notch Detector routine performed the following functions to accurately detect the termination of systole within the Pa:

1. Detect the Dicrotic Notch,
2. Accumulate Dicrotic Notch Pressure Value and Position History and Calculate Average,
3. Accumulate Systolic Time Intervals and Calculate Average,
4. Calculate the Systolic Peak to Dicrotic Notch Average Pressure Ratio.

2.2.4.1 Dicrotic Notch Detection

The dicrotic notch is a relatively small perturbation in comparison to the systolic rise. For that reason as well as the difference in Pa physiological variation, additional criteria are utilized to detect the dicrotic notch. Dicrotic notch detection involves a two gate process which occurs within set physiological constraints as seen in Figure 2-17. The physiological constraints dictate that the dicrotic notch is detected within the proper physiological time window and pressure window. The first gate is a ensures that two criteria are met, namely the current first derivative window filter exceeds a negative current window first derivative peak threshold and that one of three (second, third or second and third combination) current window derivative peak averages is exceeded. The second gate verifies that one of three current window derivatives (second, third or second and third combination) exceeds the corresponding ambient derivative window.

The physiological constraints dictated in the dicrotic notch search mandate that valid samples exist in a time window spanning from the position of the peak systolic pressure to a time period equalling 66% that of the cycle length average. The physiological constraints also dictated that Pa must be in the range of 20% of the average systolic-diastolic difference below systolic pressure for the current cardiac cycle as well as being in the range of 33% of the average systolic-diastolic difference above peak pressure for the current cardiac cycle. This criterion is mandated by physiology of the Pa trace. The dicrotic notch occurs in time after the peak pressure of systole and the dicrotic notch typically occurs at a pressure near the mean Pa.

The first gate has two criteria for detection. The first criterion ensures at least a mild downward slope has occurred prior to the occurrence of the dicrotic notch. The first criterion compares the current first derivative window with an average of the most negative current first derivative threshold for the last six cycles. The second criterion ensures either the second derivative, third derivative or a combination of the second and third derivative[1] exceeds the most positive second, third or a combination of second and third derivative (respectively) average threshold for the last six cycles. This criterion ensures that at least a small change in slope has occurred during a down going (first derivative) slope. These two criteria occur reliably within the Pa trace.

Once the first gate has been passed, the algorithm does not test for this criterion anymore. If the physiological constraints are still satisfied the Pa trace is tested against the second (or last) gate. A

---

1. The second derivative, third derivative or a combination of the second and third derivative is utilized in the detection of the dicrotic notch. The use of all three filters demonstrated a more reliable detection spectrum. This was illustrated by the tendency for the Pa trace of a single experimental model with a sinus rhythm to trigger on all three with filters with regularity.

Start Search For Dicrot-
ic Notch

Sample Number <= 2/3 Cycle Length Aver-
age + Peak Pressure Position &
33% Diastolic Pressure < Pa Sample < 80%
Systolic Pressure

NO

Physiolog-
ic   Con-
straints

Missed   Di-
crotic Notch

YES

**Current First Derivative Window < Most
Negative Average First Derivative Window
Threshold?
&
Current 2nd, 3rd or 2nd&3rd Derivative
Window > Most Positive Average 2nd, 3rd
or 2nd&3rd Derivative Window Threshold?

Gate 1

NO   YES

Current 2nd Derivative Window >
Ambient 2nd Derivative Window * Multiplier?
OR
Current 3nd Derivative Window >
Ambient 3rd Derivative Window * Multiplier?
OR
Current 2nd&3nd Derivative Window >
Ambient 2nd&3rd Derivative Wndw * Multiplier?

Gate 2

NO   YES

Pa Dicrotic Notch Detected -
Update Statistics

** After Gate 1 is sat-
isfied once, it is by-
passed in the detection
process.

Figure 2-17. Dicrotic Notch Detection Algorithm

comparison between the second derivative, third derivative or a combination of the second and
current third derivative threshold and the second derivative, third derivative or a combination of the
second and ambient third derivative window history, respectively. This second gate provides three

means by which a dicrotic notch may be detected. The ambient window history automatically raises the criterion for detection in the event the noise level within the signal increases. The digital version of a "riding clipper" takes into account that noise also contributes to increased window within the dicrotic notch deflection. Thus this detection filter rides above the noise level while still maintaining robust detection accuracy. The consequences of a premature detection of the dicrotic notch will lead to improper inflation timing. In the case of an intraaortic balloon, premature inflation can increase left ventricular afterload.

2.2.4.2 Accumulate Statistics

Once the Pa dicrotic notch is detected, several statistics can be accumulated to improve detection accuracy by numerically characterizing the Pa wave. The dicrotic notch pressure value history and position history is recorded. The systolic timer interval (STI) average is calculated from six cardiac cycles by subtracting the dicrotic notch position with the systolic rise position for the previous six heart beats as seen in Equation 2-28. Detecting the dicrotic notch allows calculation of the ratio of systolic-diastolic pressure versus dicrotic notch-diastolic pressure also referred to as the peak to notch pressure ratio. Typically this ratio is repeatable for cardiac cycles of different heart rate within the same experimental model. The ratio is calculated as seen in Equation 2-29. The average peak to notch pressure ratio is calculated over six heart beats and is utilized to predict the timing of the dicrotic notch for ectopic beats.

(2-28)

$$\text{STIAverage} = \frac{\sum_{i=0}^{n-1} \text{DicroticNotchPos}(t-i) - \text{SystolicRisePos}(t-i)}{(n-6)}$$

PeaktoNotch Ratio = (Systolic-Diastolic Pr)/(Dicrotic-Diastolic Pr)   **(2-29)**

2.2.5 Pa Running Statistics (e.g., Thresholds).

A variety of statistics utilized in the systolic rise and dicrotic notch detection are collected to provide set derivative thresholds and timing intervals for the two detection algorithms. These Pa running statistics calculated in windows independent of the detection algorithms include:

1. Systolic Rise Statistics

    1. Calculate the largest positive value of the first and second derivative per cardiac cycle

    2. Calculate the averages of the dicrotic notch derivative statistics above for first, second derivatives over several cardiac cycles

2. Dicrotic Notch Statistics

    1. Calculate the largest positive value of the second derivative and the most negative value of the second and third derivatives per cardiac cycle

    2. Calculate the averages of the dicrotic notch derivative statistics above for first, second and third derivatives over several cardiac cycles

3. Length Statistics between the Systolic Rise and Dicrotic Notch

    1. Calculate Average Length Between Systolic Rise and Maximum Value of Second Derivative in Dicrotic Notch Sampling Window

2.2.5.1   Systolic Rise Statistics

As noted in the systolic rise detection algorithm, the first and current second derivative window threshold is used for the first gate. This threshold is calculated independent from the detection algorithm in a window that spans 5/8 of a cycle length average after the position of the peak systolic pressure. The reason these statistics are calculated independent of the detection algorithm is to determine the actual maximum of these values as opposed to the values achieved at the time of detection. The maximum of the most recent six cardiac cycles are averaged to determine the dicrotic notch detection statistics for first and second derivatives.

2.2.5.2   Dicrotic Notch Statistics

As noted in the dicrotic notch detection algorithm, the first, second and current third derivative window threshold is used for the first gate. This threshold is calculated independent from the detection algorithm in a window that spans 1/3 of a cycle length average prior to the projected systolic rise to 1/4 of a cycle length average after. The reason these statistics are calculated independent of the detection algorithm is to determine the actual maximum of these values as opposed to the values achieved at the time of detection. The maximum positive value of the most recent six cardiac cycles are averaged to determine the dicrotic notch detection statistics for second derivatives. The most negative value of the most recent six cardiac cycles are averaged to determine the dicrotic notch detection statistics for first and third derivatives. For the downward slope in Pa pressure in which the dicrotic notch is present, the second derivative turns positive at the dicrotic

notch. The first and third derivative are typically negative at strategic timing points in the downward slope.

2.2.5.3   Length Statistics between the Systolic Rise and Dicrotic Notch

The length between the position of the systolic rise and peak of the current second derivative window filter within the dicrotic notch second derivative peak search window is calculated. This statistic is created to determine a more accurate measurement of the STI. Since detection of the dicrotic notch is set so that approximately 99% of the dicrotic notches are detected, the detection of the dicrotic notch may occur slightly before the peak of the second derivative. The peak of the second derivative is also considered an accurate measurement of the dicrotic notch position. Therefore utilizing the dicrotic notch detection position in the STI calculation may lead to a value slightly less than the actual STI. In addition, certain Canine Mongrel Pa wave shapes had some non-dicrotic notch "barbs" on the downward slope of systole sometimes leading to an early false positive detection of the dicrotic notch. A comparison of the two STI measurement led to the diagnosis of this phenomenon.

2.3   ECG QRS-Complex Detection (R-wave Detection)

The detection of the QRS-complex (R-wave detection[1]) within the ECG was essential to properly timing events within the cardiac cycle. The R-wave signals the onset of the cardiac systolic contraction.

The R-wave detection algorithm selected (i.e., ARGUS DD/1 utilizing preprocessed AZTEC data(25)(26)) to trigger on a wide variety of ECG signals. The DD/1 algorithm was modified to provide results for a real-time control application. The algorithm's complexity was limited by the real-time constraints placed on the CAD control application. Simple algorithms generally provide short computation time which allows complete processing between samples. The processing time between samples was 2 milliseconds (1 / 500 Hz = 2 milliseconds)[2],[3].

---

1. For this control application, detection of the R-wave would be sufficient for CAD control. However, in order to provide a high detection accuracy (i.e., with the DD/1 algorithm utilizing AZTEC data), the algorithm analyzes the entire QRS-complex for detection criterion. The delineation of the QRS-complex is available but is not utilized specifically. For the purpose of this dissertation research, R-wave and QRS-complex detection are interchangeable terms.

2. Since this is a real-time controller computational efficiency is essential, thus all calculations are done with double precision integers. No real numbers are used because of their relatively longer calculation times.

The focus of Section 2.3 describes the implementation of the AZTEC ECG preprocessing and DD/ 1 QRS-complex detection algorithm as well as modifications and additions to the algorithm for this real-time control application. A high level description of the algorithm starts with the reading in of the 12-bit data through the A/DC at 500hz. A running average of the sample values establishes a mean ECG potential (e.g., approximately to the isoelectric potential) to allow scaling of the wave. A running average of the absolute maximum deflection values of ECG potential is maintained to perform autoscaling of the wave. This autoscaling constantly maintains an R-wave potential difference in pressure of approximately 200 centered around zero[1]. A 9-point moving average low pass filter is used to filter the incoming signal to remove unwanted high frequencies.

A cardiac cycle is identified by the detection of its QRS-complex. A QRS-complex is detected with a two step process. The first step converts the ECG data samples into AZTEC data (i.e. vectorized data, a sequence of slopes and lines. The second step utilizes the AZTEC data (only slopes) to detect a QRS-complex. The QRS complex is a closely timed sequence of slopes. Statistics are collected on all the QRS-complexes to increase the detection accuracy of the upcoming QRS-complexes.

Once the R-wave heights (and corresponding autoscaling factor) are known[2], detection of the QRS-complex initiates. After QRS-complex detection occurs, detection status is changed to look for the next cardiac cycle[3].

In order to implement the ECG detection algorithm mentioned above, the following functions were developed in C language (44) using the Borland C++ compiler(45):

1. Interrupt Handling Routine

2. Definitions for Included Functions, Constants, Functions Declarations, Types, Enⓢmerations Types, and Variables

3. Data Preprocessing Routine

4. ECG AZTEC Vectorization

---

3. The selection of a 500 Hz Pa and ECG sampling rate was chosen because the ECG AZTEC algorithm is based on 500 Hz sampling rate and the Committee on Electrocardiography of the American Heart Association recommends a sampling rate of 500 samples per second. The highest useful frequency in ECGs is 100 Hz, however, for waveform recognition and feature extraction (47) 500 Hz is recommended. 500 Hz sampling was utilized for Pa pressure to maintain a consistent sampling rate for a multiprocessor CAD system.

1. Preprocessed autoscaled ECG data values are centered around zero and reduced to a systolic to diastolic amplitude difference of approximately 200 to minimize the chance of double precision integer (32-bit) overrun.

2. During the calculation of the heart rate and subsequently statistics are accumulated for detection thresholds, timing windows and ECG potential windows.

3. Noise rejection has been added to prevent false triggering in the event of substantial deviations, oscillations and random noise in the ECG wave. Detection is suspended until the noise subsides.

5. QRS-complex (R-wave) Detector

6. ECG Data Running Statistics (e.g., Thresholds).

2.3.1 Interrupt Handling Routine

The interrupt handling routine in the ECG QRS-complex detection algorithm is identical to the Pa interrupt handling routine described in Section 2.2.1. Please refer to that section for details.

The exception to the use of the interrupt handling routine occurred when the MIT/BIH database was utilized to test the implemented version of the DD/1 QRS-complex detection algorithm. In that case instead of reading the data from the port of the A/DC, the data was read from a file stored on a RAM Drive configured on the PC-AT. The use of a RAM drive allowed quick enough data access to allow the interrupt routine to run in real-time. Utilization of the regular hard disk would require too much time to perform a hard drive "seek" and would not allow the program to run in real-time.

2.3.2 Data Preprocessing Routine

The data preprocessing routine performed the following functions:

1. Maintain a sample number count

2. Maintain a updated history of non-filtered (CurrentData) and filtered data(x[0],x[1], ...)

3. Calculate a moving average mean pressure

4. Calculate an autoscale divisor

5. Calculate the autoscaled data

6. Low pass filter the data using a moving average smoother

7. Create and Store AZTEC data representation for display

2.3.2.1 Sample Number and Data History

As in Pa detection, the sample number was maintained using a 32 bit unsigned long integer. The data history was kept in traditional fashion in which the oldest sample was discarded and replaced with the more recent sample as seen in Equation 2-1 and Equation 2-2. Refer to Section 2.2.2.1 for additional details.

2.3.2.2 Moving Average Mean Value and Autoscaling

In order to scale the data value of the samples to a consistent amplitude deflection (usually for the R-wave), a moving average mean value was calculated. A moving average required a history of values to be stored. In order to reduce the computational time a ring buffer was constructed in software so only one value would have to be rewritten for each new sample. The moving average filter can be seen in Equation 2-3.

Autoscaling was accomplished by approximating the ECG R-wave signal as a thin triangular shaped deflection. The autoscale divisor was created by determining the largest difference between two samples within the smoothed LPF data. There were three sample spacings devised in which the amplitude difference was collected, namely a 20 sample spacing, a 30 sample spacing and a 40 sample spacing. The variety of windows were developed because of cases where a certain shaped ECG P- QRS-T complex would prevent the measurement of an accurate R-wave amplitude (i.e., from the isoelectric potential to the peak of the R-wave). For example for a 20 sample spacing, in some cases, the peak of the P-wave and R-wave were for 20 samples apart as well as the peak of the R-wave and the T-wave. For this reason, the amplitude would be read in smaller than the actual R-wave amplitude. An improper R-wave amplitude measurement would lead to an improper autoscaling. The mission of the autoscaling is to condition the ECG data to provide a QRS-complex that is consistent as possible to the QRS-complex detector.

The largest R-wave amplitude that occurred every 750 samples[1] was averaged to create a moving average R-wave height mean value as seen in Equation 2-30.

(2-30)

$$RwaveHeightMeanValue \, [t-0] \; = \; \frac{\sum\limits_{i\,=\,0}^{n-1} RwaveHeight \, [i]}{n}$$

---

1. An interval for the R-wave height mean value was selected as 750 samples. 750 samples correspond to 1.5 seconds and a heart rate of 40 bpm. It is assumed that 40 bpm is the lowest possible heart rate for the detection algorithm. Thus, a QRS-complex (and associated maximum R-wave height vector) should occur within this 1.5 second window.

The autoscaled data is calculated as seen in Equation 2-5. The scaling factor was defined as appropriate for display monitor within the experimental environment. In addition, damping is put within the autoscaling to ensure a quick baseline shift does not cause the autoscaling algorithm to grossly reduce the amplitude of the data.

(2-31)

$$\text{ScaledData} = (\text{DataSample} - \text{Average}) \frac{\text{DefinedScalingFactor}}{\text{RwaveHeightMeanValue}}$$

2.3.2.3 Moving Average Smoother Low Pass Filter

The signal to noise ratio (S/N) of the QRS-complex is at least an order of magnitude greater for the ECG than, for example, the dicrotic notch for the same level of noise. For this reason the LPF is not as critical as it is in Pa detection (where a Butterworth filter was employed). A 9-point moving average filter was used to smooth the data as seen in Equation 2-32.

(2-32)

$$\text{SmoothedLPFData}[t-0] = \frac{\sum\limits_{i=0}^{n-1} \text{UnfilteredData}[t-i]}{(n=9)}$$

2.3.2.4 Create and Store AZTEC Data Representation for Display

The data preprocessing routine of the DD/1 QRS-complex detection algorithm is the AZTEC data. The AZTEC data is essentially a sequence of vectors. These vectors are lines and slopes. The lines are mathematically represented by an amplitude value, a length and a starting point. The slopes are mathematically represented by a slope value, a length and a starting point. These representations must be converted into a representation that can be displayed on a monitor. In addition, a sample

history must be maintained because a line or slope cannot be displayed until it is formulated. Thus a multiple sample delay existed between the monitor display of the AZTEC data (particularly for long lines) and the current sample being processed by the detection algorithm. (For example, the representation of an AZTEC line could not be displayed on the monitor until its value was known). For this reason an algorithm to convert the AZTEC data to a contiguous set of samples that represent the lines and slopes was necessary. The display processing steps required the lines to be converted into samples that correspond to the value of the line (i.e., y = mx + b, where m= 0 and b is the value of the line) for the duration in samples of the line. The slopes are converted using the same conversion equation for the line (i.e., y = mx + b, where m= slope of the vector and b is the value at the starting point of the slope). The AZTEC display datum history spanned 64 samples to account for any lines that endure for the maximum length of any AZTEC vector (i.e., 128 milliseconds).

2.3.3 ECG AZTEC Vectorization

The original implementation of the ECG AZTEC vectorization was to process off-line data quickly for the ARGUS arrhythmia Holter monitor detector. The AZTEC algorithm would initially convert all the ECG data to lines. A line's amplitude (i.e., value) was equal to the average of the two maximum and minimum points. The termination of a line was dictated by a deflection that exceeded a specified amplitude threshold. (The AZTEC algorithm also prevented any line from being longer than 64 samples.) The start of a new line would begin on the sample that exceeded the specified threshold of the previous line. Long durations of ECG isoelectric potential in which the amplitude changes very little, lead to long lines. Quick changes in amplitude would result in very short lines typically with a length of four samples or less. The first process of the AZTEC algorithm would convert all data to lines. The second process of the AZTEC data would convert the short lines to slope vectors. The criterion for a slope was a line or consecutive sequence of lines in which the length is four samples or less. The only exception to this criterion was when there was a change in direction of the "line" heights (e.g., at the peak of a R-wave). In the case of the R-wave peak, a new slope vector starts as the peak, but follows the slopes downward. The implementation in this dissertation differs slightly from the original implementation of the AZTEC algorithm in that:

1. The amplitude threshold is a function of the R-wave height average (divided by 35) as opposed to a constant threshold,

2. Slopes as well as lines are restricted to 64 samples in length as opposed to just lines.

The amplitude threshold was set as a function of R-wave height to more consistently convert the data into vectors of equivalent dimension (e.g., slopes of equivalent height and lines of equivalent

length) for the R-wave detection algorithm. The length of a slope was restricted to 128 samples because it was found during implementation of the algorithm that a slow slope of a long duration would cause a slope to be longer than 128 samples causing the implementation of the AZTEC algorithm to crash.

2.3.4   QRS-Complex (R-wave) Detector

The R-wave detector employed was based on the DD/1 algorithm which utilizes the preprocessed ECG AZTEC data. The lines and slope of the AZTEC data are utilized by the DD/1 algorithm in a way to perform primitive image recognition on the wave. The criteria for detection includes:

1. A set of R-wave slopes which endure within a minimum amount of time and a maximum amount of time

2. At least one of the slopes that constitute the R-wave exceed a certain height threshold

3. The sum of the vector slopes must be within a certain absolute tolerance of zero[1]

4. At least one of the slopes that constitute the R-wave exceed a certain slope threshold

The dissertation differs slightly from the original implementation of the DD/1 algorithm in that:

1. The search for a sum of slopes that may constitute a R-wave is limited to 6 slope vectors

2. Additional algorithm processing was added to prevent false positives detections from occurring, namely
    1. The detection of a single R-wave twice, and
    2. The detection of a T-wave resembling an R-wave

The six slope vector limit of an R-wave was implemented because of the limitation in processing power. Implementation of seven vector detection and greater caused the processing power demand to exceed the 2 millisecond limit between samples.

2.3.4.1   Avoiding Detection of a Single QRS-complex Twice (False Positive)

The refractory period[2] of the heart prevents the heart from contracting before the end of the last contraction typically 20-100 milliseconds[3] (48). However, patients with ventricular bigeminy and

---

1. A typical QRS-complex will have a positive slope and a negative slope. When adding the vertical components of the two vectors, the sum should total close to zero because the QRS-complex inherently originates and terminates to the same isoelectric potential. A criterion for detection is that the slope vectors sum is close to zero. This prevents a single slope vector (typically a baseline shift) from being detected as a QRS-complex.

2. The refractory period is defined as the time during which an excitable membrane does not respond to stimulus whose magnitude is normally sufficient to trigger an action potential(48).

trigeminy as present in the MIT/BIH Arrhythmia database ECG (30), did demonstrate QRS-complexes occurring as quickly as 20 milliseconds apart. In order to prevent missing those contractions and yet avoid the detection of a single QRS-complex twice, appropriate detection algorithm timing was implemented.

False positive detection for the same QRS-complex twice, requires checking for the following criterion:

1. The position of the suspected R-wave (i.e., meeting the DD/1 detection criterion) is greater than 10 samples (≈20 milliseconds) from the previous R-wave

2.3.4.2   Avoiding Detection of a T-wave Resembling an R-wave (False Positive)

Within the MIT/BIH Arrhythmia database ECG (30), along with unusually shaped QRS-complexes, unusually shaped T-wave complexes were present. The profile of the T-wave complexes occasionally rivaled the tolerances of the QRS-complex detection algorithm. However, in general those complexes were typically shorter in height and longer in duration than the QRS-complex, and this fact was used to program a supplemental algorithm to avoid this type of T-wave false positive.

Detection of a T-wave resembling an R-wave (i.e., false positive) required avoiding (discarding) R-wave shaped complexes (i.e., previously meeting the DD/1 detection criterion) that meet the following criteria:

1. The new R-wave vectors endure for longer than 20 samples (40 milliseconds), and 2 or 3
2. The following criteria   o
    1. The largest R-wave slope height in the new R-wave complex is less than 80% of the previous R-wave complex slope height, and
    2. The position of the new R-wave is less than 150 milliseconds from the last R-wave, and
        1. The width of the new R-wave is greater than twice that of the previous R-wave, or
        2. The width of the R-wave exceeds 35 samples (or 70 milliseconds)
3. The following criteria are met.
    1. The new R-wave height is greater than 3 times the height of the previous R-wave, and
    2. The new R-wave starting position (i.e., start of first slope) is within 90 samples (180 milliseconds) of the previous R-wave, and
    3. The new R-wave width is greater than 75% the width of the previous R-wave, and

---

3.   The absolute refractory period of the healthy heart is 250 milliseconds(48)

4. The end position of the new R-wave is less than 175 samples from the position of the previous R-wave

The following algorithm determines if the new perspective R-wave is a T-wave based on whether the following boolean expressions (59) are true as noted in Equation 2-33, Equation 2-34, Equation 2-35, and Equation 2-36. The flow of the algorithm to avoid a T-wave type QRS-complex false positive is seen in Figure 2-18.

T-wave Resembling Perspective R-wave Detected = A * (B +C), where   **(2-33)**

$A = 1.0.0^1$ (i.e., expression 1.0.0)   **(2-34)**

B = (2.1.0) * (2.2.0) *((2.2.1) + (2.2.2))   **(2-35)**

C = (3.1.0) * (3.2.0) * (3.3.0) * (3.4.0)   **(2-36)**

The criterion for A noted in Equation 2-34, ensures the perspective T-wave endures for a period typically longer than an R-wave. The criterion for B noted in Equation 2-35, ensures the perspective T-wave has small amplitude (relative to the QRS-complex), is within the time period window adjacent to the last R-wave, and has a width that doubles that of the average or a set maximum limit. The criterion for C noted in Equation 2-36, ensures the perspective T-wave has a relaxed criterion for height, and has a start time that is within a certain window and a relaxed width and an end time within a certain window. Equation C compares the start time of the previous R-wave with the start time of the new perspective R-wave and the end time of the previous R-wave is compared with the new perspective R-wave end time. The start time and end time window are of different widths because some T-wave complexes in patients with heart disease are exceedingly long. The criterion in C covers these T-wave complexes that endure until 350 milliseconds after the end of the previous R-wave complex. This example of detection demonstrates the advantage of AZTEC data in which the ECG is not only detected but also delineated the QRS-complex.

2.3.5 ECG Data Running Statistics (e.g., Thresholds)

A variety of statistics utilized in QRS-complex detection are collected to provide set width, height, slope thresholds; and timing intervals for the two detection algorithms. These ECG running statistics calculated in time windows independent, as well as dependent on the R-wave detection algorithm includes:

---

1. Expression 1.0.0 corresponds to the above criteria in Section 2.3.4
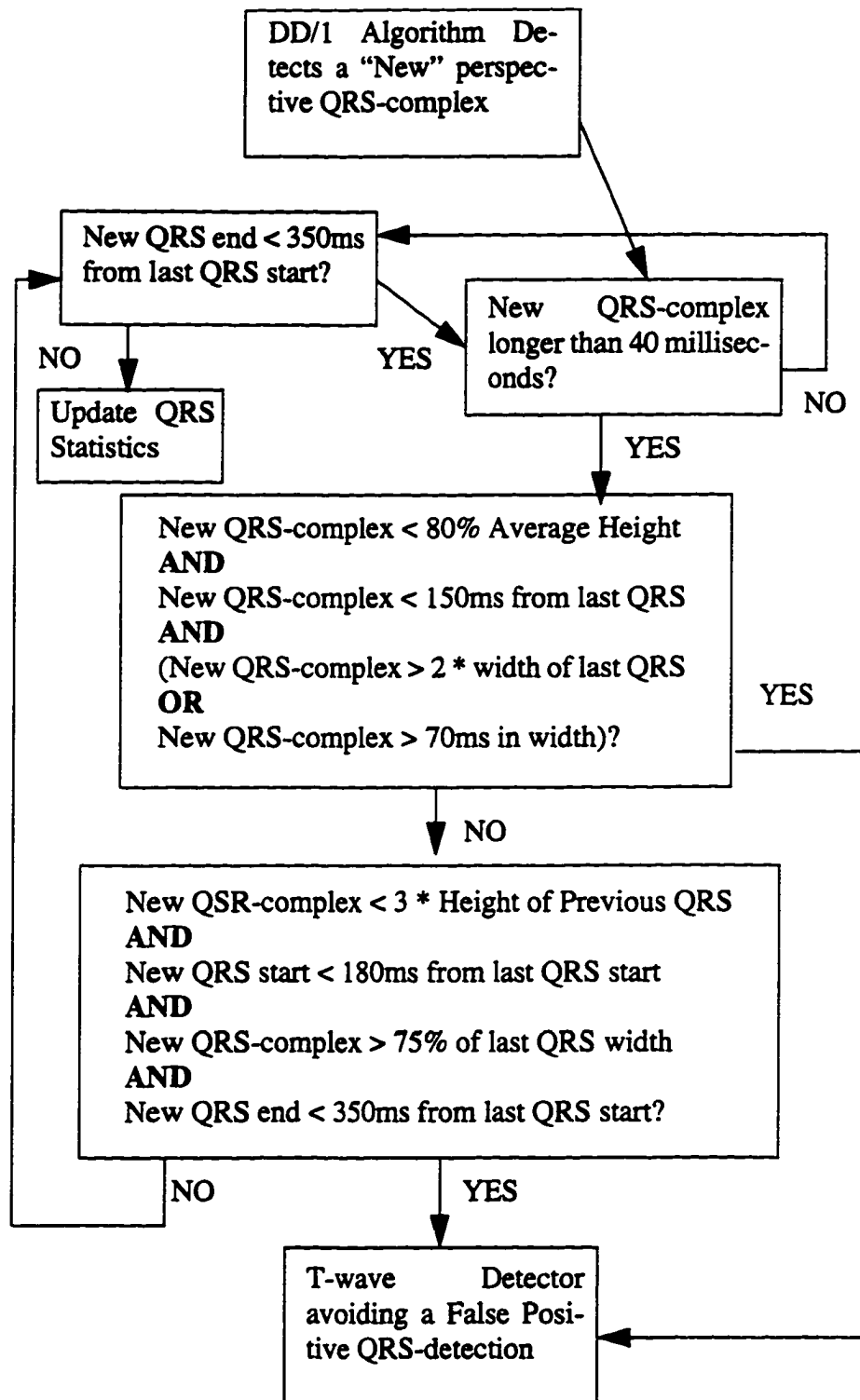
Figure 2-18. Algorithm For Avoiding QRS-Complex False Positive Detections due to T-wave

1. Statistics Independent of R-wave Detection

    1. AZTEC Slope Height History

2. AZTEC Slope Value History

3. AZTEC Slope Position History

4. AZTEC Slope Length History

5. R-wave Slope Average

6. R-wave Height Average (Documented for Autoscaling in Section 2.3.2.2)

   2. Statistics Dependent on R-wave Detection

      1. R-wave Position History

      2. R-wave Duration History

      3. Cycle Length Average and Heart Rate Average

2.3.5.1 Statistics Independent of R-wave Detection

Essential to detection of the QRS-complex was statistics about the AZTEC vector slopes. The slope vector height, value, position, and length history provided threshold information for the corresponding DD/1 algorithm detection criteria respectively. AZTEC vector line provided no information in the detection of the QRS-complex and thus statistics on the vector lines were not recorded.

The slope vector height, value, position, and length history provided threshold information that was derived independent from the R-wave detection. This independence is important because if the algorithm does not detect the first QRS-complex, these statistics may not migrate to their proper values and then the algorithm may not be able to initiate detection.

The R-wave slope average and R-wave height average are derived from the maximum values of the observed data during a 1.5 second window. Again, these statistics are accurate because the QRS-complexes are made up of slopes. Damping is implemented so that a single sharp noise excursion will not drive the average R-wave slope or height to unrealistic values. A set percentage of the R-wave slope and height averages are utilized as thresholds in the QRS-complex detection algorithm.

2.3.5.2 Statistics Dependent on R-wave Detection

The R-wave position and width history are dependent on R-wave detection. These are utilized for the QRS-complex detection algorithm. The Cycle Length Average and Heart Rate are determined in the same way as noted in Section 2.2.3.2. Damping is provided in the calculation of the cycle length average and heart rate to ensure a false positive or false negative QRS-complex detection does not cause an unrealistic cycle length average and heart rate average value.

3. CAD Control and Processor Architecture Research

Once the Pa and ECG detection algorithms were developed, the timing was established for the control algorithm of the CAD controller. The detected cardiac events are then used by the CAD control algorithm to determine when to transmit inflation/deflation signals to the pneumatic driver of the CAD. The first section describes the control for sinus rhythms and the non-sinus rhythms. The last (second) section in this chapter describes the transputer research that was conducted to investigate a fault tolerant multiprocessor based CAD control system.

3.1 Control During Sinus and Non-Sinus (Arrhythmic) Ectopic Beats

This section describes research into control during sinus and non-sinus rhythms. A closed-loop control algorithm was developed to provide inflation/deflation optimization during periods of sinus rhythms. In addition, research into a control algorithm for non sinus rhythms during ectopic beats in order to determine optimal inflation was investigated. The ectopic rhythms are abnormal isolated heart beats. In the event an abnormal beat occurs, prediction of the STI must be used to predict the timing of the dicrotic notch. The prediction of the dicrotic notch allows for optimal inflation (taking into account the delay associated with the electronic signal to inflate and the actual hemodynamic augmentation in the aortic pressure).

In order to predict the occurrence of the dicrotic notch, the STI must be predicted. Research into a STI to HR linear regression equation for a canine mongrel experimental models was investigated. The linear relationship that is prevalent in humans was demonstrated not to exist in canines. Using data from five different canine mongrel cardiac assistance experiments in which sequences of arrhythmia were recorded, five separate graphs were generated using "Cricket Graph" software. This plotting software also provided a linear regression equation for the purpose of visual analysis. The graphs plotted data points illustrating the STI to HR relationship observed in the five experiments. Through visual observation of the plotted points and their relationship, it was apparent the STI to HR relationship in the canine mongrel cardiac assistance experimental models was unacceptable for the prediction of the STI for cardiac assist experiments[1]. The criterion in

1. The author was unable to find any references on the STI to HR linear regression relationship for the canine mongrel. However, one reference (35) depicts in Figure 1-12 a relationship between the STI and the cycle length (inverse of HR) for multiple canine experimental models. From the scatter in the graph, it "appears" that a linear relationship does not exist for all canine mongrels. However, reference (35) does not document the STI to HR relationship for a single canine. The investigation examines the possibility of a specific linear regression for each canine experimental model.

determining whether the STI to HR linear regression equation was not acceptable for STI prediction was straightforward; if one canine mongrel experiment demonstrated a scatter of more than 50% for a given value of HR, the STI to HR relationship was unacceptable. In cardiac assistance, an improper inflation can lead to diminished circulation through the obstruction of the aorta during the normal pumping of the heart. The scatter of STI points around a constant value of heart rate indicates a prediction may be grossly in error. This research was conducted in an attempt to predict the STI for the canine mongrel experimental models.

A regression equation similar to that in humans did not exist for the entire set canine experimental models (n=5) studied. These results were similar to what was observed in the canine heart rate to STI research reference noted in Figure 1-12 (35). In addition, an acceptable regression equation did not exist, in general, for all of the individual canine experimental models. For example of a STI to HR graph depicted in the last of five experiments, the STI ranged from 120 -220 milliseconds for heart rates within a range of 130-140 bpm as depicted in Figure 3-1. This inherent variation in canine mongrels makes the STI to HR regression an unusable estimate for STI prediction. Chapter 5 illustrates the STI to HR plots for five different canine experimental models.

Since the STI to HR relationship did not exist in the canine experimental models, a second approach was developed to provide a prediction for the dicrotic notch. The prediction method utilizes sinusoid estimate of the systolic pressure trace that included a fault tolerant[1] algorithm in the event the estimate was unrealistic (i.e., depending upon the ratio between the estimate of the STI and the STI average). Depending upon whether the estimate was much larger than the average (i.e., > 200% of the STI average) or much smaller than the average (i.e., <50% of the STI average), one of two fault tolerant estimates was chosen for STI prediction and thus the prediction for the timing of the dicrotic notch.

3.1.1   Closed Loop Control Algorithm for Sinus Rhythms

Reliable detection of the important heart cycle events provide the necessary information to optimize cardiac assist device (CAD) control. For example, if the cardiac assist device is an intra-aortic

---

1. Fault tolerance in the prediction of the occurrence of the dicrotic notch from a STI is defined as a method of changing the method of estimate of STI using some automated logic based on a statistic collected. In this case the statistic collected in the STI average over the last five beats. In the event the sinusoid STI estimate is grossly greater than (>200%) or grossly less than (<50%) the average, an alternate method is utilized to predict the occurrence of the dicrotic notch. This is particularly useful when the aortic pressure systolic shape is peaked more toward the systolic rise.
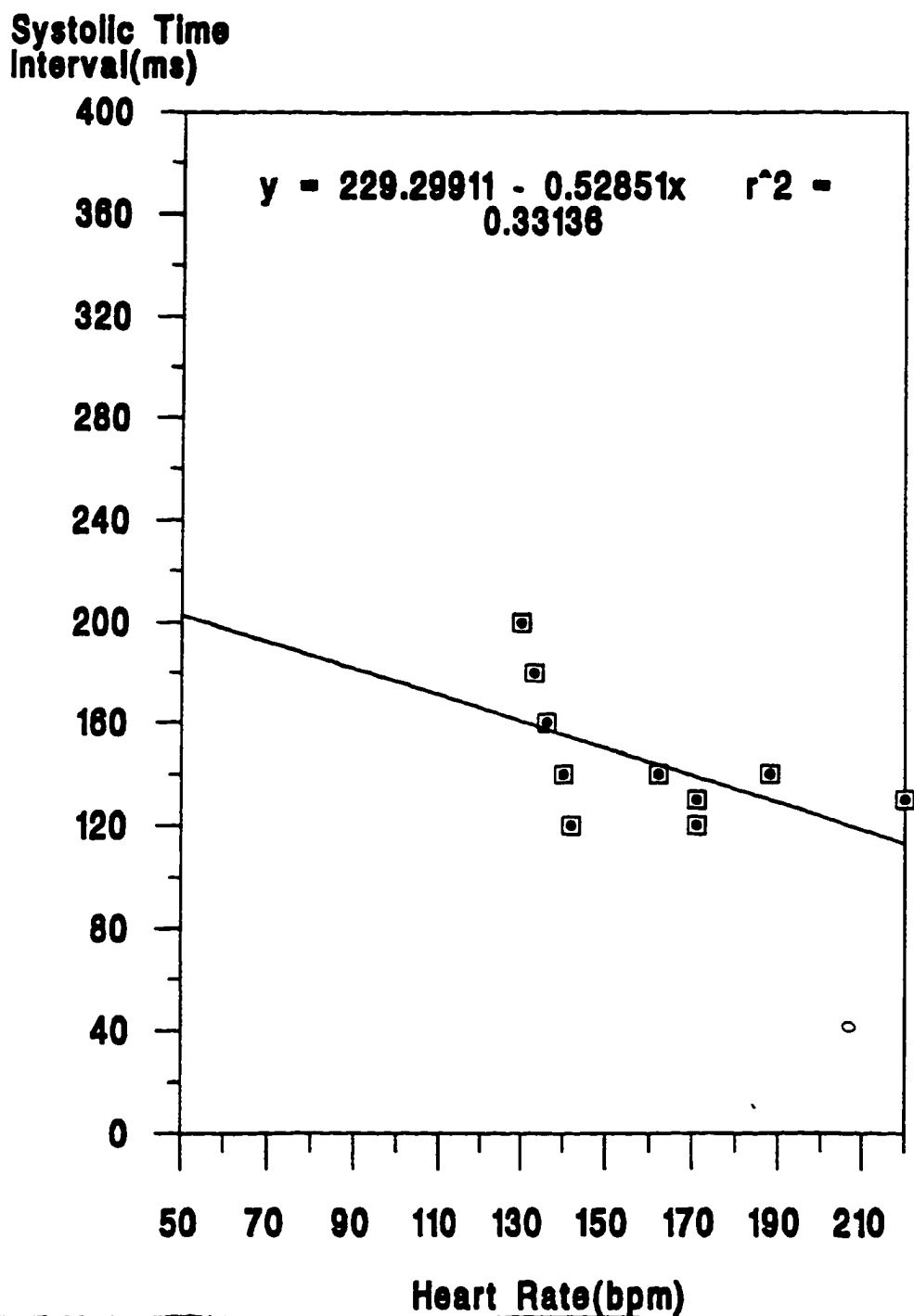
Figure 3-1. Example of Canine Mongrel Experimental Model Heart Rate to STI Plotted Points and Linear Regression Equation

balloon (IAB), optimal control of a counterpulsation cardiac assist device requires the IAB to provide pressure augmentation within the ascending aorta just as the aortic valve closes. The aortic valve closing creates the dicrotic notch within the Pa wave. The IAB should deflate in order to align the lowest point in the Pa droop exactly at the start of isovolumetric systole to minimize end

diastolic pressure and thus root aortic impedance. If the sinusoid rhythms of the heart remains constant, once reliable detection and tracking of the cardiac cycle is determined, inflation and deflation of the cardiac assist device remains periodic to provide optimal augmentation. The search for optimal inflation and deflation for a periodic heart rate occurs through the use of the developed closed loop control algorithm. Inflation of the cardiac assist device occurs exactly at the dicrotic notch. The initial pumping interval is short and slowly increases (by 2ms per cardiac cycle) until the low pressure point in the droop of the augmentation occurs just as the systolic rise in the pressure occurs.

Once the Pa detection algorithms were completed, a control algorithm was developed to optimize pumping for the cardiac assist device. The algorithm involved three different phases: passive statistics, active statistics, and optimal control. The passive statistics phase of control is an initial learning period in which filters collected threshold data for detecting the systolic rise and dicrotic notch. During the active statistics phase of control, circulatory assistance was provided at a safe interval in order to collect statistics based on the shape of the augmentation within the Pa wave. The optimal control period of the control algorithm occurs when both passive and active statistics are accumulated and the inflation interval migrates toward and eventually settles into optimal inflation and deflation timing. The control algorithm also provides intelligence to change its timing to a safe inflation interval during a single ectopic beat or a series of arrhythmic beats.

3.1.2 Control Algorithm for Non-Sinus Ectopic Rhythms

Patients with heart disease can be prone to arrhythmia. When the heart rate changes due to arrhythmia, CAD control becomes considerably more complex because of the changes imposed on CAD detection and the changes needed for CAD inflation and deflation timing. Tracking the heart requires a robust detection and control algorithm. The focus of the detection algorithm was to provide reliable detection during non optimal characteristics for detection. Once the characteristics are detected a control algorithm designed for arrhythmias had to be developed. Prediction of the duration of the systolic time interval proved to be very useful to determine when the dicrotic notch would occur once the systolic rise was determined. The position of the dicrotic notch provides the point at which the cardiac assist device should inflate. The first investigation at control through arrhythmia attempted to use the systolic interval to heart rate regression equation prevalent in humans. However, five experiments were performed that demonstrated that this relationship is not prevalent in mongrel canine experimental models. The regression proves to be even more nonlinear

when the canine experimental model is under the influence of beta-blockers commonly used in cardiothoracic laboratories to therapeutically stabilize or destabilize the heart rate. For this reason, a STI estimate was based on a Sinusoid Approximation of the systolic Pa trace.

3.1.3 STI Estimate Based on Sinusoid Approximation

Due to the nonlinear relationship between the interbeat interval (i.e., reciprocal of the heart rate) and systolic time interval (STI) of canine mongrels, an alternate algorithm had to be developed to predict inflation when an arrhythmic heart beat occurs. After a numerical review[1] of different methods to predict the timing of the dicrotic notch, the average of the systolic interval proved to be the best "overall" estimation method to determine when the dicrotic notch would occur. In an attempt to be even more accurate, a second fault tolerant sinusoid estimation algorithm was derived using a sinusoid mapping of the systolic pressure template. This sinusoid model assumed the following: (1) the aortic pressure had a sinusoid shape during systole, and (2) in each heart cycle, the relationship between the peak systolic and peak diastolic pressure difference and the peak diastolic and dicrotic pressure difference was a reproducible ratio. In order to perform the sinusoid estimate, the start of systole, the maximum pressure of systole, and the dicrotic notch must be detected for each cardiac cycle as seen in Figure 3-2.

The following assumptions are made for the sinusoid approximation model of Pa systole:

1. $t_{systole} - t_A{}^2 = t_{dicrotic} - t_{systole}$ (The "2" refers to footnote 2.)

2. $P_{tA}{}^3 = P_{tdicrotic}$ (The "3" refers to footnote 3.)

3. The peak of systole can be detected as $P_{tsystole}$ and is the center of the sinusoid

4. The Peak to Dicrotic Notch Ratio (PNR) = (Psystolic - Pdiastolic)/ (Pdicrotic-Pdiastolic) is the same for the sinus and non-sinus (ectopic) rhythms

---

1. The numerical review of the best overall estimate of the STI for canine mongrels during arrhythmia was conducted by using isolated sections of arrhythmia within the Cornell University Medical College Canine Mongrel Aortic Pressure Database. The isolated sections of Pa arrhythmia data was presented off-line to the two STI estimate methodologies and the dicrotic notch detector simultaneously. The two estimates and the actual STI values were printed on the computer screen. It was apparent from the numerical estimates of STI that the STI average was the best overall estimate. However, when the STI Pa trace was sinusoid in shape, the sinusoid estimate provided a more accurate estimate.

2. t_A is the time at which the Pa trace systolic rise crosses the estimated pressure of the upcoming dicrotic notch.

3. P_{tA} is the pressure on the systolic rise which is equivalent to the estimated pressure of the upcoming dicrotic notch.
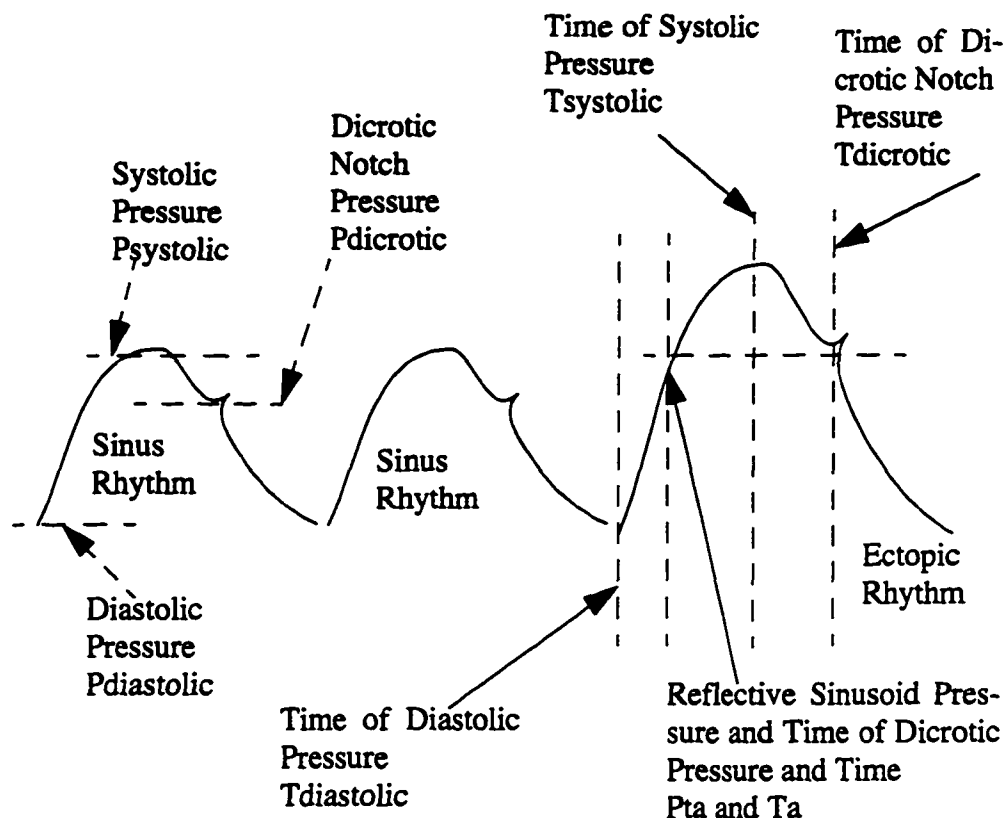
Figure 3-2. Pa Systolic Sinusoid Model for Dicrotic Notch Prediction During Ectopic Beats

5. Once the diastolic pressure (Pdiastolic) systolic peak (Psystolic) is detected, the PNR and the Psystolic - Pdiastolic difference can be used to determine the predicted pressure of the dicrotic notch [Pdicrotic = ((Psystolic - Pdiastolic)/PNR) + Pdiastolic].

6. The estimated pressure of the dicrotic notch (i.e., P_{tA} = Pdicrotic) can be used to determine the time (t_A)at which the equivalent pressure occurred on the systolic rise using a search algorithm through the data stored for the Pa trace.

7. Once the time between the $t_{systole}$ - t_A is known, the systolic time interval can be estimated as STI = ($t_{systole}$ - $t_{diastole}$) + ($t_{systole}$ - t_A).

3.1.3.1   STI Estimate Based on Average STI

Due to the unusual Pa template of systole found in various canine mongrel experimental models, sinusoid mapping STI estimates that are determined to be less than 50% or greater than 200% of the average systolic interval are discarded for an alternate method of estimation, thus providing a fault tolerant estimate. If the sinusoid estimate was less than 50% of the average, the assumption was that the estimate of the actual systolic event would occur between 50% and 100% the duration of

the average systolic interval; therefore the average (100% of the STI average) was used as a safe estimate. The average systolic interval estimate would protect the heart by providing a Pa augmentation after the dicrotic notch. This would ensure inflation after systole and thus prevent inflation of the cardiac assist counterpulsation device from hindering the normal pumping of the heart.

3.1.3.2   STI Estimate Based on Dicrotic Notch Detection

If the sinusoid estimate was greater than 200% of the average STI, the assumption was that the actual dicrotic notch would occur between 100% and 200% the duration of the average systolic interval. In order to optimize pumping without jeopardizing inflation during the systolic interval of the heart, an inflation just after the dicrotic notch was detected was utilized. This dicrotic notch inflation provides the most optimal estimate of inflation under the circumstance of unusual Pa template that is estimated improperly by a sinusoid template algorithm during an ectopic heart beat.

3.2   CAD Transputer Processor Architecture and Communications Research

This section describes the transputer research results from the fault tolerant control research that was conducted. The initial goal of the research was to develop a RISC-based (Reduced Instruction Set Computer) multiprocessor CAD controller. The multiprocessor computer was to be provided by a PC-plug in quad transputer card. The transputer would provide enough computational power to operate four algorithms independently. The four algorithms would include Pa detection, ECG detection, Arrhythmia Detection and overall CAD control. In the event either the Pa or ECG signal was compromised with severe noise or the signal was discontinued, control using the remaining signal would continue to operate.

The CAD Multiprocessor Control research involved determining the communications requirements for the CAD implementation, determining the proper transputer architecture, developing a CAD protocol and verifying the communications throughput. The quad transputer board utilized is depicted in Figure 3-3
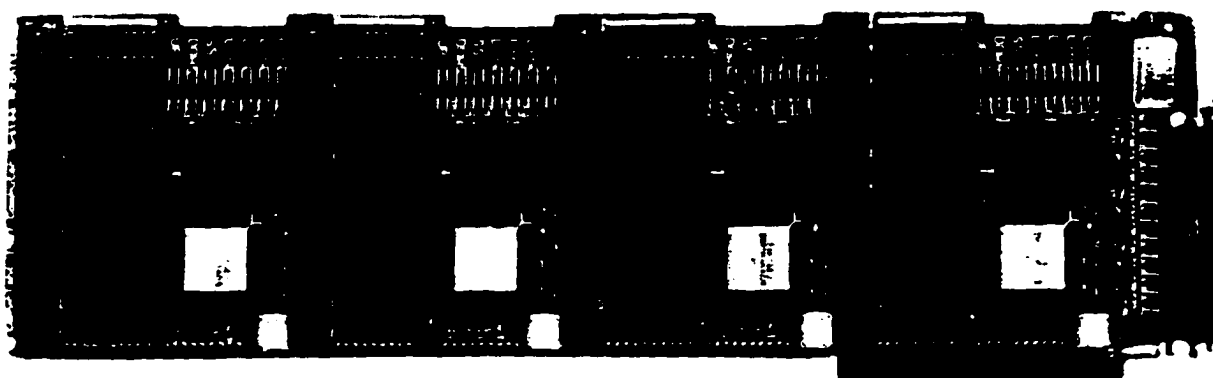
Figure 3-3. Pictorial of PC-Plug in Quad Transputer Card

3.2.1 CAD Multiprocessor Control

Once the Pa and ECG detection algorithms were developed and tested separately by a single microprocessor (33Mhz PC-AT clone), multiprocessor development began in order to work toward integrating the algorithms into a single cardiac assist device control system. In order to demonstrate that the transputer board was efficient enough in the transport of data, the communications primitives between the PC and between RISC processors would have to be designed and verified. If the communication primitives were verified, it can be assumed the cardiac assist controller system would function properly. Verification involved showing that data communications between the host processor (PC/AT) and the RISC processors would not deplete a large percentage of processor time.

The first steps to complete the research were to develop a working understanding of the transputer card and the transputer C compiler software. The transputer card was a Computer System Architects (CSA) Multi-Transputer Board with four T800 20Mhz RISC processors(60). Each processor had one megabit of local RAM available as seen in Figure 3-4. The transputer compiler software was the Computer Systems Architects LS-C (Logical Systems -C), "C Transputer Toolset for Multi-Transputer Networks from Logical Systems", Version 89.1(61)(62). The most important features of the transputer software included a C preprocessor, C compiler, Linker, Librarian, and Loader and Execution Tools for a array of transputers.

A PC server had to be written to act as interface between the transputers and the A/DC and D/AC interfaced to the PC-bus. The user written PC Server will allow the PC and transputer PC plug in
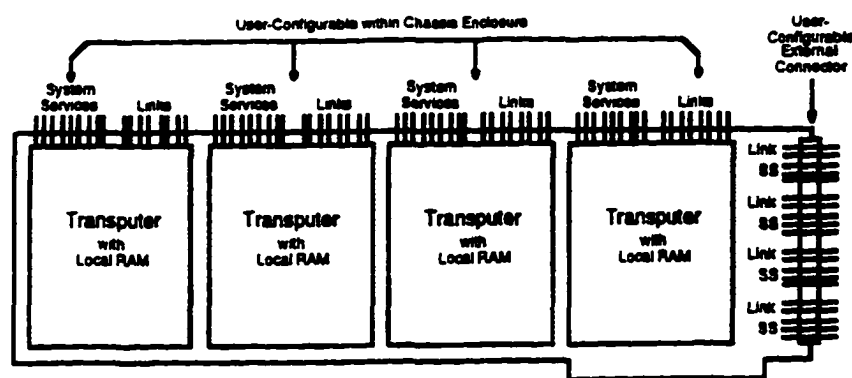
Figure 3-4. Quad Transputer Functional and Interface Block Diagram

card to operate as concurrent computing devices. The PC server will act as a platform for the transputer board allowing I/O access for the transputers.

3.2.2 CAD Multiprocessor Architecture

The CAD Control transputer architecture chosen was the farm model in which one process is assigned to one processor. That would allow debugging of the "independent process architecture" to be more straightforward[1]. The transputers are connected to each other through one of four links (L1-L4) available at the communications interface of each processor as seen in Figure 3-5. The transputers are networked physically through the physical connection of 10 pin ribbon cables. The single root node processor (control and I/O processor) communicated with the PC-bus through link 0. The three remaining node processors communicated with the root processor through links 1-3. An additional link connected Node 2 to Node 3 to allow the R-wave detector to provide timing information to the P-wave detection algorithm. The CAD control transputer architecture is depicted in network configuration illustration of Figure 3-6 and the network configuration table noted in the network information file (*.NIF) software is shown in Figure 3-7.

---

1. The farm model contrasts the pipeline model approach in which each processor (in sequence of processors) executes part of an algorithm (that can be broken into a sequence of processing steps). The pipeline approach, if implemented, would be considerably more difficult to debug because each detection algorithm could not be independently isolated.
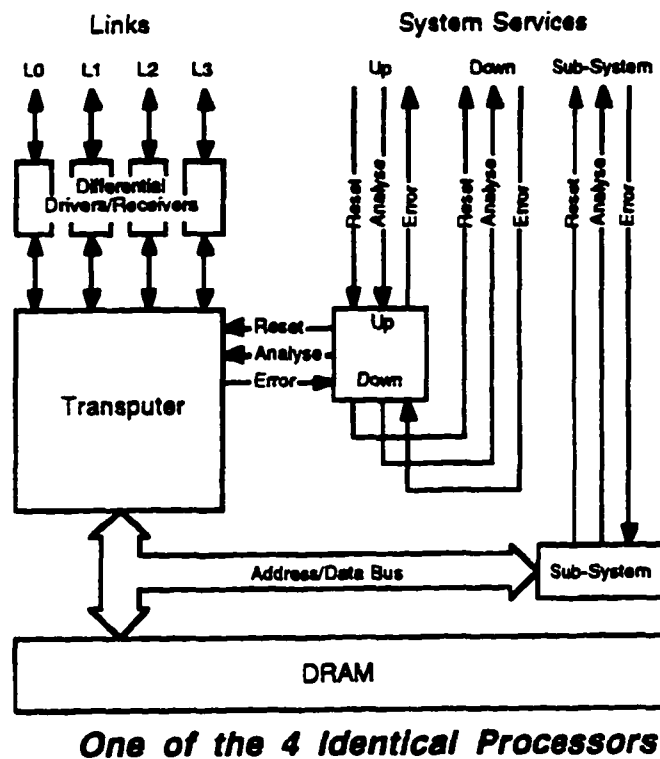
Figure 3-5. Transputer Functional Diagram illustrating Network Link Interfaces

3.2.3 CAD Multiprocessor Protocol

The transputer data communications protocol was designed to allow eight bytes to be read in through the PC-bus. Four bytes consisted of the Pa and ECG samples. Within the root processor the Pa sample was sent to the aortic pressure detection algorithm node processor in a two byte message. The ECG samples received by the root processor are transmitted to the two ECG algorithms, P-wave and R-wave in a two byte message. The root processor then awaits the response from all the detection processors. The two byte return message from each detection algorithm returns notification of when their respective events occurred. Once all three algorithms have responded back to the root processor, the root processor controller algorithm responds back to the PC-bus with an eight byte control message of when to inflate and deflate the cardiac assist device. The transputer
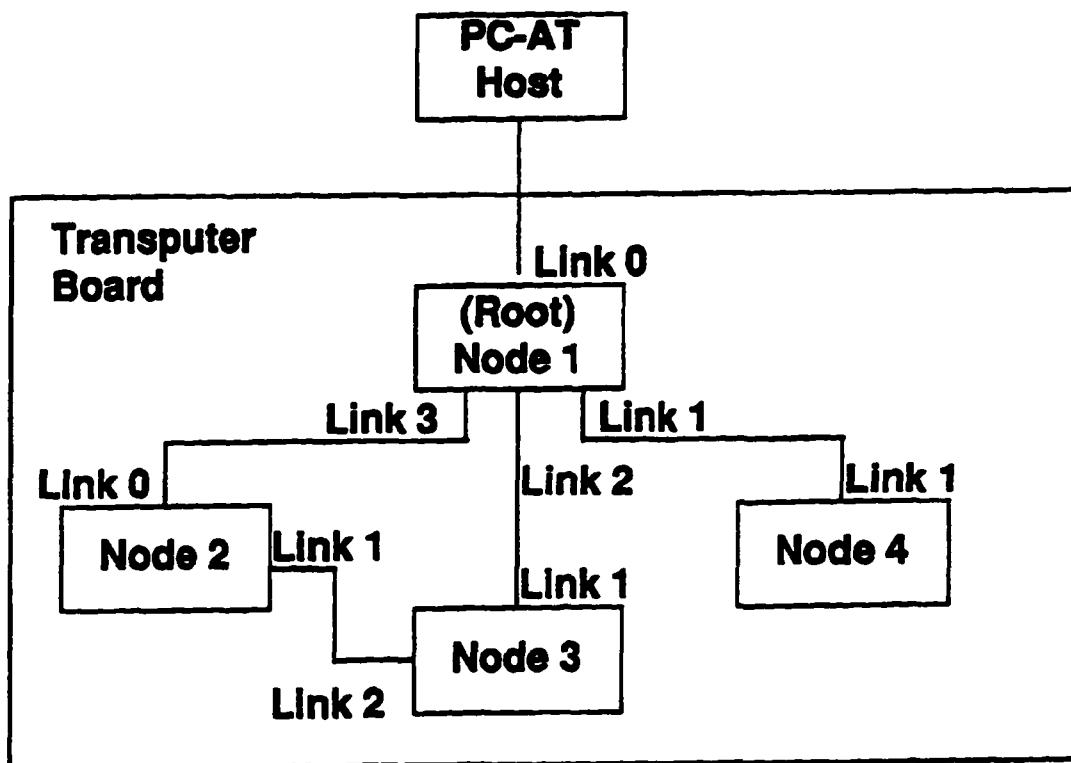
Figure 3-6. CAD Control Transputer Network Configuration

data flow moving toward the leaf nodes is described in Figure 3-8 and the transputer data flow moving away from the leaf nodes is described in Figure 3-9.

3.2.4 Communications Throughput Verification

The sampling rate of the AD/C was set at 500 Hz; therefore the maximum processing time for each processor between samples was 2 msec. Verification involved testing the rate of information flow. The information was read into the A/DC through the PC-bus (port) by using an infinite loop that would read data in from the A/DC as soon as the previous sample was processed (instead of the sending an A/DC timer generated interrupt to the host

Node #	Prog	Parent	Link 0 1 2 3
1	Cntrl	R0	0 4 3 2
2	R-w	R1	1 3
3	P-w	R2	1 2
4	Pa	S1	1

Figure 3-7. CAD Control Transputer Network Configuration Table
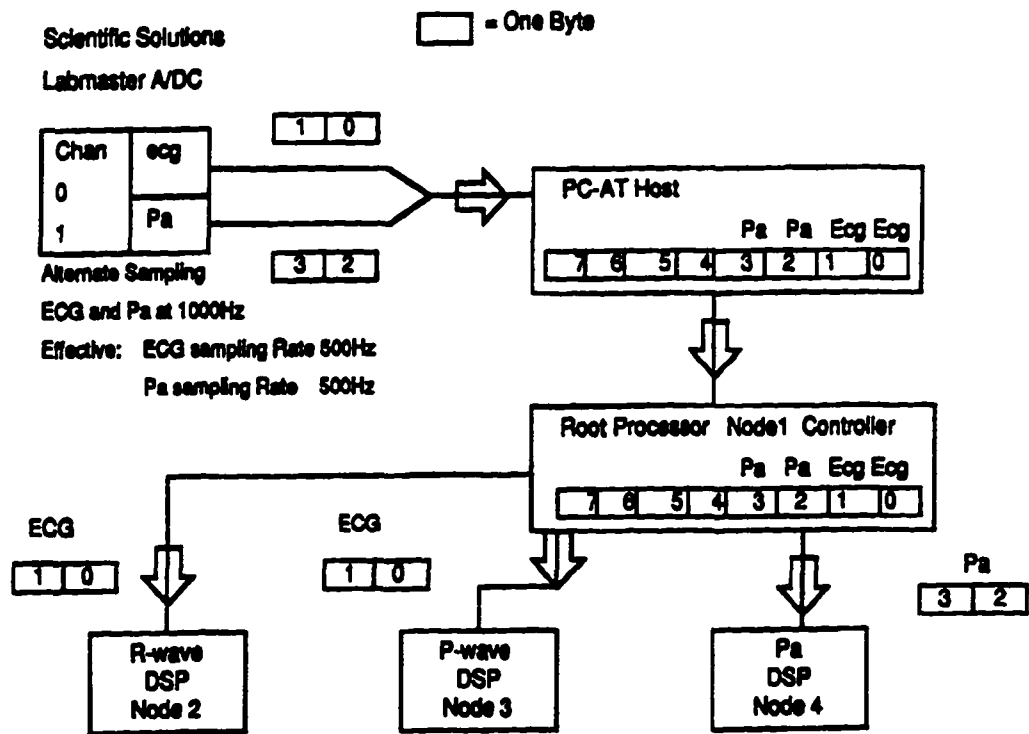
Figure 3-8. Transputer Data Traffic Flow toward the Leaf Nodes

program). The data was then transferred from the host program to the root node of the transputer
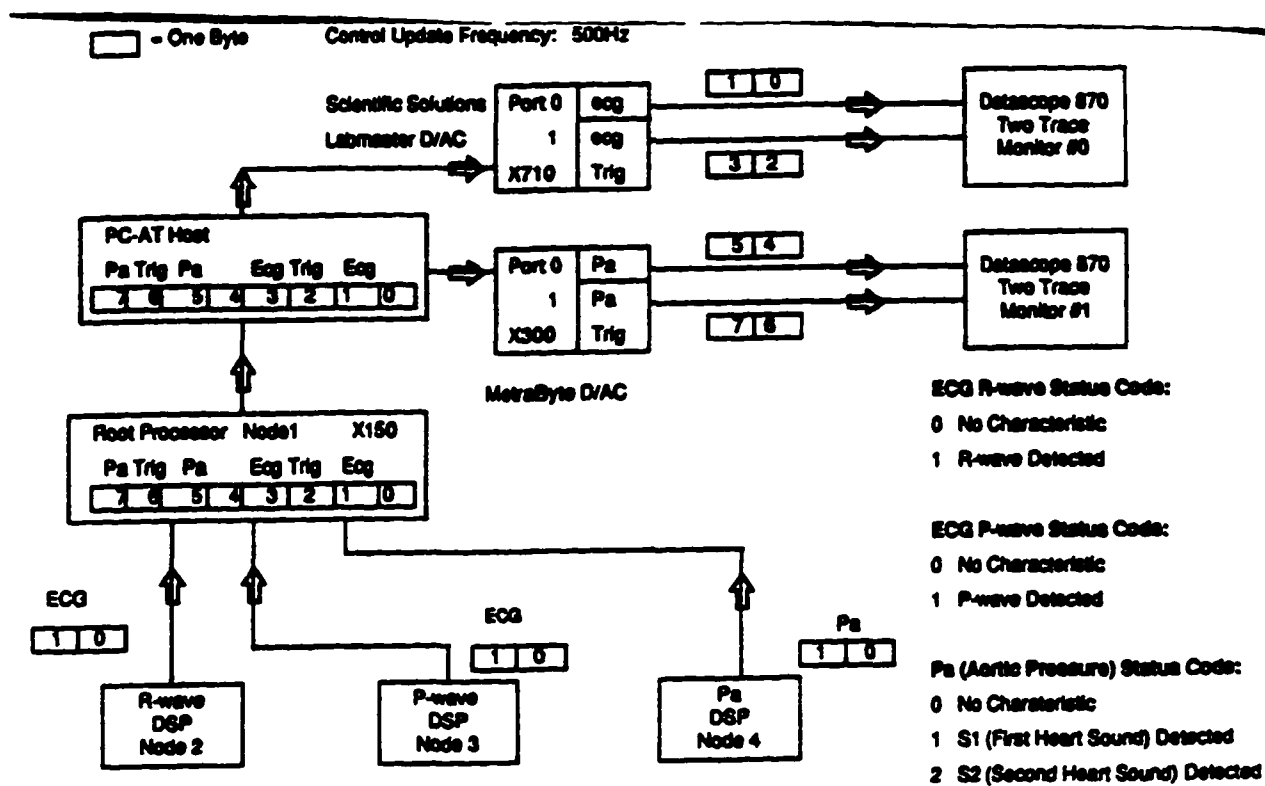
Figure 3-9. Transputer Data Traffic Flow leaving the Leaf Nodes

board and onto the detection RISC leaf nodes, back up to the root node, eventually the host program and out onto the ports of the PC-AT mapped to the D/AC. This was accomplished by rewriting the host program to utilize the transputer primitives (i.e., ChanIn() and ChanOut())

The following test configuration was utilized to demonstrate the maximum throughput of the transputer data. A running total of the data count was printed to the PC-AT screen with a period that would not create any measurable delay (i.e., once per 1000 samples passed). The number on the screen was utilized along with a stop watch to determine the throughput. A Datascope 870 patient monitor was used as further verification that the data being routed through the transputer board was not corrupted in any way as seen in Figure 3-10.

The flow of information proved to be well below the 2 msec upper limit, at 166 microsecond or 8.3% of the processor time. The improvement in Transputer throughput is described in more detail in Chapter 5. Unfortunately, by utilizing host transputer primitives to achieve the necessary data communications efficiency, the ability to write from the root processor to the host programs screen (the PC-screen) was eliminated. Implementation of the multiprocessor system is theoretically
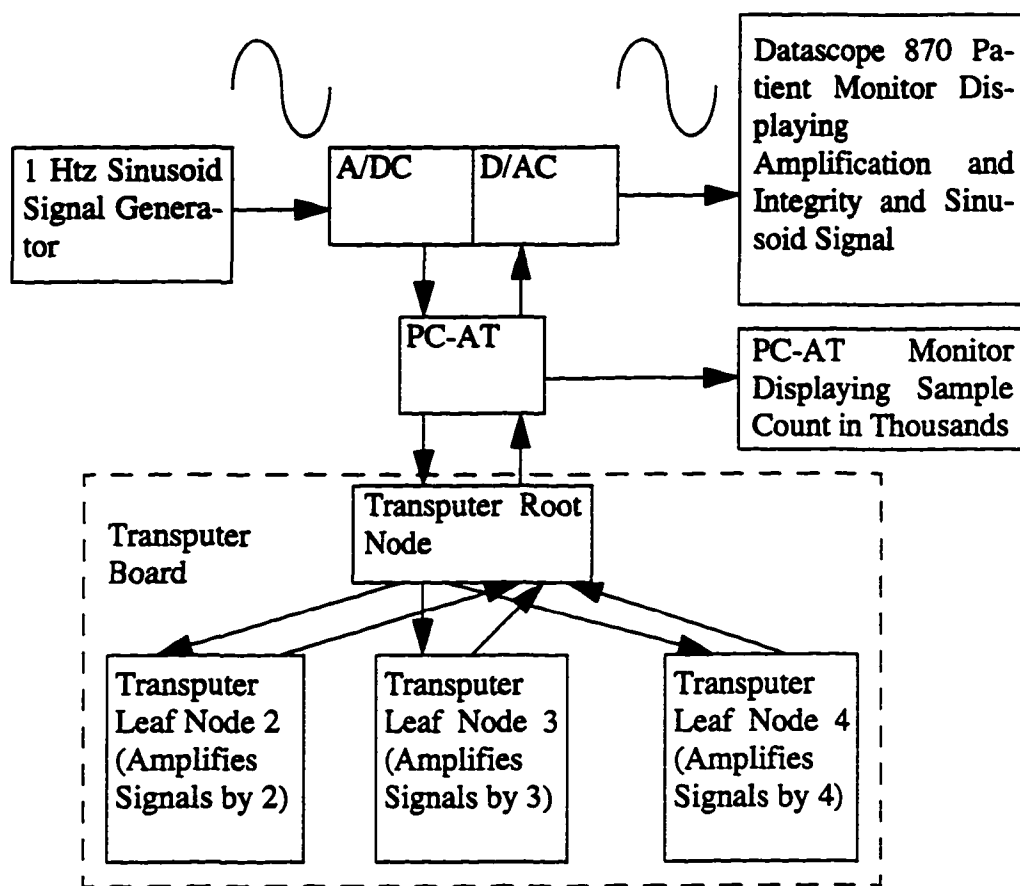
Figure 3-10. Transputer Data Throughput Performance Test Configuration

possible. However this diagnostic limitation severely handicapped the ability to integrate and debug the control system as well as verifying the simultaneous multiple process control system on experimental canine models. Transputer integration and verification of the control algorithm would prove to be a task beyond the scope of a dissertation. Therefore, simulation was deemed as the necessary alternative to demonstrate the robustness of the most complex detection algorithm developed, the Pa detection algorithm.

4. CAD Pa Modeling and Detection Simulation Verification

The developed aortic pressure trigger algorithm is the most important as well as the most sophisticated aspect of the dissertation research completed. The aortic pressure trigger algorithm establishes the timing which is the foundation for Cardiac Assist Device (CAD) control. The established timing allows the control algorithm to maintain synchronization with the cardiac cycle. The systolic rise (onset of systolic ejection) and dicrotic notch (end of systolic ejection) detection algorithms establish this synchronization by reliably detecting their respective events in the ascending aortic pressure signal.

A method to verify the accuracy of the systolic rise and dicrotic notch detection algorithms the dissertation research, the most important aspect of CAD control, was accomplished though simulated experiments.

The proposed goal of my simulation verification research was to develop a simulation platform and demonstrate the robustness of the aortic pressure detection algorithms, namely the systolic rise and dicrotic notch detector. The simulated results along with the experimental results would further verify the ability of the algorithms to accurately detect aortic pressure signals provided by canine experimental models as well as various experimental conditions simulated using a modeling platform. Simulated experimental conditions allow artifacts within the aortic pressure (e.g. changes due to respiration, noise, heart rate variability, etc.) to be controlled nominally. This provides an advantage over canine experimental model conditions in which control of such parameters would be considerably more difficult.

o

4.1 Simulation Approach

The simulation verification was accomplished through a series of research and development steps as seen in Figure 4-1. A simulation package had to be selected. Acclimation to the modeling elements in the simulation package was necessary to build and perform the various simulations. A method had to be devised to synchronize data communications between the modeling elements and detection algorithm. A method also had to be devised to display simulated Pa and respective CAD Pa triggering signals for visual inspection. The development of an aortic pressure model to run continuously in real-time to facilitate a visual method of stability verification with the use of a ECG/ aortic pressure patient monitor would also be desirable. In order to generate the aortic pressure (Pa) simulated waveform, a model for the heart(LV), aorta, aortic valve and the rest of the circulatory system (systemic system) would be necessary. Once the individual models were developed,

verification of the stability (long term simulation results) and integrity (ensure realistic and rationale results) of the heart, aorta, aortic valve and the system models separately would be completed. Integration of the four models in a logical order, one by one, ensuring the stability and integrity of the arterial pressure at strategic points within the model would be performed next. For verification of the Pa detection filters, creation of modeling filters to integrate undesirable Pa artifacts (into the Pa wave) was the last stage of development necessary to "challenge" the Pa detectors. Integration of the previously described simulation platform, Pa trace model, Pa trace biological variation and artifact models, and integration of the Pa detection algorithm provided a research analysis platform that presented various Pa traces to the aortic pressure systolic rise and dicrotic notch detectors.

4.2   Simulation Requirements

In order to demonstrate the robustness of the systolic rise and dicrotic notch aortic pressure detectors, the algorithm must be tested on a select set of Pa biological traces with artifacts observed during cardiothoracic experiments due to canine model variation and experimental impediments. When the simulations are conducted, the simulation results must properly record the detection algorithm results. The method of recording results will depend on the method of systolic rise and dicrotic notch detection implementation. This may involve a third computer running a real-time data acquisition system, a data dump to hard disk for post process printing, selected snap-shots using an oscilloscope camera, or printing selected time intervals using simulation package print feature.

4.3   Simulation Platform

In order to perform the simulation studies to verify the robustness of the aortic pressure trigger algorithm, a simulation platform had to be selected. The criteria for the platform included:

1. PC-based graphical interface
2. Cost effective implementation
3. Simulation result storage and print capabilities
4. Method to integrate software modules developed externally to the platform
5. Ability to import external data and export simulation data to/from a file
6. Real-time simulation and control capabilities

```
┌─────────────────────────────┐
│  Select Simulation Platform  │
└─────────────────────────────┘
              │
              ▼
┌─────────────────────────────┐
│  Develop Interface to Win-   │
│  dows-based VisSim Plat-     │
│  form                        │
└─────────────────────────────┘
              │
              ▼
┌─────────────────────────────┐
│  Port Pa Detection Software  │
│  to Windows DLL              │
└─────────────────────────────┘
              │
              ▼
┌─────────────────────────────┐
│  Develop Pa Trace Model      │
└─────────────────────────────┘
              │
              ▼
┌─────────────────────────────┐
│  Verify Proper Interaction   │
│  Between Pa Detection and    │
│  Simulation Package          │
└─────────────────────────────┘
              │
              ▼
┌─────────────────────────────┐
│  Verify Stability of Pa Model│
└─────────────────────────────┘
              │
              ▼
┌─────────────────────────────┐
│  Develop Pa Artifact Models  │
└─────────────────────────────┘
              │
              ▼
┌─────────────────────────────┐
│  Perform Pa Detection Simu-  │
│  lated Experiments           │
└─────────────────────────────┘
              │
              ▼
┌─────────────────────────────┐
│  Demonstrate Robustness of   │
│  Pa  Detection  Algorithm    │
│  through Simulation Results  │
└─────────────────────────────┘
```

Figure 4-1. Process Steps to Verify Pa Algorithm through Simulation

Of the three evaluated, MatLab, VisSim and Xanalog; VisSim was chosen because its features met most of the requirements. These requirements would be necessary to "import" the logic of over one-thousand (1000) lines of software code programmed in "C" into basic building "blocks" of the VisSim simulation platform. Therefore the import feature of the VisSim package was utilized to

execute the algorithm programmed in "C". Since the VisSim platform was developed on Microsoft

DOS/Windows, the method to import a software block was chosen to be a Windows Dynamic Link

Library (DLL). The DLL software module provides the framework for building a simulation

"block" which can be called from within the Simulation Platform. The DLL capability provides the

functionality to create extensions to the standard VisSim "block" set. This functionality allowed the

C program (i.e. the systolic rise and dicrotic notch detector) to be implemented as a "block" within

model configuration as seen in Figure 4-2[1].
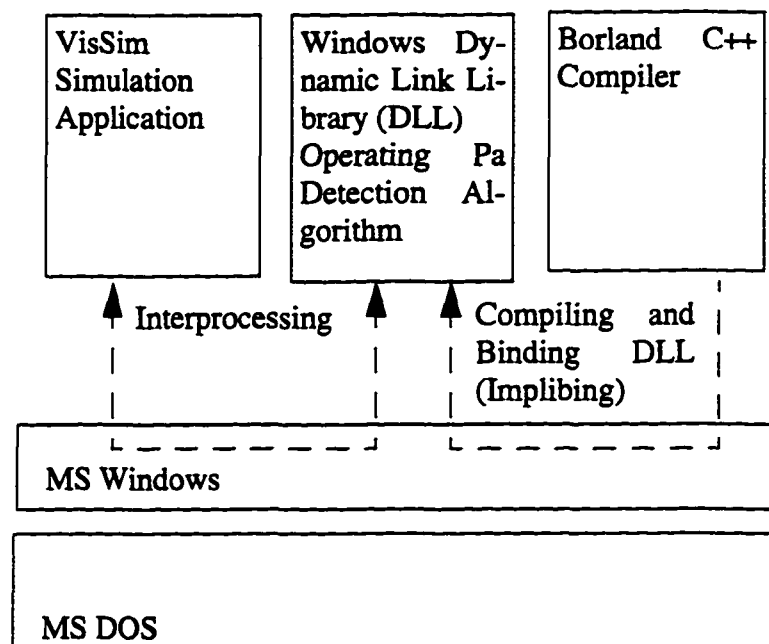
Figure 4-2. Simulation Software Architecture for Creating and Importing Windows DLLs

4.4 Interface to Simulation Package

Implementation of the "C" program into a DLL required two major steps, the development of the

framework for a DLL and the modification of the "C" program detection algorithm into more

manageable functions to interface with the DLL framework.

---

1. Implibing in this Dissertation refers to importing a library to create the MS Windows DLL for third party software (i.e., Visual Solutions Inc., VisSim Simulation Package (49)).

4.4.1 Interface Requirements

The DLL framework included the development of three different files, the VisSim header file, the Borland C++ windows header file, and a main file with PASCAL far exportable functions.

4.4.1.1 Vissim Header File

The main file included methods to import and export variables as well as function calls for the following: import and export variables, initialization for the start of the simulation, end of simulation departure, function to allocate DLL parameters, and a function to initialize the DLL instance. A function is required to specifically initialize a DLL instance for a Windows DLL since Windows functions can be called (e.g. clicked on or selected) more than once.

4.4.2 Borland C++ Compiler Settings

Once the program functions, compiler settings, and definition file setting were determined and programmed, a Borland C++ 3.1 program within the Borland Integrated Development Environment (IDE) could be developed to execute as a DLL within the Microsoft Windows 3.1 based simulation package VisSim. The DLL was created by compiling the resource and source files, binding the resource compiler files to the compiled source module and then marking the module as executable, the initial verification of the software module functionality could be determined by calling the module into the VisSim package. Integrating the DLL into the VisSim package required the external executable block to be placed in the directory corresponding to other internal blocks. Once the test "user function block" DLL was imported into the simulation platform "work area," verification that the DLL framework was functioning properly was determined by conducting a test simulation. Within the software module, the output was programmed to follow the input. After applying a sine wave to the input, a sine wave of equal amplitude was verified on the output during each time interval or "step" during the simulation. A graph block was used to display the input signal presented to the DLL and the output signal emanating from the DLL. Again, the identical graph of both signals demonstrated the proper behavior. This experiment also verified that the DLL was not crashing the VisSim package, at least for this simple DLL. Modification of the DLL sample program to double and full-wave rectify the sinusoid input (after re-compiling and binding the DLL), demonstrated that the DLL framework was functioning properly with the VisSim simulation package as seen in Figure 4-3 and Figure 4-4 (at least for this very terse program).

Plot Block Comparatively Displays
Original Sinusoid as well as Output of
Imported Simulation Block

VisSim Simulation Platform

Internal Sinu-
soid Block

Internal Plot
Block

Imported Exter-
nal Windows
DLL Amplifier
and Rectifier
Block

External
Windows
DLL Block
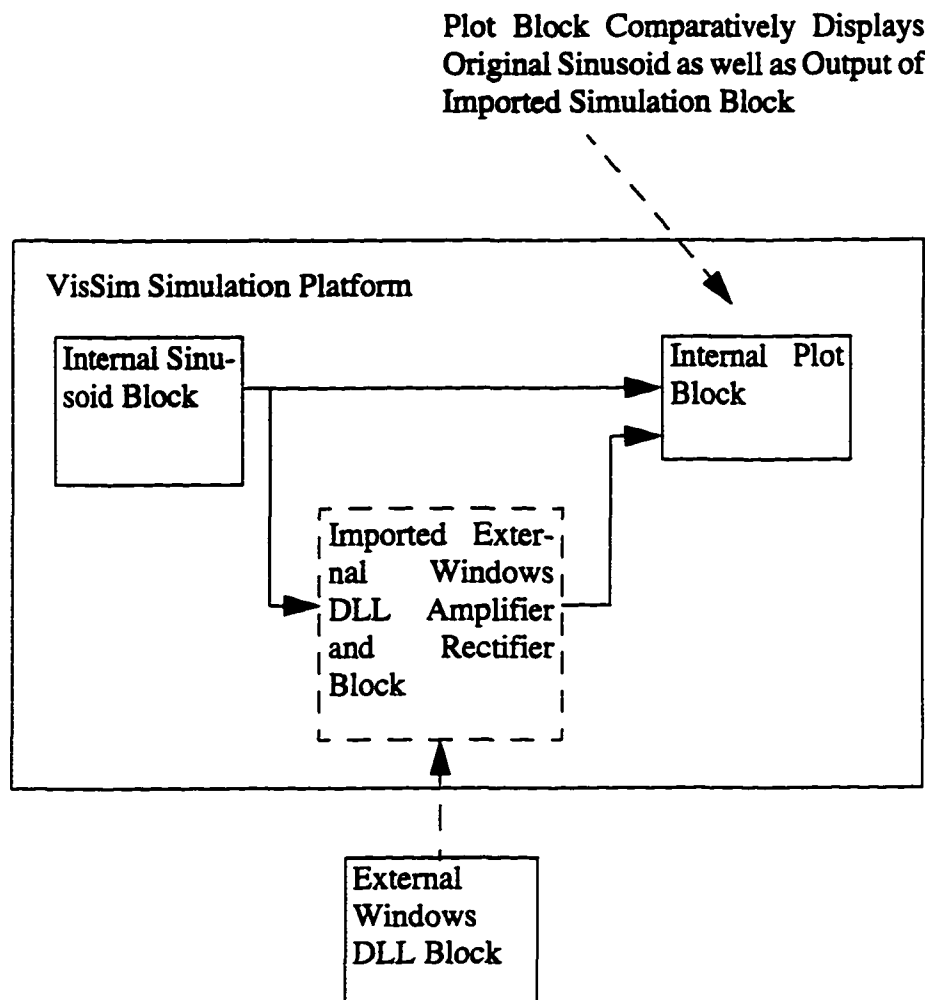
Figure 4-3. Simulation Software Verifying Windows DLLs Functioning as a VisSim Simulation Block

4.4.3 Modification of Pa Detector Software for Simulation

Once the DLL framework was worked out, the Pa real-time detector program had to be modified to integrate into a DLL. Since the software was originally written to execute as efficiently as possible for real-time control, all software algorithms resided within a single function. The reason for this was that in real-time control, functions (i.e. sub functions calls) increase execution time by having to pass variables; and allocate memory for local variables and function overhead. Refer to Section
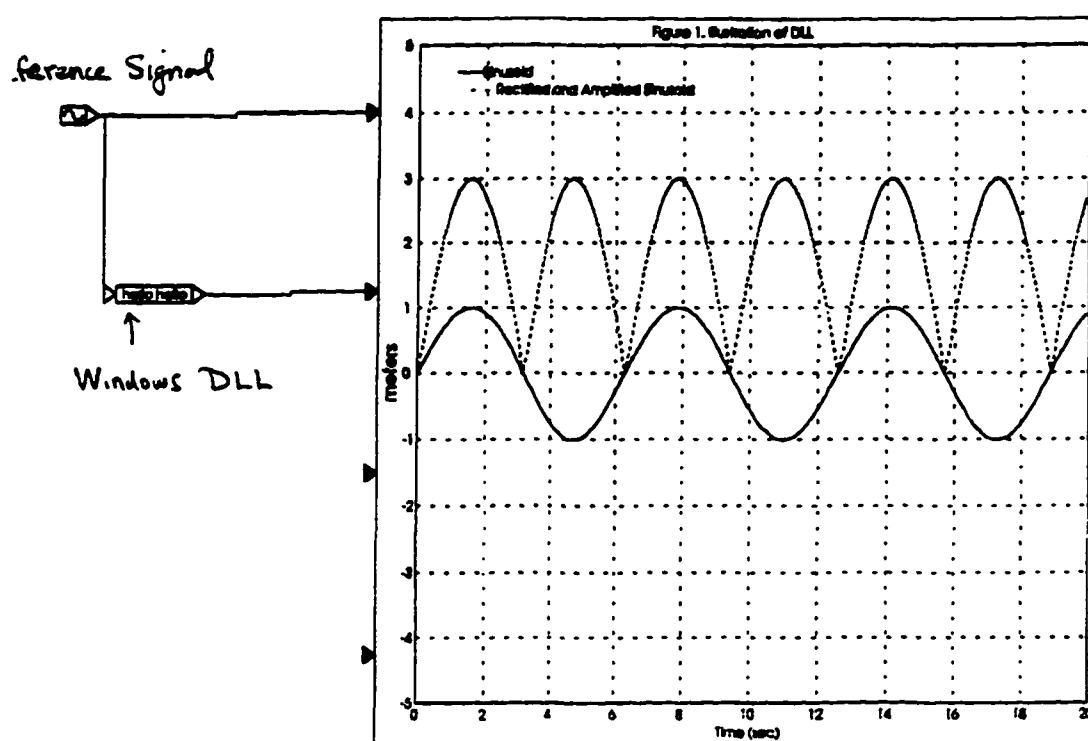
Figure 4-4. Simulation Diagram Verifying Windows DLLs Functioning as a VisSim Simulation Block (Note that Sinusoid is Rectified and Amplified by Three)

2.2. "Pa Systolic Rise and Dicrotic Notch Detection," page 2–41 for further details on the Pa digital filter detection algorithms.

4.4.3.1   Software Partitioning

In order to implement the software on the VisSim platform, the software single function had to be partitioned into several functions. The partitioning of functions would provide a more graceful way of debugging the integration of the software into the DLL one function at a time.

The list of functions included variable initialization, prefilter processing, systolic rise detector, dicrotic notch detector, and Pa waveform characteristic collection, and main function to call all previously listed functions as seen in Figure 4-5. Detection algorithm variables had to be mapped to VisSim input and output signal array variables. In order to ensure that single detection DLL would function error free, each function was verified one by one in a sequence of tests. In order to

perform these tests, a select set of "diagnostic" variables would have to be presented to the output signals of the DLL.

```
┌─────────────────────────────┐
│ Enable Execution of Variable Ini- │
│ tialization Function and Demon- │
│ strate "Rectifier" DLL functioning │
│ properly │
└─────────────────────────────┘
              │
              ▼
┌─────────────────────────────┐
│ Enable Execution Prefilter Process- │
│ ing Function and Demonstrate "Rec- │
│ tifier" DLL functioning properly │
└─────────────────────────────┘
              │
              ▼
┌─────────────────────────────┐
│ Enable Execution of Systolic Rise Detec- │
│ tion Function and Demonstrate "Rectifier" │
│ DLL functioning properly │
└─────────────────────────────┘
              │
              ▼
┌─────────────────────────────┐
│ Enable Execution of Dicrotic Notch Detec- │
│ tion Function and Demonstrate "Rectifier" │
│ DLL functioning properly │
└─────────────────────────────┘
              │
              ▼
┌─────────────────────────────┐
│ Enable Execution of Pa Waveform │
│ Characteristic Collection Function │
│ and Demonstrate "Rectifier" DLL │
│ functioning Properly │
└─────────────────────────────┘
              │
              ▼
┌─────────────────────────────┐
│ Enable Main Function of "Pa" DLL │
│ with Pa Detection Function Variables │
│ Mapped to "Pa" DLL and Demonstrate │
│ all previous Functions noted Executing │
│ Properly and Interacting Properly with │
│ the Simulation Package Software │
└─────────────────────────────┘
```

Figure 4-5. Software Function Verification/Debugging Process Flow

4.4.3.2   Variable Mapping from Pa Detection to Simulation Platform

Of the twenty four signals (24) entering and leaving the Pa detection DLL through the signal array variables, two (2) were input signals and twenty-two (22) were detection and diagnostic output signals. The output variables can be grouped into several categories including information timing and transfer, filter signals, detection signals, and detection filter signals.

4.4.3.2.1   Input Signals

The inputs signals of the systolic rise and dicrotic notch detector DLL were defined as follows:

1. Aortic Pressure Simulation Signal
2. 500 Hz Impulse Train

The input signals presented to the CAD detector consist of the simulated aortic pressure signal and the 500 hertz impulse train. The aortic pressure signal is provided to the CAD detector for digital signal detection processing. The 500 Hz sampling signal is provided to the CAD detector to establish a 500 Hz sampling interval for the simulated aortic pressure wave. This allows the CAD detector digital filter sampling frequency to be isolated from the aortic pressure (Pa) simulation "time step" (or simulation computational interval). (The Euler integration method was utilized because the VisSim package evaluates the DLL block once per time step. All other integration methods evaluate the DLL block more than once per time step.)

4.4.3.2.2   Output Signals

The output signals of the systolic rise and dicrotic notch detector DLL were defined as follows:

1. Simulated Pa Sample Number Processed
2. Aortic Pressure Simulation Signal Received
3. 24 Hz LPF Filtered Data
4. Running Average of Unfiltered Data
5. Rectified Average of the Unfiltered Data
6. First Derivative Window Value
7. First Derivative Ambient Window
8. Second Derivative Window Value
9. Second Derivative Ambient Window

Figure 4-6. Visual Model Configuration illustrating the Pa Detection Algorithm Receiving Input Signals

10. Third Derivative Window Value

11. Third Derivative Ambient Window

12. Second and Third Derivative Window Value

13. Second and Third Derivative Ambient Window

14. S1 Detector Trigger

15. Diastolic Valley Position

16. Diastolic Valley Value

17. Systolic Peak Position

18. Systolic Peak Value

19. S2 Detector Trigger

20. S2 Position

21. S2 Value

22. Autoscale Multiplier

The majority of the output signals were utilized to determine that each functional section of the CAD detector was implemented properly in the CAD detector DLL block as seen in Figure 4-7.
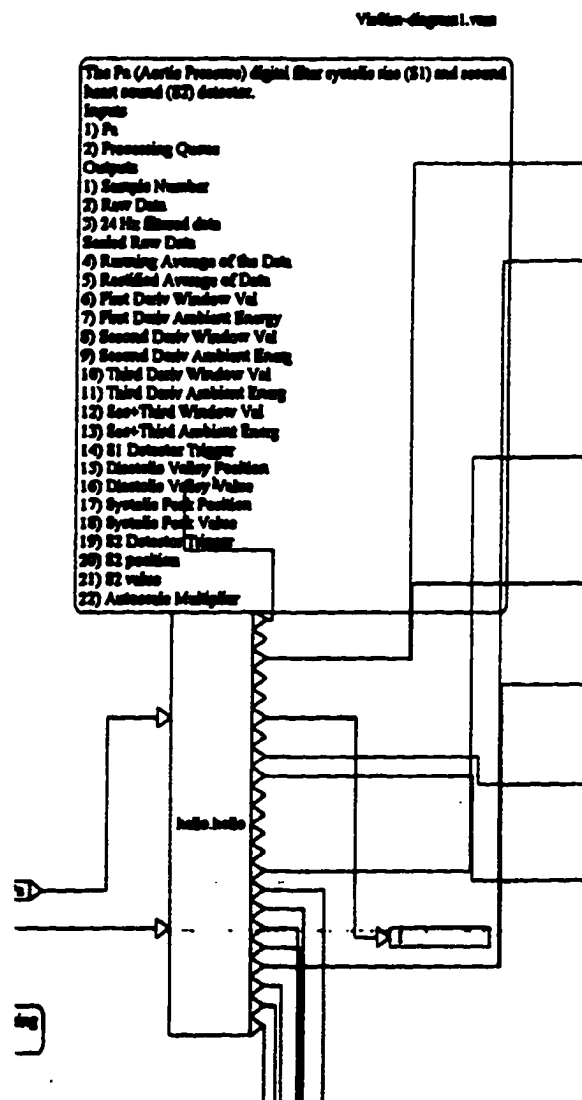
Figure 4-7. Visual Model Configuration illustrating the Pa Detection Algorithm Generating Output Signals

Output signal 1 provides the total of the simulation samples (i.e. time steps) processed. Signal 2 retransmits the aortic pressure signal provided to the DLL. Signal 3 transmits the Pa signal filter by

the 24 Hz low pass filter. Signal 4 provides the running average of unfiltered data. Signal 5 provides the average rectified value of the aortic pressure signal. Signals 6 through 13 are the derivative signals used for detection. The derivative window is compared with the ambient derivative window to determine if there is a substantial increase in the derivative window. The first order derivative is used to detect the systolic rise in aortic pressure. The second, third and a combination of the second and third derivative are utilized to detect the dicrotic notch. Output signal 14 is a detection signal which has a positive slope when detecting the systolic rise. The first negative slope of output signal 14 indicates the detection of the systolic peak pressure and the second negative slope indicates the detection of the dicrotic notch. Signals 15-18 refresh each cardiac cycle with the updated systolic and diastolic extreme pressure and timing position. Output signal 19 illustrates when a dicrotic notch may be detected (i.e. active detection time window) using the derivative techniques. Signal 20 and 21 present updated dicrotic notch pressure and position. Signal 22 provide the value of the autoscale multiplier.

4.4.3.3   Windows DLL and VisSim Interaction Verification

After the set of diagnostic variables were selected and mapped to the output of the DLL, the Pa detection algorithm was verified. A sample sinusoid waveform was presented to the Pa input as well as a 500 Hz sampling timing was presented to the sample/hold input of the Pa detection algorithm. Filters were verified by comparing the input signal to the output of the filter (an algorithm diagnostic variable). The autoscaling multiplier variable was modified from an integer to a real variable to provide more smoothing fidelity in scaling factor.

4.5   Pa and Pa Artifact Model Development

After considering the requirement to test the Pa detector DLL, it was determined that the development of a complete model of the circulatory system to simulate the heart (i.e. left ventricle), aortic valve, systemic system was not necessary because detection verification would only address the detection from pressure at the ascending aorta. This ascending aorta location is where the pressure catheter would be located and not throughout the arterial system.

4.5.1   Pa Model

Investigation into arterial pressure wave shapes led to one that is extremely close to those observed in human patients as seen in far superior to that (in shape as compared to a human Pa trace) provided by canine experimental models. The focus of the Pa modeling aspect of research was focused around simulating the less than ideal patient conditions through wave form distortion. These waveform distortion contributions to the ideal Pa model would simulate non-ideal conditions similar to that observed during experimental model cardiothoracic research.

Figure 4-8. Simulated Aortic Pressure (Pa) Trace Modelling Elements

The development of the aortic pressure simulator to verify the Pa systolic rise and dicrotic notch detector required the development of the ideal Pa trace as well as the additional artifact models which would distort the ideal Pa trace. The integration of the Pa distortion artifacts with the ideal Pa trace can be seen in Figure 4-9.

```
┌─────────────────┐     ┌─────────────────┐
│ Ideal  Pa  Model│     │ Pa  Summing  or │
│ Signal          │────▶│ Multiplier  Junc-│
│                 │     │ tion   Dependent│
│                 │     │ Upon   Distortion│        ▶
└─────────────────┘     │ Type            │    Pa Signal with
                        │                 │────▶  Artifacts
┌─────────────────┐     │                 │
│ Pa    Distortion│     │                 │
│ Model           │────▶│                 │
│                 │     │                 │
└─────────────────┘     └─────────────────┘
```

Figure 4-9. Integration of Pa Distortion Artifacts and Ideal Pa Trace

The ideal aortic pressure trace simulator was developed by combining three different wave shapes including a half wave rectified sinusoid, sawtooth wave and an inverted half wave rectified sinusoid. The difference equation of the sawtooth wave generator was modelled after the following differential equation.

$$y = (4/3)(t - dy/dt) \tag{4-1}$$

The combination of the halfwave rectified sinusoid and the sawtooth wave together form the basis for systolic and diastolic pressure. The sharp systolic rise (i.e. the end of diastole and the start of systole) is created by a combination of both these waves rising simultaneously. The transition from systole to diastole is simulated by the end of the halfwave rectified sinusoid contribution. The saw tooth wave continues to contribute to the wave by simulating the damped discharge of aortic pressure within the aorta as seen in Figure 4-10.

4.5.1.1   Pa Dicrotic Notch

The dicrotic notch is simulated by a high frequency half wave inverted sinusoid timed to contribute a depression precisely where systole ends.

In order to facilitate the dicrotic notch to occur within the aortic pressure wave just prior to the change in Pa slope due to the end of the contribution of the half wave sinusoid, the sinusoid frequency which forms the dicrotic notch depression was chosen to be a multiple of the heartbeat frequency. The heart beat sinusoid is supplied to the dicrotic notch sub block fed through a zero crossing detector, inverted and then clipped to provide a pulse only during the negative slope zero

Aotic Pressure Simulator

Graph axes: vertical axis values 110, 100, 90, 80, 70, 60, 50, 40, 30, 20, 10, 0, -10. Horizontal axis "Time (sec)" with values 0, .25, .5, .75, 1, 1.25, 1.5, 1.75, 2, 2.25, 2.5, 2.

Legend: Damped Sinusoid, Half Wave Rectified Sinusoid, Dicrotic Notch Half Sinusoid, Composite Aortic Pressure Signal
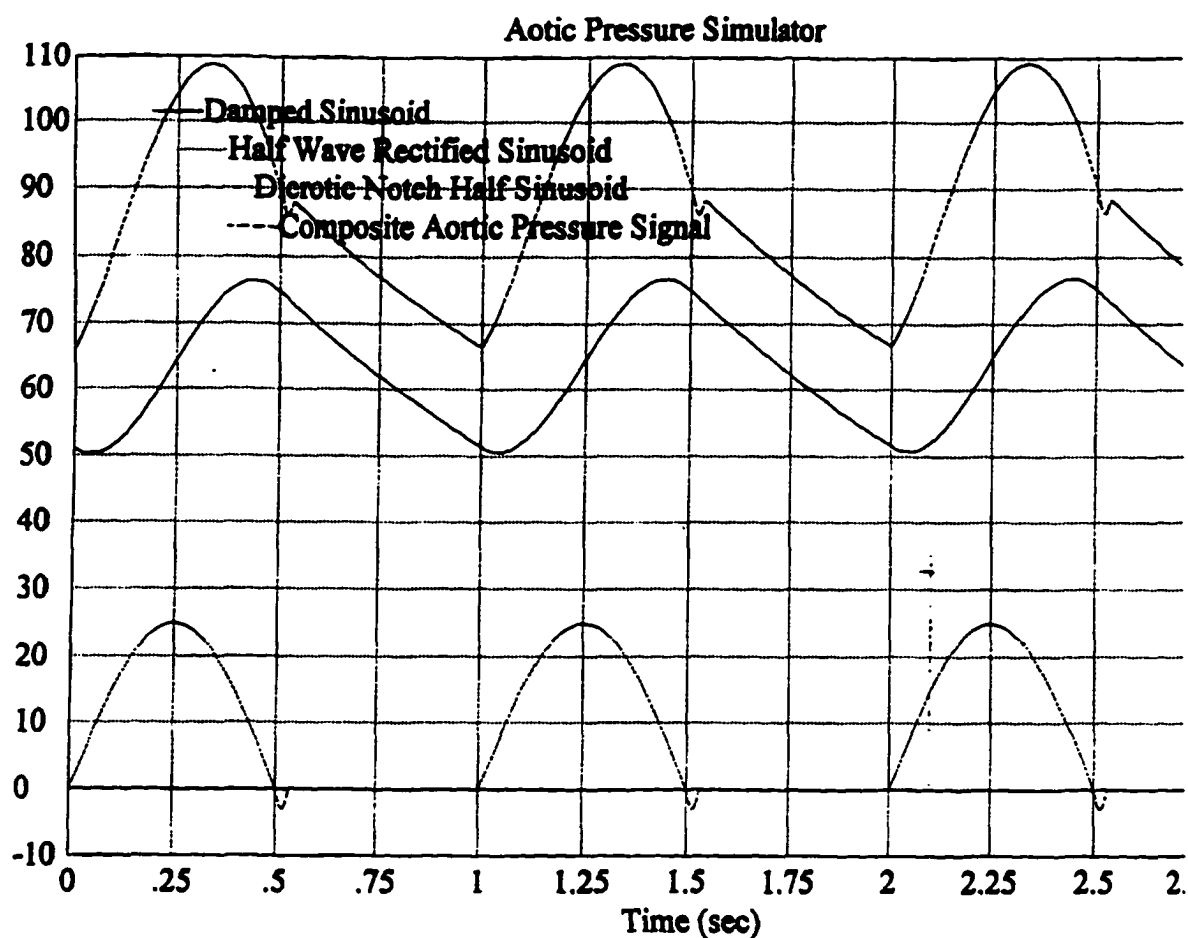
Figure 4-10. Combined Wave Shapes that Constitute the Ideal Pa Trace

crossing. The same processing is performed on the high frequency sinusoid providing the dicrotic notch. When both timing signals are present, the negative contribution due to the inverted half cycle is combined with the aortic pressure wave to create the dicrotic notch depression as seen in Figure 4-11.
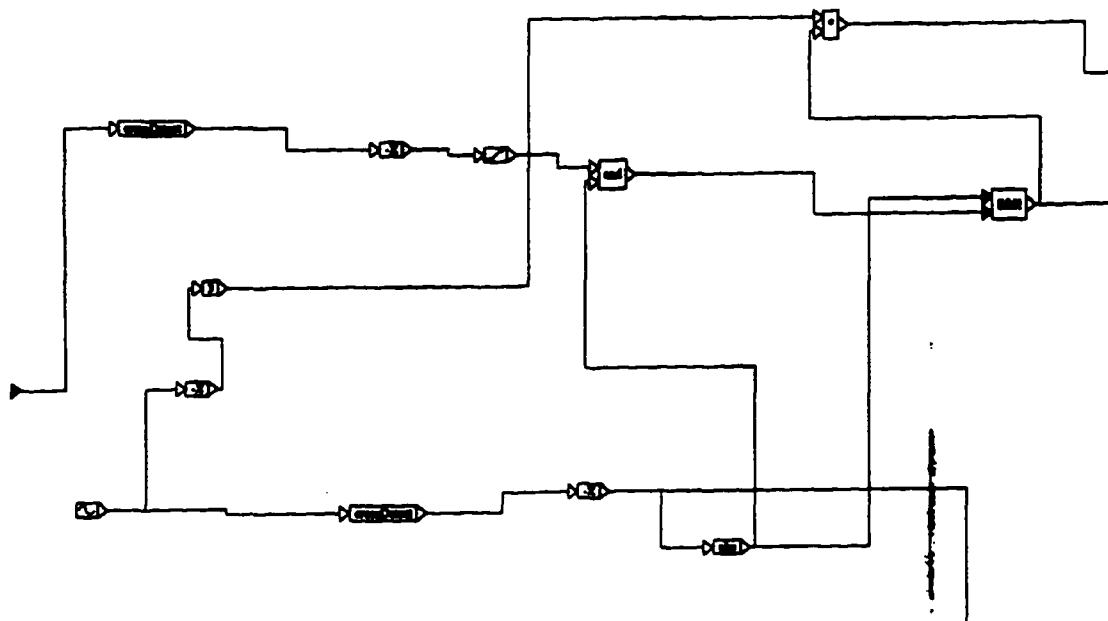
Figure 4-11. Diagram of Simulation Blocks that Generate the Dicrotic Notch

4.5.1.2 Pa Model Transformation to Mimic A/DC Digital Values

The aortic pressure wave[1] is amplified and shifted to create a systolic to diastolic difference of 200 ranging between 900 and 1100 to simulate the associated deflection of a millar pressure catheter[2] introduced to a 12 bit resolution analog to digital converter as seen in Equation 4-2.

$$\text{A/DC Pa Value [nT]} = (\text{Ideal Aortic Pressure[nT]} -80) * 5 + 900 \qquad (4\text{-}2)$$

4.5.2 Pa Biological Variation and Artifact Models

Pa Biological Variation and Artifact Models were constructed for the following variations in Pa:

1. Long term simulation to determine stability of the Pa model for the Pa Biological Variation and Artifact Models

2. Lack of Dicrotic Notch Deflection

3. Mechanical Ventilation

4. Pa Transducer Position or Sensitivity

---

1. The values of the ideal aortic pressure range from diastolic (80 mmHg) to systolic (120 mmHg).

2. The range of numerical values between 900 to 1100 was typically observed during canine mongrel experimental model studies in which a Millar catheter pressure transducer was received by a patient monitor and then transmitted to the A/DC PC-AT card. In order to simulate the same type of numerical excursion observed within a Cardiothoracic surgical operating environment, the simulated Pa trace numbers were modified through a first order equation, i.e., y = mx +b.

5. Uniformly Distributed Noise

6. Gaussian Distributed Noise

7. Heart Rate Variability Due to Respiration

The type of Pa biological variation and artifact model developed was dependent upon on the type of simulated variation or disturbance to be imposed on the ideal Pa trace. The following sections describe how the Pa disturbances were modelled within the simulation experiments.

4.5.2.1 Long Term Simulation to Determine Stability of the Pa Model for the Pa Artifact Models

In order to ensure the Pa model was stable and that no subtle drift was occurring during the simulations, a long term simulation was configured for execution. A simulation lasting 600 simulated seconds (10 minutes) would provide a way of determining if the model was stable. The simulation start and end parameters were set at 0 and 600 seconds respectively. Of important note was the bug found within the impulse simulation block. The impulse generator stopped generating impulses after approximately 6 minutes (6 minutes * 60 seconds * 500 samples) or 180,000 impulses. The bug was verified by VisSim and an update version of the software was provided with the bug fixed.

4.5.2.2 Missing Dicrotic Notch Deflection

The model for the missing dicrotic notch was created by breaking the connection between the dicrotic notch generator and the Pa systolic-diastolic generator. Figure 4-12 illustrates the simulation block configuration for generating the Pa trace without a dicrotic notch.

4.5.2.3 Mechanical Ventilation (MV)

When simulating the aortic pressure variation due to mechanical ventilation (MV) the slow variation in Pa baseline is imposed with the addition of a sinusoid wave form. The sinusoid waveform must be properly scaled in frequency and amplitude domain to address a typical experimental model breath rate (i.e. 12 breaths per minute) and the appropriate deflection due to the intra-thoracic pressure (i.e. 10, 20 or 40 mmHg deflection in Pa) as seen in Equation 4-3. The mechanical ventilation pressure variation artifact is created by generating the appropriate sinusoid of amplitude and frequency with a sinusoid block and integrating the pressure variation using an adder block into the ideal pressure waveform as see in Figure 4-13.
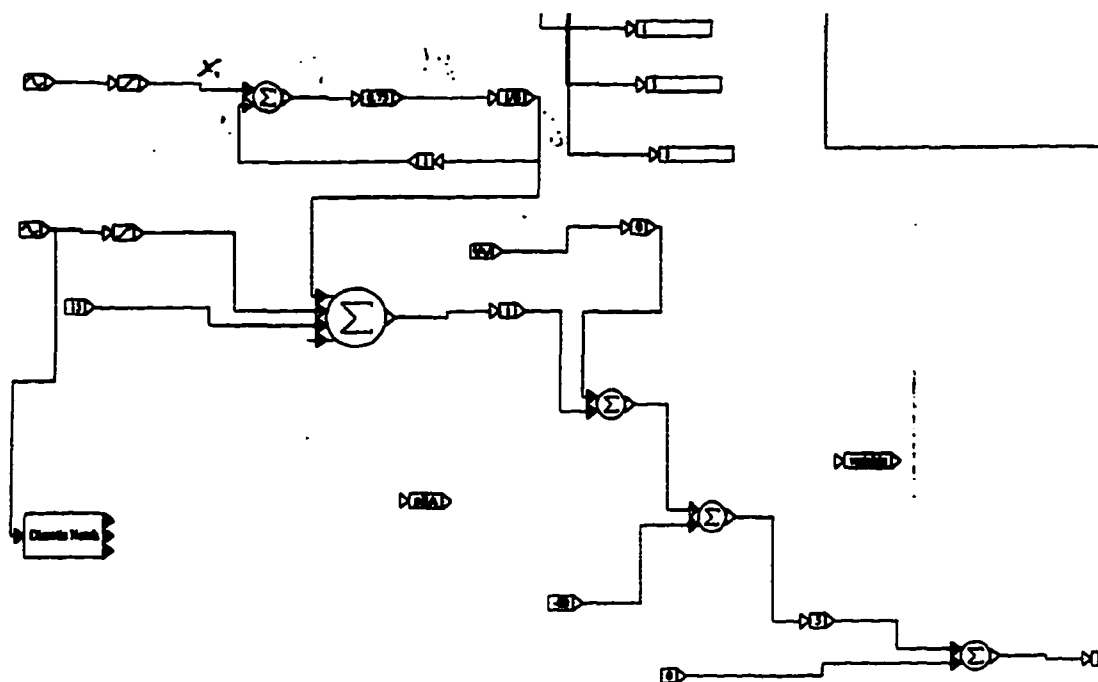
Figure 4-12. Simulation Block Configuration for Pa Trace without Dicrotic Notch Deflection

$$AV(10/20/40mmHg) = 50/100/200 * Sin [(75.24 \text{ rad }/min) * 500Hz *nT] \qquad (4\text{-}3)$$
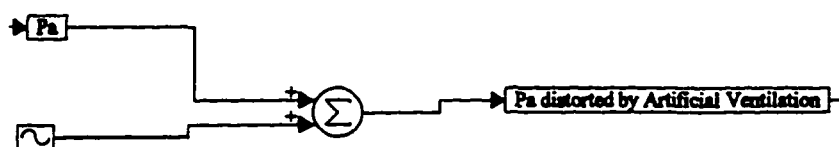
Figure 4-13. Simulation Block Configuration for Pa Trace with Pa Baseline Deflection due to Mechanical Ventilation

4.5.2.4 Change in Pa Transducer Position or Sensitivity

When simulating changes due to variations in Aortic Pressure Amplitude (APA) due to changes in transducer sensitivity or positioning the ideal Pa wave form must be modified using a sinusoidally driven scaling factor. Again, the sinusoid must be properly scaled in the frequency and amplitude domain to address a typical experimental model variation in scaling. The variations in transducer

sensitivity are due to change in catheter positioning within the ascending aorta or blood coagulation on the catheter tip.

The APA sinusoid was driven at 0.2 hertz (one cycle every 5 seconds) and the amplitude was varied between 100% to 200% of its ideal amplitude as seen in Equation 4-4 where the amplitude ranges from 0.667 to 1.333. The pressure variation due to changes in transducer sensitivity or positioning artifact is created by generating the appropriate sinusoid of amplitude and frequency with a sinusoid block and scaling the ideal pressure waveform using a multiplier block with the sinusoid and the ideal pressure waveform as inputs as seen in Figure 4-14.

$$\text{APA Scaling Factor} = 1.0 + 0.333 * \text{Sin} [(1.254 \text{ rad /sec}) * 500\text{Hz} * nT] \qquad (4\text{-}4)$$
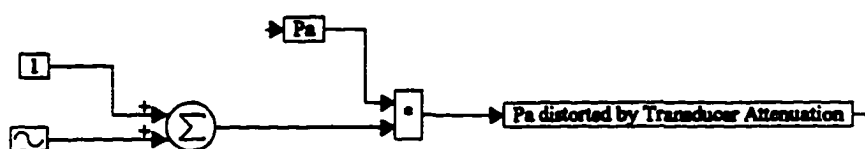
Figure 4-14. Simulation Block Configuration for Pa Trace with Pa Amplitude Variation due to change in Transducer Position or Sensitivity

4.5.2.5 Uniformly and Gaussian Distributed Noise

When simulating changes due to variations in aortic pressure amplitude due to contributions of noise, the ideal Pa wave form must be modified using a uniformly distributed and a Gaussian random noise source as described in Equation 4-5 and Equation 4-6, respectively. The noise source must be properly scaled and added to the ideal Pa wave. Noise contributions may come from several sources within the cardiothoracic experimental model environment including 60Hz noise, electrocautery, and acoustical noise due to vibrations introduced through the pressure catheter transducer. The uniformly and Gaussian distributed pressure variation artifact simulate these types of experimental noise. The uniformly distributed noise source has a mean of 1/2 mmHg and a standard deviation of 0.289 mmHg. This noise level was generated by multiplying the uniformly distributed random noise block (mean=5/2 simulation units and variance = 25/12 simulation units^2) by the mmHg to simulation unit ratio (i.e., 1.0 mmHg/ 5.0 simulation units). The Gaussian (or normal) distributed noise source has a mean of zero mmHg and a standard deviation of 0.6 mmHg.

This noise level was generated by multiplying the Gaussian random noise block (mean=0 and variance = 1 simulation units^2) by the mmHg to simulation unit ratio (i.e., 1.0 mmHg/ 5.0 simulation units).The noise distortion to the ideal pressure wave are created by generating the noise source with appropriate simulation block (i.e. uniformly or Gaussian distributed). The noise contribution is integrated into the ideal pressure waveform using an adder block as seen in Figure 4-15.

(4-5)

$$\text{UniformDistributionRandomVar}(x) = \frac{1}{x_2 - x_1} \qquad x_1 \leq x \leq x_2$$

$$= 0 \qquad \text{Otherwise}$$

$$x_1 = 0 \qquad x_2 = 2 \qquad \begin{array}{l} \eta(\text{mean}) = 1/2\text{mmHg} \\ \sigma^2(\text{variance}) = 1/12\text{mmHg}^2 \end{array}$$

(4-6)

$$f(x) = \frac{1}{\sigma \cdot \sqrt{2 \cdot \Pi}} \cdot e^{-(x-\eta)^2/(2 \cdot \sigma^2)} \qquad \text{for} \qquad -\infty \leq x \leq \infty$$

$$\eta(\text{mean}) = 0 \qquad \sigma^2(\text{variance}) = 9/25\text{mmHg}^2$$
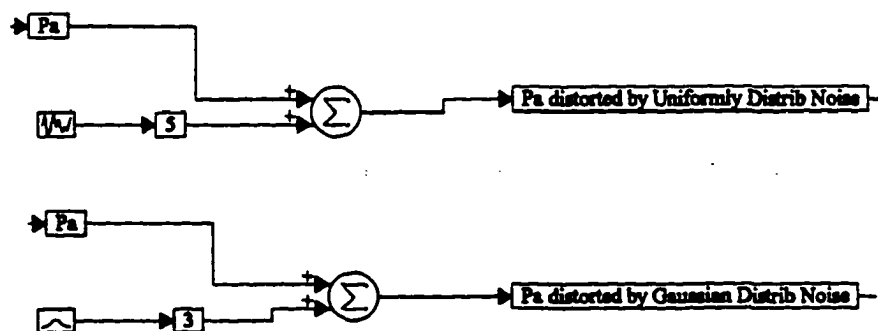
Figure 4-15. Simulation Block Configuration for Pa Trace with Pa Amplitude Variation due to Contributions of Uniformly and Gaussian Distributed Noise

4.5.2.6 Heart Rate Variability Due to Respiration

The purpose of the simulation was to illustrate the systolic rise and dicrotic notch filters detecting accurately during heart rate variability due to respiration. The method to simulate Pa heart rate variation due to respiration differed from the Pa during other disturbances. The variation in the Pa trace could not be imposed with a VisSim simulation arithmetic block (i.e., adder or summer). The variation had to occur to the fundamental sinusoid of the Pa trace. A method within the VisSim simulation package to vary the frequency of the sinusoid was not available. In order to work around this limitation, a method of oversampling the data was used. The simulation "step size" was decreased to create a set of data that was oversampled. The oversampled data was stored in a file using the Signal Consumption "export" block. A "C" program was then used to sample the data with a varying frequency to simulate a change in heart rate as seen in Equation 4-7 through Equation 4-11.

Pa Detection software was designed to receive Pa signal sampled at the following frequency:

$$f_{s\_Pa\_detection\_filter} = 500 \text{ samples/sec} \tag{4-7}$$

The 60 bpm Pa signal was oversampled at the following rate:

$$f_{s\text{-oversampling}} = 3000 \text{ samples/sec for Pa waveshape hr=60bpm} \tag{4-8}$$

To achieve a simulated heart rate = 60bpm for the 500Hz-based Pa detection filter, the oversampled wave must be selectively sampled as follows:

$$\tag{4-9}$$

$$fsOverSampledWaveFor60bpm = \frac{3000hz}{60bpm} \times \frac{1NewSample}{6OldOverSampled} = \frac{500Hz}{60bpm}$$

To achieve a simulated heart rate of 80bpm for the 500Hz-based Pa detection filter, the oversampled wave must be selectively sampled as follows:

$$\tag{4-10}$$

$$fsOverSampledWaveFor80bpm = \frac{3000hz}{60bpm} \times \frac{1NewSample}{8OldOverSampled} = \frac{500Hz}{80bpm}$$

The software equation that provided the selective sampling interval (i.e. varying between every 6th to 8th sample) to provide the varying heart rate is as follows:

$$\text{SampleFreqPerSimStep} = \text{ceil}^1(6.5 - 1 * \sin((nT+1) * 2 * 3.14/ (4.0 * 3000))) \qquad (4\text{-}11)$$

The modified data within the new file was then used as data for the simulation. The data was introduced to the Pa algorithm within the simulation platform using the Signal Producer "import" block. The methodology to perform the hear rate variability simulation is illustrated in Figure 4-16.

The simulation was designed for the heart rate of the model to cycle between 60 beats per minute (bpm) and 80 bpm every four seconds (15 breaths per minute). The model is illustrated in Figure 4-17. The change in heart rate due to respiration is exaggerated to more effectively illustrate the phenomenon and to further challenge the detection algorithms.

---

1. The "ceil"ing function provided an integer value approximation based on the total of the constant and the sinusoid.

Generate Over Sampled Data by a Factor of 6. (3000 Samples per Second instead of 500 for all other simulations)

Store Over Sampled Data in File Using Export Block Function

Write "C" Program to Selectively Choose Samples to Vary Heart Rate Between 60 and 80 Beats per Minute and Store Pa Trace in a Different Data File

Open Data File in Word Processor and Cut and Paste Sections of Undistorted Data (Data Distorted After Approximately 16 Seconds of Simulation due to Bug in Simulation Package

Configure Pa Detection Algorithm DL to Receive Data Utilizing the Import Data Block Display Results to Plot Block for Data Stability and Detection Verification

Figure 4-16. Methodology for Heart Rate Variability Simulation due to Respiration

Figure 4-17. Simulation Block Configuration for Pa Trace with Heart Rate Variation due to Respiration

5. Canine Mongrel Experimental Model Procedure and Results

This chapter discusses the experimental procedures and experimental results for the research conducted in this dissertation paper, namely, CAD control canine mongrel experimental model research. Section 5.1 discusses canine mongrel experimental model CAD detection and CAD control results. Section 5.2 describes the results of the quad-transputer (multiprocessor) research. Section 5.3 documents the research examining the heart rate (HR) to systolic time interval (STI) relationship for canine mongrel experimental models for the purpose of inflation prediction during canine mongrel experimental model ectopic rhythms.

5.1 Canine Mongrel Experimental Model Procedure and Results

Cardiothoracic Research utilizing canine mongrel experimental models for the advancement of Cardiac Assist Device Research involves a rigorous surgical preparation and CAD electronic and pneumatic equipment to perform complicated experiments in which the experimental model is exposed to surgical conditions typical to patients undergoing life saving pre- and postoperative heart surgery. Section 5.1.1 describes the experimental procedures followed in order to perform CAD experimental research. The results of the experiments are summarized in Section 5.1.2. The results of the experimental research is described in Section 5.1.3.

5.1.1 Experimental Model, Materials, Equipment and Procedure

The configuration for experiments with canine experimental models included four major stations. The first station was the PC-based CAD controller station (with A/DC an D/AC) which received the cardiac signal (Pa or ECG from the pressure transducer catheter or patient monitor respectively depending on the experiment) and generated the CAD control information to be sent to the pneumatic driver station. The pneumatic driver, the second station, was a Datascope System 83 Intraaortic Balloon Pump system modified to be utilized as a pneumatic driver for the experiments. Upon signaling from the CAD controller the pneumatic driver would inflate or deflate the CAD (IAB or EACD depending on the experiment) located within the experimental model surgical area (i.e., the third station). The experimental model station consisted of an anesthetized canine mongrel fastened in a supine (for IABP experiments) or right decubitous (for EACD experiments) position on a pediatric operating table. Appropriate surgical measures were taken to position (IABP) or attach (EACD) the CAD within or to the experimental canine model's aorta. Necessary instruments were surgically or otherwise fastened to the canine model to provide experimental control signals.

The control signals included ECG which was provided via ECG monitor with three alligator clip leads fastened in an Einthoven triangle configuration and Pa which was provided via a Millar pressure catheter inserted into the right femoral artery up to the ascending aorta. The experimental model station included a signal junction box that provided a means to connect to the data acquisition system. The data acquisition system, the fourth station, allowed "experimental runs" to be recorded during the experiments to capture Pa, ECG and solenoid timing (CAD pneumatic driver) signals.

5.1.1.1   CAD Controller Station Experimental Equipment

The following equipment was used for CAD Controller Station of the canine mongrel experiments (Refer to Figure 2-1 for illustration of experimental configuration):

1. FM Tape Recorder - Honeywell 5600

    1. FM Tapes - Scotch 10.5 inch reels, 0.5 inch magnetic tapes to record PA and ECG Signal of mongrel dogs),

2. PC-AT 25/33Mhz 64Kb Cache 80387 - Datatech Enterprises Co., Ltd. DTK PEM2501/3301 (Controller Computer),

3. Two Trace Monitor - Datascope 870.

5.1.1.2   Pneumatic Driver, Experimental Model, and Data Acquisition Stations

The equipment used for Pneumatic Driver, Experimental Model Surgical and Data Acquisition Stations of the canine mongrel experiments are illustrated in Figure 2-1.

5.1.1.3   CAD Canine Mongrel Experimental Configuration

The CAD canine mongrel experimental stations were positioned in two different rooms due to limitations of floor space within the Cornell University Medical College (CUMC) Cardiothoracic Research lab.

1. Pneumatic Driver, Experimental Model Surgical, and Data Acquisition stations were located in "Room A" (CUMC Room A-829),

2. The CAD Controller station was located in "Room B" (CUMC Room A-831).

5.1.2 Experimental Log

The experimental log was compiled to note the progress of the advancing research experiments conducted utilizing canine mongrel experimental models. Each experiment was conducted to establish or refine an area of CAD detection and control research.

Initial experiments demonstrated cardiac assist device control using the two different control signals, aortic pressure and ECG separately. The Pa control algorithm demonstrated augmentation using an intra-aortic balloon (IAB) and an extra-aortic counterpulsation device (EACD). The ECG control algorithm also demonstrated augmentation utilizing the IAB. Twenty-nine experiments, using canine experimental models, were performed in order to finalize the development of the aortic pressure and ECG detection algorithms and aortic pressure and ECG control algorithms.

The first experiment (experiment 0A/B) was performed on a canine being exsanguinated. (Each experiment was performed on a different experimental canine model.) This first experiment demonstrated that the Pa control trigger algorithm properly tracked cardiac cycle events during an experiment as well as verifying the control signal were being properly received by the CAD controller station. Experiments 1 and 2 were performed to remove gross and fine phasing errors between the Pa CAD control algorithm and the experimental model. The third experiment demonstrated the Pa CAD control algorithm augmenting the experimental model Pa with an IAB. Experiments 4 through 6 were used to correct a problem associated with large Pa augmentation in which the control algorithm was triggering on the rise of the augmentation. Experiment 7 demonstrated the IAB being controlled by an ECG CAD control signal. Experiments 8 through 12 were conducted to further refine the Pa control algorithm for the IABP as well as to perform initial experiments on the EACD CAD with Pa control. Experiment 13 demonstrated the EACD being controlled by the CAD controller with the use of the Pa signal. The Pa augmentation due to the EACD was considerably more pronounced than the IAB due to the method of cardiac assistance. The IAB utilized displacement of volume within the aorta while the EACD utilizes a piston-cylinder type action which provided more pronounced augmentation results and thus hemodynamic benefits.

Experiments 14-18 were performed to develop a heart rate to systolic time interval regression equation for predicting the dicrotic notch in the event of an ectopic beat. Prediction of the dicrotic notch provided an optimal inflation time for the CAD. Experiments verified that a heart rate to systolic time interval regression equation relationship present in humans was not present in canines particularly when the canine models were treated with beta-blockers.

Experiment 19 demonstrated the control algorithm tracking quick variations in heart rate. The changes in heart rate were performed with an adjustable pacemaker system. Experiments 20-25 were performed to adjust the CAD controller to account for the inflation delay time and deflation delay time. Experiment 26 demonstrated the CAD control algorithm properly tracking the cardiac cycle and augmenting Pa during both cut and coagulate mode of the electrocautery performed with a Valley Lab Cauterizer. This CAD Pa control immunity to electrocautery noise is particularly important to fault tolerant CAD control. In this surgical situation, the ECG is not a viable control signal because electrocautery electrical interference eliminates the possibility of deriving the ECG.

Experiments 27-29 focused on deflation timing CAD control adjustments. The end of augmentation had to be determined to adjust deflation. The lowest point of the augmentation droop occurred as systole begins. This timing allowed the mean root aortic impedance to be minimized as the heart's aortic valve opens.

Table 5-1. Canine Mongrel CAD Experimental Log

Exp #	Exp Date	Experimental Purpose/Observation
0A	10/30/91	Exsanguination /Triggering On Live Pa Data #1
0B	10/31/91	Triggering On Live PA Data #2
1	11/1/91	Check Instrumentation Set Up /Test IABP Pa Trigger Test
2	11/5/91	Fix Gross PA Phase Errors /Observe Fine Phase Errors
3	11/6/91	Fix Fine PA Phase Errors /IABP PA Control Working
4	11/21/91	Worked on PA Inflation-Deflation Delay Times, Record Data
5	12/13/91	Test Pumping on Observation Beats, Test PVC Detection
6	12/19/91	Exam Double Phasing Problem, Test ECG Triggering
7	12/20/91	Work on PA Double Phasing Problem /IABP ECG Control Working
8	12/23/91	Test Pa EACD/ Large Augmentation - observe phase problem
9	1/2/92	Test Pa PVC Determine/Eliminate Most of Double Phasing Problems
10	1/9/92	Test Pa Optimal Timing/ Observed Pumping Too Long
11	1/14/92	Test Pa EACD/ Late and Elongated Inflation Causing Problems

Table 5-1. Canine Mongrel CAD Experimental Log

Exp #	Exp Date	Experimental Purpose/Observation
12	1/16/92	Test Pa Opt Tim/ Pumping Too Long cause Pos Feedback/ Need To Adjust Calibrate Pump Timing
13	1/21/92	Test Pa EACD Triggering /EACD Pa Control Working
14	1/28/92	Worked on Inflation/Deflation Times
15	2/11/92	Worked on Inflation/Deflation Times, HR-STI Regression Data, Ring in Pa
16	2/12/92	Worked on Double Phasing Problem
17	2/13/92	Worked on Triggering For Exp With Ring in Pa
18	2/19/92	Test Augmentation Sensing, HR-STI Regression Data
19	3/5/92	Work on Opt Deflation timing, Test Pa algorithm ability to track changing Heart Rates
20	3/10/92	Test New Augmentation Detection Area Technique/ Test Ectopic Beat Algorithm For S2 Prediction i.e. Inflation
21	3/12/92	Test Optimal Deflation timing, Aug Detector, IDT/DDT
22	3/17/92	Test Algorithm in very low pressure, Aug Detector
23	4/2/92	Adjust Opt Deflation Timing, Aug Detector/ Adjust Ectopic Beat Determination Thresholds
24	4/16/92	Test Proposed Protocol EXP I, Test New "C" Program, /Test Pressure Trigger Adjustments For Close Chest Dog/Respiration Has Greater Affect On Close Chest Dog
25	4/17/92	EXP II, Test Autoscaling with more damping/ He Gas Escaping From DataScope System 83
26	4/21/92	Take Electrocautery Noise on Dead Dog Through Pressure Channel- StoreAT.Pas
27	4/30/92	EXP III, Taking Auto and Manual Timing runs, Adjusted Opt Deflation Timing
28	5/8/92	Suffolk Sheep EXP IV, Test Algorithm On Different Animal/ Weak S1 Pressure Wave Causing A S1 Detection Problem/ Test Change to S1 Detector, No More Cycle Length Average (CLA) /7 Intervals
29	5/13/92	EXP V, Analyze Response to Ring in Aug/ Lengthened CAD S1 Blanking Interval

All CAD Experiments Noted in Experimental Log Use the IABP Unless Otherwise Noted

5.1.3   Experimental Results

The canine experimental models, having hemodynamic characteristics similar to those of human patients, were exposed to a Cardiothoracic surgery environment and Cardiothoracic complications similar to those experienced by human patients with heart disease. The CAD experimental results noted in the following subsections were collected utilizing canine mongrel experimental models. The results verify the robustness of the Pa and ECG detection algorithms and Pa and ECG control algorithms.

The aortic pressure(Pa) signal is susceptible to mechanical interference causing pressure changes like respiration, mechanical ventilation, coughing or surgical procedures performed about the heart. ECG leads are immune to aortic pressure changes, although ECG leads are susceptible to electrical disturbances i.e. electromyographic interference, 60 Hz powerline interference, baseline drift and abrupt baseline shift. The Pa and ECG signal interference caused by these artifacts challenge the Pa and ECG detection algorithms.

Prior to performing experiments "on-line"[1] experiments, "off-line"[2] testing was performed on the detection algorithms to ensure the algorithms were "ready" for use with canine mongrel experimental models. The off-line results are presented prior to the "on-line" experimental results.

5.1.3.1   Off-line Testing of Pa and ECG Recorded Traces

Off-line verification testing was performed on both Pa (systolic rise and dicrotic notch) traces and ECG (R-wave) traces. Off-line Pa detection verification was performed using the Cornell University Medical College Canine Mongrel Pa Database. The Pa traces were recorded during various types of Cardiothoracic experiments within the Cornell University Medical College (CUMC) research laboratory. The traces were recorded on reel-to-reel magnetic FM tapes. The tapes recorded a variety of Pa traces from canine mongrel, sheep and pig experiments. This variety of animals coupled with various experimental conditions provided a wide range of Pa traces to test the Pa detection algorithms off-line. The recorded canine experimental Pa traces were particularly applicable to the CAD canine mongrel model experiments that followed.

---

1. On-line refers to experimentation with a Canine Mongrel Experimental Model.

2. Off-line testing refers to CAD detection and CAD control signal experimentation with digitized data from the Cornell University Medical College (CUMC) Canine Mongrel Aortic Pressure Database.

The MIT/BIH ECG Arrhythmia Database was utilized in preparation for off-line ECG R-wave detection. The Cornell University Medical College Canine Mongrel Pa Database had ECG recorded on a secondary channel, however, the MIT/BIH ECG Arrhythmia Database provided the greatest variation of ECG trace sets that were organized beat-by-beat and thus provided a very accurate method of determining exact detection accuracy.

5.1.3.1.1   Off-line Testing of Recorded Canine Experimental Model Pa

Off-line testing was performed to verify detection accuracy had exceeded 90% for the dicrotic notch for Pa traces recorded within the Cornell University Medical College (CUMC) Canine Mongrel Pa Database. This would ensure that, on average, 9 of 10 dicrotic notches were detected for the most severe cardiothoracic surgical conditions. The systolic rise event was assumed to be 100% accurate because of the much larger signal to noise ratio than the dicrotic notch. It was necessary to develop a robust systolic rise detection in order to provide a detection timing precursor for the dicrotic notch detection. The off-line dicrotic notch detection was determined to be 99% accurate for 95% of the CUMC Canine Mongrel aortic pressure wave traces stored on magnetic tape. For nineteen in twenty Pa canine traces, the detection algorithm would detect 99% of the Pa dicrotic notches presented to the Pa detection algorithm.[1] Thus, the overall dicrotic notch detection accuracy for the Cornell University Medical College Canine Mongrel Pa Database was 0.99 * 0.95 = 94%.

The axes of the off-line Pa detection figures must be known to interpret the results. The axes are Pa (vertical) and time (horizontal). The numerical coordinate across the bottom of all the traces (parallel to the title) is time in seconds. The vertical coordinates correspond to mmHg for the Pa signal. The vertical coordinates for the detection signal "square wave" are in arbitrary units. However, a "square wave" transition in the detection signal indicates something has been detected.

In the figures, the Pa signal and the detection signal which intersects the Pa trace are illustrated. The Pa signal is a representation of the recorded Pa signal of a Canine Mongrel Experimental Model. The "square wave" detection signal signifies the detection of the systolic rise and the dicrotic notch. The systolic rise detection is signified by the positive going transition. The dicrotic notch detection is signified by the negative going transition.

---

1.   Although unrelated to the Canine Mongrel Pa Detection, an interesting detection behavior was experienced with Suffolk sheep Pa traces, where some Pa systolic rise contours presented a slope that was too weak to detect (false negative).

The success of a Pa detection using a recorded canine mongrel experimental Pa signal can be determined by evaluating the relationship in the signals within the figure. The relationship between the Pa signal and the detection signal "square wave" must be aligned. A 90% dicrotic notch detection success is used as criterium. The positive transition of the "square wave" detection signal should occur shortly after the start of the systolic rise. The negative transitions of the "square wave" detection signal should occur slightly after or during the dicrotic notch deflection. If the dicrotic notch is detected for 90% of the cardiac cycles displayed, once the Pa detection filter is trained[1], the detection experiment is considered a success.

The detection trace figures were created by photographic images taken of the DataScope 870 patient monitor used for detection algorithm development and verification. The thin black traces are the reverse video (white to black performed with an image processor) image of the green phosphor trace on the black background of the DataScope 870 patient monitor.

The fast transitions within signals (e.g., particularly the detection signals) are typically invisible because the DataScope 870 monitor did not illuminate the thin transition traces very well. After the photographic images were taken and processed, the thin traces did not display. The first two images (Figure 5-1 and Figure 5-2) include some image processor enhancement lines that connect the appropriate upper and lower plateau of the square wave to help illustrate the detection by intersecting the Pa signal.

The effect of transitioning between the different trace speeds on the Datascope 870 monitor, (i.e., 25 or 50 mm/sec) causes the timescale to shrink or expand. The 50 mm/sec trace speed provide a more detailed view of a shorter length of time. The amplitude does not change when switching between a trace speed of 25 or 50 mm/sec.

Figure 5-1 and Figure 5-2 demonstrate off-line detection of Pa using data from Canine Mongrel Experimental Model "A"[2]. Figure 5-1 and Figure 5-2 show the detection of the systolic rise slightly after the systolic rise has occurred on the Pa trace. Those figures also show the detection of the dicrotic notch slightly after the start of the dicrotic notch on the Pa trace.

---

1. Pa detection filter "training" refers to the time it takes for the detection filter to develop thresholds and statistics which mathematically characterize the wave to ensure accurate detection.

2. Experimental Model A, Experimental Model B, etc., refers to a unique Canine Mongrel Experimental Model Pa trace of a distinct Cardiothoracic experiment either recorded in the Cornell University Medical College Canine Mongrel Pa Database (i.e., off-line) or performed within the CUMC Cardiothoracic Surgery Research Laboratory for the purpose of this Dissertation Research (i.e., on-line).
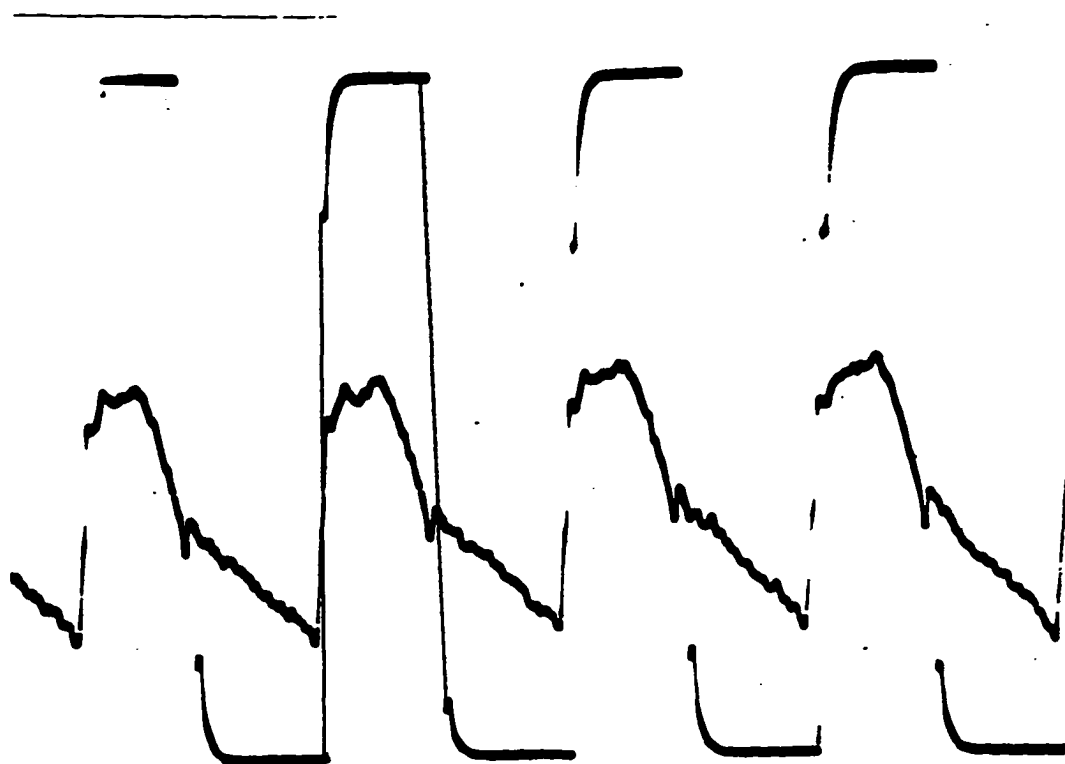
Figure 5-1. Detection of Canine Mongrel Aortic Pressure Wave A. The Positive Transition of the Square Wave illustrates the Detection Timing of the Systolic Rise. The Negative Transition of the Square Wave illustrates the Detection Timing of the Dicrotic Notch. (Datascope 870 Patient Monitor set at 25mm/s Trace Speed)
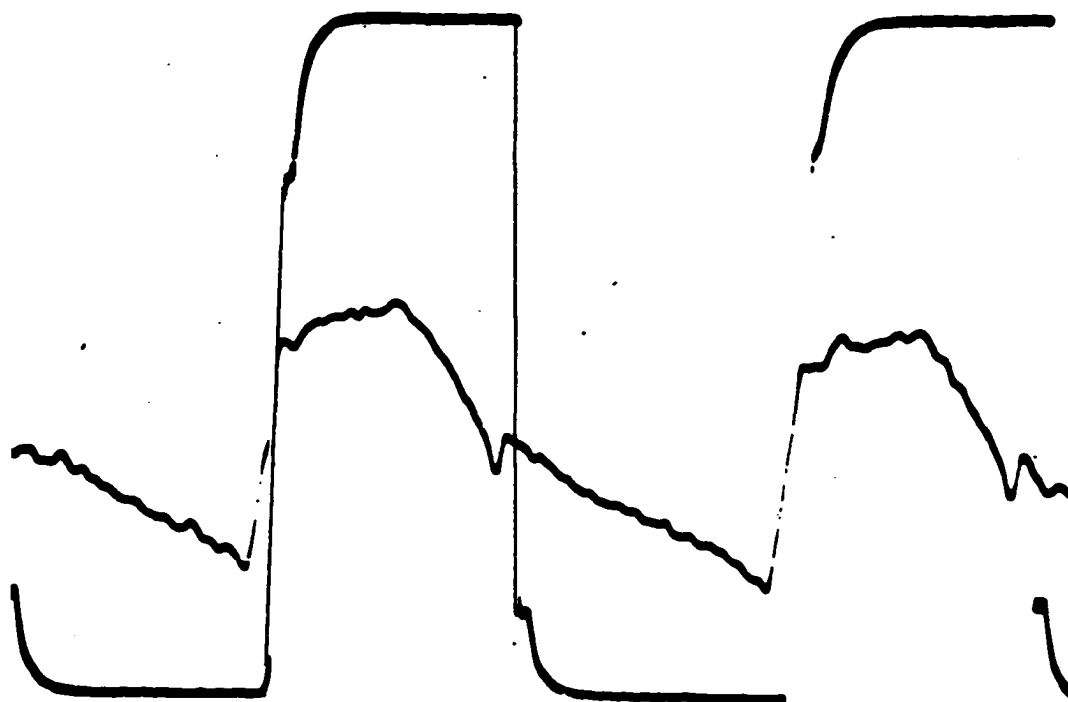
Figure 5-2. Exploded View of Figure 5-1 shows Detection of Canine Mongrel Aortic Pressure Wave A. The Positive Transition of the Square Wave illustrates the Detection Timing of the Systolic Rise. The Negative Transition of the Square Wave illustrates the Detection Timing of the Dicrotic Notch.(Datascope 870 Patient Monitor set at 50mm/s Trace Speed)

5.1.3.1.2 Off-line Testing of ECG MIT/BIH Arrhythmia Database

Investigations into the accuracy and phase delay of real-time QRS detection led to the real-time detection (i.e., not real-time control detection) portion of ARGUS (Arrhythmia Guard System) called DD1 (Detection and Delineation 1) (26) which quotes an accuracy of 99.5%. For this real-time control application, a modified version of the DD1 algorithm was implemented. The published DD1 detection accuracy was not a not achieved because ARGUS is typically performed on recorded Holter data in which detection phase delay is not crucial to success. For real-time control, phase delay in detection diminishes the ability to optimally control the CAD.

Efforts were made to modify the DD1 algorithm to reduce the detection phase delay to acceptable levels without significantly compromising the high detection accuracy. The Real-time QRS-complex detector achieved 96.56% accuracy when tested using the MIT/BIH Arrhythmia Database.

The method utilized to tabulate detection accuracy specified (42) the following table headings: MIT/BIH Record (100-234), Number of Beats, False Positives (FP), False Negatives (FN), Double Detections (DD), Failed Detections (FP+ FN) and Failed Detection Percentage (FP+FN)/Total.

The MIT/BIH Record refer to the ECG trace numbers within the MIT/BIH Arrhythmia Database. The Number of Beats notes the number or heart beats within the particular Record. The False Positives noted the number of times the QRS-detection algorithm detected a ECG artifact other than a QRS-complex. The False Positives noted the number of times the QRS-detection algorithm failed to detect a QRS-complex. The Double Detection column notes the number of times a QRS-complex was detected twice. (Double Detections count toward the failed detection percentage.) The Failed Detection column note the total of False Positives and False Negatives for the Record. The Failed Detection Percentage is a calculation of the number of Failed Detections divided by number of heart beats within the Record. 100% minus a total of the Failed Detection divided by the Total Number of Beats * 100% provides detection accuracy which is 96.56%[1].

o

---

1. As noted in the MIT/BIH detection methodology reference (42) to tabulate detection accuracy, Ventricular Flutter was excluded from the detection accuracy experiments in this Dissertation.

MIT/BIH Record	Number of Beats	FP	FN	DO	Failed Det (FP+FN)	Failed Det % (FP+FN)/Total
100	2267	0	0		0	0
101	1859	2	1		3	0.161
102 Pac	2181	1	0		1	0.045
103	2081	0	2		2	0.096
104 Pac	2224	30	32		62	2.790
105 P	2564	44	25		69	2.690
106	2024	6	9		15	0.741
107 Pac	2131	0	38		38	1.78
108 N,P	1757	507	159		666	37.9
109	2526	0	0		1	0.039
111 T	2120	424	0		424	20.0
112	2536	2	0		2	0.094
113	1791	16	1		17	0.949
114 N.2	1872	63	5	418	496	26.5
115	1945	0	0		0	0
116	2409	3	1		4	0.166
117	1532	2	0		2	0.131
118	2273	11	1		12	0.527
119	1985	0	0		0	0
121	1858	4	2		6	0.323
122	2471	0	0		0	0
123	1514	0	0		0	0
124	1613	0	9		9	0.558
200	2595	3	19		22	0.848
201	1946	2	31		33	1.70
202	2134	2	5		7	0.328
203 N,V	2976	54	299		353	11.9
205	2650	0	22		22	0.830
207 •	1856	7	18		25	1.35
208 N,V23	2953	9	176		185	1.26
209	2999	15	2		17	0.567
210	2645	6	101		107	4.06
212	2746	54	0		54	1.97
213 N,V	3245	5	3		8	0.247
214 V	2255	1	40		41	1.82
215 A	3357	6	19		25	0.745
217 Pac	2202	1	6		7	0.318
219	2150	0	0		0	0
220	2041	0	0		0	0
221	2422	9	11		20	0.826
222 N,P	2492	335	114		449	18.0
223 Vbig	2603	72	107		179	6.88
228 N,Vbg	2048	60	260		320	15.6
230	2252	1	0		1	0.044
231	1566	0	0		0	0
232	1719	19	1		20	1.16
233	3135	0	36		36	1.14
234	2747	0	2		2	0.073

| Totals | 109267 | 1776 | 1986 | | 3762 | 3.448 -> 96.56% acc |

Figure 5-3. Tabulated Results of DD/1 QRS-Complex Algorithm (modified for Real-time Cardiac Assist Device Control) Detection Accuracy when tested against the MIT/BIH ECG Arrhythmia Database.

5.1.3.2 On-line Canine Experimental Model Verification and Experimental Results Utilizing Pa

Off-line testing was conducted (prior to On-line experimentation) to ensure the detection algorithms were operating properly for a wide physiological spectrum of Pa traces. The off-line experimentation was the necessary step prior to utilizing Canine Mongrel Experimental Models.

The Canine Mongrel Model Experiments (On-line) utilized the Pa control signal demonstrating the robust detection and control algorithms researched and developed in this dissertation. The canine experimental model Pa control results demonstrate the CAD control algorithm advancing augmentation toward optimal deflation. The experimental results also demonstrate the control algorithm tracking increases in heart rate from 120 beats per minute (bpm) to 180 bpm. The control algorithm additionally tracks the heart cycle to provide cardiac assist device augmentation during a decreasing heart rate starting at 120 bpm and ending at 90 bpm. Cardiac assist device control and tracking of the cardiac cycle is further demonstrated during electrocautery - the most severe source of noise within a Cardiothoracic surgical environment. Results are collected during both cut and coagulate mode of electrocautery.

Experiments were performed using Pa as the control signal. The experiments demonstrated CAD detection and control results using both the IABP and the EACD after the left ventricle of the Canine Mongrel Experimental Model was infarcted by tying off coronary arteries.

5.1.3.2.1 Intra-aortic Balloon (IAB)

This section illustrates experimental results in which the Pa trace was utilized as the control signal for the IAB CAD. The majority of the CAD results are in Section 5.1.3.2 utilize the IAB as the CAD. Utilization of the IAB (as oppose to the EACD) is due to the less complicated surgical procedure (compared to the EACD) in which this CAD can be surgically implanted within the canine experimental model. Pa control proves to be more challenging that ECG control with regard to detection. The relative difference in the signal to noise amplitude ratio for the cardiac events that must be detected for the ECG is greater

than that of the Pa trace. The R-wave typically has a signal to noise amplitude ratio of at least 2.0 with other signals within the ECG trace (i.e., P-wave and T-wave). The most difficult Pa detection cardiac event, the dicrotic notch, has a signal to noise ratio with the Pa systolic rise of typically less than 0.2. Thus the detection of the Pa dicrotic notch is considerably more difficult to detect than the ECG R-wave.

The results in Section 5.1.3.2.1 are broken into the following subsections:

1. IABP Timing Signals Recorded Using the DataScope 870 Patient Monitor

2. IABP Timing Signals and Augmentation Recorded Using the Cornell University Medical College (CUMC) Cardiothoracic Research Laboratory Data Acquisition System

IABP control signals and Pa augmentation figures recorded using the DataScope 870 patient monitor are interpreted in the following way. The numerical coordinate across the bottom of the all traces (parallel to the title) is time in seconds. The vertical coordinates correspond to mmHg for the Pa signal. The vertical IAB trigger control signal "square wave" are in arbitrary units. However, a "square wave" transition in the control signal indicates that either the IAB (CAD) is either being inflated or deflated (activated or deactivated).

The figures illustrate the Pa signal and the IABP control signal which intersects the Pa trace. The Pa signal is a representation of the live (on-line) Pa signal of a Canine Mongrel Experimental Model. The "squarewave" control signal indicates the inflation or deflation of the IAB. The inflation of the IAB is signified by the positive going transition. The deflation of the IAB is signified by the negative going transition.

The evaluation of an Pa Detection using on-line canine mongrel experimental Pa signal can be determine by evaluating the relationship in the signals within the figure. The relationship between the Pa signal and the control signal "square wave" must be aligned. The positive transition of the "square wave" control signal should occur approximately at the dicrotic notch. The negative transitions of the "square wave" detection signal should occur prior to the systolic rise. For the purpose of demonstrating the control signal with the proper timing with respect to the cardiac cycle, a positive transition at the dicrotic notch and a negative transition prior to the systolic rise the control experiment is illustrated.

The fast transitions within signals (e.g., particularly the control signals) are typically invisible because the DataScope 870 monitor did not illuminate the thin transition traces very well. After the photographic images were taken and processed, the thin traces did not display. The two images to follow, (i.e., Figure 5-4 and Figure 5-5) include some image processor enhancement lines that

connect the appropriate upper and lower plateau of the square wave to help illustrate the control signal by intersecting the Pa signal. The same type of visual approach for connecting the control signal transitions should be used to evaluate the rest of the transitions within the figures.

IABP control signals recorded using the DataScope 870 patient monitor are illustrated in the following figures. Figure 5-4 and Figure 5-5 demonstrate proper IAB control triggering prior to engaging[1] pneumatic solenoids of the pneumatic source[2] that cause the IAB to create a pressure augmentation within the aortic pressure wave of Canine Mongrel Experimental Model D. The high and low duration of the pneumatic solenoids square wave illustrates the periods of IAB (CAD) inflation and deflation respectively. As can be seen in Figure 5-4 and Figure 5-5, for proper inflation, the square positive transition wave occurs approximately at the dicrotic notch. For proper deflation, the square wave negative transition occurs just prior to the systolic rise.

1. When the pneumatic solenoids of the pneumatic source are not engaged, the CAD pneumatic source driving gas is not enabled. Typically, the CAD control timing signal relationship to the Pa signal is observed prior to engaging the pneumatic solenoids (i.e., prior to providing cardiac assistance). This precautionary observation ensures that the CAD control timing will provide proper circulatory assistance and not hinder circulation. An improper CAD control timing, particularly IAB inflation during systole, can impede the normal pumping function of the heart by obstructing the aorta during systole.

2. The CAD pneumatic source was provided by a Datascope IABP System 83 which was modified to allow control signals from the CAD control algorithm developed within this Dissertation to inflate and deflate the CAD (by activating and deactivating the appropriate pressure and vacuum pneumatic solenoids)
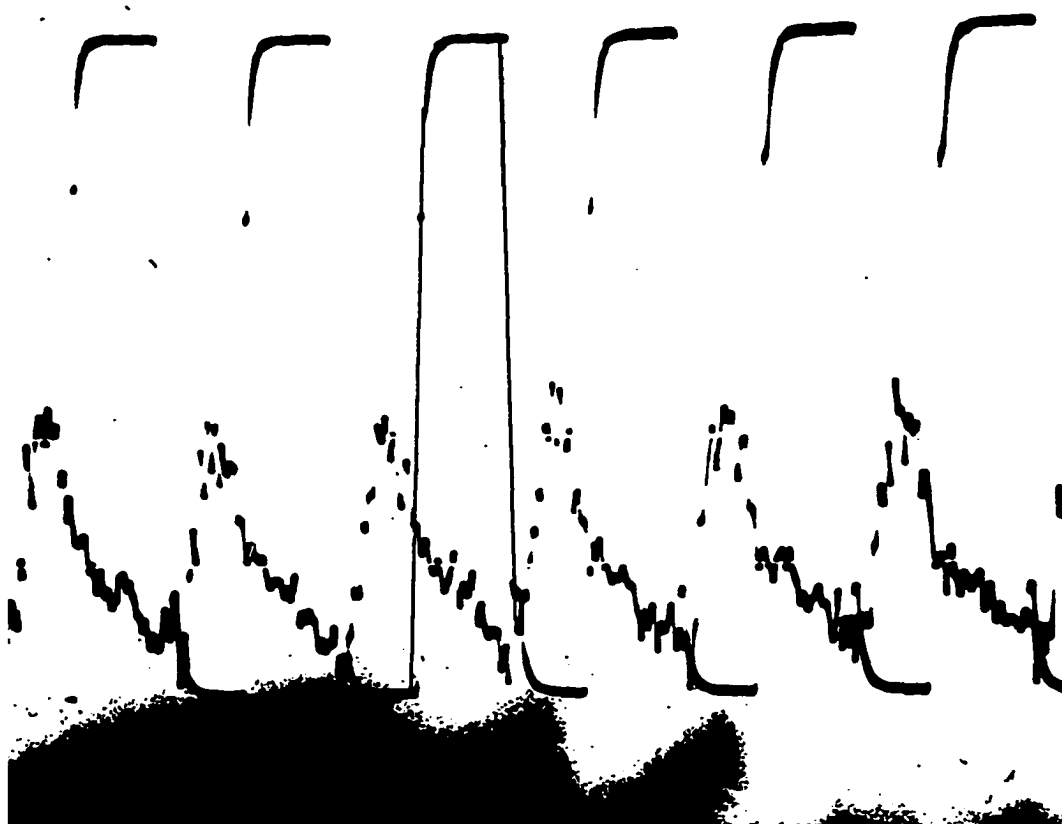
Figure 5-4. IAB Control Triggering Signal derived using Pa Trace of Canine
Experimental Model D. The Positive Transition of the Square Wave
illustrates the CAD Control Inflation Timing at the Pa Dicrotic Notch.
The Negative Transition of the Square Wave illustrates the CAD Control
Deflation Timing just prior to the Pa Systolic Rise. (Datascope 870
Patient Monitor set at 25mm/s Trace Speed)
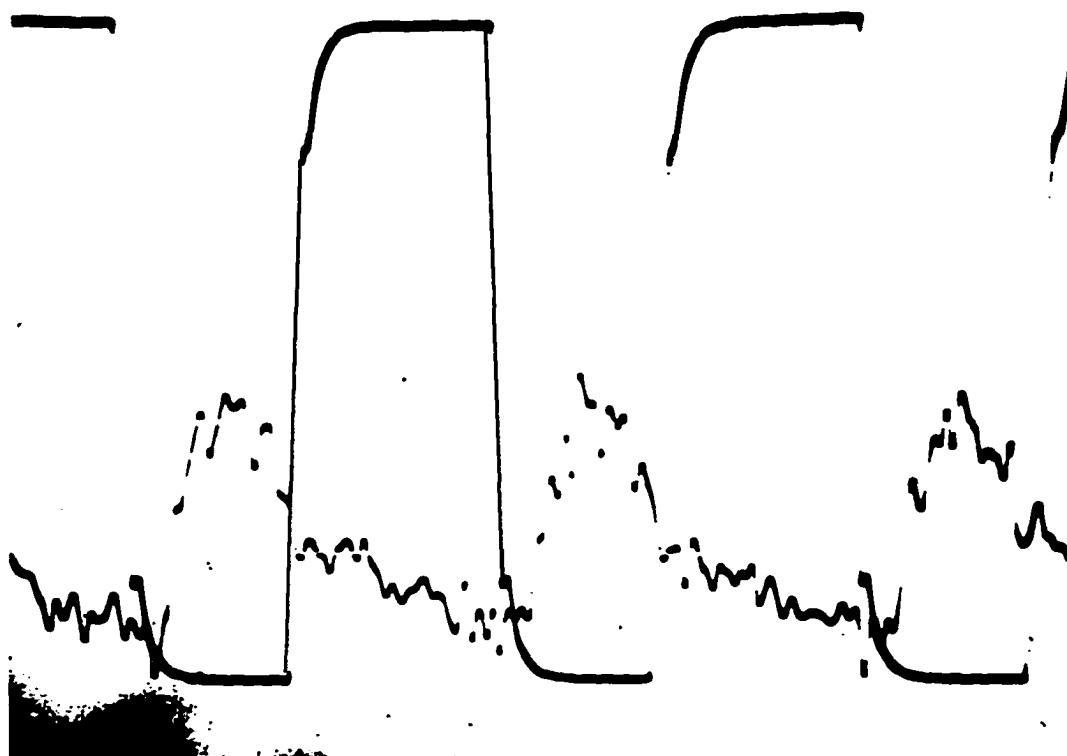
Figure 5-5. Exploded View of Figure 5-4 shows IAB Control Triggering Signal derived using Pa Trace of Canine Experimental Model D. The Positive Transition of the Square Wave illustrates the CAD Control Inflation Timing at the Pa Dicrotic Notch. The Negative Transition of the Square Wave illustrates the CAD Control Deflation Timing just prior to the Pa Systolic Rise. (Datascope 870 Patient Monitor set at 50mm/s Trace Speed.)

IAB timing control signals and Pa augmentation recorded using the Cornell University Medical College (CUMC) cardiothoracic surgery research laboratory data acquisition system are illustrated in the following manner. The CUMC Cardiothoracic Surgery Research Laboratory Data Acquisition System provided an electronic means of capturing the data of canine mongrel CAD experiments electronically through an set of analog to digital converter channels[1]. The figures within Section 5.1.3.2.1 illustrate the Pa detection algorithm tracking the cardiac cycle for slow, moderate and fast heart constant heart rates, changing heart rates, and during extreme cases of Pa signal interference due to the Cardiothoracic Surgery environment. Additional figures within

---

1. A graphical representation of the digital data is then available for print through a print screen feature of a word processor.

Section 5.1.3.2.1 further illustrate the ability of the Pa detection algorithms to properly track the cardiac cycle when challenged by noise due to electrocautery, and cardiac arrhythmia, namely, bradycardia and tachycardia.

IAB control results using Pa from canine mongrel experimental models recorded using the data acquisition system are interpreted in the following manner. The numerical coordinate across the bottom of the all traces is time in seconds. The coordinate units shown vertically on the middle trace (e.g., Figure 5-6B) are mmHg for the Pa signal. The coordinates shown vertically on the top and bottom traces (e.g., Figure 5-6A and Figure 5-6C, respectively) are D/AC amplitude units. The vertical coordinate values for the top trace ECG (labelled R-wave) correspond to millivolts. The D/ AC amplitude unit vertical coordinates of the IAB control timing signal "square wave" (labelled Solenoid Timing on the bottom trace) are in arbitrary units. However, a "square wave" transition in the IAB control timing signal square wave indicates that either the IAB control state has changed to either inflated or deflated (from the previous state of deflation or inflation, respectively).

All illustrations within Section 5.1.3.2.1 have three traces which will be referred to as the "top," "middle" and "bottom" trace (starting with the top of the page and moving downward, respectively, e.g., Figure 5-6A, Figure 5-6B and Figure 5-6C). The three traces were created simultaneously during a single canine mongrel experimental model "data run." Each data run illustrated the ECG (top trace), Pa pressure signal with associated counterpulsation Pa augmentation (middle trace), and IAB control inflation/deflation timing signal (bottom trace).

The top trace illustrates the ECG signal. The middle trace illustrates the Pa signal. The bottom trace illustrates the "square wave" IAB control inflation/deflation timing signal. The start of IAB pneumatic inflation pressure[1] is indicated by the positive going transition of the square wave in the bottom trace. The start of IAB pneumatic deflation vacuum[2] is indicated by the negative going transition of the square wave in the bottom trace.

The success of the a IAB canine mongrel experiment using Pa as the control signal can be determined by studying the middle trace and evaluating the relationship between the Pa augmentation created by the IAB within the Pa trace and the relative timing of the dicrotic notch and systolic rise within the Pa trace. The top ECG trace (e.g., Figure 5-6A) and the IAB control timing (e.g., Figure 5-6C) are provided as a visual aid to help distinguish between the Pa deflection

---

1. Pneumatic force in the form of pressurized helium is applied in order to inflate the IAB.

2. Pneumatic vacuum in the form of a evacuated chamber is exposed to the aperture of the IAB catheter in order to deflate the IAB.

caused by systole of the heart and the Pa augmentation due to the IAB in the middle trace (e.g., Figure 5-6B). The ECG trace provides a reference for the Pa deflection due to systole. The bottom IAB control timing trace provides a reference for the Pa augmentation due to the IAB.

The relationship between the Pa cardiac cycle and the Pa augmentation due to the IAB should be as follows:

1. The rise of the Pa augmentation, due to the IAB inflation, should occur at approximately the dicrotic notch.

2. The fall of the Pa augmentation, due to the IAB deflation, should stop just at the pressure of the start of systole.

If the rise and fall of the Pa augmentation occur at the proper times, due to the timing of the IAB inflation and deflation, the experiment is considered a success. In fact, more fundamentally, tracking the cardiac cycle through the Pa detection algorithm during arrhythmia (e.g., changing heart rate) and electrocautery is a substantial contribution to the field of counterpulsation cardiac assistance research.

A Pa observation beat is provided once every 10th heart beat to allow an unassisted heart cycle to occur. This allows the observation of the Pa dicrotic notch and systolic rise timing to be evaluated without the obstruction of the Pa augmentation due to counterpulsation assistance.

Figure 5-6, Figure 5-7, and Figure 5-8 illustrate IAB control triggering (inflation/deflation) using the Pa signal as the control signal during constant moderate (HR=140 bpm), slow (HR=120 bpm) and fast heart rates (HR=180 bpm) respectively of Canine Mongrel Experimental Model E.

Once every ten heart cycles, assistance is prevented through the control signal, augmentation does not occur illustrating the "observation" cycle (i.e., observation heart beat). The cardiac cycle observation beat in Figure 5-6B (between 16.75 to 17.1 seconds) allows the Pa Trace to be observed unassisted (without Pa augmentation due to the absence of IAB inflation) for a single cardiac cycle. By viewing the Pa unassisted cardiac cycle, the timing relationship of the dicrotic notch and systolic rise with the Pa cardiac cycle trace can be viewed. The timing relationship of the dicrotic notch and systolic rise can then be visually applied to those heart beats in which assistance is provided (Pa augmentation due to the presence of IAB inflation). The comparison can allow the evaluation to determine if the appropriate inflation and deflation timing of the IABP is occurring.

In Figure 5-6B, Figure 5-7B, and Figure 5-8B; the first, fourth and sixth heart cycles respectively demonstrate observation beats.

R-wave (Chan 0)

2250.000

1993.000

15.0   16.0   17.0   18.0   19.0   20.0

Aortic Pressure (Chan 1)

78.947

mm Hg

52.632

15.0   16.0   17.0   18.0   19.0   20.0

Solenoid Timing (Chan 5)

2218.000

1852.000

15.0   16.0   17.0   18.0   19.0   20.0
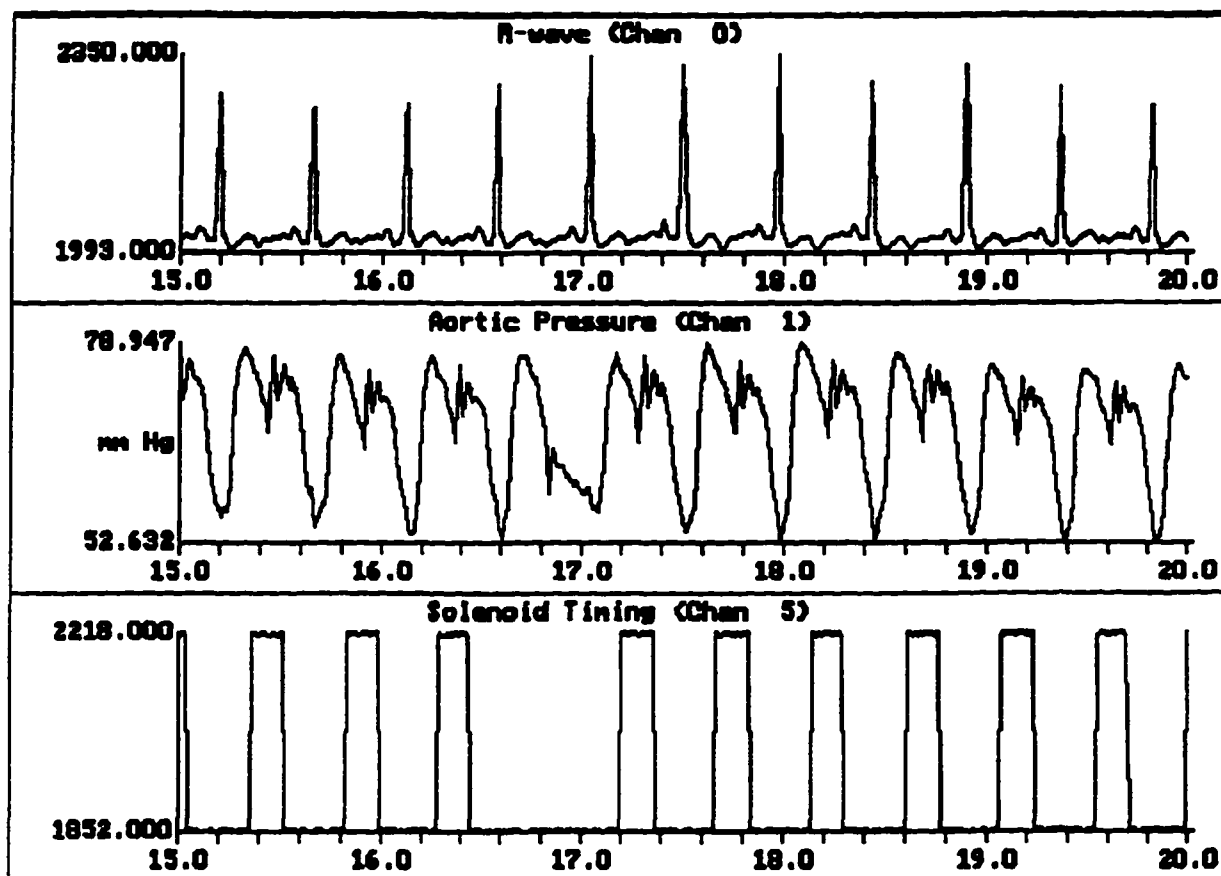
Figure 5-6. IABP Triggering Control derived using Pa Trace of Canine Mongrel Experimental Model E illustrates Pa Augmentation during Moderate Heart Rate of 140 bpm as seen in Figure 5-6B (middle trace). ECG provided an Pa Cardiac Cycle Timing Reference as seen in Figure 5-6A (top trace). IAB Inflation/Deflation Control Signal as seen in Figure 5-6C (bottom trace) provided a Pa Augmentation Timing Reference. The Cardiac Cycle Observation Beat (in Figure 5-6B between 2.0 to 2.4 seconds) illustrated the Dicrotic Notch and Systolic Rise of Cardiac Cycle without Pa Augmentation due to IAB Inflation.

Figure 5-7. IABP Triggering Control derived using Pa Trace of Canine Mongrel Experimental Model E illustrates Pa Augmentation during Slow Heart Rate of 120 bpm as seen in Figure 5-7B (middle trace). ECG provided an Pa Cardiac Cycle Timing Reference as seen in Figure 5-7A (top trace). IAB Inflation/Deflation Control Signal provided a Pa Augmentation Timing Reference as seen in Figure 5-7C (bottom trace). The Cardiac Cycle Observation Beat (in Figure 5-7B between 16.75 to 17.1 seconds) illustrated the Dicrotic Notch and Systolic Rise of Cardiac Cycle without Pa Augmentation due to IAB Inflation.

Figure 5-8. IABP Triggering Control derived using Pa Trace of Canine Mongrel Experimental Model E illustrates Pa Augmentation during Fast Heart Rate of 180 bpm as seen in Figure 5-8B (middle trace). ECG provided an Pa Cardiac Cycle Timing Reference as seen in Figure 5-8A (top trace). IAB Inflation/Deflation Control Signal provided a Pa Augmentation Timing Reference as seen in Figure 5-8C (bottom trace). The Cardiac Cycle Observation Beat (in Figure 5-8B between 1.7 to 2.0 seconds) illustrated the Dicrotic Notch and Systolic Rise of Cardiac Cycle without Pa Augmentation due to IAB Inflation.

Figure 5-9 illustrates IAB Pa triggering during electrocautery coagulation mode interference to Canine Mongrel Experimental Model E. The interference due to electrocautery almost completely abolishes the ECG signal in Figure 5-9A. The observation cycle pattern can be easily seen once every ten beats in the Solenoid Timing signal of Figure 5-9C. Figure 5-10 and Figure 5-11 are exploded illustrations of Figure 5-9. Figure 5-10B and Figure 5-11B demonstrate the application of

electrocautery to the Canine Experimental Model going from a state off to on and on to off, respectively.

Figure 5-9. IABP Triggering Control derived using Pa Trace of Canine Mongrel Experimental Model E illustrated Pa Augmentation during use of Electrocautery in Coagulation Mode on Canine Model as seen in Figure 5-9B (middle trace). ECG provided a Timing Reference for when the Electrocautery was started (at 1 second and at 23 seconds) and stopped (at 12 seconds) as seen in Figure 5-9A (top trace). Note the ECG Trace went Off Scale during Electrocautery. IAB Inflation/Deflation Control Signal demonstrated Periodic Timing of IAB Control Signal as seen in Figure 5-9C (bottom trace). The Missing Control Pulse of the Periodic Cardiac Cycle Observation Beat once every Ten Beats (in Figure 5-9C at 2.5, 5.6, 8.7, 11.8, etc. seconds) illustrated Control Synchronization with the Sinus Rhythm Cardiac Cycles (which are also periodic).
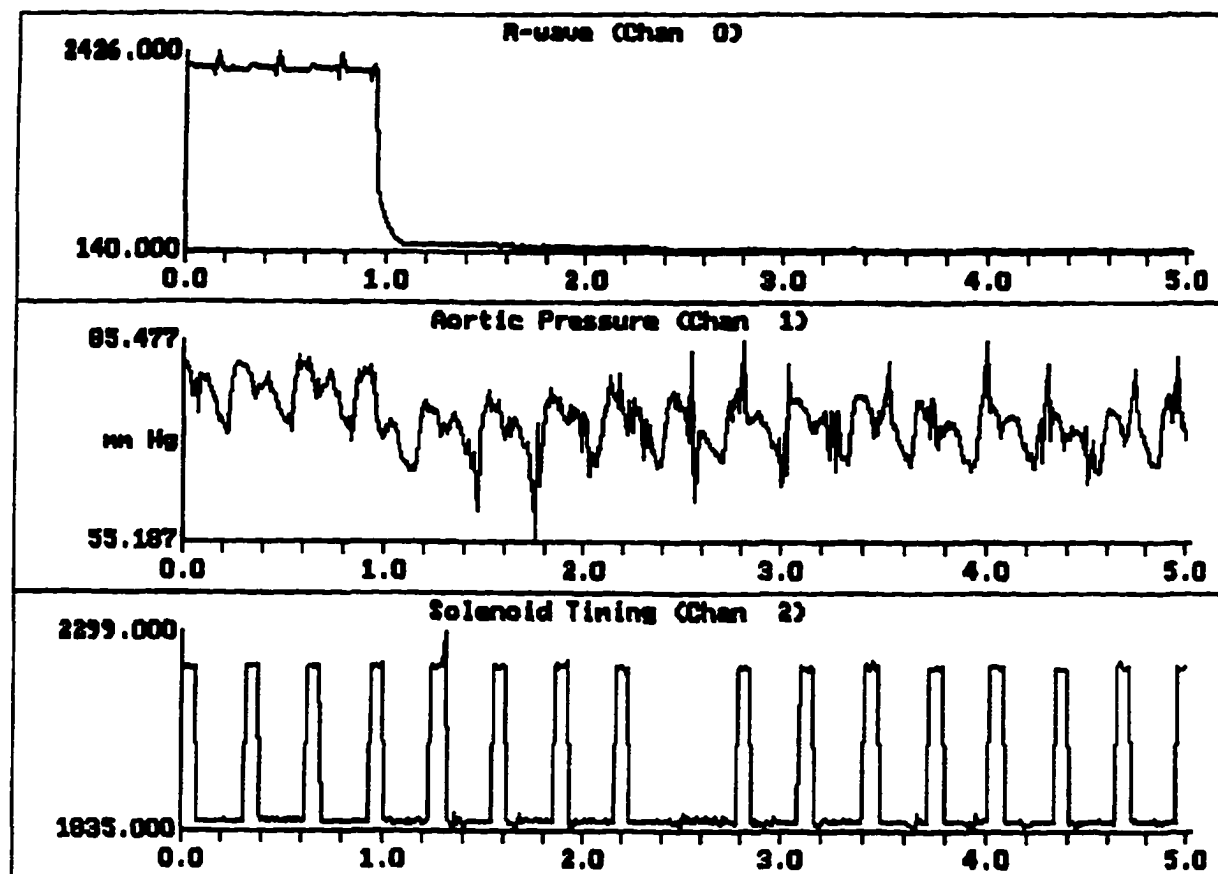
Figure 5-10. Exploded View of Figure 5-9 showed IABP Triggering Control derived using Pa Trace of Canine Mongrel Experimental Model E which illustrated Pa Augmentation during use of Electrocautery in Coagulation Mode on Canine Model as seen Figure 5-10B (middle trace). ECG provided a Timing Reference for when the Electrocautery was started (at 1 second) as seen Figure 5-10A (top trace). Note the ECG Trace went Off Scale during Electrocautery. IAB Inflation/Deflation Control Signal demonstrated Periodic Timing of IAB Control Signal as seen Figure 5-10C (bottom trace). The Periodic Cardiac Cycle Observation Beat once every Ten Heart Beats is illustrated by the missing IAB Control Signal Pulse (in Figure 5-10C at 2.5 seconds).
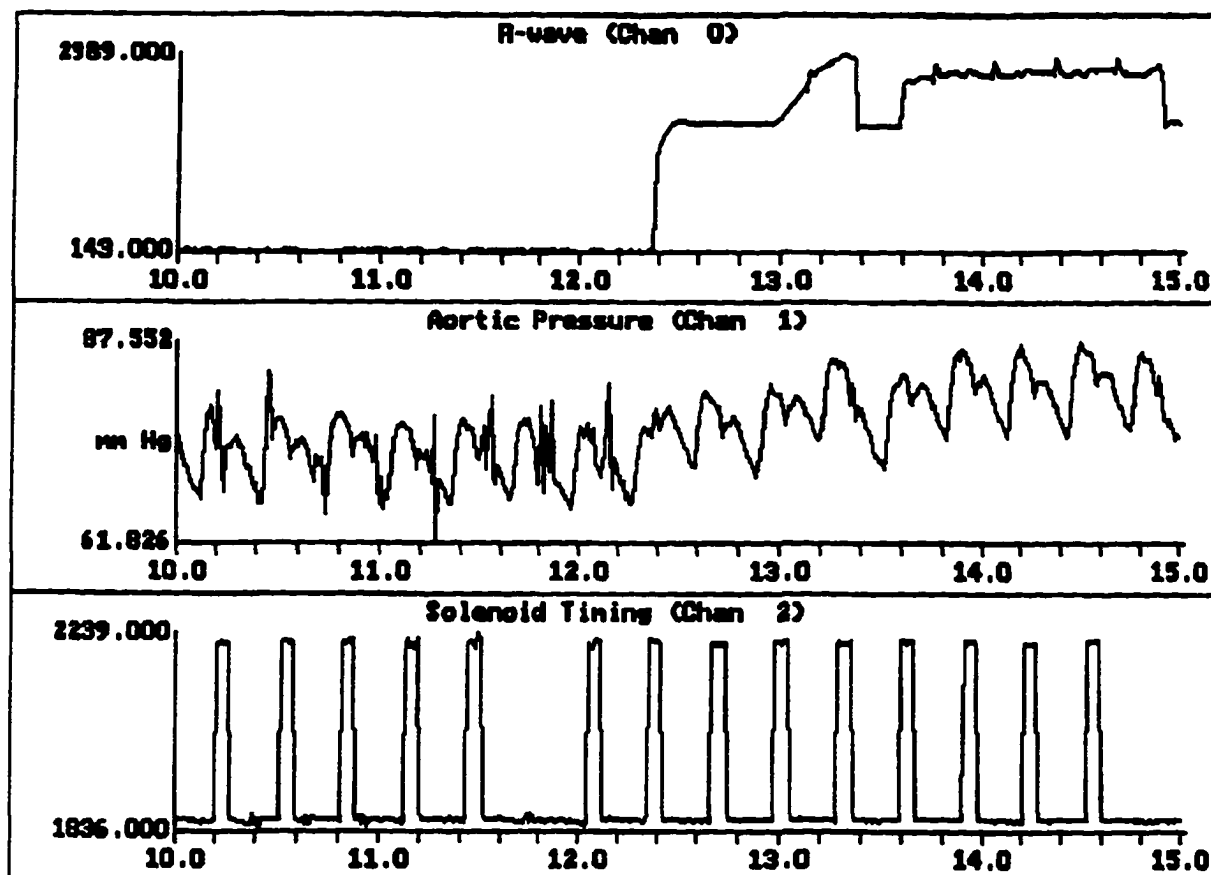
Figure 5-11. Exploded View of Figure 5-9 showed IABP Triggering Control derived using Pa Trace of Canine Mongrel Experimental Model E which illustrated Pa Augmentation during use of Electrocautery in Coagulation Mode on Canine Model as seen in Figure 5-11B (middle trace). ECG provided a Timing Reference for when the Electrocautery was stopped (at 12.4 seconds) as seen in Figure 5-11A (top trace). Note the ECG Trace went Off Scale during Electrocautery. IAB Inflation/Deflation Control Signal demonstrated Periodic Timing of IAB Control Signal as seen in Figure 5-11C (bottom trace). The Periodic Cardiac Cycle Observation Beat once every Ten Heart Beats is Illustrated by the missing IAB Control Signal Pulse (in Figure 5-11C at 11.8 seconds).

Figure 5-12 illustrates IAB Pa triggering during electrocautery cut mode interference to Canine Mongrel Experimental Model E. The interference due to electrocautery adds a considerable amount of noise to the Pa (Figure 5-12B) and ECG signal (Figure 5-12A). Figure 5-13 and Figure 5-14 are

exploded illustrations of Figure 5-12. Figure 5-13B and Figure 5-14B demonstrate the electrocautery going from a state off to on and on to off respectively.
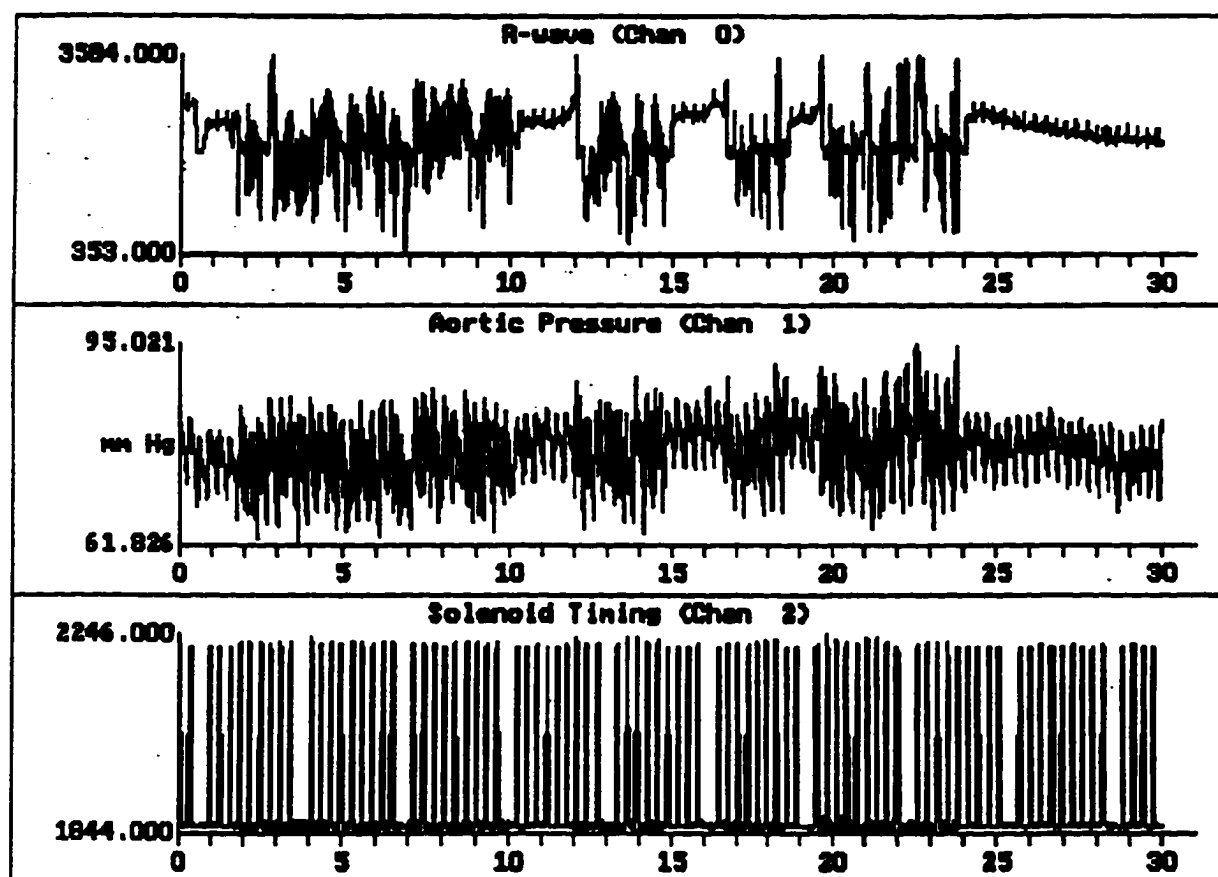
Figure 5-12. IABP Triggering Control derived using Pa Trace of Canine Mongrel Experimental Model E illustrated Pa Augmentation during use of Electrocautery in Cut Mode on Canine Model as seen in Figure 5-12B (middle trace). ECG Provided a Timing Reference for when the Electrocautery was Started (at 1.5, 12.0, 16.5, and 19.5, seconds) and Stopped (at 10.2, 15.0, 18.5, and 24.0 seconds) as seen in Figure 5-12A (top trace). Note the ECG Trace became Extremely Noisy during Electrocautery. IAB Inflation/Deflation Control Signal demonstrated Periodic Timing of IAB Control Signal as seen in Figure 5-12C (bottom trace). The Missing Control Pulse of the Periodic Cardiac Cycle Observation Beat once every Ten Beats (in Figure 5-12C at 3.8, 6.8, 9.8, 12.8, etc. seconds) illustrated Control Synchronization with the Sinus Rhythm Cardiac Cycles (which are also periodic).
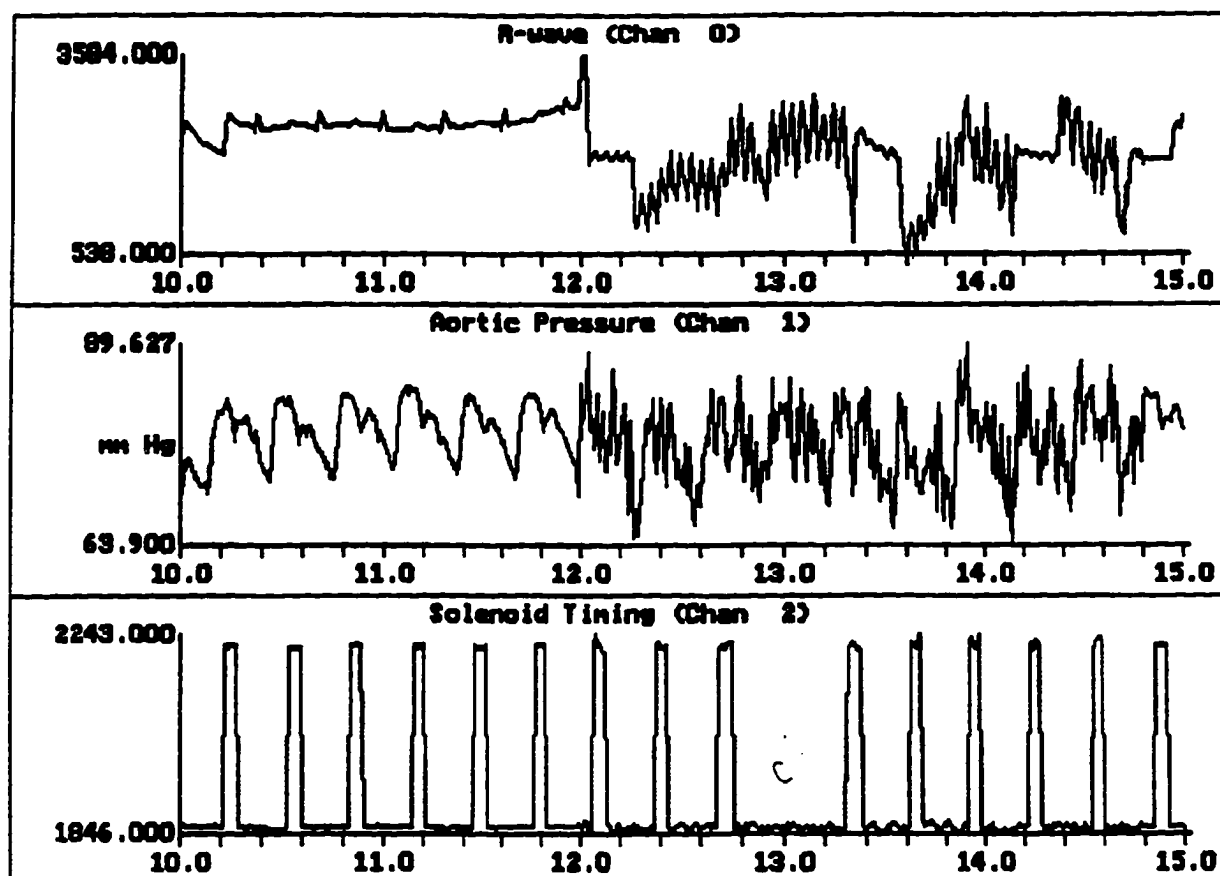
Figure 5-13. Exploded View of Figure 5-12 showed IABP Triggering Control derived using Pa Trace of Canine Mongrel Experimental Model E which illustrated Pa Augmentation during use of Electrocautery in Cut Mode on Canine Model as seen in Figure 5-13B (middle trace). ECG provided a Timing Reference for when the Electrocautery was Started (at 12.0 seconds) as seen in Figure 5-13A (top trace). Note the ECG Trace became Extremely Noisy During Electrocautery. IAB Inflation/Deflation Control Signal demonstrated Periodic Timing of IAB Control Signal as seen in Figure 5-13C (bottom trace). The Periodic Cardiac Cycle Observation Beat once every Ten Heart Beats is illustrated by the Missing IAB Control Signal Pulse (in Figure 5-13C at 12.8 seconds).
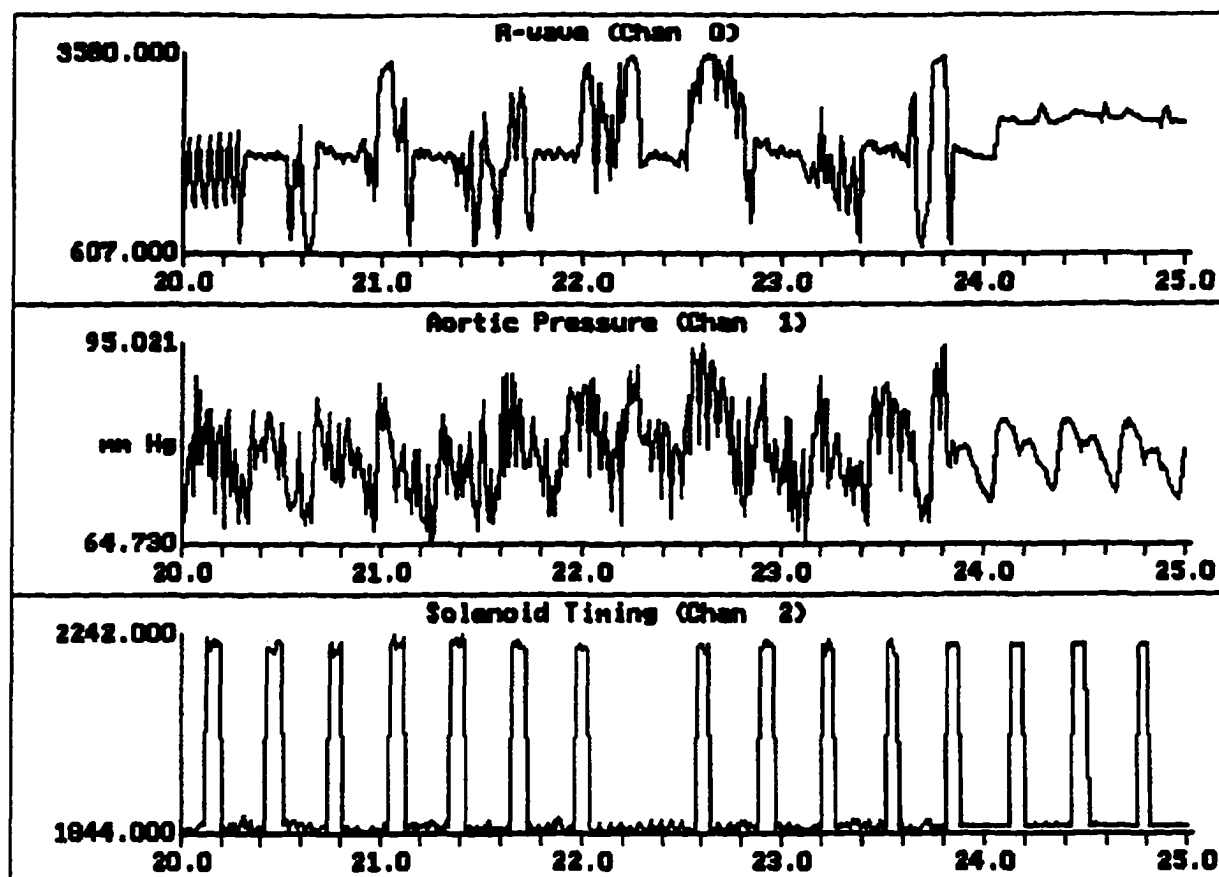
Figure 5-14. Exploded View of Figure 5-12 showed IABP Triggering Control derived using Pa Trace of Canine Mongrel Experimental Model E which illustrated Pa Augmentation during use of Electrocautery in Cut Mode on Canine Model as seen in Figure 5-14B (middle trace). ECG provided a Timing Reference for when the Electrocautery was Stopped (at 24.0 seconds) as seen in Figure 5-14A (top trace). Note the ECG became Extremely Noisy during Electrocautery. IAB Inflation/Deflation Control Signal demonstrated Periodic Timing of IAB Control Signal as seen in Figure 5-14C (bottom trace). The Periodic Cardiac Cycle Observation Beat once every Ten Heart Beats is Illustrated by the Missing IAB Control Signal Pulse (in Figure 5-14C at 22.3 seconds).

Figure 5-15 illustrates the IAB Pa triggering during changing canine heart rate (bradycardia arrhythmia) of Canine Experimental Model E. The heart rate starts at 120 beats per minute(bpm) then quickly changes to 90 bpm for six cycles (during period of 22.5 to 27.5 seconds). Two

observation heart cycles are present at the seventh and seventeenth beat in Figure 5-15C. Note that the IABP control algorithm tracks the changing heart rate to provide cardiac assistance during bradycardia in Figure 5-15B.
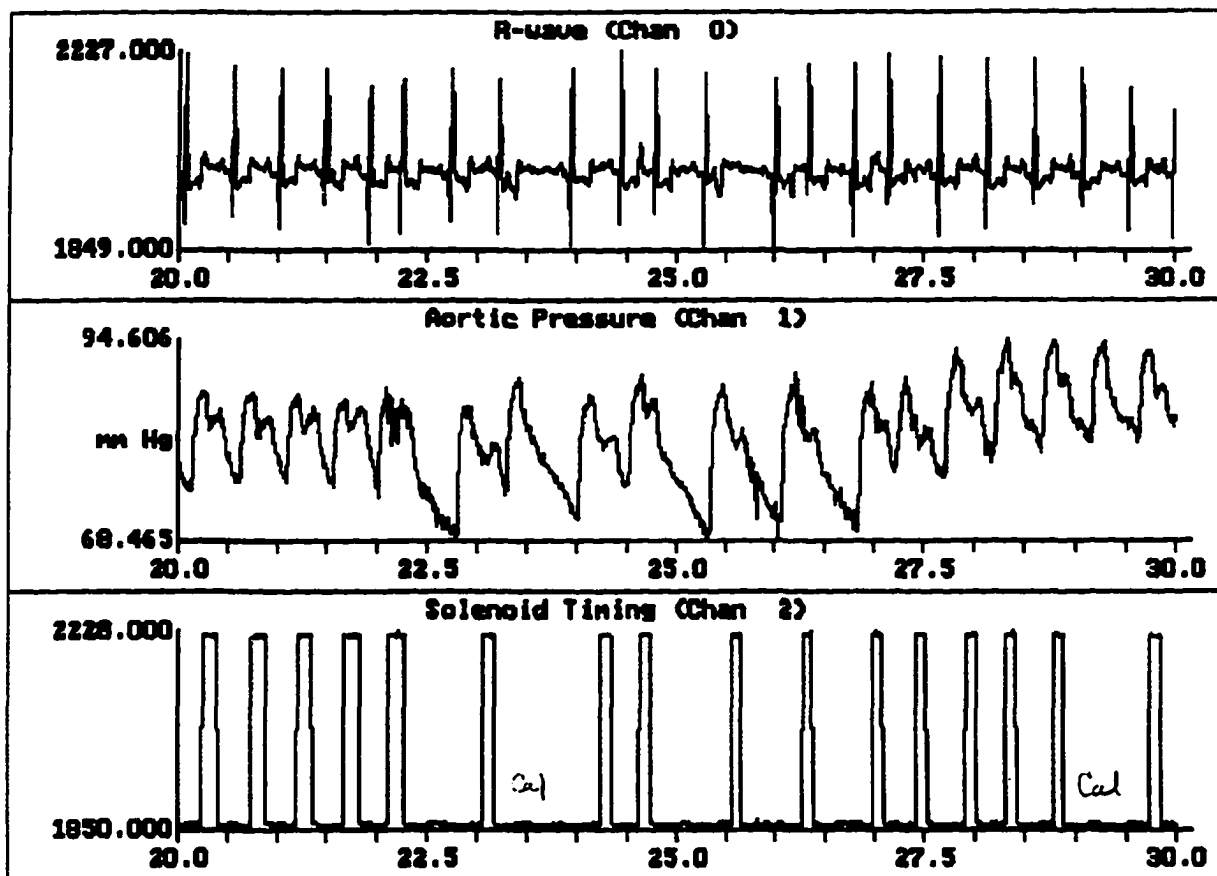
Figure 5-15. IABP Triggering Control derived using Pa Trace of Canine Mongrel Experimental Model E illustrates Pa Augmentation during Changing Heart Rate ranging from Moderate to Slow (120 to 90 bpm as seen in Figure 5-15B (middle trace)). ECG Provided a Pa Cardiac Cycle Timing Reference as seen in Figure 5-15A (top trace). IAB Inflation/Deflation Control Signal provided an Pa Augmentation Timing Reference as seen in Figure 5-15C (bottom trace). The Cardiac Cycle Observation Beat (in Figure 5-15C at 23.5 and 29.5 seconds) Illustrated the Dicrotic Notch and Systolic Rise of Cardiac Cycle without Pa Augmentation due to IAB Inflation.

Figure 5-16 illustrates IAB Pa triggering during an increasing canine heart rate (tachycardia arrhythmia) of a range changing from 120 bpm (0 to 5 seconds) to 180 bpm (during period of 5 to 22 seconds). Figure 5-17 and Figure 5-18 are exploded views of Figure 5-16 demonstrating IAB Pa triggering at heart rates 180 and 120 bpm, respectively.
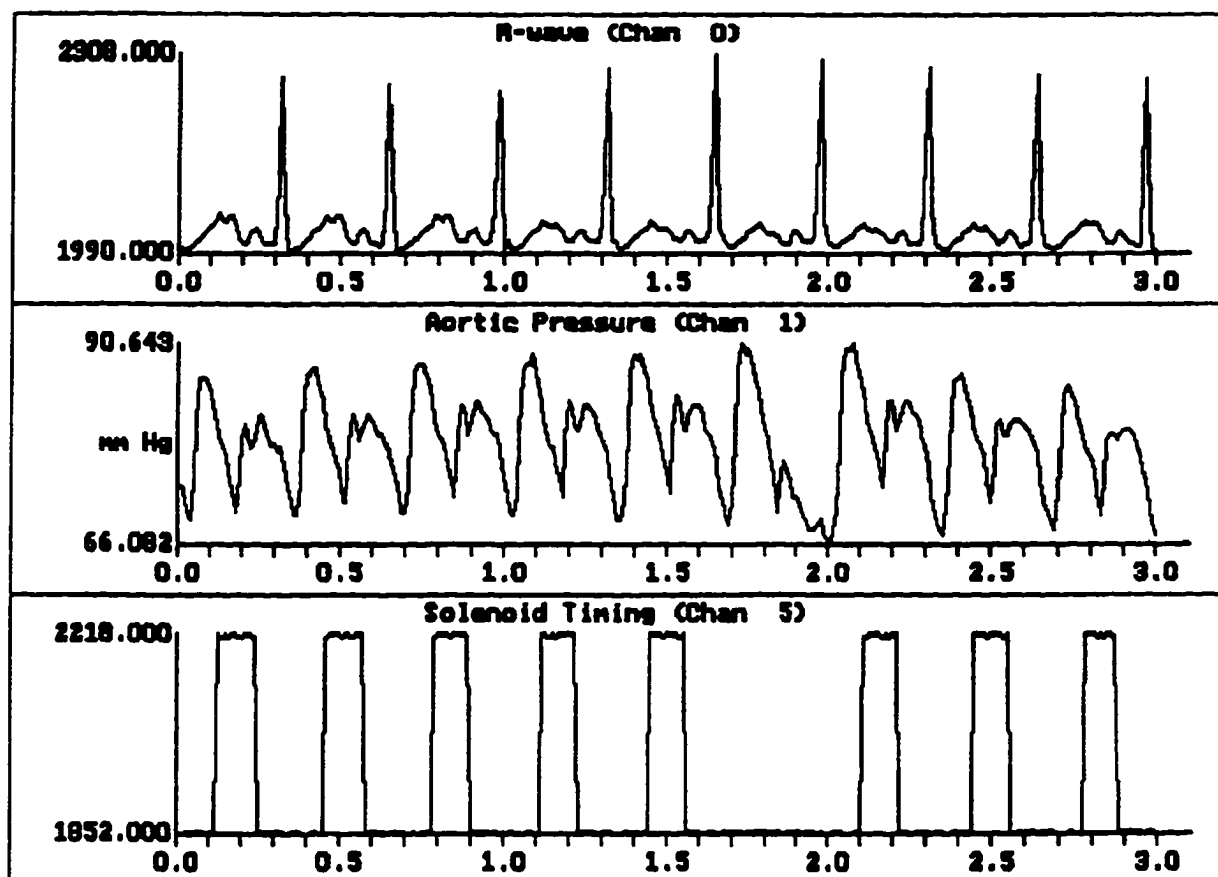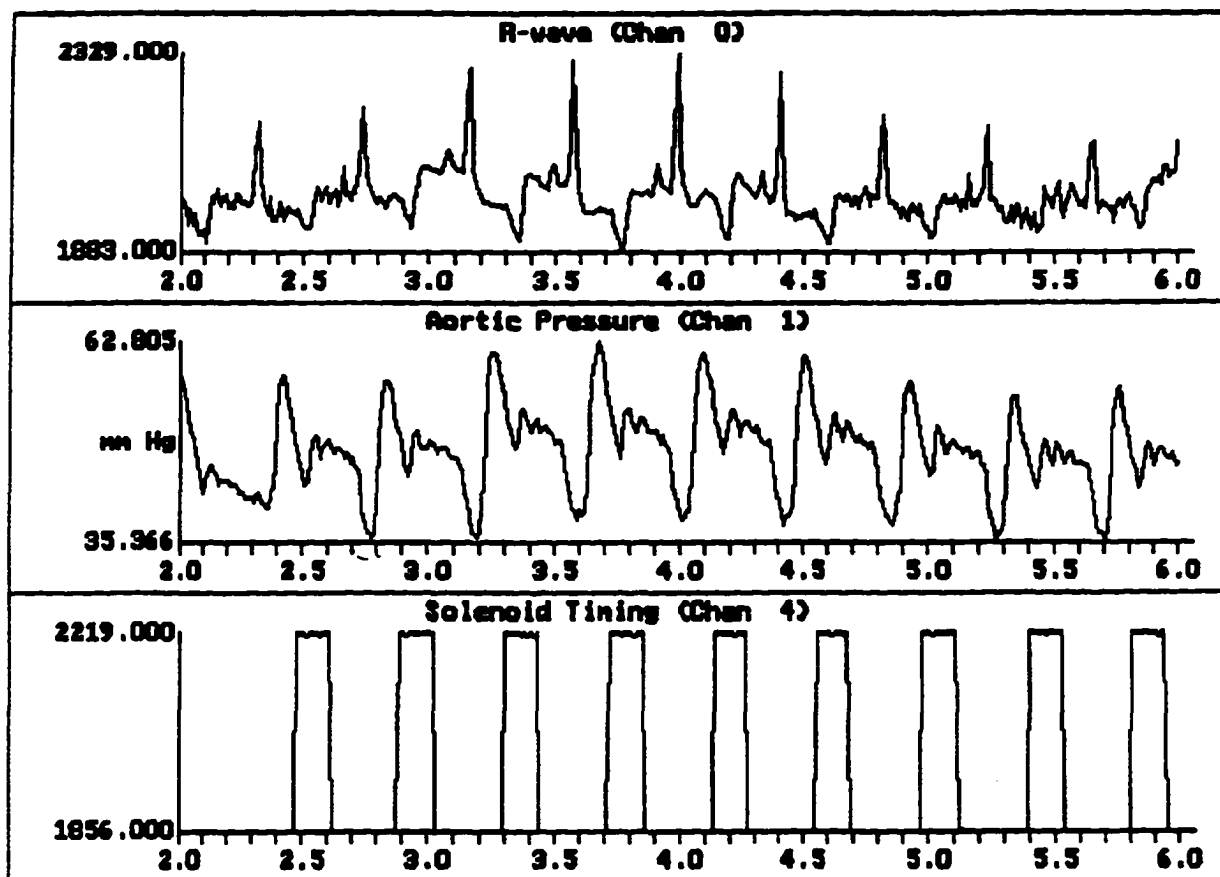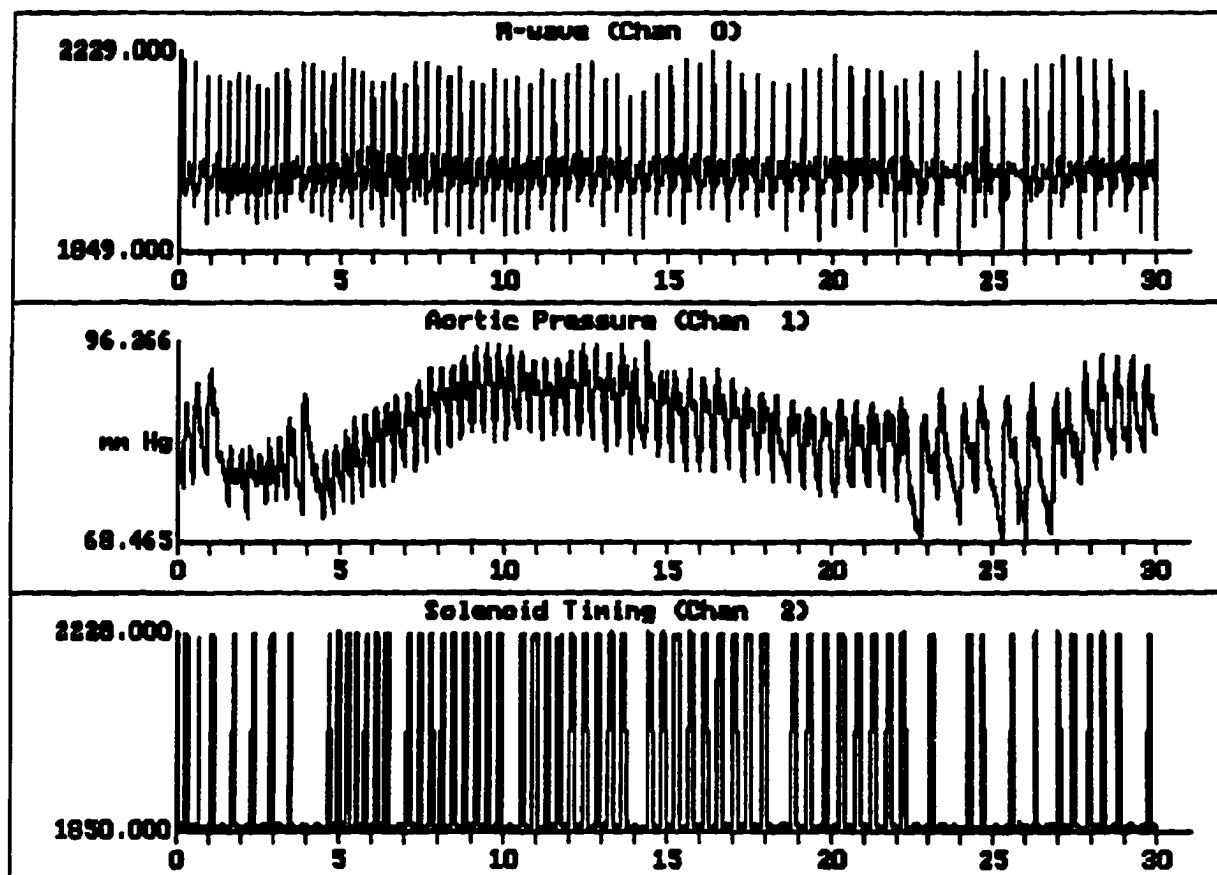
Figure 5-16. IABP Triggering Control derived using Pa Trace of Canine Mongrel Experimental Model E illustrates Pa Augmentation during changing Heart Rate ranging from Moderate to Fast (120 to 180 bpm as seen in Figure 5-16B (middle trace)). ECG provided an Pa Cardiac Cycle Timing Reference as seen in Figure 5-16A (top trace). IAB Inflation/ Deflation Control Signal provided an Pa Augmentation Timing Reference as seen in Figure 5-16C (bottom trace). The Cardiac Cycle Observation Beat (in Figure 5-16C at 4.0, 6.8, 10.2, 14.0, etc.) illustrated the Dicrotic Notch and Systolic Rise of Cardiac Cycle without Pa Augmentation due to IAB Inflation.
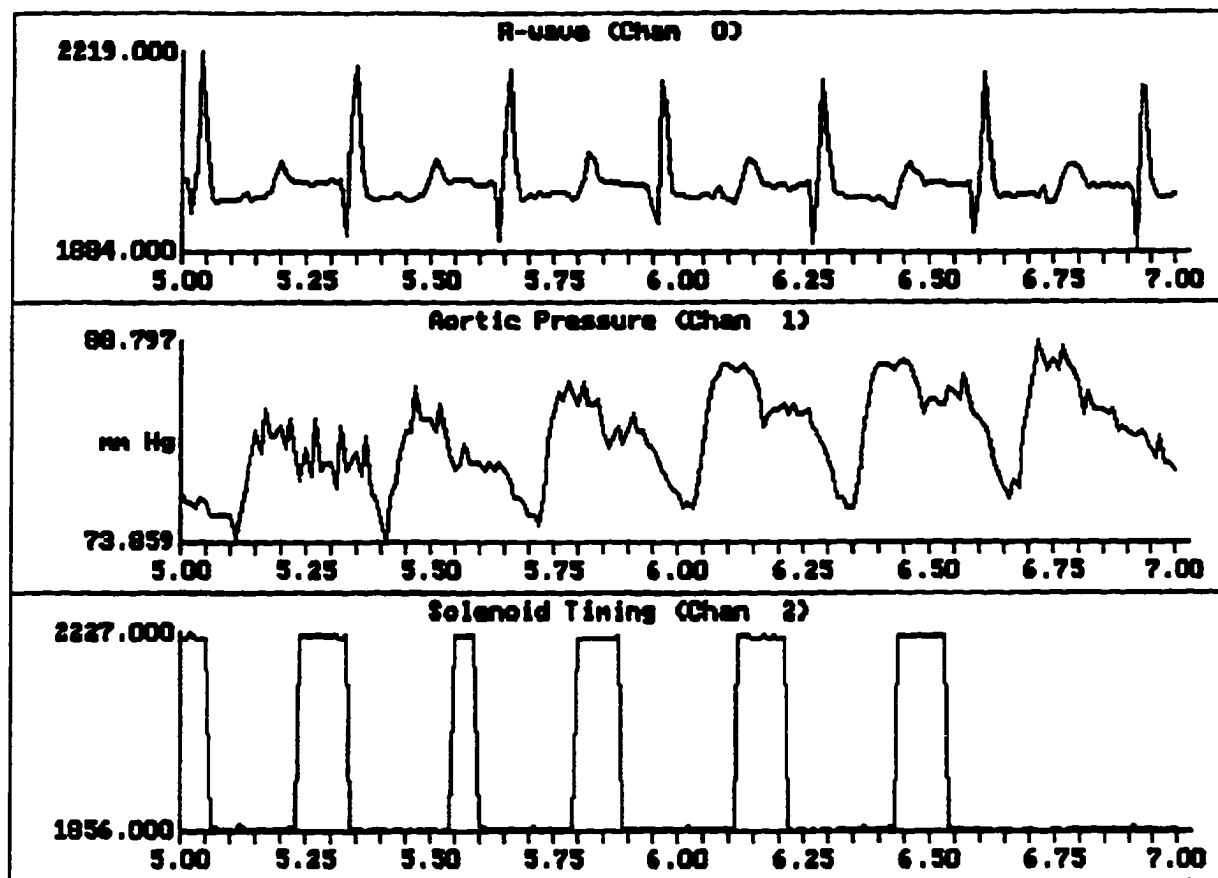
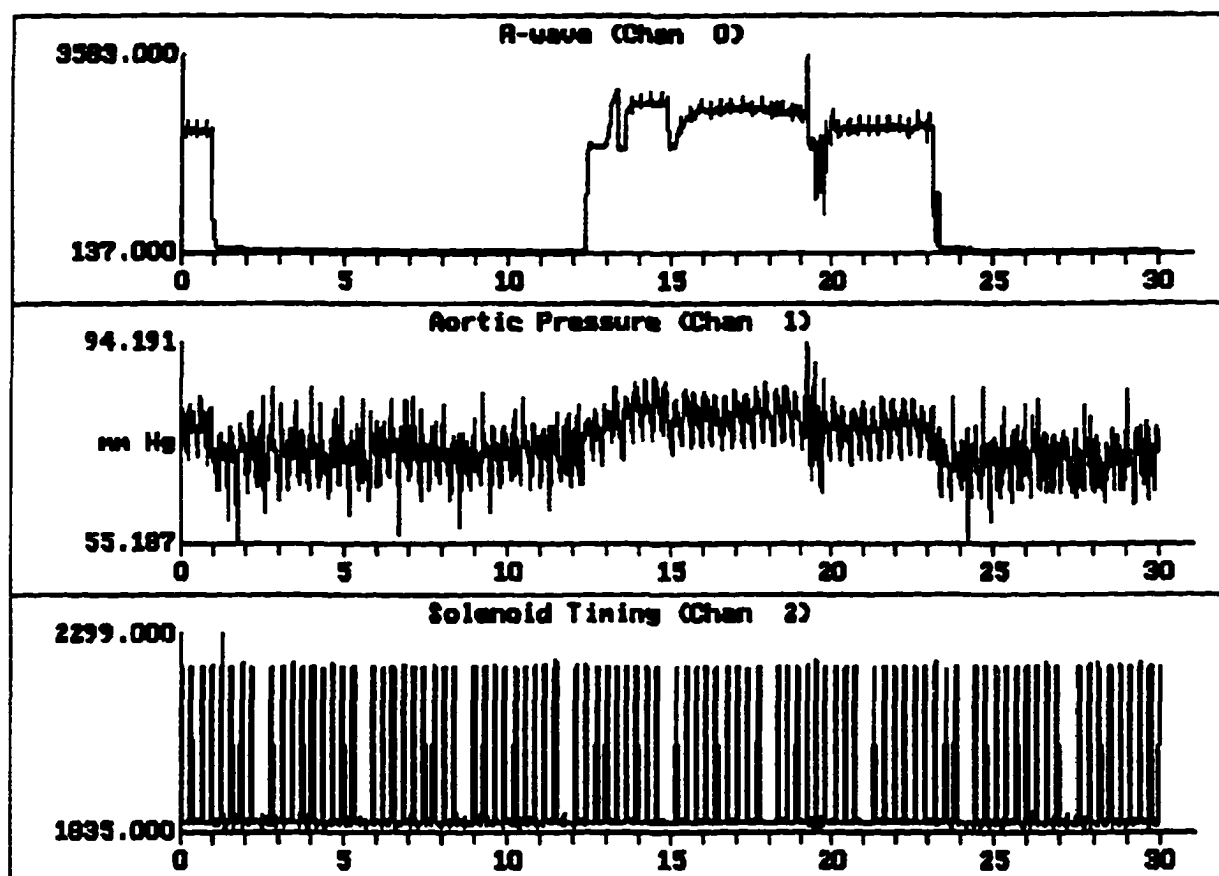**Figure 5-17.** Exploded View of Figure 5-16 showed IABP Triggering Control derived using Pa Trace of Canine Mongrel Experimental Model E illustrates Pa Augmentation during Start of Fast to Moderate Changing Heart Rate (at 180 bpm as seen in Figure 5-17B (middle trace)). ECG provided an Pa Cardiac Cycle Timing Reference as seen in Figure 5-17A (top trace). IAB Inflation/Deflation Control Signal provided an Pa Augmentation Timing Reference as seen in Figure 5-17C (bottom trace). The Cardiac Cycle Observation Beat (in Figure 5-17C at 6.8 seconds) illustrated the Dicrotic Notch and Systolic Rise of Cardiac Cycle without Pa Augmentation due to IAB Inflation.
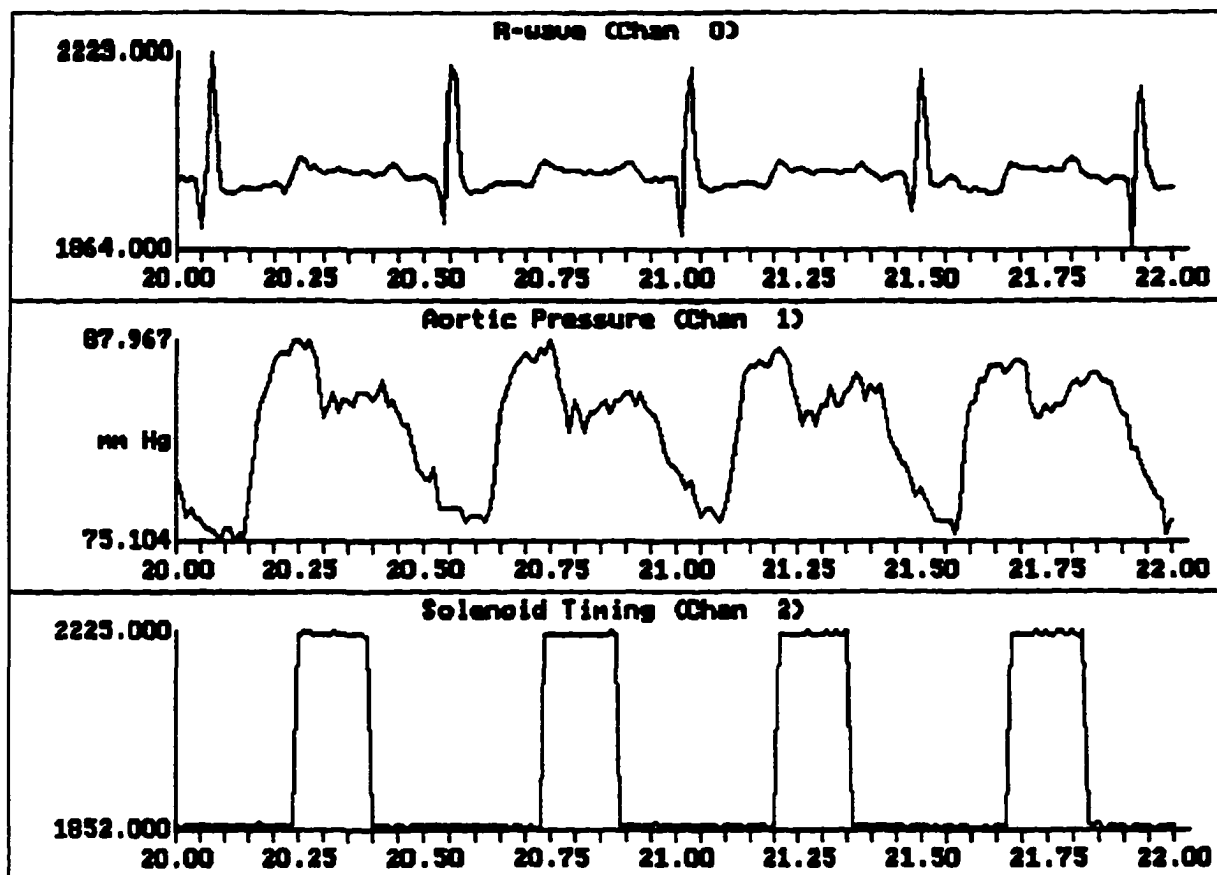
Figure 5-18. Exploded View of Figure 5-16 showed IABP Triggering Control derived using Pa Trace of Canine Mongrel Experimental Model E illustrates Pa Augmentation during end of Fast to Moderate Changing Heart Rate (at 120 bpm as seen in Figure 5-18B (middle trace)). ECG Provided an Pa Cardiac Cycle Timing Reference as seen in Figure 5-18A (top trace). IAB Inflation/Deflation Control Signal provided an Pa Augmentation Timing Reference as seen in Figure 5-18C (bottom trace).

5.1.3.2.2   Extra-Aortic Counterpulsation Device (EACD)

Figure 5-19B illustrates the Pa control augmentation advance toward optimization created by the EACD through Pa signal triggering[1]. The first three heart cycles in Figure 5-19B demonstrate retrograde fill (aortic regurgitation) where deflation occurs a bit too soon thus causing a small amount of blood to flush back into the aorta. The small amount of blood causes a little pressure rise

which can be seen at the end of the augmentation "droop". Once the augmentation interval is lengthened (i.e. deflation occurs a bit later in time relative to the cardiac cycle) the retrograde fill is eliminated as can be seen by the last three full heart cycles. Figure 5-19B demonstrates the deflation timing advance toward optimal EACD Pa timing.

---

1. Note that the peak Extra-Aortic Counterpulsation Device (EACD) augmentation pressure is greater than the peak systolic pressure due to the flushing of blood into the ascending aorta via a piston-cylinder type action.

R-wave (Chan 0)

2158.000

1980.000

5.0   5.5   6.0   6.5   7.0   7.5   8.0

Aortic Pressure (Chan 2)

74.000

mm Hg

23.000

5.0   5.5   6.0   6.5   7.0   7.5   8.0

Solenoid Timing (Chan 5)

2222.000

1858.000

5.0   5.5   6.0   6.5   7.0   7.5   8.0
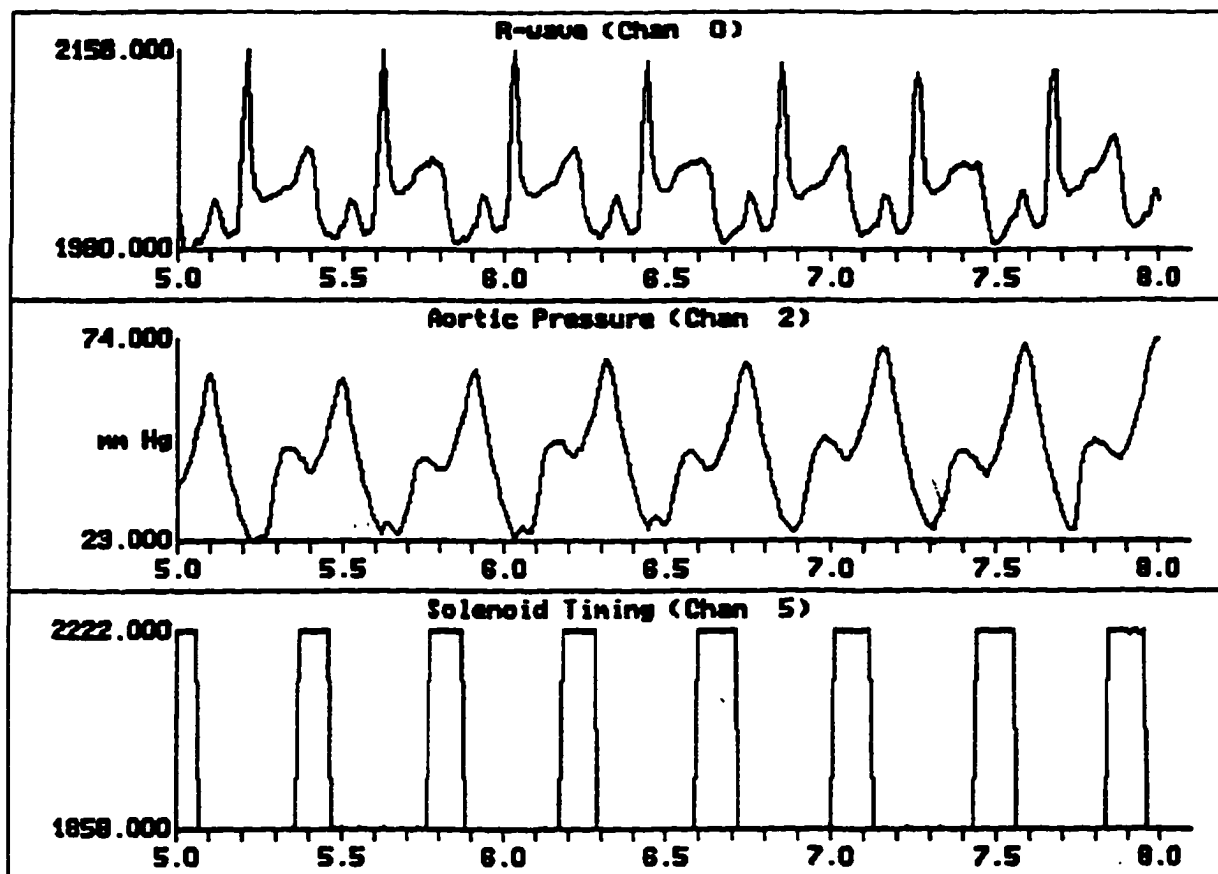
Figure 5-19. EACD Triggering Control derived using Pa Trace of Canine Mongrel Experimental Model F illustrates Pa Augmentation during Moderate Heart Rate of 150 bpm as seen in Figure 5-19B (middle trace). ECG provided a Pa Cardiac Cycle Timing Reference as seen in Figure 5-19A (top trace). IAB Inflation/Deflation Control Signal provided an Pa Augmentation Timing Reference as seen in Figure 5-19C (bottom trace). The Pa Augmentation is the Triangular Shaped Excursion (in Figure 5-19B e.g., between 5.4 and 5.6 seconds). Aortic Regurgitation is the Small Perturbation in the Pa Trace just after the End of the Pa Augmentation (e.g., between 5.6 and 5.7 seconds in Figure 5-19B). Figure 5-19B illustrates the Advancement of Deflation Timing Relative to the Cardiac Cycle (i.e., extending the Inflation Interval) which eliminates the Aortic Regurgitation to provide Optimal Control Deflation Timing of the EACD (e.g., at 6.8 seconds and thereafter).

5.2 Transputer Communication Throughput Results

The results of the transputer research used to demonstrate acceptable communications throughput (as to not use too much transputer processor time) was accomplished in two steps. The first step involved the evaluation of two transputer compilers to determine which was more efficient. A methodology for comparing the effect of different transputer compilers on data throughput of the CAD Control Application was implemented.

Using the Computer Systems Architects (CSA) "CIO" Host I/O driver[1] for "C" language on the transputer host/root processor the two versions of the CSA compiler were analyzed to determine which compiler would provide superior throughput. The representative Pa and ECG signal data was routed to the processing transputers (i.e., leaf processors) via the A/DC to the host processor (PC-AT), then to the root transputer and on the leaf processor. The control information followed the same processor path outward and then onto the port of the D/AC via PC Ports. When taking this route the CSA Compiler version 88.3 provided a throughput rate of 4KBytes/sec. The same communication path was utilized for the CSA Compiler 89.1 and provided a throughput rate of 8KBytes/sec. Thus the superior throughput performance was provided by CSA Compiler 89.1. The second step was to modify the communications software to improve communications efficiency if necessary.

The maximum transfer data rate achieved after evaluating the transputer compilers was 8K bytes / second in which 4 bytes had to be transferred represented a transaction rate of 2K transactions/sec. The sampling rate was set at 500Hz and thus 25% of the CPU time would be used for data transfer. This was deemed unacceptable[2]. A second step was necessary to modify the communications software to improve communications efficiency.

In order to increase the data throughput for the transputer based system, a user written PC-AT host server had to be implemented. This server had to be simplistic to provide a more efficient method of transporting data from the host back and forth to the root transputer processor. Although throughput would increase, additional bytes of data had to be transmitted to replace the more

---

1. The Computer Systems Architects (CSA) CIO host (PC-AT) I/O driver was a high level C language general I/O application written to allow the PC-AT host process to communicate with the root transputer processor application (60) (61) (62).

2. Since the 20Mhz transputer processor was comparatively less powerful than the 33 Mhz PC-AT processor in which the algorithms operated independently during development, it was apparent that the processing power exhaust due to communications should be reduced to less than 10%. This would allow most of the processing power of the transputer processors to be utilized on the CAD control application algorithms.

sophisticated commands provided by the compiler's PC-AT host server. Powerful commands like printf() were no longer available with the user written server. Instead of requiring 4 bytes of data per transfer, 8 bytes of data per transfer are required to allow for very basic diagnostics. Even though twice as many bytes of data were being transferred (four to eight), throughput was still increased by three fold. The percentage of CPU time used for data transfer decreased from 25% to 8.3% because the data rate went from 2Khz to 6Khz transfers/sec.

Previously CPU time used for data transfer (CSA Compiler 89.1, CIO program) $0.5K^1/2K = 25\%$ (5-1)

After R&D (CSA Compiler 89.1, Using Primitive Root Processor Commands) $0.5K/6K = 8.3\%$ (5-2)

5.3 STI to HR Regression Equation Research for Prediction of Dicrotic Notch Timing Using Canine Mongrel Experimental Model Data

This section describes results of the study to determine if a HR vs. STI regression relationship exists for the Cardiothroracic Research Canine Mongrel Experimental Model based on data studied, compiled and analyzed during Canine Mongrel Experiments. For a series of normal heart beats, prediction of the dicrotic notch is relatively simple since the STI is identical for each beat; thus an average can be used. Experimentally where an ischemic heart can cause ectopic beats, a method must be derived to predict the occurrence of the dicrotic notch for the abnormal beat to optimize inflation timing. The strict linear relationship between the heart rate and systolic time intervals in humans gave rise to the possibility that this relationship may potentially exist for canines. Experiments to empirically determine whether the HR to STI relationship exists for canines were performed.

5.3.1 Interpretation of Heart Rate to Systolic Time Interval (STI) Graphical Figures

The numerical coordinate across the bottom of the all graphs (parallel to the title) is heart rate in beats per minute (bpm). The vertical coordinate is milliseconds for the Pa trace systolic time interval of a single heart beat of the canine mongrel experimental model.

---

1. Since data sampling occurs at 500Hz, 500 (0.5K) data transfers/second are required.

In the graphs, each point represents the relationship between the Heart Rate and STI measured from of a single heart beat of the Pa trace of a canine mongrel experimental model.

The line within the graph is the first order linear regression estimate of the plotted points illustrating Heart Rate to STI relationship. The equation for the linear regression is noted at the top of the graph.

The ischemic model reference in parentheses of the graph title indicates that the canine mongrel experimental model had an ischemic heart due to the procedure of tying off certain coronary arteries of the heart. A normal model reference in parentheses of the graph title indicates that the canine experimental model did not have the coronary arteries obstructed (i.e., tied off).

The inderal reference in parentheses of the graph title indicates that inderal (a beta-blocker) was administered to the canine mongrel. The no inderal reference in parentheses indicates that inderal was not administered.

The potential use of the heart rate to STI regression equation for inflation prediction requires the plotted graph points (actual data) to be located closely to the regression equation (numerical estimate). The more the data is scattered from the estimate, the less likely the estimate can be used to predict the dicrotic notch accurately during a non-sinus rhythm of a canine mongrel experimental model. The method of determining if a heart rate to STI regression equation is providing a reasonable estimate is if all plotted points are within 15% of the linear regression STI estimate. For example if the plotted point is located at heart rate = 120 bpm and STI = 230 milliseconds. That plotted point would be right on the boundary of acceptance if the heart rate to regression equation provided an STI estimate (at a heart rate = 120bpm) equal to 200 milliseconds.

All experiments must indicate the heart rate to STI regression equation will provide an accurate prediction of when the dicrotic notch will occur (once the systolic rise is detected) to make the estimate viable for CAD inflation prediction during non-sinusoid rhythms in canine mongrel experimental models.

The STI to HR plots were created with Cricket Graph software.

5.3.2 Results of STI to HR Regression Equation Research for Prediction of Dicrotic Notch Timing Using Canine Mongrel Experimental Model Data

The Canine Mongrel Experimental Models used in Cardiothoracic Research experiments are typically subjected to intravenous drug therapy (i.e beta-blockers) as well as the physiological conditions common to Cardiothoracic Surgery. For reasons beyond the scope of this dissertation,

the linear relationship between the heart rate and the systolic time interval in canines does not exist as it does in humans. The absence of a strict heart rate vs. STI relationship present in humans contrasts the results found for canines. The nonlinear relationship between the experimental canine heart rate and systolic time interval is demonstrated in Figure 5-20 through Figure 5-24. Canine Mongrel Experimental Models S, T, and W (i.e., Figure 5-20, Figure 5-21, and Figure 5-24) demonstrate variation in STI for a given Heart Rate of greater than 15% which was determined to be unacceptable for dicrotic notch prediction. Canine Mongrel Experimental Models U and V (i.e., Figure 5-22 and Figure 5-23) demonstrate more predictable values as seen from the graphs. However, because the HR to STI regression does not exist for all of the experimental models, the HR to STI regression technique was not chosen for dicrotic notch prediction.

Systolic Time Interval(ms)

400 —

360 —

$$y = 194.81436 - 0.12822x \quad r^2 = 0.02270$$

320 —

280 —

240 —

200 —

160 —

120 —

80 —

40 —

0 —

50   70   90   110   130   150   170   190   210
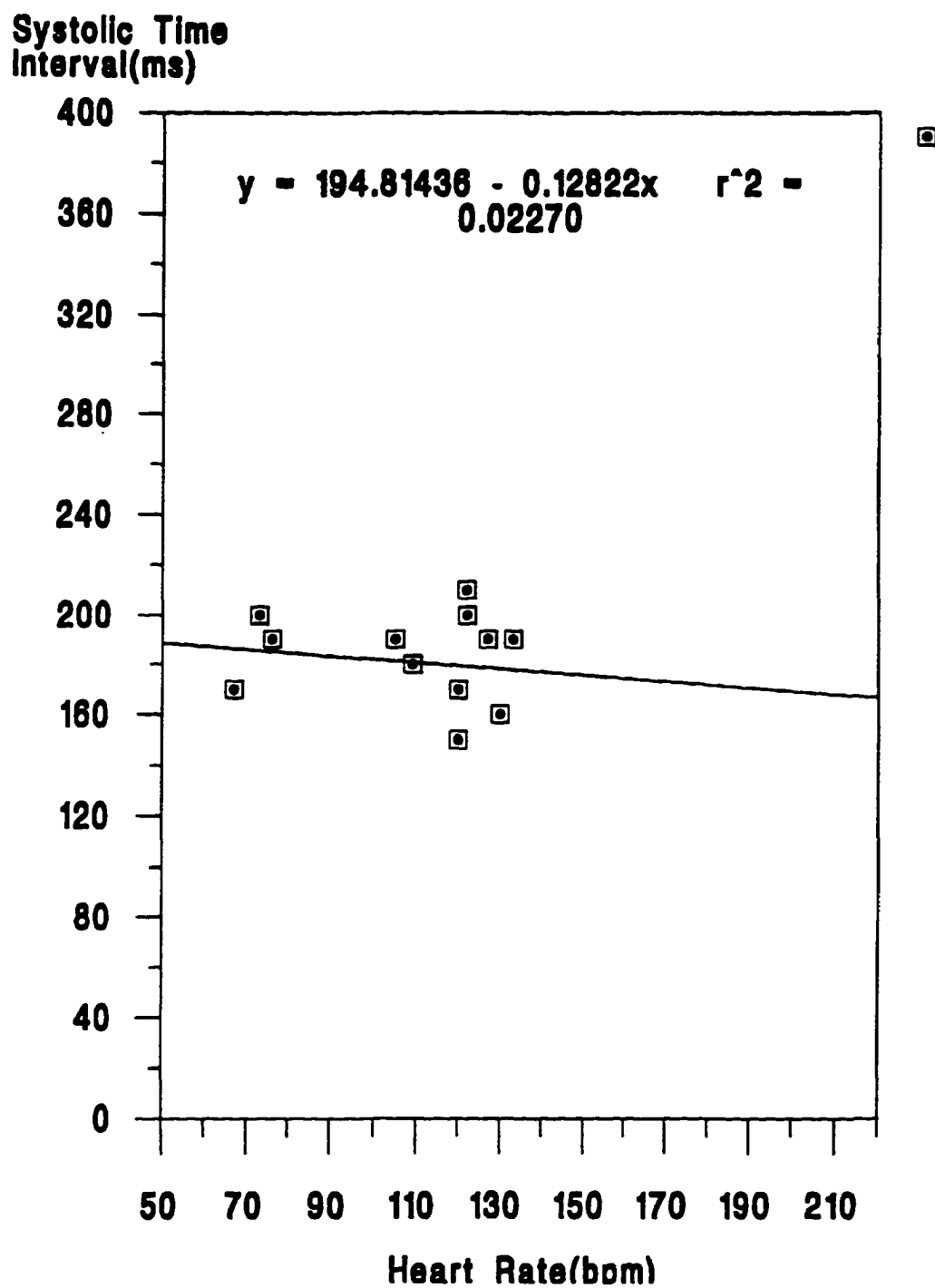
Heart Rate(bpm)

Figure 5-20. Canine Mongrel Experimental Model Heart Rate to STI Plotted Points and Linear Regression Estimate Equation for Canine Mongrel Experimental Model S (Healthy Model, No Drug Therapy)
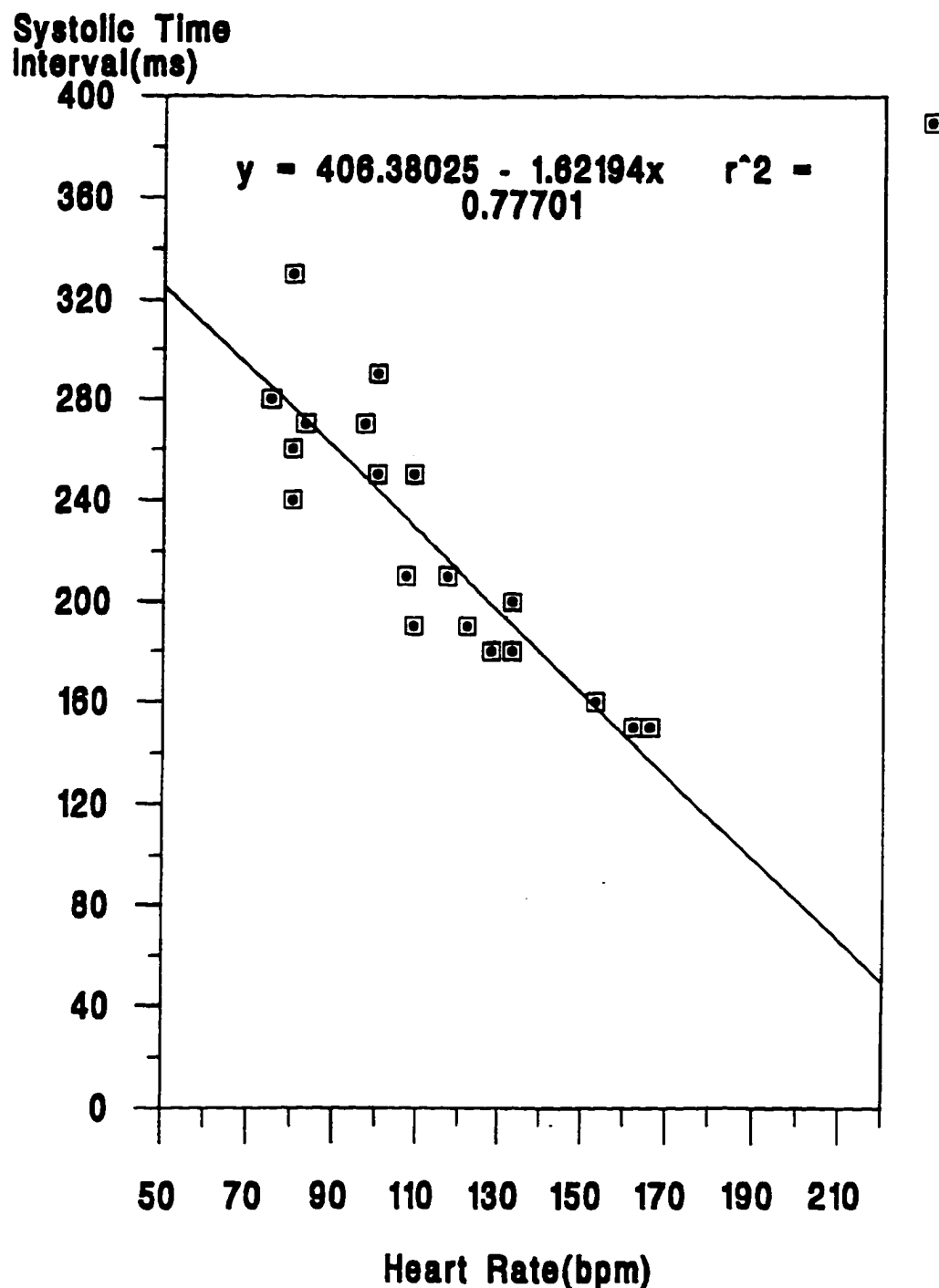
Figure 5-21. Canine Mongrel Experimental Model Heart Rate to STI Plotted Points and Linear Regression Estimate Equation for Canine Mongrel Experimental Model T (Ischemic Model, Inderal Therapy)

Systolic Time Interval(ms)

$$y = 203.65523 - 0.33129x \qquad r^2 = 0.44255$$
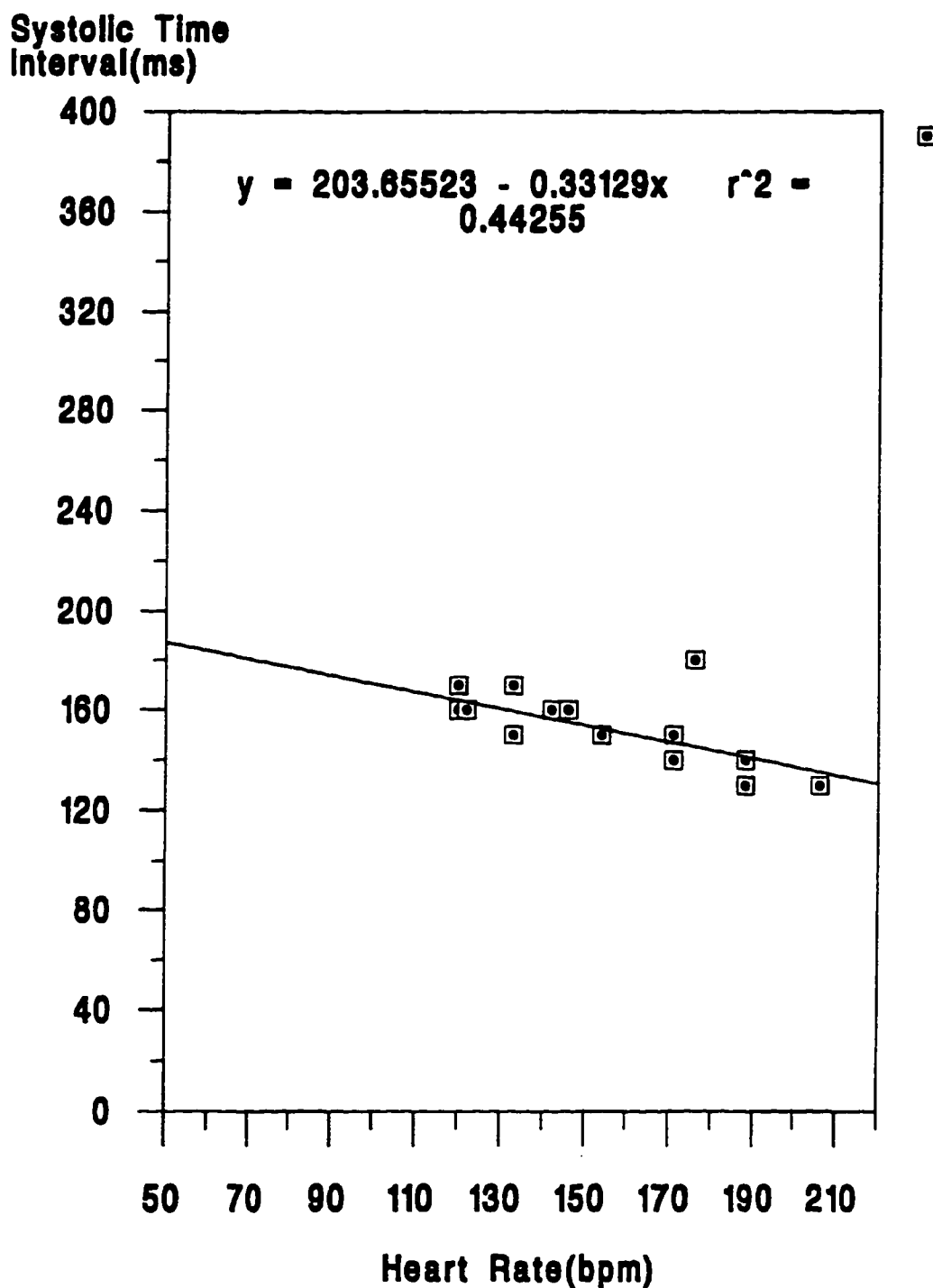
Heart Rate(bpm)

Figure 5-22. Canine Mongrel Experimental Model Heart Rate to STI Plotted Points and Linear Regression Estimate Equation for Canine Mongrel Experimental Model U (Healthy Model, Inderal Therapy)

Sytolic Time Interval(ms)
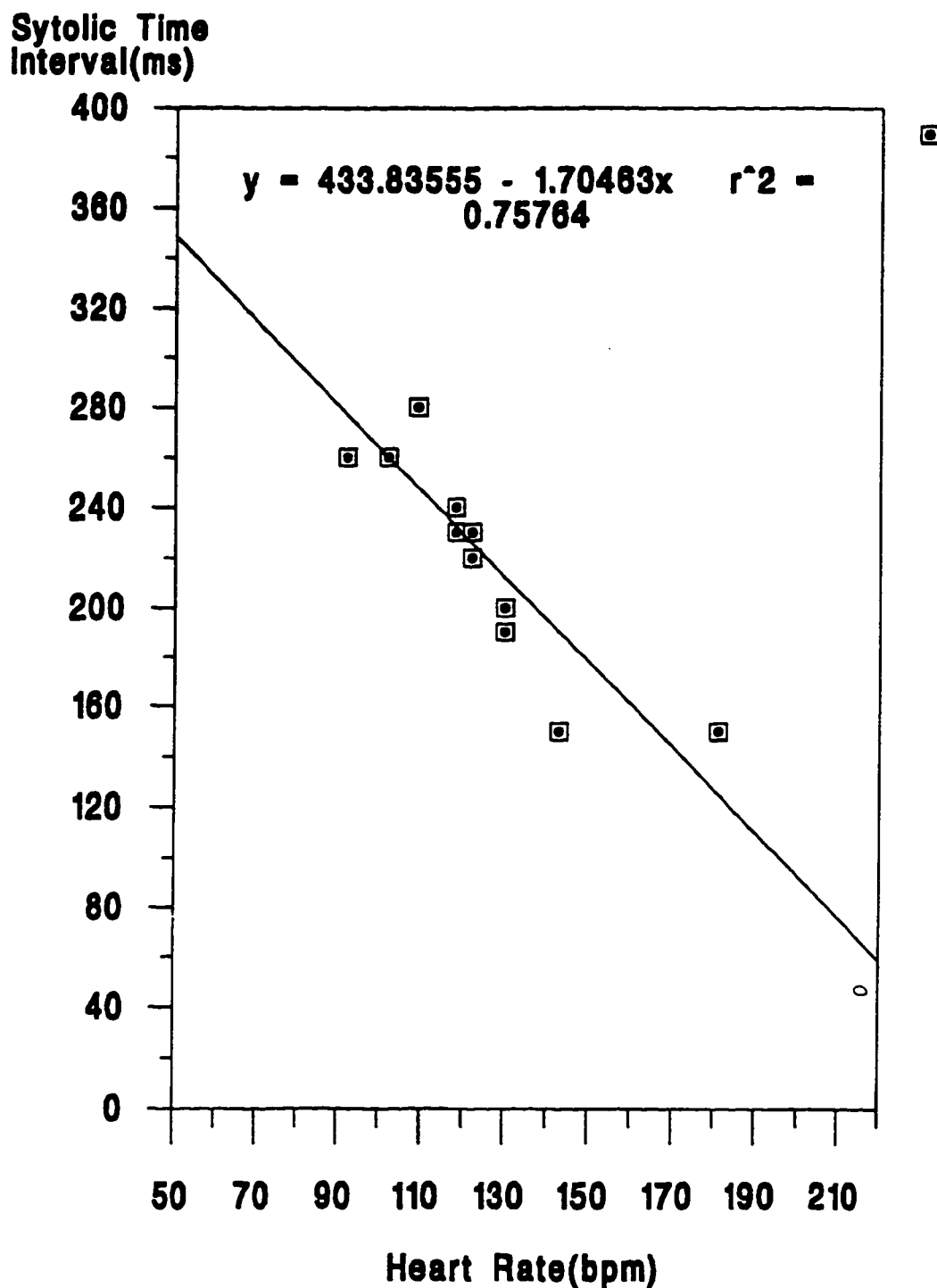
Heart Rate(bpm)

Figure 5-23. Canine Mongrel Experimental Model Heart Rate to STI Plotted Points and Linear Regression Estimate Equation for Canine Mongrel Experimental Model V (Ischemic Model, Inderal Therapy)
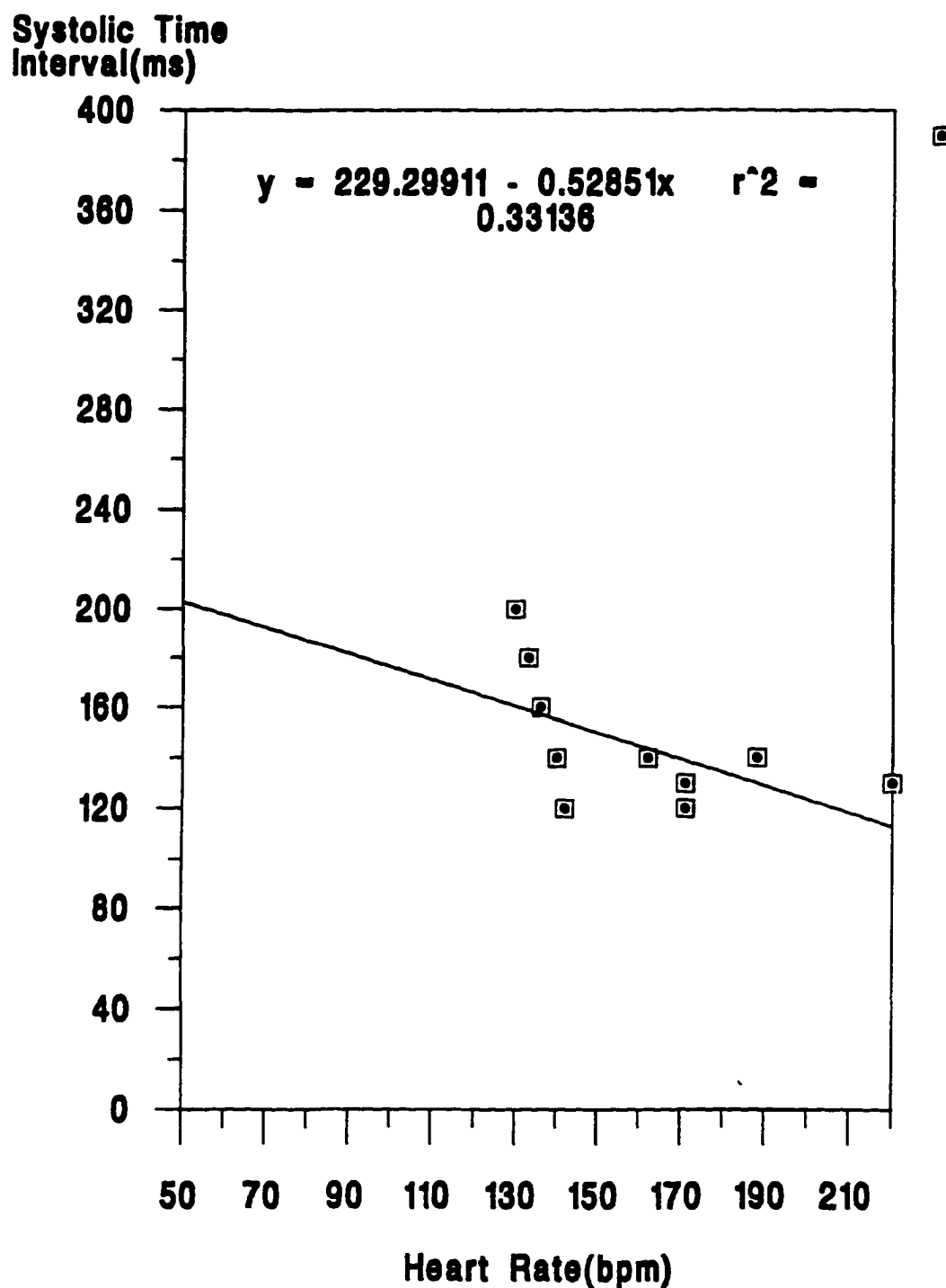
Figure 5-24. Canine Mongrel Experimental Model Heart Rate to STI Plotted Points and Linear Regression Estimate Equation for Canine Mongrel Experimental Model W (Ischemic Model, No Drug Therapy)

6. Pa Model Detection Simulation Experimental Procedure and Results

This chapter discusses the simulation experimental procedures and experimental results of research conducted in this dissertation paper, namely, CAD control Pa detection simulation research. The development of the experimental Pa trace model, Pa distortion models and simulation integration development is described in Chapter 4. Section 6.1 describes the experimental procedures followed to perform the Pa detection simulation experiments. Section 6.2 lists the experimental log for the simulation research. Section 6.3 describes and illustrates the results from the experiments performed with development of the CAD control Pa detection simulation research.

6.1   Experimental Procedure

The Simulation Experimental procedures were similar to the actual experiments except that a simulated Pa trace was utilized as opposed to the Pa control signal originating from a canine mongrel experimental model.

The procedure for the simulated experiments was as follows:

1. Execute VisSim Application version 1.2 (Later version 1.5 with "impulse block" Bug corrected) using Mouse from Windows 3.1 running on IBM 486 PC-AT clone with 16M of RAM and 350M harddisk.

2. Import VisSim appropriate diagram with Pa trace model, Pa dicrotic notch model, Pa trace artifact model, and detection algorithm external block.

3. Configure simulation parameters as appropriate within the "Simulate" pull-down menu.

    1. The "Simulation Setup" menu is selected and the following parameters must be populated:

        1. Length of Simulation (Populate: Range Start, Range End)

        2. The "Integration Algorithm" selection chosen was Euler. (Euler was chosen as opposed to other integration algorithm because it only executed the Pa detection imported DLL block once per simulation step as desired.)

        3. Simulation Interval (Populate: Step Size = 0.002 seconds = 500Hz)

    2. The "Control Panel" was selected several times to offer a step by step control of the simulation execution. The "Step" option was particularly useful in debugging certain simulations.

4. Assuming all models are built, configure appropriate connections for simulation (e.g., connect Pa trace to Pa detection algorithm external DLL block.

5. Determine appropriate signals to be displayed.

6. Determine appropriate methods to collect data (i.e. type and number of graphs (i.e., plot blocks

7. Execute Simulation using the "Go" command in the "Simulate" pull-down menu. Stopping the simulation prematurely requires using the "Stop" command in the "Simulate" pull-down menu.

8. Review results graphically and numerically (if appropriate) to determine if desired research results were achieved.

9. Format graph for to display desired section of the graphical result.

10. Output results to printer.

The experimental procedure also included progressively challenging the Pa systolic rise and dicrotic notch detection algorithms to find the disturbance severity at which the algorithm could no longer reliably detect the targeted cardiac events. This involved numerically increasing the Pa disturbance. The advantage to simulation was that the disturbances could be precisely adjusted empirically to provide a very accurate threshold for algorithm detection competence. This would be considerably more difficult or impossible when performing experiments using a canine mongrel experimental model in a Cardiothoracic Surgical Environment.

6.2   Experimental Log

Once the Pa trace model, Pa dicrotic notch model, Pa trace artifact models, and detection algorithm external DLL block were developed, experimentation was the next step. (The Pa simulation experiment "block" diagrams are described and illustrated in Chapter 4, entitled 4, "CAD Pa Modeling and Detection Simulation Verification," page 4–98.) The categories of experimental simulations conducted are itemized below.

1. Stability Simulation

2. Ideal Pa Trace with No Dicrotic Notch Perturbation

3. Ideal Pa Trace with Pa Dicrotic Notch Perturbation

4. Pa Trace Varying Baseline Due to Effects of Mechanical Ventilation

5. Pa Trace Amplitude Variation Due to Catheter Pressure Transducer Tip Positioning and Sensitivity

6. Pa Trace Distorted by Uniformly Distributed Noise

7. Pa Trace Distorted by Gaussian Distributed Noise

8. Heart Rate Variability Due to Respiration

6.3   Experimental Results

As noted in Section 6.2, several categories of simulations were conducted. The results of these simulations are depicted graphically in Section 6.3.2 through Section 6.3.8. The simulation results demonstrate the robustness of the Pa systolic rise and dicrotic notch detection algorithm (i.e.,

cardiac assist device detector). The following section, Section 6.3.1, provides a general overview of the Simulation Illustrations coordinates, traces, and signals. Section 6.3.1 also provides a methodology for interpreting a successful simulation.

6.3.1 Interpretation of Simulation Results

6.3.1.1 Reference to Figures with "Top," "Middle" and "Bottom" Traces

The majority of simulation illustrations within this section have three traces which will be referred to as the A (top), B (middle), and C (bottom) trace (starting with the top of the page and moving downward, as seen in Figure 6-1, i.e., Figure 6-1A (top trace), Figure 6-1B (middle trace), and Figure 6-1C (bottom trace), respectively). The three traces were created simultaneously during a single simulation to illustrate detection signals (top trace), output of detection filters (middle trace), and unobstructed Pa trace (bottom trace).

6.3.1.2 Figure Coordinates

The numerical coordinate across the bottom of the all traces is time in seconds (e.g., as labelled across the bottom of the all three traces in Figure 6-1). The coordinates shown vertically on the trace are amplitude simulation units which correspond to mmHg for the Pa and detection states for the digital filter detector signals (e.g., as labelled on the left side of all three traces of Figure 6-1). The vertical coordinate values for the detection signal "square wave" are in arbitrary units. However, a "square wave" transition in the detection signal indicates something has been detected (as seen in Figure 6-1A) or indicates a detection window[1] has opened or closed (as seen in lower part of Figure 6-1A).

6.3.1.3 Signals within the Simulation Traces

In all of the figures with three traces (i.e., top, middle and bottom trace), the top trace illustrates the Pa signal, the detection signal which intersects the Pa trace, and at the very bottom of the trace, the dicrotic notch detection window signal (e.g., as seen in Figure 6-1A). The Pa signal is a

---

1. A detection window is a time interval in which a cardiac cycle event may be detected e.g., the dicrotic notch detection window indicates when the dicrotic notch may be detected based on criteria within the Pa detection algorithm.

representation of the output of the Pa trace model. The "squarewave-like" detection signal signifies the detection of the systolic rise, peak systolic pressure and the dicrotic notch. The systolic rise detection is signified by the first positive going transition. The detection of peak systolic pressure is signified by the first negative going transition. The dicrotic notch detection is signified by the second negative going transition. The positive going slope of the dicrotic notch detection window trace (e.g., as seen at the lower part of Figure 6-1A) signifies the dicrotic notch detection algorithm can detect a dicrotic notch and the negative going slope of the dicrotic notch detection window indicates either the dicrotic notch is detected or the detection algorithm can no longer detect the dicrotic notch.

The middle trace has four signals, the Pa signal, the current second derivative window signal and the ambient second derivative window signal and the dicrotic notch detection window (e.g., as seen in the Figure 6-1B). Again, the Pa signal is a numerical representation of the Pa model. The more current second derivative window signals is a numerical representation of the current second derivative window. The ambient second derivative window signal is a numerical representation of the overall Pa trace second derivative window. (The distinction between the two second derivative signals may be viewed more easily in Figure 6-3, which is an amplified view of Figure 6-1B. The current second derivative window is the "spike" with the leading phase as compared to the ambient second derivative window signal.) A comparison of the current second derivative window signal and the ambient second derivative window signal is used in the detection of the dicrotic notch and is included here to illustrate timing of this detection signal with respect to the systolic rise and dicrotic notch occurrence. The second derivative signals are also illustrated to show the large amplitude generated by the Pa detection filter which provided a strong signal for detection. The positive going slope of the dicrotic notch detection window signal (e.g., as seen at the bottom of Figure 6-1B) signifies the dicrotic notch detection algorithm can detect a dicrotic notch and the negative going slope of the dicrotic notch detection window indicates either the dicrotic notch is detected or the detection algorithm can no longer detect the dicrotic notch.

The bottom trace has one signal, the Pa signal, it is shown alone so it may be viewed unobstructed from any other signals (e.g., as seen in Figure 6-1C).

6.3.1.4   Evaluating the Success of a Pa Trace Model Detection Simulation

The success of the a Pa Trace Model Detection Simulation can be determine by evaluating the signals within the top trace (e.g. the signals of Figure 6-1A). The relationship between the Pa signal

and the detection signal "square wave" must be aligned. A 100% detection is used as criterium for all Pa cardiac events to be detected, namely, the systolic rise, peak systolic pressure and the dicrotic notch. The positive transition of the "square wave" detection signal should occur shortly after the start of the systolic rise. The first of two negative transitions of the "square wave" detection signal should occur shortly after the peak of systolic pressure. The second of two negative transitions of the "square wave" detection signal should occur slightly after or during the dicrotic notch deflection. If all three cardiac events are detected for all cardiac cycles displayed, once the Pa detection filter is trained[1], the simulation is considered a success.

6.3.1.5   Reference to Figures with a Single Trace

A subset of the simulation illustrations have a single trace. Again, the numerical coordinate across the bottom of the traces is time in seconds. The single trace figures are amplified vertically to provide a better view of the signals within the trace. The vertical coordinate units are simulation units which represent mmHg for all of the following signals: the Pa trace(e.g., as seen in Figure 6-3), the current second derivative window signal (e.g., as seen in Figure 6-3), the ambient second derivative window signal (e.g., as seen in Figure 6-3), uniformly distributed noise (e.g., as seen in Figure 6-17), Gaussian distributed noise (e.g., as seen in Figure 6-20), and the inverted half-wave rectified sinusoid (which creates the dicrotic notch deflection (e.g., as seen in Figure 6-17 and Figure 6-20). The vertical coordinate values for the detection signal "square wave" are in arbitrary units. However, a "square wave" transition in the detection signal indicates something has been detected (e.g., as seen in Figure 6-24) or indicates a detection window has opened or closed (e.g., as seen in Figure 6-24). Additional detail will be provided with the description of each figure with a single trace.

6.3.2   Stability Simulation

The stability of the aortic pressure simulator and CAD detector was demonstrated by illustrating a continuous aortic pressure simulator signal and CAD detector that detects the Pa systolic rise and dicrotic notch for 600 seconds (or 10 minutes).

---

1. Pa detection filter "training" refers to the time it takes for the detection filter to develop thresholds and statistics which mathematically characterize the wave to ensure accurate detection.

6.3.2.1 Top Trace

The Figure 6-1A illustrates the detection of the systolic rise (positive transition of the squarewave), peak systolic pressure (first negative transition of the square wave), and dicrotic notch (second negative transition of the square wave). The positive transition of the small pulse in the lower part of Figure 6-1A illustrates the start of the dicrotic notch detection window. The negative transition of the small pulse in the lower part of Figure 6-1A illustrates the close of the dicrotic notch detection window. The close of the dicrotic notch detection window of Figure 6-1A is initiated by the detection of the dicrotic notch[1]

6.3.2.2 Middle Trace

Figure 6-1B illustrates the dicrotic notch detector signals, namely the current second derivative window filter and the ambient second derivative window filter of the Pa trace. The second derivative window is strongest during the change in the rate of slope due to the systolic rise and dicrotic notch within the Pa signal.

6.3.2.3 Bottom Trace

Figure 6-1C illustrates the Pa signal without any other signals so it may be viewed unobscured to ensure the Pa signal reflects the type of simulation being conducted (e.g., a stability simulation).

6.3.2.4 Simulation Technique and Significance

The simulation technique that was used to derived the results of the simulation illustrated in Figure 6-1 was to generate the ideal Pa trace with the Pa trace model and provide that signal to the Pa detection filter. (Refer to Section 4.5.1 for a description of the Pa model.)

The significance of the stability simulation illustrated in Figure 6-1 was to demonstrate that the VisSim-based Pa detection Simulation Platform is stable (e.g., no software crashes) and provides realistic[2] and rational[3] results over a relatively long period of time (i.e., 10 minutes). In addition the

---

1. The dicrotic notch detection window is the timing window which will allow a dicrotic notch to be detected. This timing of the window is based on certain criteria including reference to the peak systolic pressure and the diastolic pressure. The dicrotic notch detection window will close for two reasons. The first reason the dicrotic notch closes is the detection of the dicrotic notch. The second reason the dicrotic notch detection closes is that the algorithm determines that the appearance of the dicrotic notch is no longer possible (this would indicate the dicrotic notch was missed i.e., a false positive). Since the criterium for a successful detection simulation is 100% detection accuracy, the dicrotic notch detection window closing because of a missed detection is not displayed.

ideal Pa trace signal (and associated Pa trace profile) does not vary from cardiac cycle to cardiac cycle. It is important that the Pa trace profile of the ideal Pa trace is unchanged from cardiac cycle to cardiac cycle because the Pa trace is used as the "control" signal for simulations that follow in Section 6.3.3 through Section 6.3.8. The simulations in Section 6.3.3 through Section 6.3.8 vary the ideal "control" Pa signal to demonstrate the Pa detection algorithms immunity to various forms of biological variation (e.g,. hart rate variability due to respiration) and Pa signal artifact (e.g., noise).

As was described in the criteria for a successful Pa detection simulation in Section 6.3.1.4, the systolic rise, peak systolic pressure, and dicrotic notch in Figure 6-1A are all detected for every cardiac cycle.

Figure 6-2 provides a closer look (expanded time scale) at the last five seconds of the same stability simulation illustrated in Figure 6-1. (The description of Figure 6-1A (in Section 6.3.2.1), Figure 6-1B (in Section 6.3.2.2), and Figure 6-1C (in Section 6.3.2.3) also describes the corresponding traces in Figure 6-2, namely, Figure 6-2A, Figure 6-2B and Figure 6-2C.) The additional simulation information that is illustrated in Figure 6-2 is as follows. Figure 6-2C provides a closer look at the stable aortic pressure wave in the last five seconds of the stability run of Figure 6-1. The Pa template is repeatable and very similar the Pa trace observed in man. Figure 6-2A illustrates the accurate CAD detection for each of the last five heart beats. The accuracy of the detection is more easily observed in Figure 6-2.A

Figure 6-3 provides a closer look (expanded time scale and amplitude scale) at the last second of the same stability simulation illustrated in Figure 6-1. (The description of Figure 6-1B in Section 6.3.2.2 also describes Figure 6-3.) The additional simulation information that is illustrated in Figure 6-3 is as follows. Figure 6-3 illustrates the second derivative dicrotic notch detector signals. The second derivative detector trace with the leading phase response (i.e., the "spike" at the time of the second derivative) is proportional to the current second derivative window. The second derivative detector trace with the lagging phase "spike" is proportional to the ambient second derivative window. A comparison of these second derivative based signals leads to a very accurate and robust

---

2. A realistic result in simulation is one in which the result is possible, however, may or may not be applicable (i.e., rational or unrational) to the simulation being conducted. For example, a blood pressure of zero mmHg is possible in a deceased person, however is not possible (i.e., not rational) in these simulations where the Pa is of the living patient. A Pa with negative values within the signal would be an unrealistic simulation result.

3. A rational result in simulation is one in which the result is possible (i.e, realistic) and also possible for the particular simulation conducted. A Pa trace ranging from 120 mmHg to 80 mmHg in a simulation modelling a healthy patient is rational. A Pa trace ranging from 60 mmHg to 40 mmHg in a simulation modelling a healthy patient is not rational.

dicrotic notch CAD detection methodology for CAD control. The CAD control detection filter responses were accurate for detecting "ideal" Pa signals as well as Pa signals with various degrees[1] of biological variation (e.g,. heart rate variability due to respiration) and with Pa signal artifact (e.g., noise).

o

---

1. Heart rate variability due to respiration may appear as a 1 beat per minute variation in one patient and as a 2 beat per minute variation in a second patient.
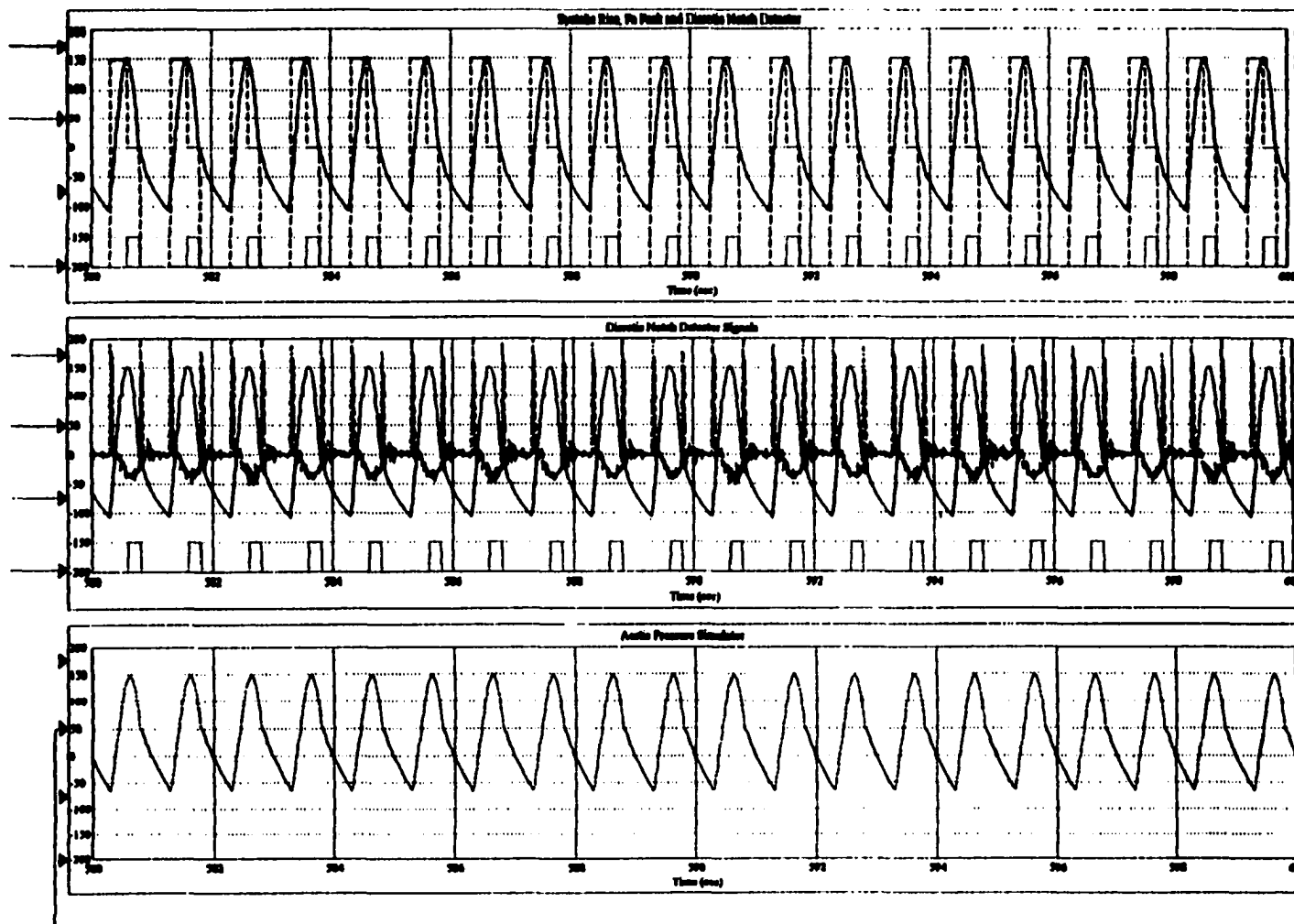
Figure 6-1. Figure 6-1A (top trace) illustrates Pa Detection of Systolic Rise, Peak Systolic Pressure and Dicrotic Notch. Figure 6-1B (middle trace) illustrates Second Derivative Window Filter Output used to Detect the Dicrotic Notch. The Last 20 Seconds of Ten Minute Simulation illustrated a Stabile Aortic Pressure Signal is shown in Figure 6-1C (bottom trace).

174
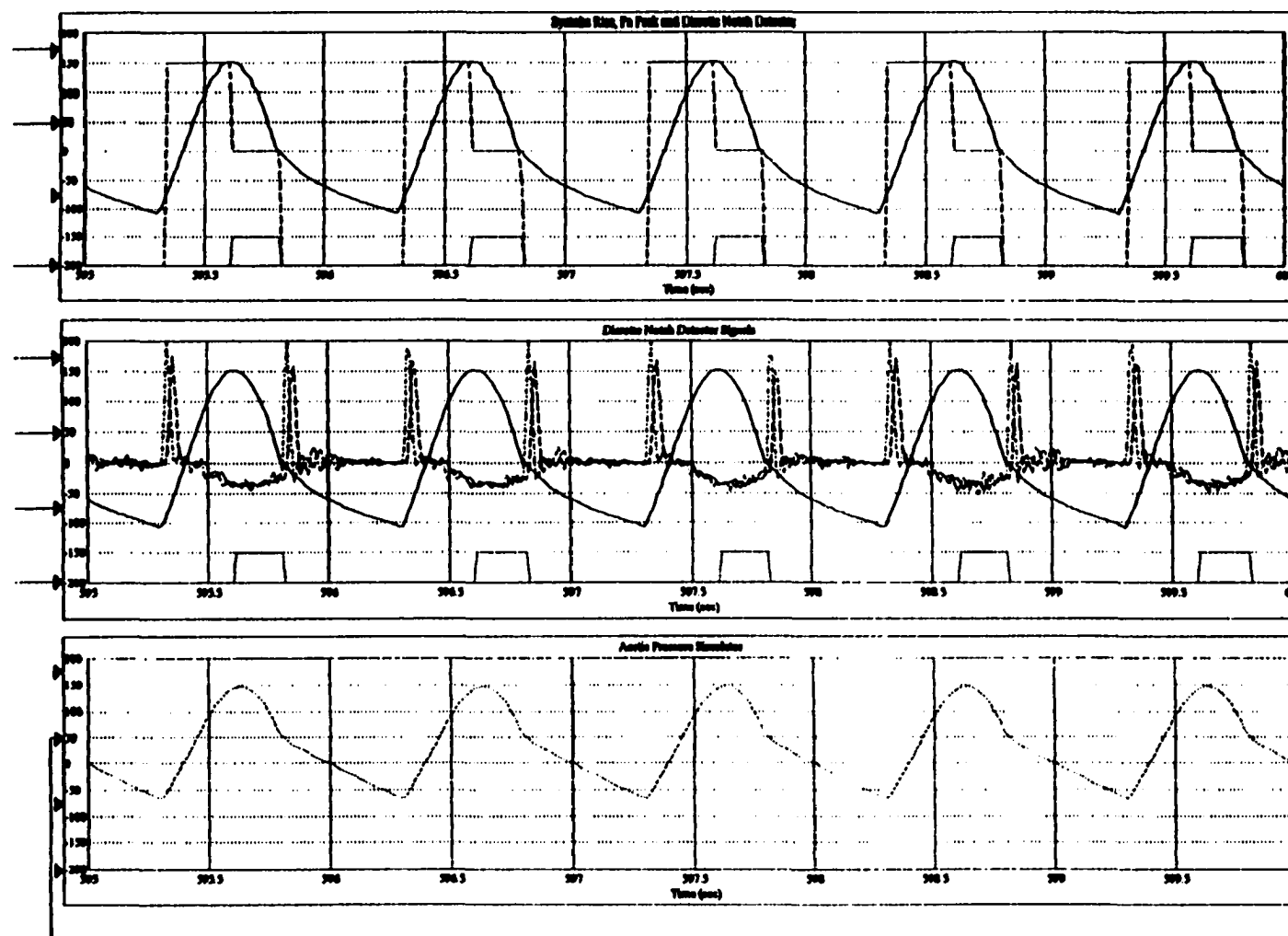
Figure 6-2. The Last 5 Seconds of Ten Minute Simulation in Figure 6-1 Illustrates Accurate Pa Detection as shown in Figure 6-2A (top trace). Figure 6-2B (middle trace) illustrates the Dicrotic Notch Detector Signals. Figure 6-2C (bottom trace) illustrates the Pa Signal.

Dicrotic Notch Detector Signals
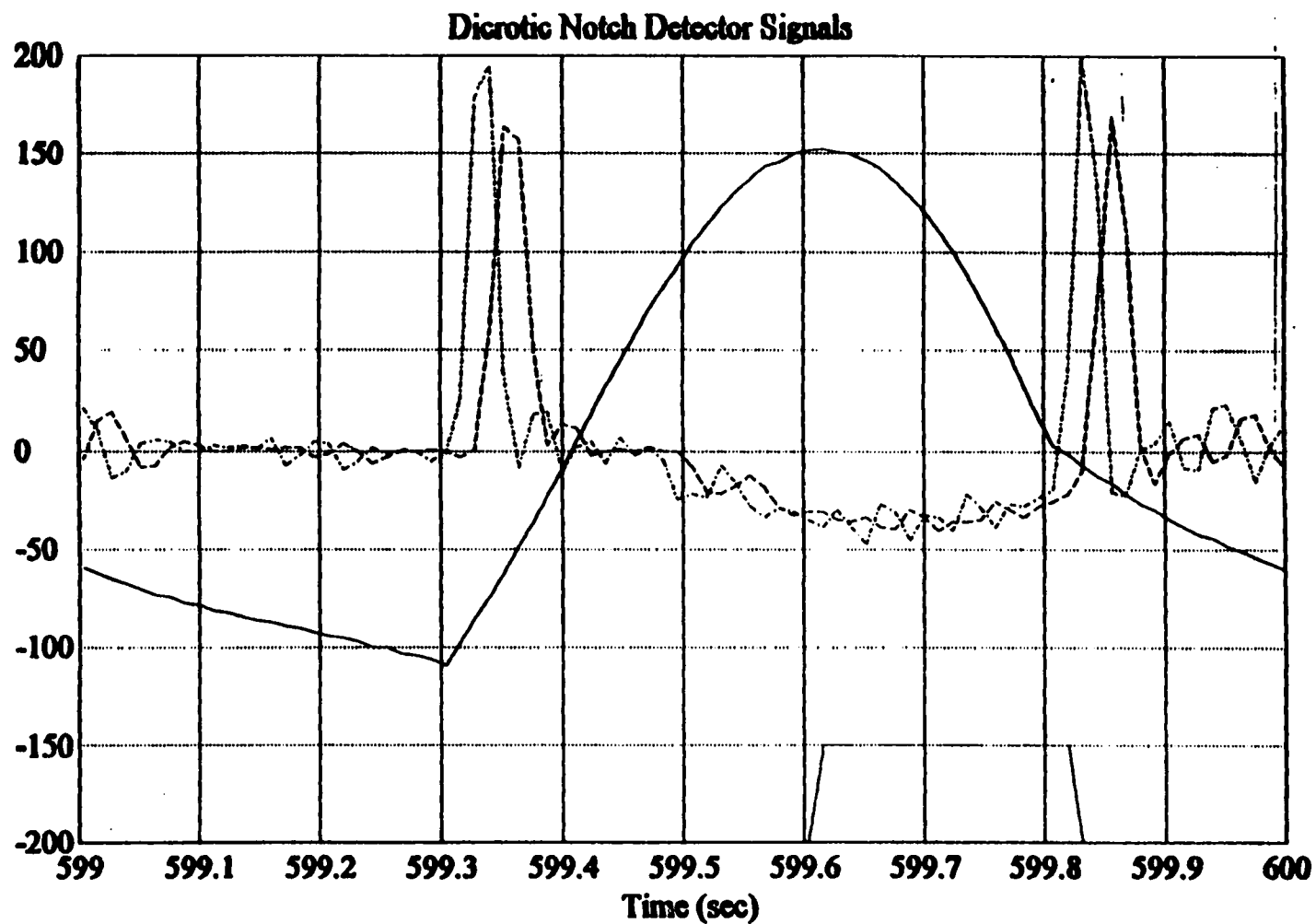
Figure 6-3. An Amplified View of the Second Derivative Dicrotic Notch Pa Detector Signals from Stability Simulation of Figure 6-1. The Leading Phase Current Second Derivative Window Signal is the taller of the Two "Spikes." The Lagging Phase Ambient Second Derivative Window Signal is the Shorter of the Two "Spikes."

178

6.3.3 Ideal Pa Trace with No Dicrotic Notch Perturbation

The ability of the CAD Pa detector to detect a Pa signal without a dicrotic notch perturbation is demonstrated in Figure 6-4. The relationship between the simulated Pa trace signal and CAD detector signal demonstrates detection of the Pa systolic rise, peak systolic pressure and dicrotic notch of the Pa wave with no dicrotic notch perturbation.

Figure 6-4 provides a closer look (expanded time scale) at the last second of the stability simulation illustrated in Figure 6-1. (The description of Figure 6-1A (in Section 6.3.2.1), Figure 6-1B (in Section 6.3.2.2), and Figure 6-1C (in Section 6.3.2.3) of Figure 6-1 also describes the corresponding traces of Figure 6-4.) The additional simulation information that is illustrated in Figure 6-4 is as follows. Figure 6-4 illustrates the detection of the very subtle dicrotic notch that is represented only by a small change in slope. The delay of the dicrotic notch detector illustrated in Figure 6-4A (the timing of the second negative transition of the squarewave in relation to the change in slope of the Pa trace) is shown to be approximately 10 milliseconds after the occurrence of the dicrotic notch slope deflection.

The simulation technique that was used to derive the results of the simulation illustrated in Figure 6-4 was to generate the ideal Pa trace with Pa trace model and provide that signal to the Pa detection filter. The dicrotic notch perturbation model was not integrated into the Pa trace model for this simulation. (Refer to Section 4.5.1 for a description of the Pa model.)

The significance of the Pa detection simulation with no dicrotic notch perturbation illustrated in Figure 6-4 was to demonstrate that detection is occurring accurately even though no "notch" shape is present in the aortic pressure wave. The lack of the dicrotic notch perturbation reduces the amount of second derivative window amplitude at the dicrotic notch as compared to a Pa signal with a dicrotic notch perturbation. The reduced amount of amplitude makes detection more difficult.[1] Only a small change in slope represents the dicrotic notch. This represents one extreme of biological variation that is encountered when detecting the dicrotic notch, namely, a Pa trace with a dicrotic notch perturbation of zero mmHg. The Pa detection algorithm has the capability to detect a dicrotic notch with no dicrotic notch perturbation.

---

1. The derivative based detection filters use changes in slope associated with the systolic rise and dicrotic notch as criteria for detection.

As was described in the criteria for a successful Pa detection simulation in Section 6.3.1.4, the systolic rise, peak systolic pressure, and dicrotic notch in Figure 6-4A were detected within the single cardiac cycle displayed.

O
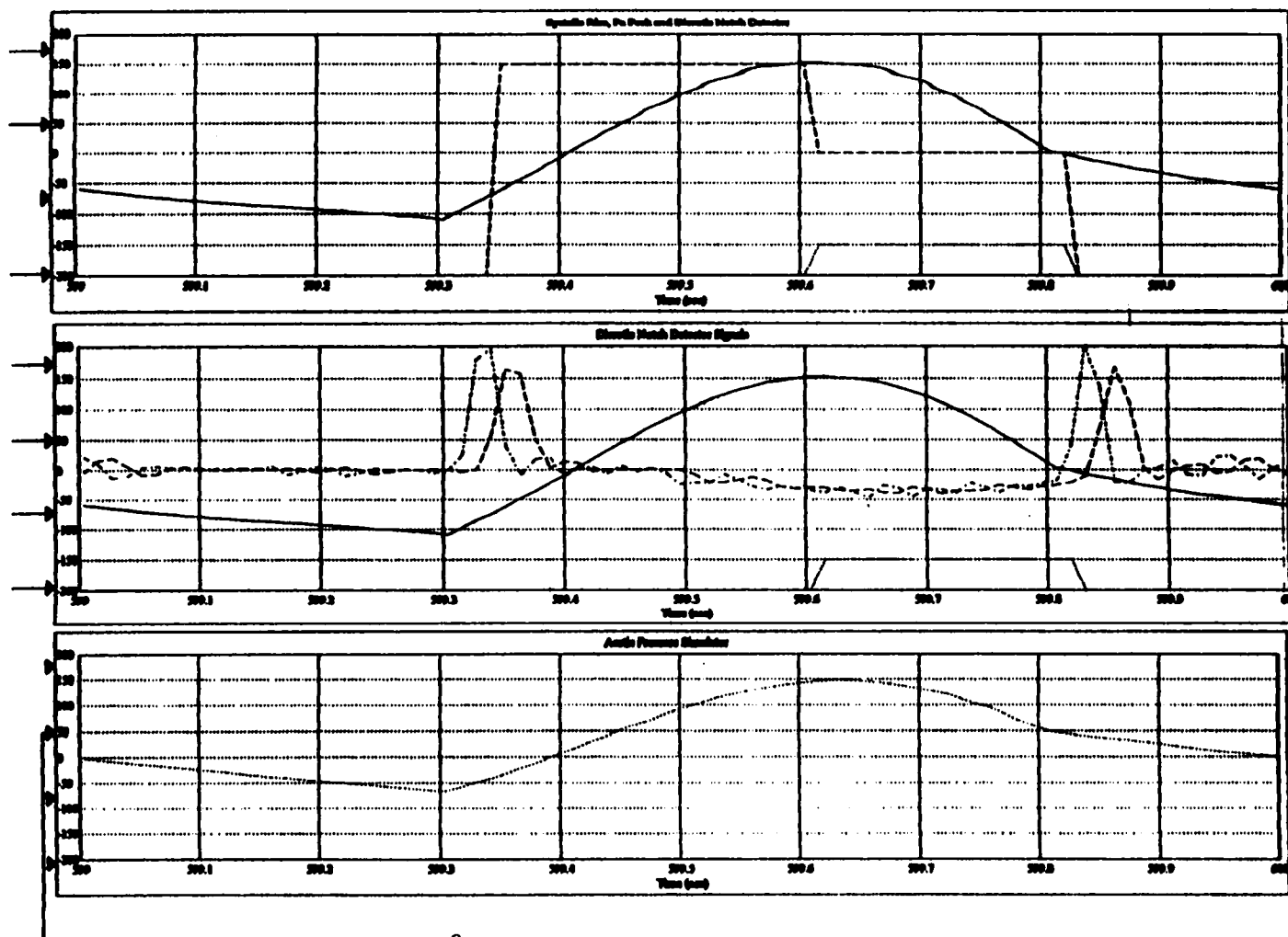
Figure 6-4. The Accuracy of Aortic Pressure (Pa) Detector for Dicrotic Notch without Pa Overshoot (from Figure 6-1) is displayed in Figure 6-4A (top trace). Detection Occurs Approximately 10 milliseconds after the Dicrotic Notch (Second Negative Transition) of the Detection Square Wave as seen in the Figure 6-4A. Figure 6-4B (middle trace) illustrates the Dicrotic Notch Detector Signals. Figure 6-4C (bottom trace) illustrates the Pa Signal.

179

6.3.4 Ideal Pa Trace with Pa Dicrotic Notch Perturbation

The ability of the CAD Pa detector to detect an Pa signal with a dicrotic notch perturbation (modelled with a half-wave rectified inverted sinusoid) is demonstrated in Figure 6-5 and Figure 6-6. The relationship between the simulated Pa trace signal and CAD detector signal demonstrates detection of the Pa systolic rise, peak systolic pressure and dicrotic notch of the Pa wave with a dicrotic notch perturbation.

Figure 6-5 illustrates the detection of the dicrotic notch with a pressure perturbation. (The description of Figure 6-1A (in Section 6.3.2.1), Figure 6-1B (in Section 6.3.2.2), and Figure 6-1C (in Section 6.3.2.3) of Figure 6-1 also describes the corresponding traces in Figure 6-5.) The additional simulation information that is illustrated in Figure 6-5 is as follows. Figure 6-5 illustrates the detection of the dicrotic notch that is represented by a 3 mmHg sinusoidal deflection (i.e., depression) exactly at the change in slope of the Pa trace. Figure 6-5A illustrates quick training of the CAD detection filter which occurs within 17.5 seconds. The filter is accurately detecting all three cardiac events within 17.5 seconds as seen in Figure 6-5A.

The simulation technique that was used to derive the results of the simulation illustrated in Figure 6-5 was to generate the ideal Pa trace with the Pa trace model and combine the ideal Pa trace with output of the Pa dicrotic notch perturbation model. The combined Pa signal with Pa dicrotic notch perturbation is then provided to the Pa detection filter. (Refer to Section 4.5.1 for a description of the Pa model. Refer to Section 4.5.1.1 for a description of the dicrotic notch model.)

The significance of the Pa detection simulation with a dicrotic notch perturbation illustrated in Figure 6-5 was to demonstrate that detection is occurring accurately during the "notch" shape present in the aortic pressure wave. This represents one extreme of biological variation that is encountered when detecting the dicrotic notch, namely, a Pa trace with a dicrotic notch perturbation of 3 mmHg. The Pa detection algorithm has the capability to detect a dicrotic notch with a 3 mmHg dicrotic notch perturbation. Figure 6-5 demonstrates the Pa detection algorithms immunity to the form of biological variation due to the variance in the dicrotic notch perturbation. Figure 6-4A in the previous section (Section 6.3.3) illustrates reliable detection for the other extreme of biological variation, a dicrotic notch with no dicrotic notch perturbation (i.e., 0 mmHg). Thus the Pa detection algorithm has biological variation dicrotic notch perturbation immunity between 0 to 3 mmHg.

As was described in the criteria for a successful Pa detection simulation in Section 6.3.1.4, the systolic rise, peak systolic pressure, and dicrotic notch in Figure 6-5A were detected for all the cardiac cycles displayed.

Figure 6-6 provides a closer look (expanded time scale) of the last four seconds of the same simulation illustrated in Figure 6-5. (The description of Figure 6-1A (in Section 6.3.2.1), Figure 6-1B (in Section 6.3.2.2), and Figure 6-1C (in Section 6.3.2.3) of Figure 6-1 also describes the corresponding traces in Figure 6-6.) The additional simulation information that is illustrated in Figure 6-6 is as follows. The Pa template generated is very similar to the Pa trace (with dicrotic notch perturbation) observed in humans. The accuracy of the detection is more easily observed in Figure 6-6. The delay of the dicrotic notch detector illustrated in Figure 6-6A (the timing of the second negative transition of the squarewave in relation to the start of the Pa perturbation) occurs approximately 10 milliseconds prior to the end of the dicrotic notch. The detection occurs at approximately 20 milliseconds after the start of the dicrotic notch.
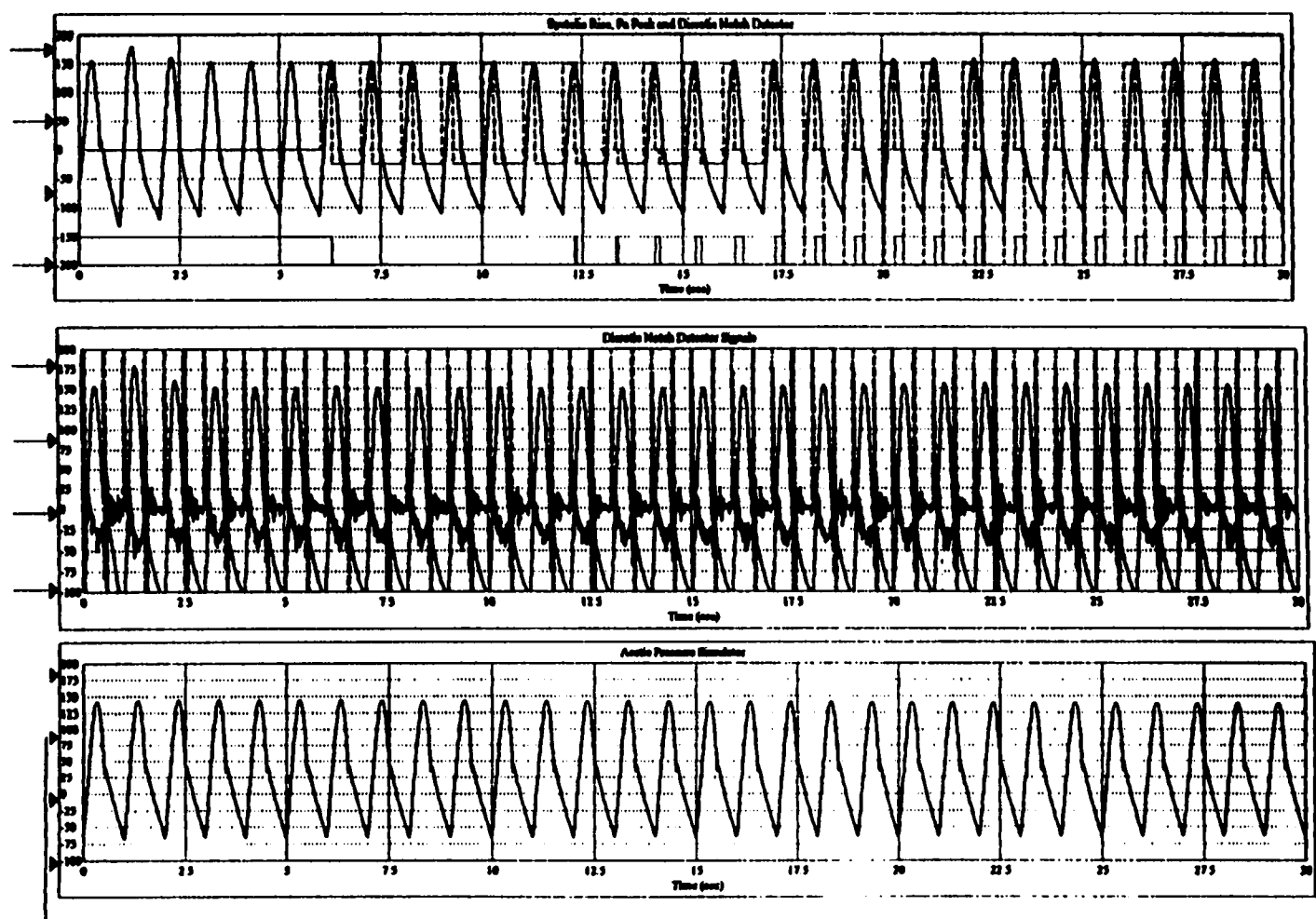
Figure 6-5. Simulated Aortic Pressure (Pa) Detection of Dicrotic Notch with Pa Overshoot is shown Figure 6-5A (top trace). Accurate Detection Occurs 17.5 Seconds after the Pa Trace Initiates as indicated by the Second Negative Going Transition in Figure 6-5A. Figure 6-5B (middle trace) illustrates the Dicrotic Notch Detector Signals. Figure 6-5C (bottom trace) illustrates the Pa Signal.
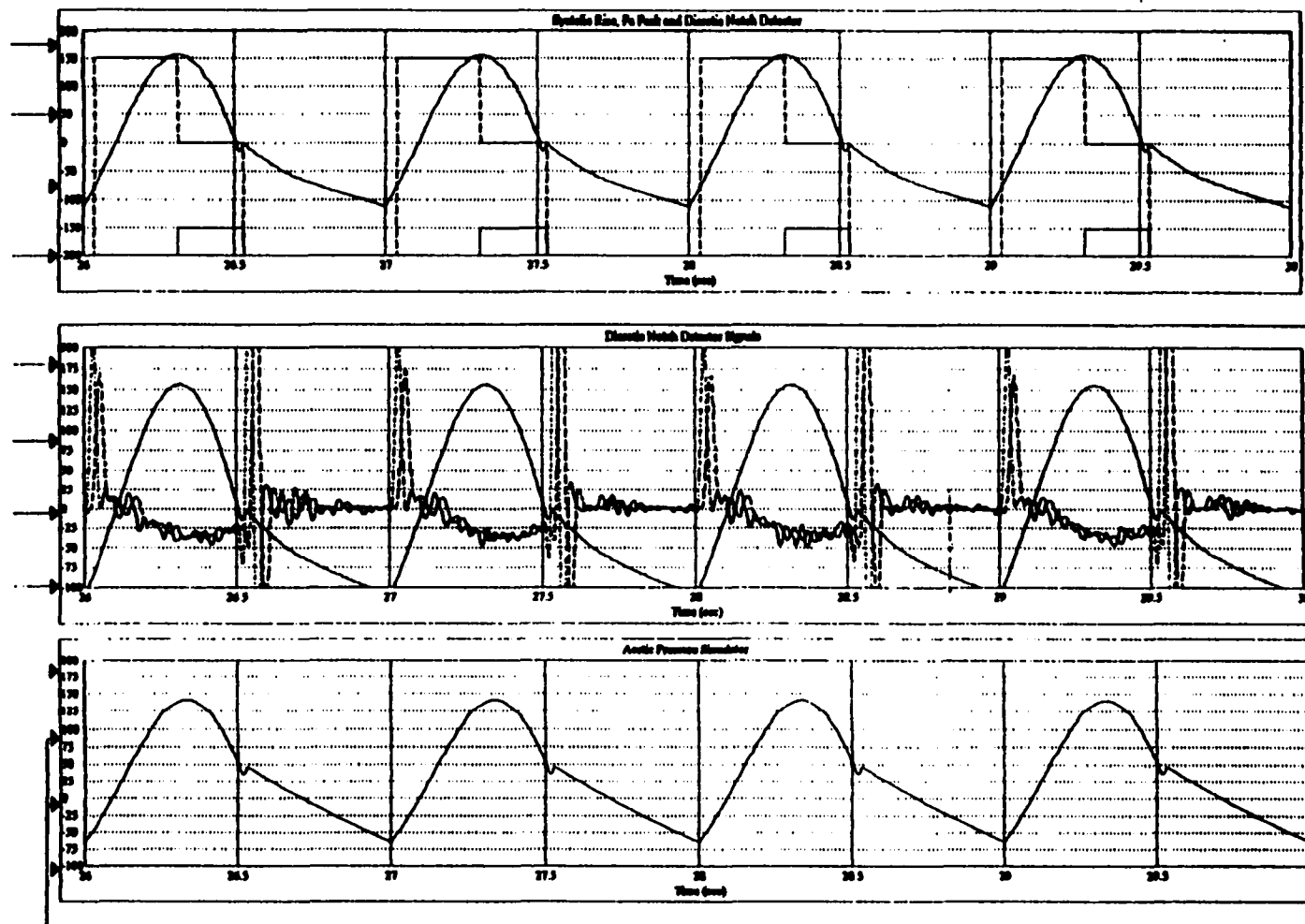
Figure 6-6. The Accuracy of Simulated Aortic Pressure (Pa) Detection of Dicrotic Notch with Pa Overshoot of the Simulated Pa Waveform of Figure 6-5 can be more easily viewed in Figure 6-6A (top trace). Detection occurs at Exactly the Dicrotic Notch Deflection as seen in Figure 6-6A. Figure 6-6B (middle trace) illustrates the Dicrotic Notch Detector Signals. Figure 6-6C (bottom trace) illustrates the Pa Signal.

6.3.5 Pa Trace Varying Baseline Due to Effects of Mechanical Ventilation

The ability of the CAD Pa detector to detect an Pa signal with a baseline pressure variation (also known as baseline wander) due to mechanical ventilation is demonstrated in Figure 6-7 and Figure 6-8. The relationship between the simulated Pa trace signal and CAD detector signal demonstrates detection of the Pa systolic rise, peak systolic pressure and dicrotic notch of the Pa wave with baseline variation due to mechanical ventilation.

Figure 6-7 illustrates the detection of the dicrotic notch with baseline variation due to mechanical ventilation. (The description of Figure 6-1A (in Section 6.3.2.1), Figure 6-1B (in Section 6.3.2.2), and Figure 6-1C (in Section 6.3.2.3) of Figure 6-1 also describes the corresponding traces in Figure 6-7.) The additional simulation information that is illustrated in Figure 6-7 is as follows. Figure 6-7 illustrates the detection of the dicrotic notch during baseline wander due to a modelled breath rate of 12 breaths per minute. The baseline wander causes a fluctuation of 10 mmHg in the baseline. Figure 6-7A illustrates quick training of the CAD detection filter which occurs within 17.5 seconds. The filter is accurately detecting all three cardiac events within 17.5 seconds as seen in Figure 6-7A.

The simulation technique that was used to derive the results of the simulation illustrated in Figure 6-7 was to generate the ideal Pa trace with the Pa trace model and combine the ideal Pa trace with output of the Pa dicrotic notch perturbation model. The Pa trace with the dicrotic notch perturbation is then combined with the mechanical ventilation baseline wander model. The combined Pa signal with Pa dicrotic notch perturbation and baseline wander is then provided to the Pa detection filter. (Refer to Section 4.5.1 for a description of the Pa model. Refer to Section 4.5.1.1 for a description of the dicrotic notch model. Refer to Section 4.5.2.3 for a description of the mechanical ventilation baseline wander model.)

The significance of the Pa detection simulation with a baseline wander illustrated in Figure 6-7 was to demonstrate that detection is occurring accurately during the baseline wander at the frequency of the mechanical ventilator in the aortic pressure wave. Baseline wander due mechanical ventilation represents one artifact of the cardiothroracic surgery operating room that can be encountered when detecting the dicrotic notch. The Pa detection algorithm has the capability to detect a dicrotic notch with a 10 mmHg baseline wander at a breath rate of 12 breaths per minute[1]. Figure 6-7A demonstrates the Pa detection algorithms immunity to the type of artifact due to the cardiothroracic surgery operating room. Figure 6-1 in a previous section (Section 6.3.2) illustrates reliable detection

---

1. The frequency of the baseline wander is dictated by the breath (i.e., ventilation) rate of the mechanical ventilator.

for the other extreme of baseline wander, an Pa trace with no baseline wander (i.e., 0 mmHg). From the simulation results illustrated in Figure 6-7A and Figure 6-1A, the Pa detection algorithm mechanical ventilation baseline wander immunity has been demonstrated to be between 0 mmHg to 10 mmHg.

As was described in the criteria for a successful Pa detection simulation in Section 6.3.1.4, the systolic rise, peak systolic pressure, and dicrotic notch in Figure 6-7A were detected in all cardiac cycles displayed.

Figure 6-8 provides a closer look (expanded time scale) at the last four seconds of the same simulation illustrated in Figure 6-7. (The description of Figure 6-1A (in Section 6.3.2.1), Figure 6-1B (in Section 6.3.2.2), and Figure 6-1C (in Section 6.3.2.3) of Figure 6-1 also describes the corresponding traces in Figure 6-8.) The additional simulation information that is illustrated in Figure 6-8 is as follows. The Pa template generated is very similar to a Pa trace with baseline wander due to mechanical ventilation observed in man. The accuracy of the detection is more easily observed in Figure 6-8A. The dicrotic notch detection, illustrated in Figure 6-8A (the timing of the second negative transition of the squarewave in relation to the dicrotic notch perturbation of the Pa trace) occurs approximately 5 milliseconds prior to the end of the dicrotic notch. The dicrotic notch detection occurs at approximately 25 milliseconds after the start of the dicrotic notch.

Figure 6-9 is the result of a simulation identical to the simulation results illustrated in Figure 6-7 (10 mmHg baseline wander) except for the fact that the baseline wander has been increased to 20 mmHg. The increase in wander of the Pa baseline can be observed in Figure 6-9C. The result of the simulation documented in Figure 6-9 are identical to that of the simulation illustrated in Figure 6-7 (10 mmHg baseline wander) including that the CAD Pa detection of dicrotic notch occurs within 17.5 seconds and detection occurs at approximately 5 milliseconds prior to the end of the dicrotic notch. Figure 6-10 provides a closer look (expanded time scale) at the last four seconds of the same simulation illustrated in Figure 6-9 to demonstrate the detection accuracy.

Figure 6-11 is the result of a simulation identical to the simulation results illustrated in Figure 6-7 (10 mmHg baseline wander) except for the fact that the baseline wander has been increased to 40 mmHg. The increase in wander of the Pa baseline can be observed in Figure 6-11C. The result of the simulation documented in Figure 6-11 are different to that of the simulation illustrated in Figure 6-7 (10 mmHg baseline wander) in that CAD Pa detection of dicrotic notch occurs within 27.5 seconds and the detection occurs at approximately at the end of the dicrotic notch (30 milliseconds after the start of the dicrotic notch). Figure 6-12 provides a closer look (expanded time scale) at the

last four seconds of the same simulation illustrated in Figure 6-11. Due to the extreme variation in baseline pressure, dicrotic notch detection does not start until 27.5 seconds have elapsed as seen in Figure 6-11A (in contrast to the 17.5 seconds in Figure 6-7A and Figure 6-9A).

From the simulation illustrated in Figure 6-7 through Figure 6-12, the Pa detection algorithm mechanical ventilation baseline wander immunity has been demonstrated to be between 0 to 40 mmHg.
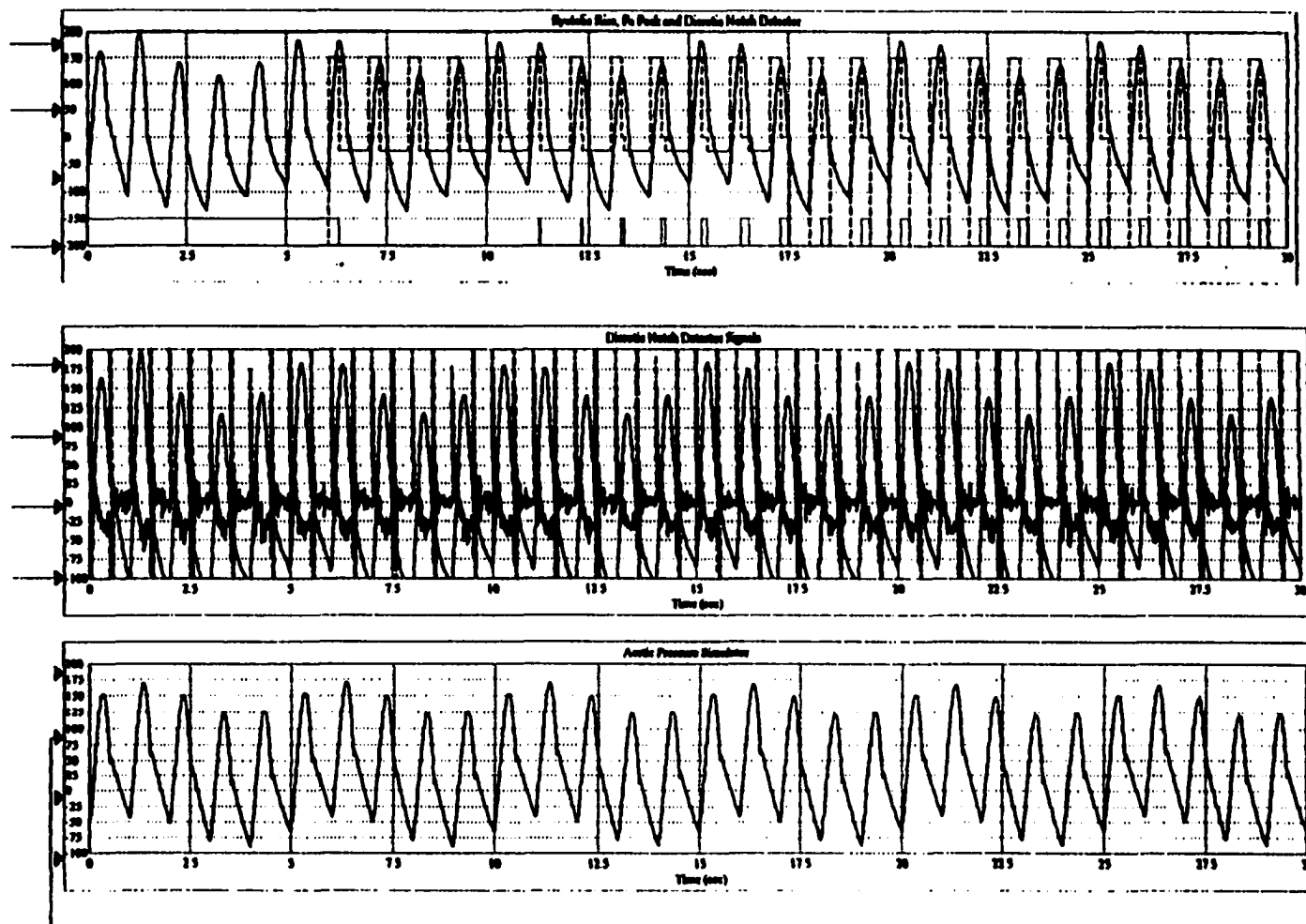
Figure 6-7. Simulated Aortic Pressure (Pa) Detection with 10 mm Hg Pa Variation due to Respiration is illustrated in Figure 6-7A (top trace). Figure 6-7B (middle trace) illustrates the Dicrotic Notch Detector Signals.The Variation in the Pa Baseline can be viewed in Figure 6-7C (bottom trace).
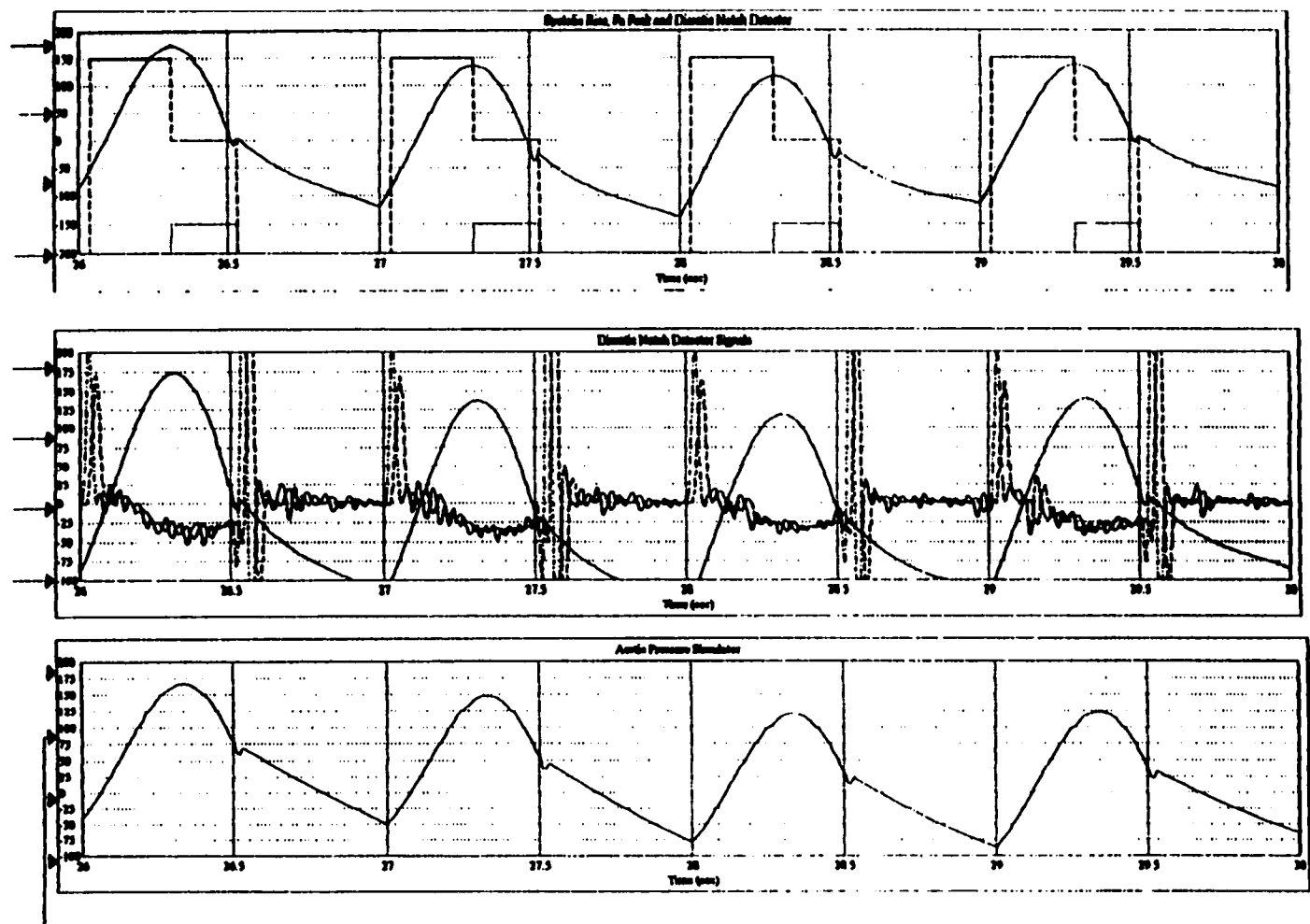
Figure 6-8. The Accuracy of Simulated Aortic Pressure (Pa) Detection of Figure 6-7 with 10 mm Hg Pa Variation due to Respiration can be seen in Figure 6-8A (top trace). Figure 6-8B (middle trace) illustrates the Dicrotic Notch Detector Signals. Figure 6-8C (bottom trace) illustrates the Pa Signal.
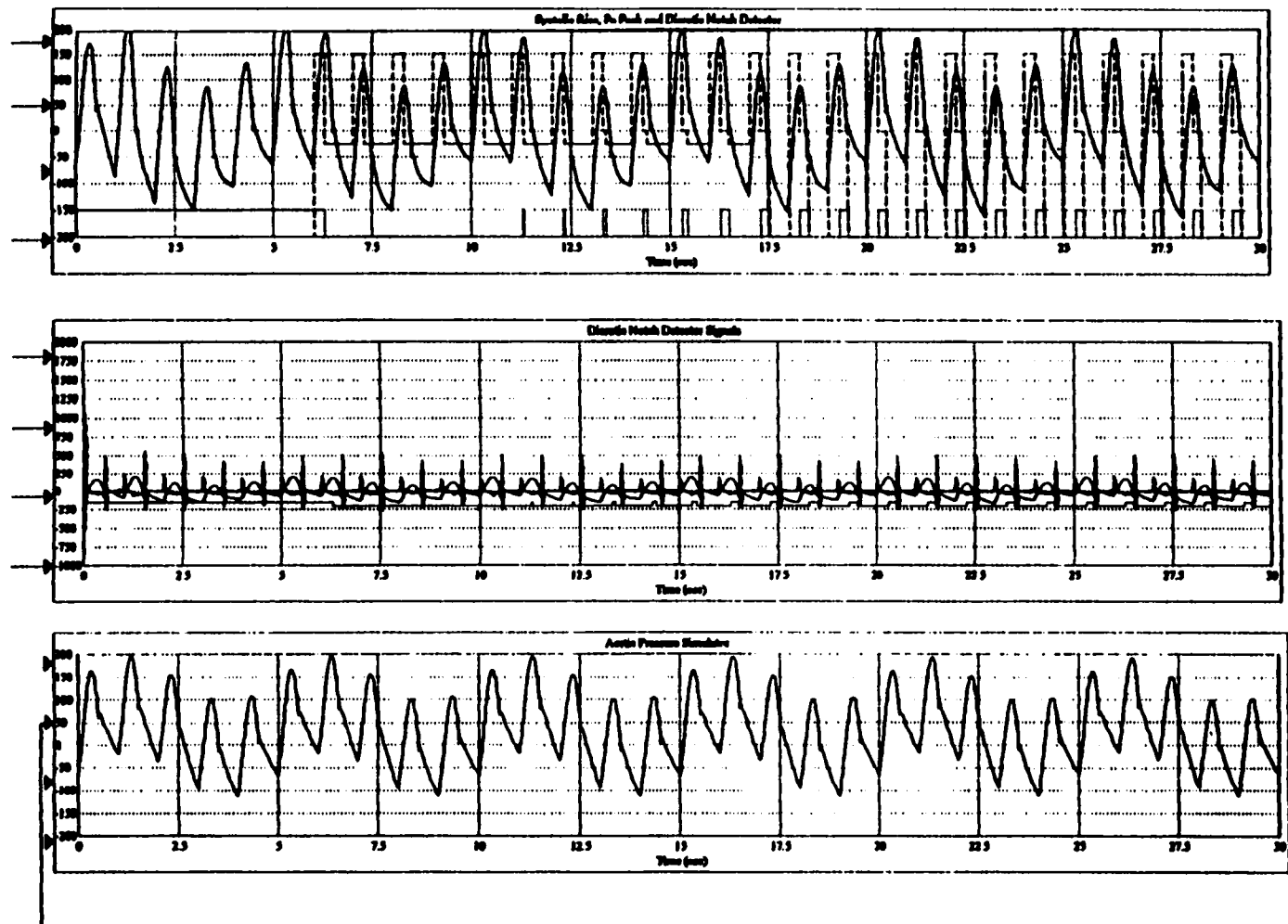
Figure 6-9. Simulated Aortic Pressure (Pa) Detection with 20 mm Hg Pa Variation due to Respiration is illustrated in Figure 6-9A (top trace). Figure 6-9B (middle trace) illustrates the Dicrotic Notch Detector Signals. The Variation in the Pa Baseline can be viewed in Figure 6-9C (bottom trace).
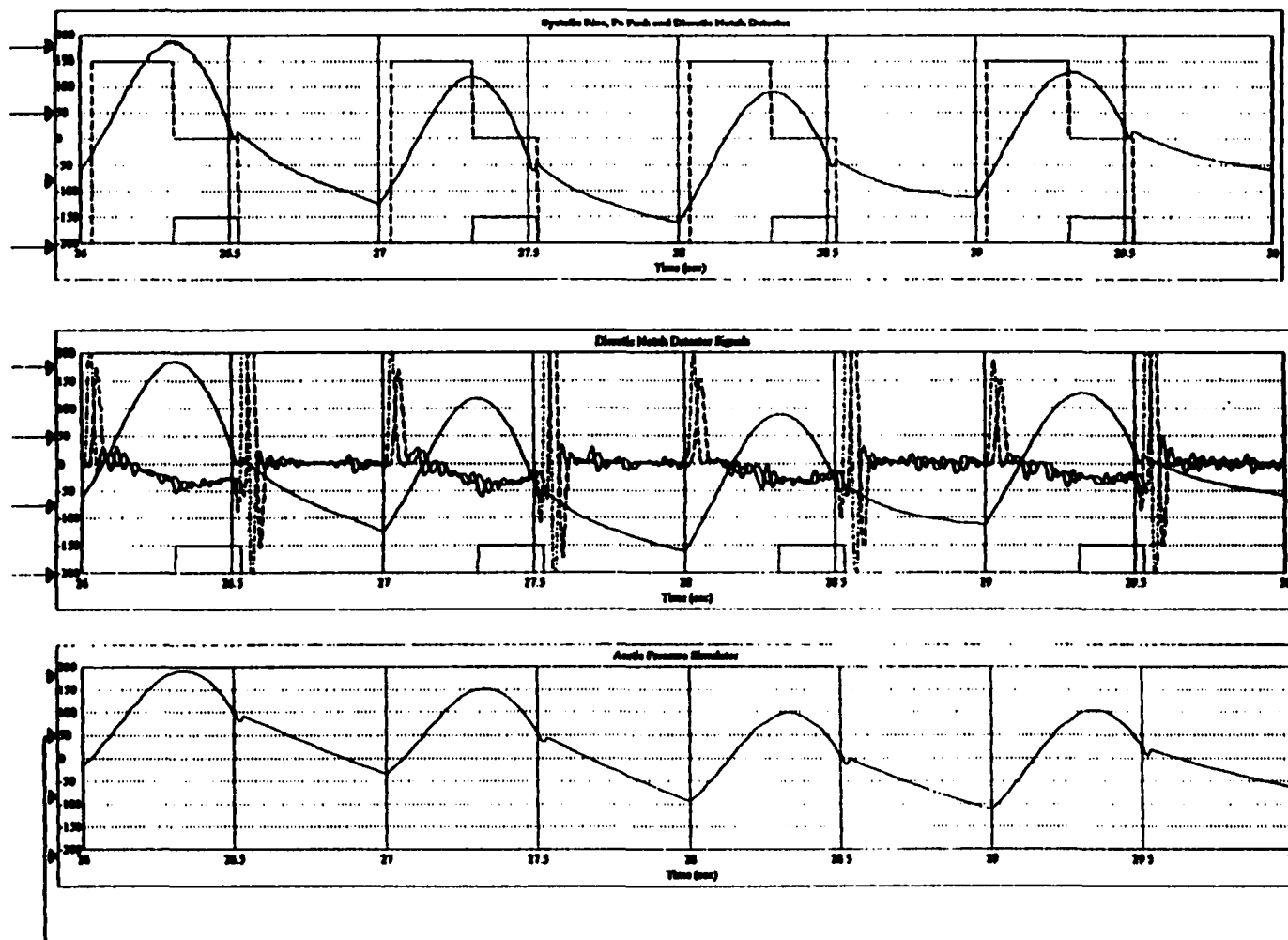
Figure 6-10. Accuracy of Simulated Aortic Pressure (Pa) Detection of Figure 6-9 with 20 mm Hg Pa Variation due to Respiration can be seen in Figure 6-10A (top trace). Figure 6-10B (middle trace) illustrates the Dicrotic Notch Detector Signals. Figure 6-10C (bottom trace) illustrates the Pa Signal.
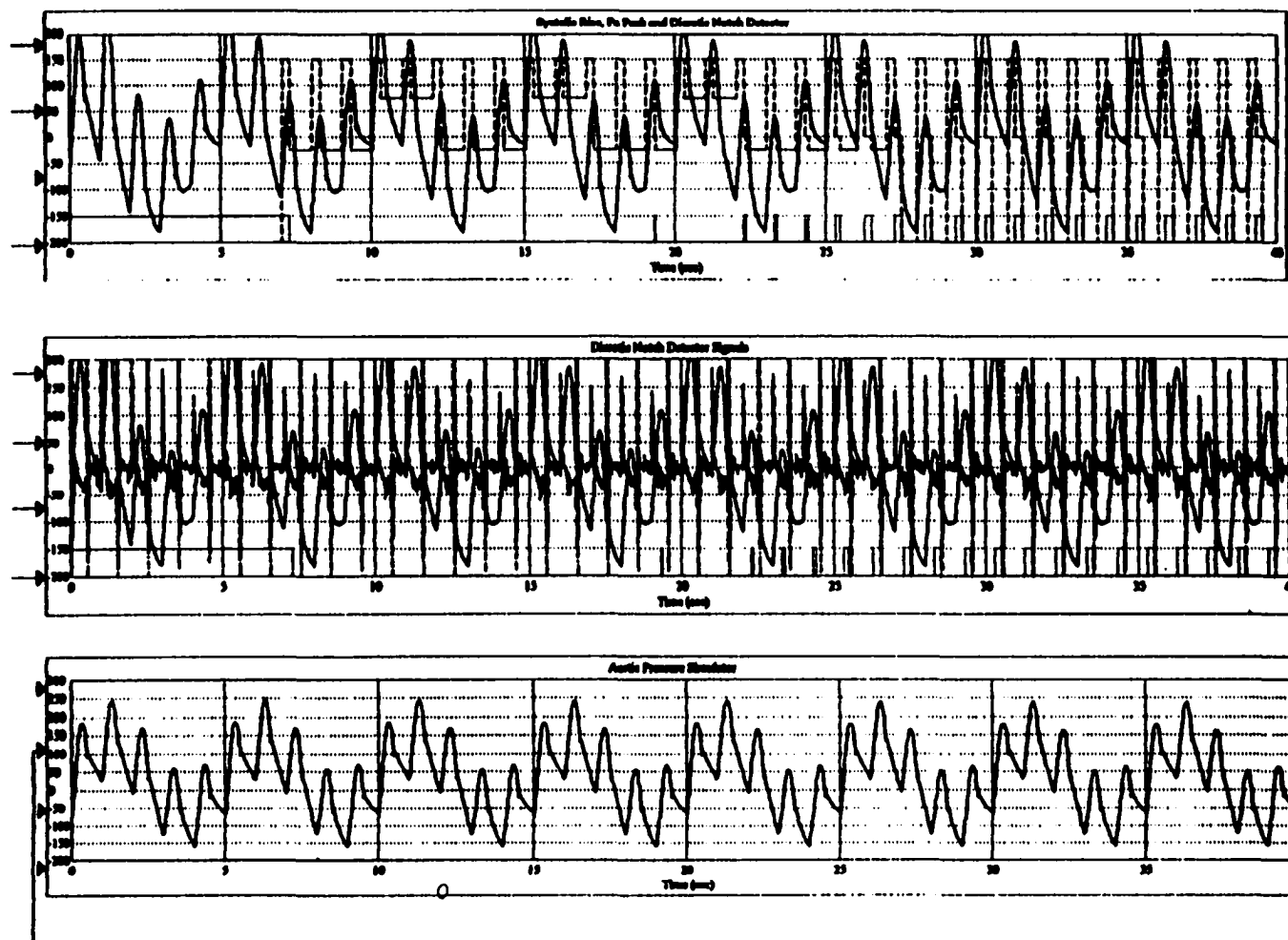
Figure 6-11. Simulated Aortic Pressure (Pa) Detection with 40 mm Hg Pa Variation due to Respiration is illustrated in Figure 6-11A (top trace). Figure 6-11B (middle trace) illustrates the Dicrotic Notch Detector Signals. The Variation in the Pa Baseline can be viewed in Figure 6-11C (bottom trace).

e
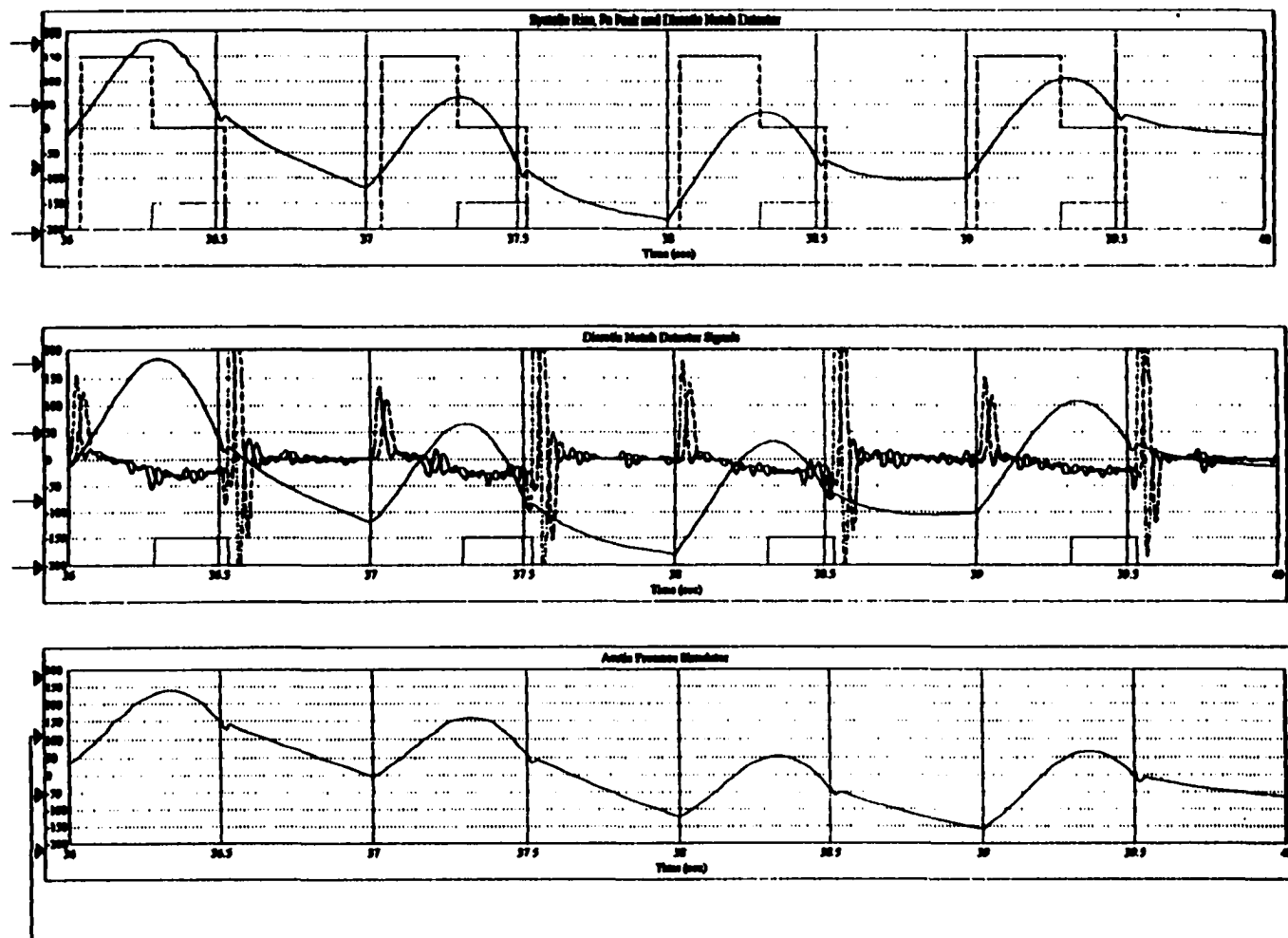
Figure 6-12. Accuracy of Simulated Aortic Pressure (Pa) Detection of Figure 6-11 with 40 mmHg Pa Variation due to Respiration can be seen in Figure 6-12A (top trace). Figure 6-12B (middle trace) illustrates the Dicrotic Notch Detector Signals. Figure 6-12C (bottom trace) illustrates the Pa Signal.

6.3.6 Pa Trace Amplitude Variation Due to Catheter Pressure Transducer Tip Positioning and Sensitivity

The ability of the CAD Pa detector to detect an Pa signal with pressure amplitude variation due to transducer tip positioning and sensitivity is demonstrated in Figure 6-13 and Figure 6-14. The relationship between the simulated Pa trace signal and CAD detector signal demonstrates detection of the Pa systolic rise, peak systolic pressure and dicrotic notch of the Pa wave with amplitude variation due to transducer tip positioning and sensitivity.

In a cardiothoracic surgery operating room environment, amplitude variation of the Pa trace (due to transducer tip positioning and sensitivity) is due to mechanical ventilation and blood coagulation on the pressure catheter tip. Amplitude variation due to mechanical ventilation is caused by the mechanical ventilation slightly repositioning (reorienting) the one-sided pressure catheter tip (one side exposes the piezoelectric transducer to the aortic blood hemodynamic pressure). The repositioning (reorienting) can cause the pressure presented to the pressure catheter tip to vary the amplitude of the Pa trace provided to the CAD controller Pa detection filter. Blood coagulation, the second cause of Pa amplitude variation, is due to the blood's physiologic propensity to adhere to foreign objects within the aorta (or body). As the amount of blood adhering (to the side of the pressure catheter tip's piezoelectric transducer) increases, the sensitivity of the piezoelectric transducer decreases and thus the amplitude of the Pa trace diminishes.

Figure 6-13 illustrates the detection of the dicrotic notch with amplitude variation due to transducer tip sensitivity and positioning. (The description of Figure 6-1A (in Section 6.3.2.1), Figure 6-1B (in Section 6.3.2.2), and Figure 6-1C (in Section 6.3.2.3) of Figure 6-1 also describes the corresponding traces in Figure 6-13.) The additional simulation information that is illustrated in Figure 6-13 is as follows. The rate of amplitude variation occurs at a faster rate due to the mechanical ventilation (i.e., at the rate of the ventilation) as oppose to blood coagulation. Thus the more challenging signal artifact was modelled to demonstrate the more severe signal interference for the Pa trace, namely, amplitude variation due to mechanical ventilation.

Figure 6-13 illustrates the detection of the dicrotic notch during amplitude variation due mechanical ventilation in which the a breath rate modelled at 12 breaths per minute. The amplitude variation causes a fluctuation in the systolic to diastolic Pa difference to range between 100% and 200% every 2.5 seconds. Figure 6-13A illustrates quick training of the CAD detection filter which occurs within 17.5 seconds. The filter is accurately detecting all three cardiac events within 17.5 seconds as seen in Figure 6-13A.

The simulation technique that was used to derived the results of the simulation illustrated in Figure 6-13 was to generate the ideal Pa trace with the Pa trace model and combine the ideal Pa trace with output of the Pa dicrotic notch perturbation model. The Pa trace with the dicrotic notch perturbation is then combined with the mechanical ventilation amplitude variation model. The combined Pa signal with Pa dicrotic notch perturbation and amplitude variation is then provided to the Pa detection filter. (Refer to Section 4.5.1 for a description of the Pa model. Refer to Section 4.5.1.1 for a description of the dicrotic notch model. Refer to Section 4.5.2.4 for a description of the mechanical ventilation amplitude variation model.)

The significance of the Pa detection simulation with a amplitude variation illustrated in Figure 6-13 was to demonstrate that detection is occurring accurately during the amplitude variation (at the frequency of the mechanical ventilator) in the aortic pressure wave. Amplitude variation due mechanical ventilation represents one artifact of the cardiothroracic surgery operating room that can be encountered when detecting the dicrotic notch. The Pa detection algorithm has the capability to detect a dicrotic notch with a 100% change in amplitude (from 100% to 200% and 200% to100%) at a breath rate of 12 breaths per minute[1]. Figure 6-13 demonstrates the Pa detection algorithm's immunity to the type of artifact due to the cardiothroracic surgery operating room. Figure 6-1 in a previous section (Section 6.3.2) illustrates reliable detection for the other extreme of amplitude variation, an Pa trace with no amplitude variation (i.e., 0% amplitude change). From the simulation illustrated in Figure 6-13A and Figure 6-1A, the Pa detection algorithm mechanical ventilation amplitude variation immunity has been demonstrated to be between 100% to 200% (of the ideal Pa trace) at a breath rate of 12 breaths per minute.

As was described in the criteria for a successful Pa detection simulation in Section 6.3.1.4, the systolic rise, peak systolic pressure, and dicrotic notch in Figure 6-13A were detected in all cardiac cycles displayed.

Figure 6-14 provides a closer look (expanded time scale) of the last four seconds of the same simulation illustrated in Figure 6-13. (The description of Figure 6-1A (in Section 6.3.2.1), Figure 6-1B (in Section 6.3.2.2), and Figure 6-1C (in Section 6.3.2.3) of Figure 6-1 also describes the corresponding traces in Figure 6-14.) The additional simulation information that is illustrated in Figure 6-14 is as follows. The Pa template generated is very similar to a Pa trace with amplitude variation due to mechanical ventilation observed in man. The accuracy of the detection is more

---

1. The frequency of the amplitude variation is dictated by the breath (i.e., ventilation) rate of the mechanical ventilator.

easily observed in Figure 6-14. The dicrotic notch detection, illustrated in Figure 6-14A (the timing of the second negative transition of the squarewave in relation to the change in slope of the Pa trace) occurs approximately 5 milliseconds prior to the end of the dicrotic notch. The dicrotic notch detection occurs at approximately 25 milliseconds after the start of the dicrotic notch.

From the simulation illustrated in Figure 6-13 and Figure 6-14, the Pa detection algorithm mechanical ventilation amplitude variation immunity has been demonstrated to be between 100% and 200% of the ideal Pa trace at a mechanical ventilation breath rate of 12 breaths per minute.
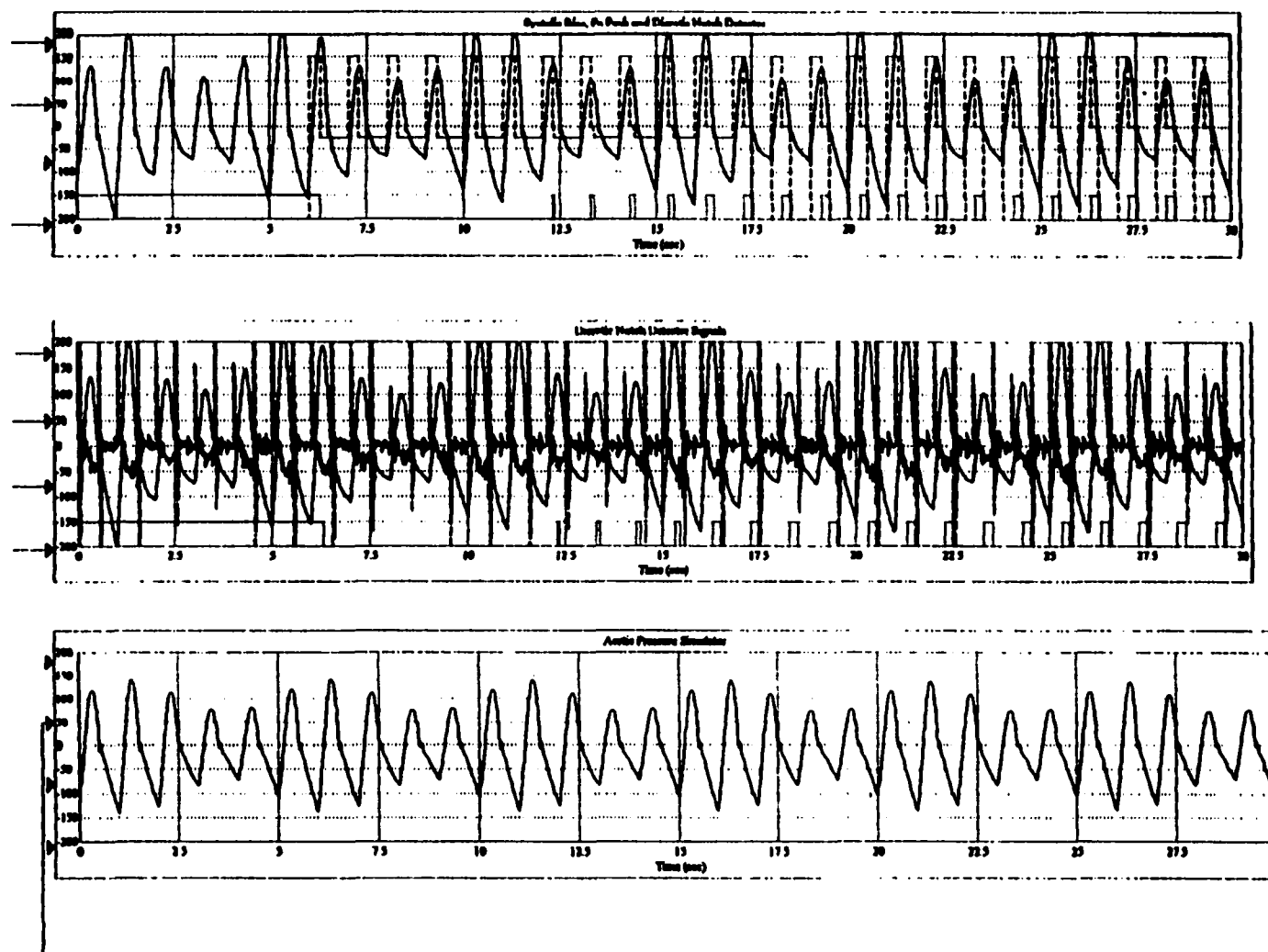
Figure 6-13. Simulated Aortic Pressure (Pa) Detection with Pa Variation due to Transducer Attenuation can be seen in Figure 6-13A (top trace). Figure 6-13B (middle trace) illustrates the Dicrotic Notch Detector Signals. The Variation in the Pa Amplitude can be viewed in Figure 6-13C (bottom trace).

O
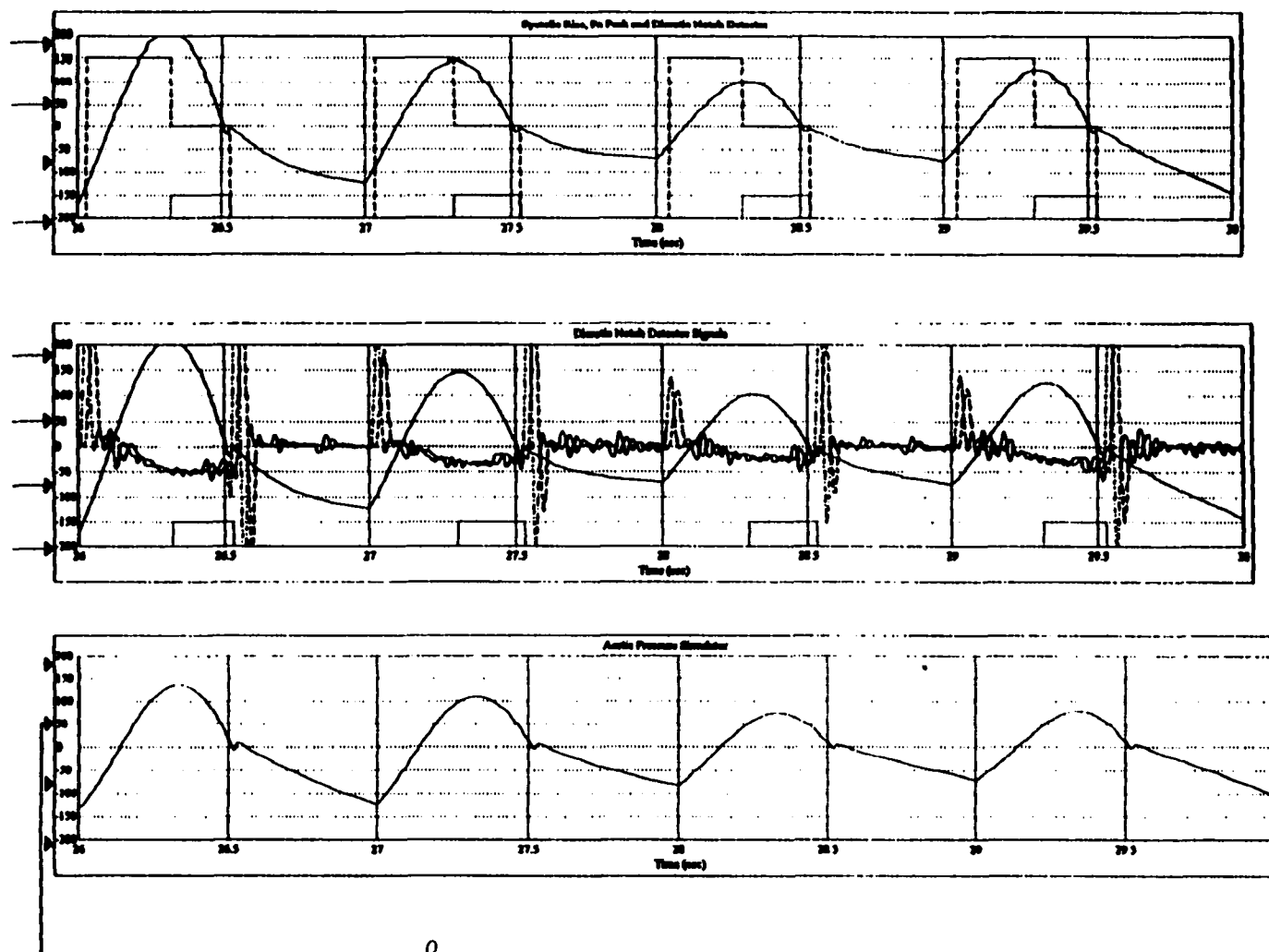
Figure 6-14. The Accuracy of Simulated Aortic Pressure (Pa) Detection of Figure 6-13 with Pa Variation due to Transducer Attenuation can be seen in Figure 6-14A (top trace). Figure 6-14B (middle trace) illustrates the Dicrotic Notch Detector Signals. Figure 6-14C (bottom trace) illustrates the Pa Signal.

6.3.7   Pa Trace Distorted by Uniformly Distributed Noise

The ability of the CAD Pa detector to detect an Pa signal distorted by uniformly distributed noise due to cardiothoracic surgery operating room environment is demonstrated in Figure 6-15 and Figure 6-16. The relationship between the simulated Pa trace signal and CAD detector signal demonstrates detection of the Pa systolic rise, peak systolic pressure and dicrotic notch of the Pa wave with artifacts due to uniformly distributed noise.

The causes of unwanted noise (artifacts due to the cardiothoracic operating room environment) within the Pa signal include artifacts due to powerline interference, muscle contraction (e.g., due to coughing), baseline drift and amplitude modulation with mechanical ventilation, instrumentation noise generated by electronic devices used in signal processing, and electrosurgical noise (22). A single sinusoid noise source with a constant frequency and amplitude (e.g., powerline interference) was modelled by a uniformly distributed noise source.

In a cardiothoracic surgery operating room environment, 60 Hz powerline interference is present on all electronic signals and creates variation of the Pa trace. The Pa signal is sampled at 500 Hz. The 60 Hz powerline interference shows up as an artifact on the continuous (analog) Pa trace as a 60 Hz sinusoid. The 60 Hz sinusoid powerline interference sampled (using an A/DC) at 500 Hz provides a distribution that may be approximated by a uniformly distributed noise source. Thus a uniformly distributed noise is utilized to model the 60 Hz powerline noise.

Figure 6-15 illustrates the detection of the dicrotic notch with Pa variation due to uniformly distributed noise. (The description of Figure 6-1A (in Section 6.3.2.1), Figure 6-1B (in Section 6.3.2.2), and Figure 6-1C (in Section 6.3.2.3) of Figure 6-1 also describes the corresponding traces in Figure 6-15.) The additional simulation information that is illustrated in Figure 6-15 is as follows. Figure 6-15 illustrates the detection of the dicrotic notch during Pa artifact variation due to uniformly distributed noise. The Pa trace uniformly distributed noise variation causes "hair" within the Pa trace. Figure 6-15A illustrates quick training of the CAD detection filter which occurs within 17.5 seconds. The filter is accurately detecting all three cardiac events within 17.5 seconds as seen in Figure 6-15A. Figure 6-15B demonstrates the increased amount of "ambient" derivative window amplitude within the current second derivative window filter and the ambient second derivative window filter (utilized to detect the dicrotic notch). The increase in noise challenges the Pa dicrotic notch detection algorithm because derivative based filters are typically extremely sensitive to noise.

The simulation technique that was used to derived the results of the simulation illustrated in Figure 6-15 was to generate the ideal Pa trace with the Pa trace model and combine the ideal Pa trace with

output of the Pa dicrotic notch perturbation model. The Pa trace with the dicrotic notch perturbation is then combined with the uniformly distributed noise variation model. The combined Pa signal with Pa dicrotic notch perturbation and noise is then provided to the Pa detection filter. (Refer to Section 4.5.1 for a description of the Pa model. Refer to Section 4.5.1.1 for a description of the dicrotic notch model. Refer to Section 4.5.2.5 for a description of the uniformly distributed noise variation model.)

The significance of the Pa detection simulation with a uniformly distributed noise illustrated in Figure 6-15 was to demonstrate that detection is occurring accurately while the artifact of a uniformly distributed noise source distorted the aortic pressure wave. Uniformly distributed noise modeling 60 Hz powerline interference represents one artifact of the cardiothroracic surgery operating room that can be encountered when detecting the dicrotic notch. The Pa detection algorithm has the capability to detect a dicrotic notch while uniformly distributed noise (with a mean = 0.5 mmHg and a standard deviations = 0.289 mmHg) is imposed on the Pa signal. Figure 6-15 demonstrates the Pa detection algorithms immunity to the type of artifact due to the cardiothroracic surgery operating room. Figure 6-1A in a previous section (Section 6.3.2) illustrates reliable detection for the other extreme of the addition of uniformly distributed noise, an Pa trace with no variation due to noise (i.e., mean and standard deviation = 0 mmHg). From the simulation illustrated in Figure 6-15A and Figure 6-1A, the Pa detection algorithm uniformly distributed noise immunity has been demonstrated to range between a Pa wave with no noise (i.e., ideal Pa trace) and a Pa wave with mean = 0.5 mmHg and standard deviation = 0.289 mmHg of uniformly distributed noise imposed.

As was described in the criteria for a successful Pa detection simulation in Section 6.3.1.4, the systolic rise, peak systolic pressure, and dicrotic notch in Figure 6-15A were detected in all cardiac cycles displayed.

Figure 6-16 provides a closer look (expanded time scale) at the last four seconds of the same simulation illustrated in Figure 6-15. (The description of Figure 6-1A (in Section 6.3.2.1), Figure 6-1B (in Section 6.3.2.2), and Figure 6-1C (in Section 6.3.2.3) of Figure 6-1 also describes the corresponding traces in Figure 6-16.) The additional simulation information that is illustrated in Figure 6-16 is as follows. The Pa template generated is very similar to a Pa trace observed in man with uniformly distributed noise. The accuracy of the detection is more easily observed in Figure 6-16. The dicrotic notch detection, illustrated in Figure 6-16A (the timing of the second negative transition of the squarewave in relation to the dicrotic notch perturbation of the Pa trace) occurs

approximately 10 milliseconds prior to the end of the dicrotic notch. The dicrotic notch detection occurs at approximately 20 milliseconds after the start of the dicrotic notch.

Figure 6-17 illustrates the signal to noise comparison of the dicrotic notch deflection and uniformly distributed noise contribution during the first second of the simulation shown if Figure 6-15. The amplitude of the dicrotic notch deflection (3 mmHg half-cycle inverted sinusoid) can be compared with the mean of the noise source signal (0.5 mmHg) for a signal to noise comparison. This comparison further illustrates the robustness of the dicrotic notch filter noise immunity because the detection filters implemented are derivative based which are typically extremely sensitive to noise.

From the simulation illustrated in Figure 6-15 through Figure 6-17, the Pa detection algorithm uniformly distributed noise immunity (modelling 60 Hz powerline interference) has been demonstrated to range between a Pa signal without noise (ideal Pa trace) and a Pa trace with mean = 0.5 mmHg and standard deviation = 0.289 mmHg of uniformly distributed noise imposed.
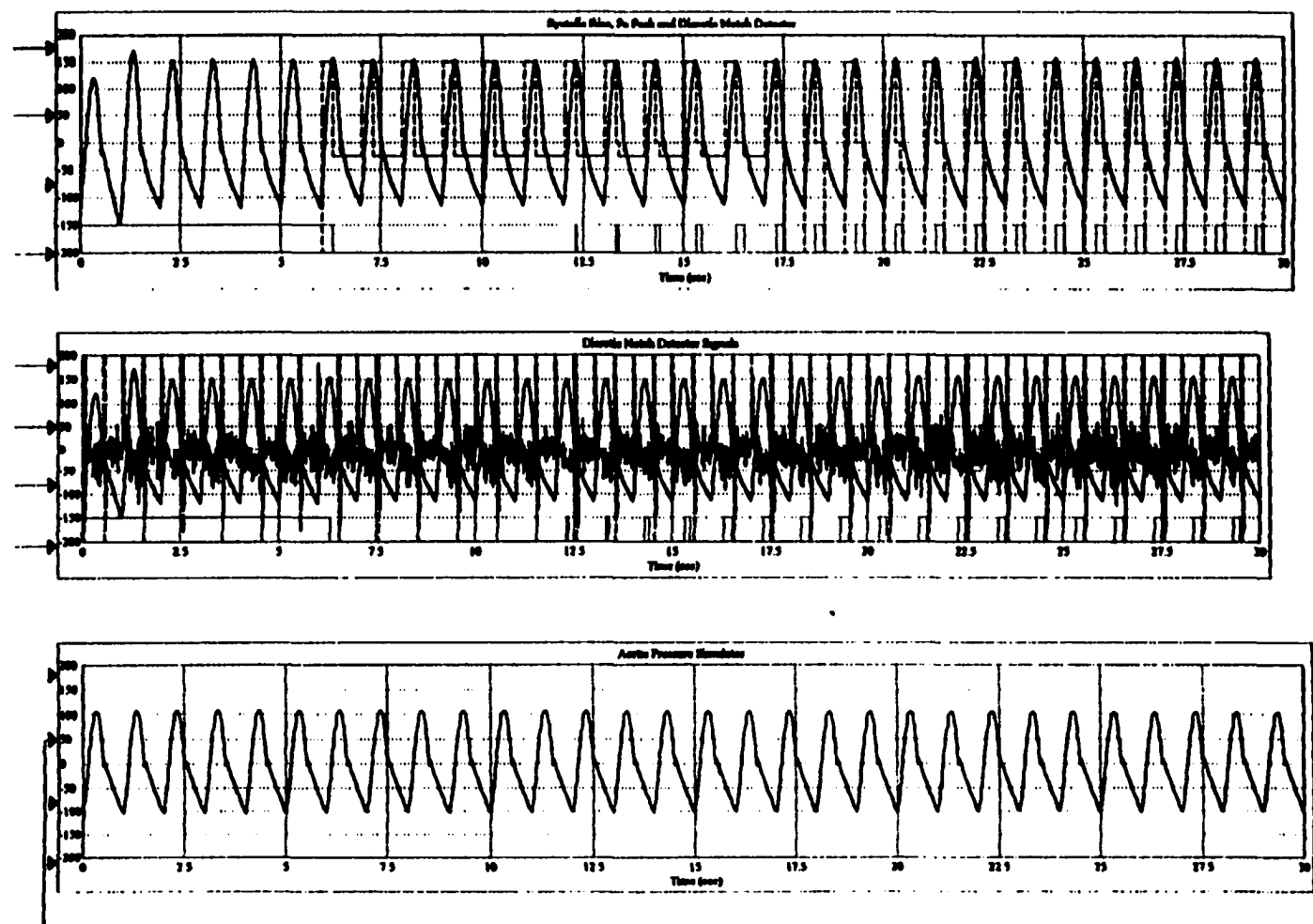
Figure 6-15. The Simulated Pa Detection with Pa Variation due to Uniformly Distributed Noise can be seen in Figure 6-15A (top trace). The Increased Amplitude in Second Derivative Filter Signals can be seen in Figure 6-15B (middle trace). Figure 6-15C (bottom trace) illustrates the Pa Signal.
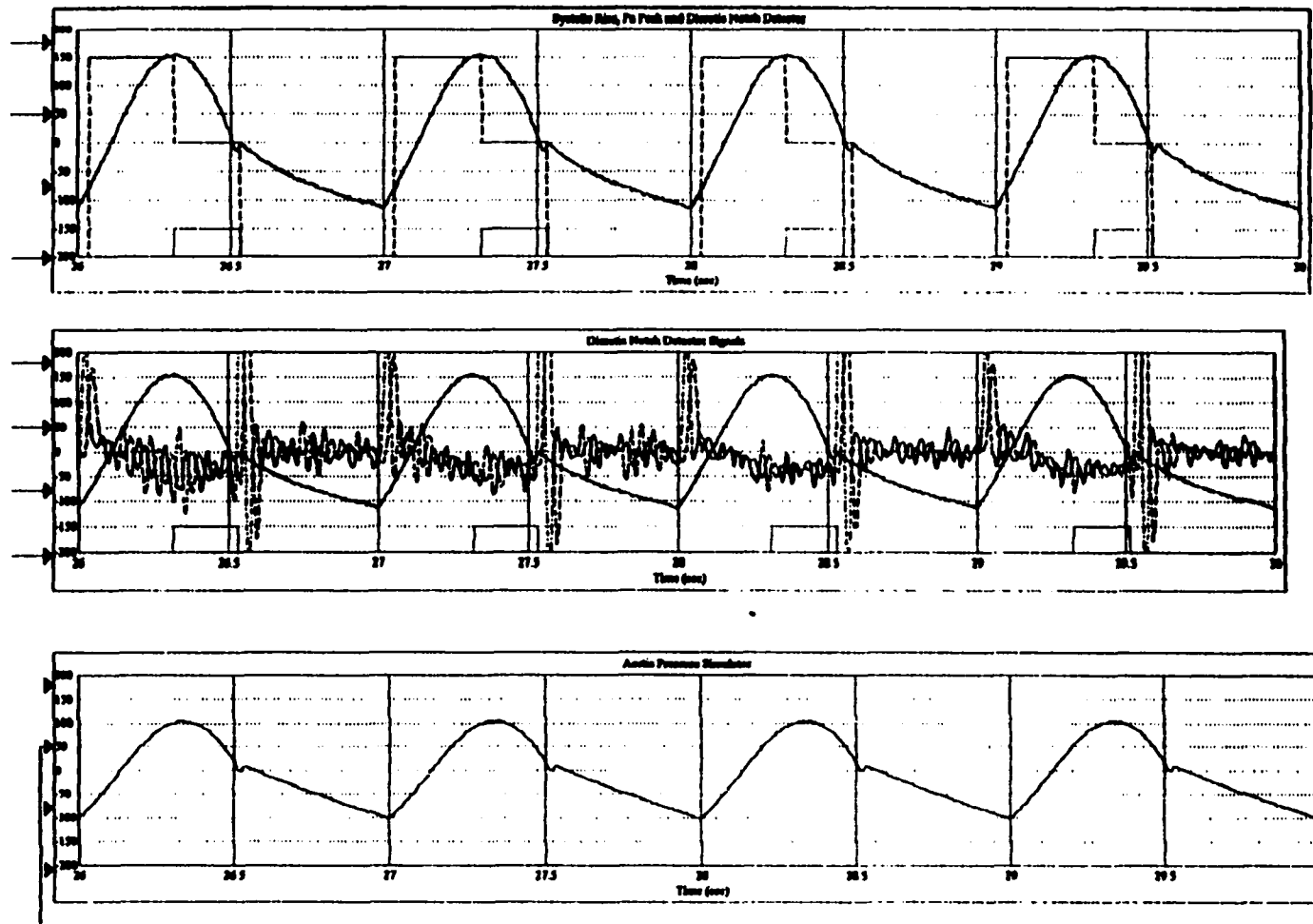
Figure 6-16. The Accuracy of Simulated Pa Detection of Figure 6-15 with Pa Variation due to Uniformly Distributed Noise can be seen in Figure 6-16A (top trace). The Increased Amplitude in Second Derivative Filter Signals can be seen in Figure 6-16B (middle trace). Figure 6-16C (bottom trace) illustrates the Pa Signal.
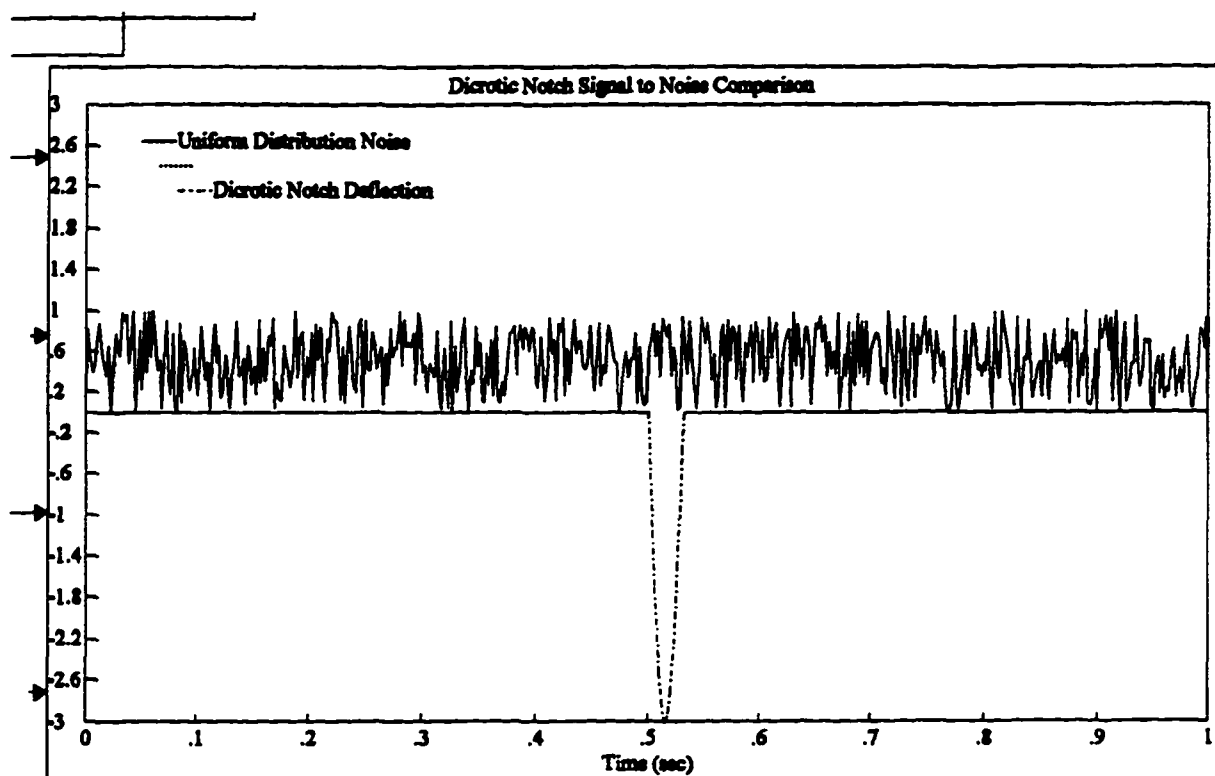
Figure 6-17. A Comparison of Dicrotic Notch Deflection (Inverted Halfwave Rectified Sinusoid) and Pa Variation of Simulation due to Uniformly Distributed Noise in Figure 6-15 Demonstrates the Atypical Noise Immunity of the Derivative based Dicrotic Notch Detector

o

6.3.8 Pa Trace Distorted by Gaussian Distributed Noise

The ability of the CAD Pa detector to detect an Pa signal distorted by Gaussian distributed noise due to cardiothoracic surgery operating room environment is demonstrated in Figure 6-18 and Figure 6-19. The relationship between the simulated Pa trace signal and CAD detector signal demonstrates detection of the Pa systolic rise, peak systolic pressure and dicrotic notch of the Pa wave with artifacts due to Gaussian distributed noise.

The causes of unwanted noise (artifacts due to the cardiothoracic operating room environment) within the Pa signal include artifacts due to powerline interference, muscle contraction (e.g., due to coughing), baseline drift and amplitude modulation with mechanical ventilation, instrumentation noise generated by electronic devices used in signal processing, and electrosurgical noise (22). The

contribution of several cardiothoracic surgery noise sources combined was modelled by a Gaussian distributed noise source.

In a cardiothoracic surgery operating room environment, the combination of interference noted in the previous paragraph, is present on all electronic signals and creates variation in the Pa trace. The Pa signal is digitally sampled at 500 Hz. The combined interference shows up as an artifact on the continuous (analog) Pa trace in a random fashion. The combined Pa interference sampled (using an A/DC) at 500 Hz provides a distribution that may be approximated by a Gaussian distributed noise source. Thus a Gaussian distributed noise is utilized to model the combination of unwanted noise artifacts due to the cardiothoracic operating room environment.

Figure 6-18 illustrates the detection of the dicrotic notch with Pa variation due to Gaussian distributed noise. (The description of Figure 6-1A (in Section 6.3.2.1), Figure 6-1B (in Section 6.3.2.2), and Figure 6-1C (in Section 6.3.2.3) of Figure 6-1 also describes the corresponding traces in Figure 6-18.) The additional simulation information that is illustrated in Figure 6-18 is as follows. Figure 6-18 illustrates the detection of the dicrotic notch during Pa artifact variation due to Gaussian distributed noise. The Pa trace Gaussian distributed noise variation causes "hair" within the Pa trace. Figure 6-18A illustrates quick training of the CAD detection filter which occurs within 17.5 seconds. The filter is accurately detecting all three cardiac events within 17.5 seconds as seen in Figure 6-18A. Figure 6-18B demonstrates the increased amount of amplitude within the current second derivative window filter and the ambient second derivative window filter (utilized to detect the dicrotic notch). The increase in noise challenges the Pa dicrotic notch detection algorithm because derivative based filters are typically extremely sensitive to noise.

The simulation technique that was used to derived the results of the simulation illustrated in Figure 6-18 was to generate the ideal Pa trace with the Pa trace model and combine the ideal Pa trace with output of the Pa dicrotic notch perturbation model. The Pa trace with the dicrotic notch perturbation is then combined with the Gaussian distributed noise variation model. The combined Pa signal with Pa dicrotic notch perturbation and noise is then provided to the Pa detection filter. (Refer to Section 4.5.1 for a description of the Pa model. Refer to Section 4.5.1.1 for a description of the dicrotic notch model. Refer to Section 4.5.2.5 for a description of the Gaussian distributed noise variation model.)

The significance of the Pa detection simulation with a Gaussian distributed noise illustrated in Figure 6-18 was to demonstrate that detection is occurring accurately while the artifact of a Gaussian distributed noise source distorted the aortic pressure wave. Gaussian distributed noise due

to combined cardiothoracic surgery operating room environment interference represents a combinations of noise artifacts of the cardiothroracic surgery operating room that can be encountered when detecting the dicrotic notch. The Pa detection algorithm has the capability to detect a dicrotic notch while Gaussian distributed noise (with a mean ▪ 0.0 mmHg and a standard deviations▪ 0.6 mmHg) is imposed on the Pa signal. Figure 6-18A demonstrates the Pa detection algorithms immunity to this type of artifact due to the cardiothroracic surgery operating room. Figure 6-1A in a previous section (Section 6.3.2) illustrates reliable detection for the other extreme of the addition of Gaussian distributed noise, an Pa trace with no variation due to noise (i.e., mean and standard deviation ▪ 0 mmHg). From the simulation illustrated in Figure 6-18 and Figure 6-1, the Pa detection algorithm Gaussian distributed noise immunity has been demonstrated to range between a Pa wave with no noise (i.e., ideal Pa trace) and a Pa wave with mean ▪ 0.0 mmHg and standard deviation ▪ 0.6 mmHg of Gaussian distributed noise imposed.

As was described in the criteria for a successful Pa detection simulation in Section 6.3.1.4, the systolic rise, peak systolic pressure, and dicrotic notch in Figure 6-18A were detected in all cardiac cycles displayed.

Figure 6-19 provides a closer look (expanded time scale) at the last four seconds of the same simulation illustrated in Figure 6-18. (The description of Figure 6-1A (in Section 6.3.2.1), Figure 6-1B (in Section 6.3.2.2), and Figure 6-1C (in Section 6.3.2.3) of Figure 6-1 also describes the corresponding traces in Figure 6-19.) The additional simulation information that is illustrated in Figure 6-19 is as follows. The Pa template generated is very similar to a Pa trace observed in humans with Gaussian distributed noise. The accuracy of the detection is more easily observed in Figure 6-19. The dicrotic notch detection, illustrated in Figure 6-19A (the timing of the second negative transition of the squarewave in relation to the dicrotic notch perturbation of the Pa trace) occurs approximately 10 milliseconds prior to the end of the dicrotic notch. The dicrotic notch detection occurs at approximately 20 milliseconds after the start of the dicrotic notch.

Figure 6-20 illustrates the signal to noise comparison of the dicrotic notch deflection and Gaussian distributed noise contribution during the first second of the simulation shown if Figure 6-18. The amplitude of the dicrotic notch deflection (3 mmHg half-cycle inverted sinusoid) can be compared with the standard deviation of the noise source signal (0.6 mmHg) for a signal to noise comparison. This comparison further illustrates the robustness of the dicrotic notch filter noise immunity because the detection filters implemented are derivative based which are typically extremely sensitive to noise.

From the simulation illustrated in Figure 6-18 through Figure 6-20, the Pa detection algorithm Gaussian distributed noise immunity (modelling a combination of cardiothroracic surgery operating room interference) has been demonstrated to be between a Pa signal without noise (ideal Pa trace) and a Pa trace with mean ▬ 0.0 mmHg and standard deviation ▬ 0.6 mmHg of Gaussian distributed noise imposed.
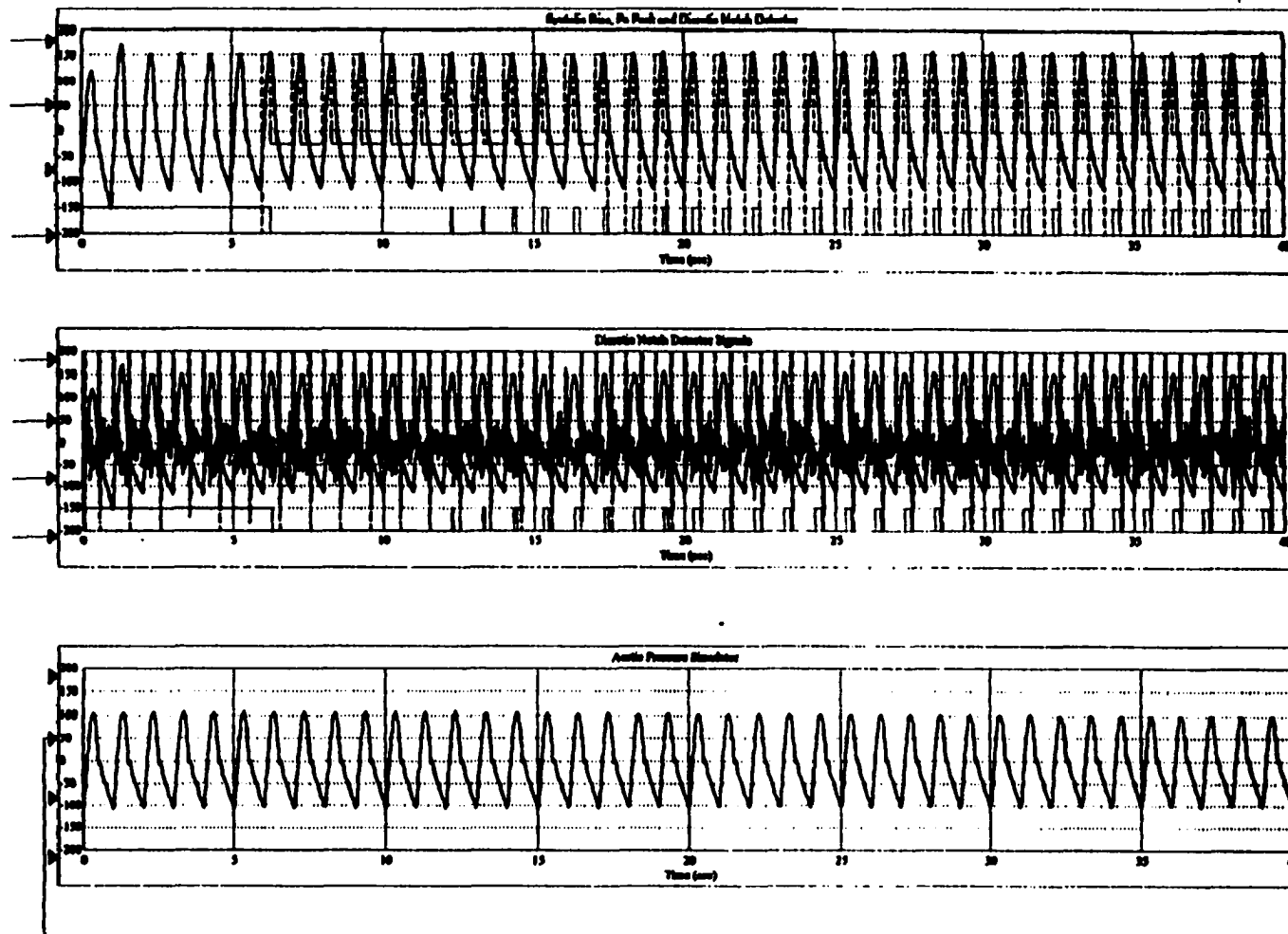
Figure 6-18. Simulated Pa Detection with Pa Variation due to Gaussian Distributed Noise can be seen in Figure 6-18A (top trace). The Increased Amplitude in Second Derivative Filter Signals can be seen in Figure 6-18B (middle trace). Figure 6-18C (bottom trace) illustrates the Pa Signal.
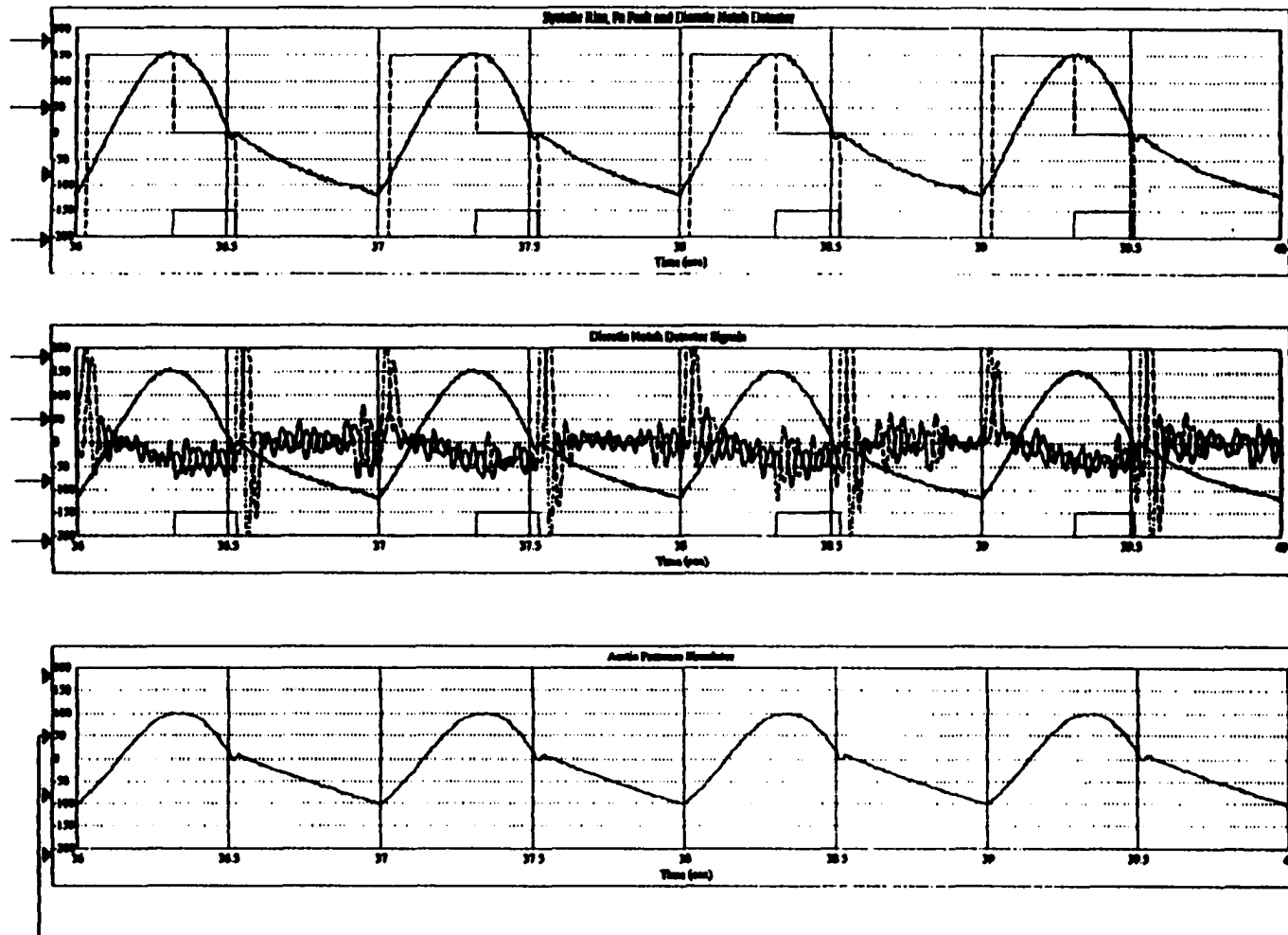
Figure 6-19. The Accuracy of Simulated Pa Detection with Pa Variation of Figure 6-18 due to Gaussian Distributed Noise can be seen in Figure 6-19A (top trace). The Increased Amplitude in Second Derivative Filter Signals can be seen in Figure 6-19B (middle trace). Figure 6-19C (bottom trace) illustrates the Pa Signal.
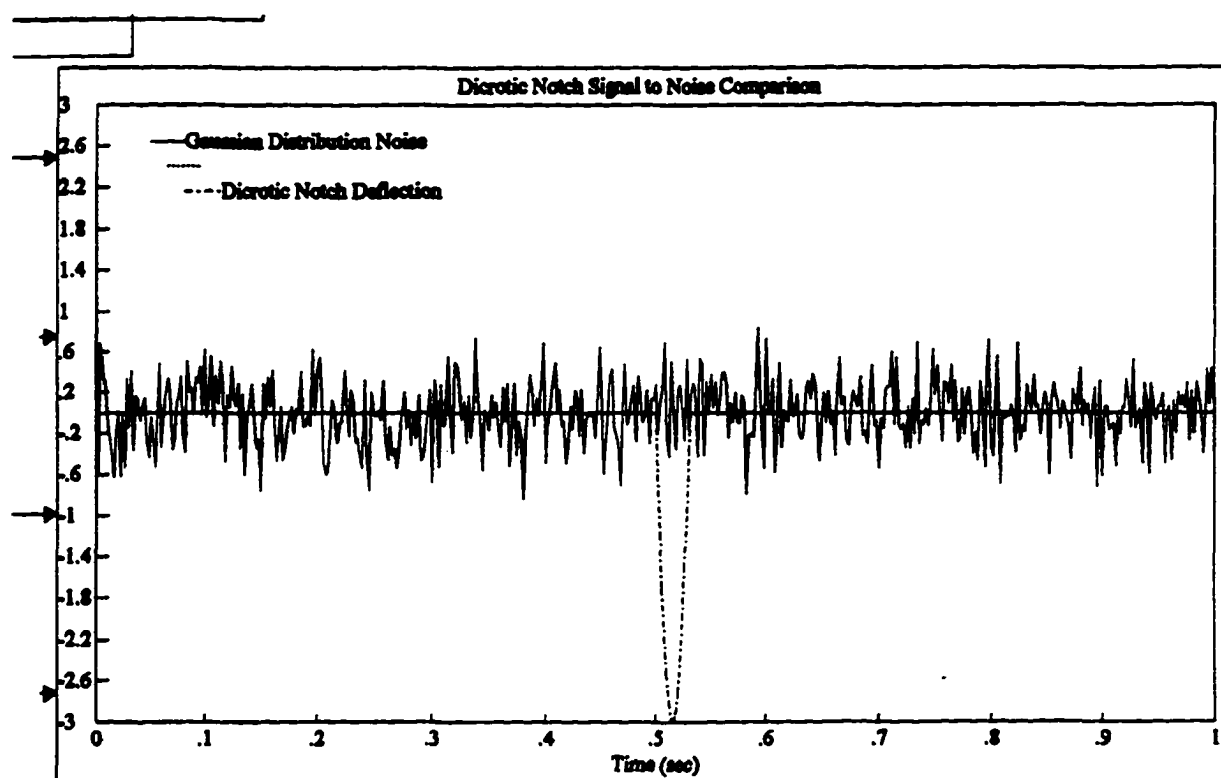
Figure 6-20. Comparison of Dicrotic Notch Deflection (Inverted Halfwave Rectified Sinusoid) and Pa Variation due to Gaussian Distributed Noise of Figure 6-18 Demonstrates the Atypical Noise Immunity of the Derivative based Dicrotic Notch Detector.

6.3.9 Heart Rate Variability Due to Respiration

The ability of the CAD Pa detector to detect a Pa signal with heart rate variability due to respiration is demonstrated in Figure 6-21 through Figure 6-24. The relationship between the simulated Pa trace signal and CAD detector signal demonstrates detection of the Pa systolic rise, peak systolic pressure and dicrotic notch of the Pa wave with heart rate variability due to respiration.

Figure 6-21 illustrates the detection of the dicrotic notch with heart rate variability due to respiration. (The description of Figure 6-1A (in Section 6.3.2.1), Figure 6-1B (in Section 6.3.2.2), and Figure 6-1C (in Section 6.3.2.3) of Figure 6-1 also describes the corresponding traces in Figure 6-21.) The additional simulation information that is illustrated in Figure 6-21 is as follows. Figure 6-21 illustrates the detection of the dicrotic notch in an Pa trace with a changing heart rate due to respiration. Figure 6-21A illustrates quick training of the CAD detection filter which occurs within

15.2 seconds. The filter is accurately detecting all three cardiac events within 15.2 seconds as seen in Figure 6-21A.

The simulation technique that was used to derive the results of the simulation illustrated in Figure 6-21 was to generate the ideal Pa trace with the Pa trace model and combine the ideal Pa trace with output of the Pa dicrotic notch perturbation model. The combined ideal Pa trace with dicrotic notch perturbation model was simulated at a sampling rate of 3000 samples per second (i.e., oversampled 6 times faster as compared to the Pa detection filter of 500 Hz). The results of the oversampled Pa trace simulation data was stored to a file. A separately written "C" program then sampled the oversampled Pa wave data (to modify the data for the 500 Hz detection filter). The "C program sampling ranged from 6 to 8 samples creating a changing heart rate oscillating between 60 to 80 beats per minute every 4.3 seconds simulating a Pa trace with a respiration of 14 breaths per minute. The Pa data modelling a Pa trace with heart rate variability due to respiration is then provided to the Pa detection filter. (Refer to Section 4.5.1 for a description of the Pa model. Refer to Section 4.5.1.1 for a description of the dicrotic notch model. Refer to Section 4.5.2.6 for a description of the Pa trace with heart rate variability due to respiration model.)

The significance of the Pa detection simulation with heart rate variability due to respiration illustrated in Figure 6-21 was to demonstrate that detection is occurring accurately during the change in heart rate present in the aortic pressure wave. This represents one extreme of biological variation that is encountered when detecting the dicrotic notch, namely, a Pa trace with a 20 beats per minute variation in heart rate. (The change in heart rate due to respiration is exaggerated to more effectively illustrate the phenomenon and to further challenge the Pa systolic rise, peak systolic pressure and dicrotic notch detection algorithms.) The Pa detection algorithm has the capability to detect a dicrotic notch with a 20 beats per minute variation in heart rate. Figure 6-21 demonstrates the Pa detection algorithms immunity to the form of biological variation due to variance in heart rate due to respiration. Figure 6-5 in a previous section (Section 6.3.4) illustrates reliable detection for the other extreme of biological variation, a Pa trace with no variation in heart rate due to respiration (i.e., 0 beats per minute in variation). Thus the Pa detection algorithm has biological variation heart rate variability (due to respiration) immunity between 0 to 20 beats per minute ranging between a heart rate of 60 to 80 beats per minute for a respiration rate of 14 breaths per minute.

As was described in the criteria for a successful Pa detection simulation in Section 6.3.1.4, the systolic rise, peak systolic pressure, and dicrotic notch in Figure 6-21A were detected for all the cardiac cycles displayed.

Figure 6-22 provides a closer look (expanded time scale) at the last ten seconds of the same simulation illustrated in Figure 6-21. (The description of the Figure 6-1A (in Section 6.3.2.1), Figure 6-1B (in Section 6.3.2.2), and Figure 6-1C (in Section 6.3.2.3) of Figure 6-1 also describes the corresponding traces in Figure 6-22.) The additional simulation information that is illustrated in Figure 6-22 is as follows. The Pa template generated is very similar to the Pa trace with heart rate variability due to respiration observed in man. The heart rate variability of the Pa trace can be more easily viewed in Figure 6-22C. A complete respiration cycle in the Pa trace (heart rate variability changing from 60 beats per minute (bpm) to 80 bpm to 60 bpm) can be seen starting at 37.7 seconds and ending at 42.0 seconds. The heart rate variation cycle in 4.3 seconds demonstrates a breath rate of 14 breaths per minute. The cyclical variation in heart rate (frequency modulation) is equal to the breath rate.

Figure 6-23 provides a closer look (expanded time scale) at the last five seconds of the same simulation illustrated in Figure 6-21. (The description of the Figure 6-1A (in Section 6.3.2.1), Figure 6-1B (in Section 6.3.2.2), and Figure 6-1C (in Section 6.3.2.3) of Figure 6-1 also describes the corresponding traces in Figure 6-23.) The additional simulation information that is illustrated in Figure 6-23 is as follows. The dicrotic notch detector signals, namely, the current second derivative window and the ambient second derivative window of the Pa trace can be more easily viewed in Figure 6-23B. The dicrotic notch detector signals provided accurate dicrotic notch detection by following the heart rate variation (frequency modulation) due to respiration (e.g., at 42.2 seconds a strong current second derivative window and subsequent ambient second derivative window amplitude is generated indicating the dicrotic notch is present).

Figure 6-24 provides a closer look (expanded time scale and amplitude scale) of the last five seconds of the same simulation illustrated in Figure 6-21. (The description of Figure 6-1A (in Section 6.3.2.1) of Figure 6-1 also describes Figure 6-24.) The additional simulation information that is illustrated in Figure 6-24 is as follows. The accuracy of the dicrotic notch detection is more easily observed in Figure 6-24. The delay of the dicrotic notch detector illustrated in Figure 6-24 (the timing of the second negative transition of the squarewave in relation to the dicrotic notch of the Pa trace) occurs approximately 20 milliseconds prior to the end of the dicrotic notch. The detection occurs at approximately 10 milliseconds after the start of the dicrotic notch.

Again, the Pa detection algorithm has biological variation heart rate variability (due to respiration) immunity between 0 to 20 beats per minute ranging between a heart rate of 60 to 80 beats per minute for a respiration rate of 14 breaths per minute.
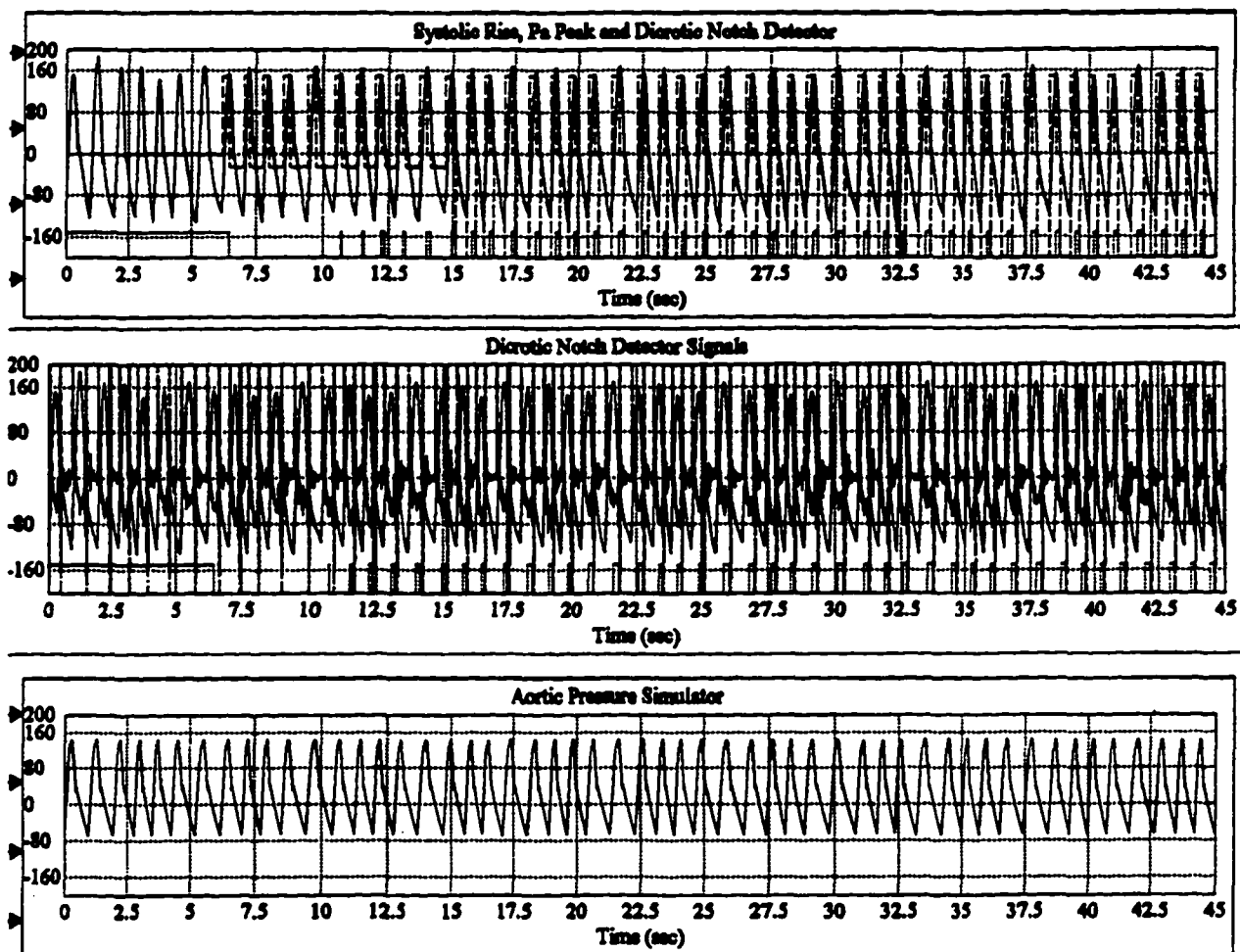
Figure 6-21. Detector Stability for 0 - 45 seconds is illustrated in Figure 6-21A (top trace). Figure 6-21B (middle trace) illustrated the Dicrotic Notch Detector Signals. The Aortic Pressure (Pa) Signal with Heart Rate Variability Simulator (60-80 bpm, 15 breaths per minute) is illustrated in Figure 6-21C (bottom trace).
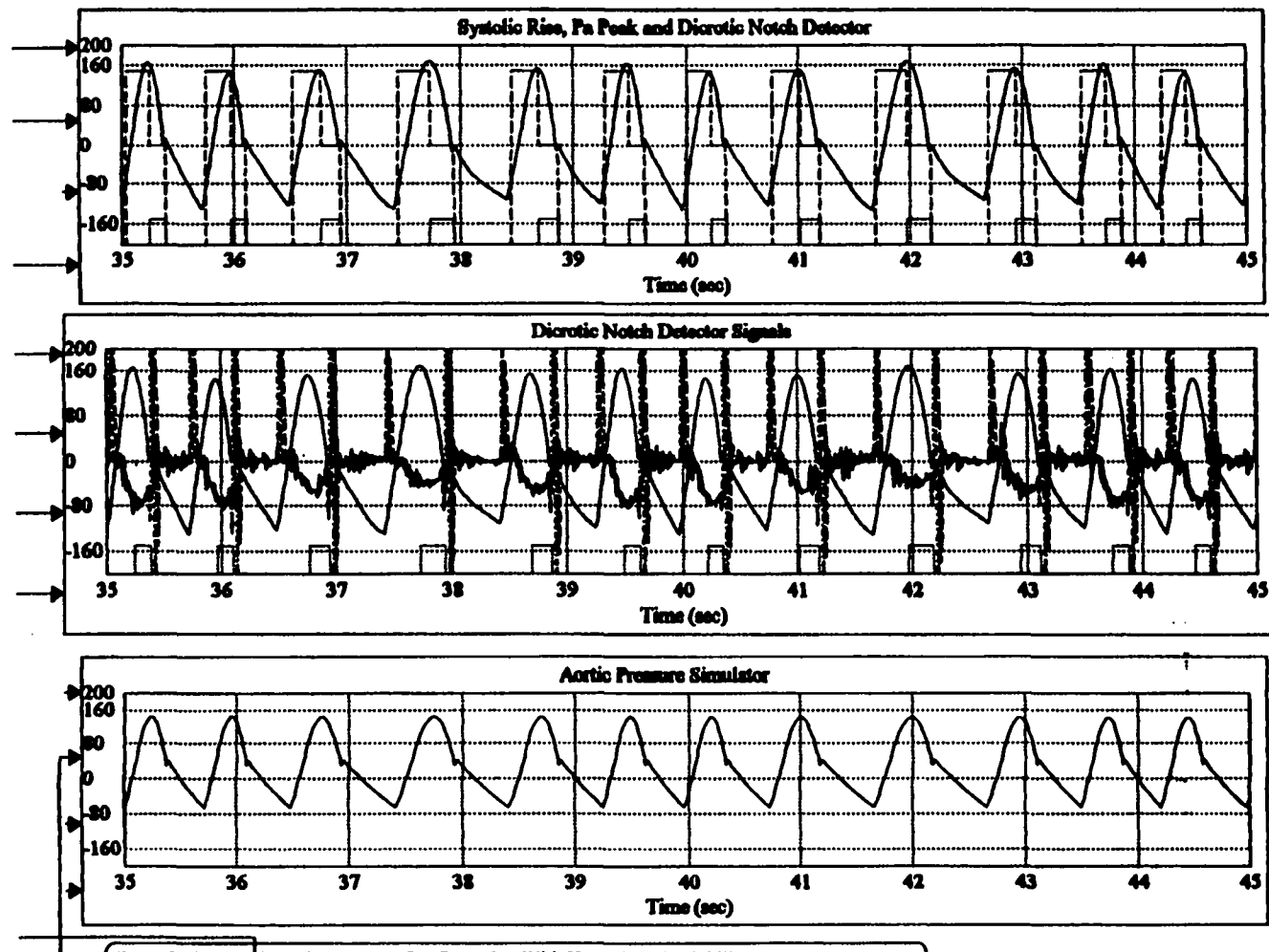
Figure 6-22. Simulated Aortic Pressure (Pa) Detection with Heart Rate Variability due to Respiration (35-45 seconds of Figure 6-21, 60-80 bpm, 15 breaths per minute) is illustrated in Figure 6-22A (top trace). Figure 6-22B (middle trace) illustrates the Dicrotic Notch Detector Signals. Figure 6-22C (bottom trace) illustrates the Pa Signal.
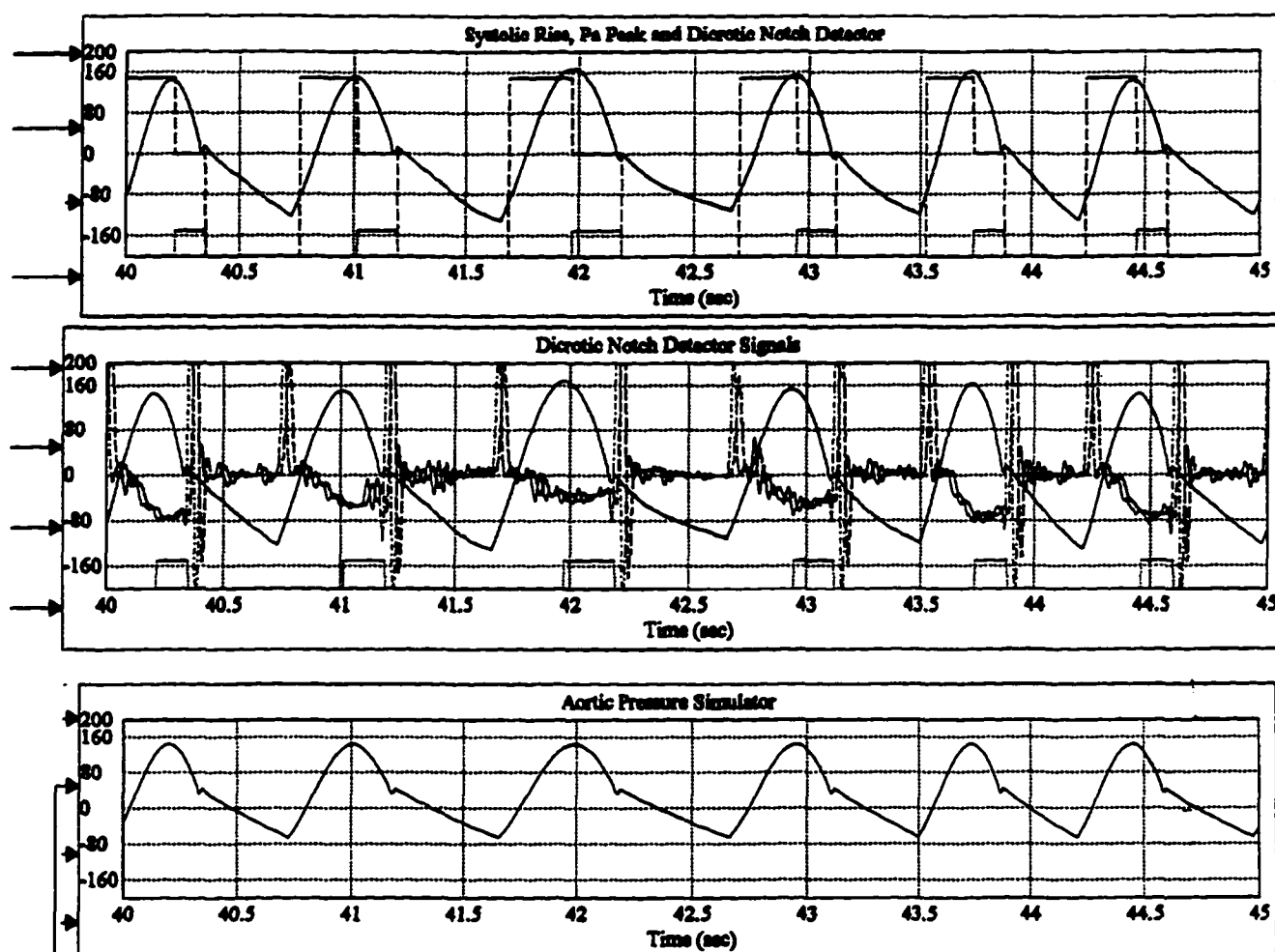
Figure 6-23. Pa Systolic Rise and Dicrotic Notch Detection is illustrated in Figure 6-23A (top trace). Heart Rate Variability Simulation Pa Systolic Rise and Dicrotic Notch Detector Signals (40-45 seconds of Figure 6-21, 60-80 bpm, 15 breaths per minute) are illustrated in Figure 6-23B (middle trace). Note the Amplitude of the Second Derivative Window at the Dicrotic Notch in Figure 6-23B. Figure 6-23C (bottom trace) illustrates the Pa Signal.

Figure 4 HR Var Sim of Dicrotic Notch Det (60-84 bpm, 15 breaths/min)
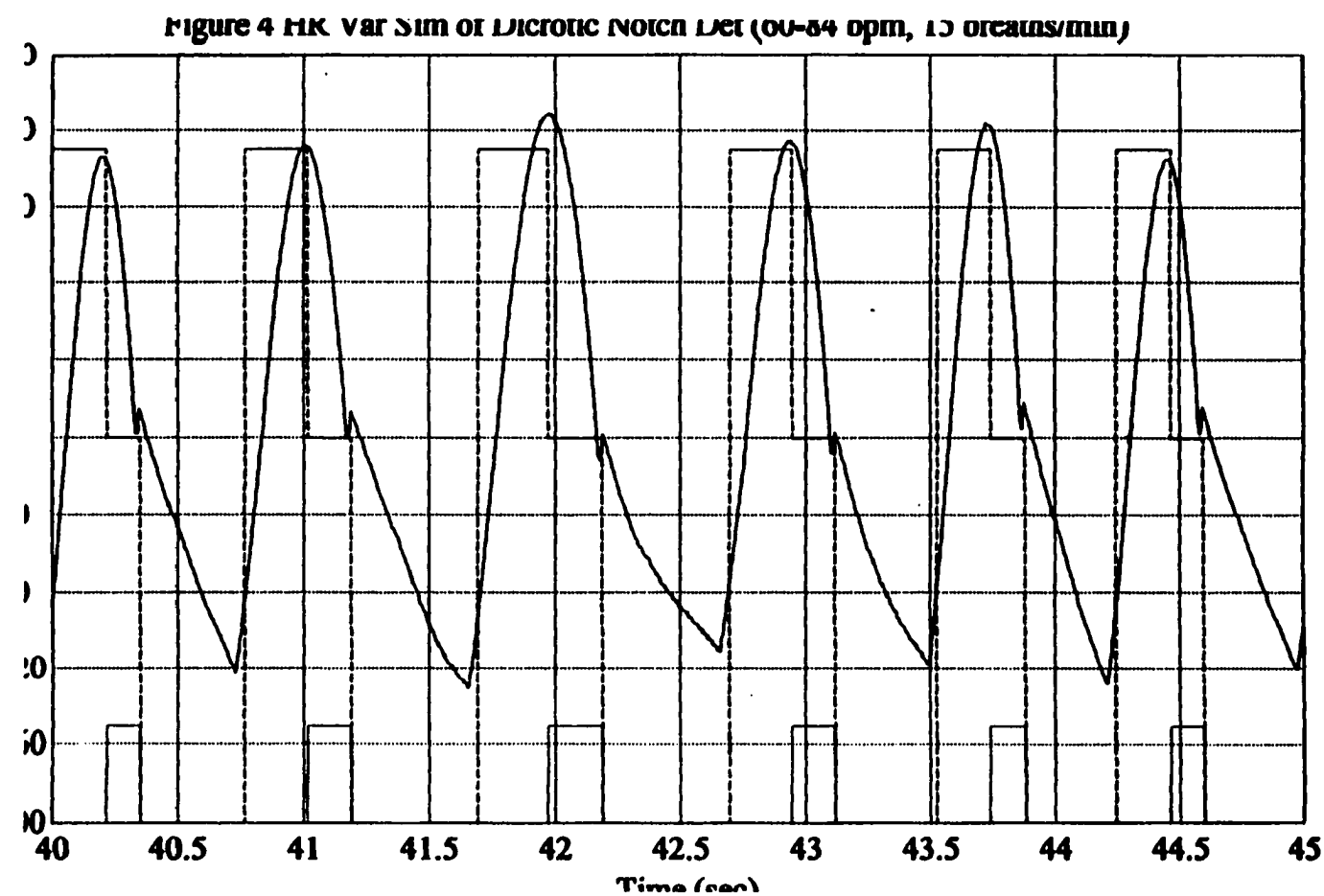
Figure 6-24. Exploded Amplitude View of Systolic Rise, Pa Peak and Dicrotic Notch Detection Signals illustrated during Heart Rate Variability Simulation of Dicrotic Notch Detection (40-45 seconds of Figure 6-21, 60-80 bpm, 15 breaths/minute). Note the Accuracy of the Detection of the Dicrotic Notch.

7. Discussion and Conclusion

Chapter 7 discusses the results of the counterpulsation CAD control dissertation research in Section 7.1 and then states conclusions that have been reached from those results in Section 7.2.

7.1 Discussion of CAD Control Research Results Using Canine Experimental Model and Pa Simulation Model

The CAD control research results using canine mongrel experimental models is discussed in Section 7.1.1 and Pa trace model and detection simulation experiments in is discussed Section 7.1.2

7.1.1 Canine Mongrel Experimental Model Results

The results of Section 7.1.1 are divided into three sections. Section 7.1.1.1 describes the Pa and ECG CAD detection and control results. Section 7.1.1.2 discusses the results of the transputer (multiprocessor) communications research. Section 7.1.1.3 discusses the results of the heart rate to systolic time interval linear relationship and its potential application for dicrotic notch prediction during ectopic heart beats.

7.1.1.1 Pa and ECG CAD Detection and Control Results

Section 7.1.1.1 describes the results of Pa and ECG CAD detection and control results utilizing off-line (recorded data) and on-line (canine mongrel experimental model data).

Off-line detection experiments were necessary to ensure the reliability and accuracy of the Pa and ECG detection algorithms prior to utilizing the algorithms in canine mongrel CAD control experiments. The off-line testing ensured that no unexpected detection behavior (e.g., algorithm crash, malfunction, improper or missed detection, etc.) would occur for a variety of some of the most challenging Pa and ECG traces.

Detection of the Pa trace required determination of the systolic rise and dicrotic notch. The detection of the Pa systolic rise utilized two basic detection criteria, the inherent strong first derivative and the difference in diastolic and systolic pressure in the Pa signal trace.

One aspect that challenges the systolic rise detection is arrhythmia, (e.g., premature ventricular contractions) in which the left ventricle does not fill to the volume of the prior beat. This behavior typically creates a smaller systolic to diastolic pressure difference. Arrhythmias causing a decreased

systolic to diastolic Pa difference present a challenge to the systolic rise detection algorithm. Thus during arrhythmia, one of the two criteria for systolic rise detection (the systolic to diastolic mmHg difference) is somewhat compromised. However, the systolic rise detection algorithm provides tolerances for a diminished systolic and diastolic difference at the systolic rise by using a fraction of the systolic rise Pa difference along with the first derivative criteria to ensure detection of the systolic rise during arrhythmias. An example of the variation in systolic to diastolic pressure difference due to arrhythmia can be observed in Figure 2-3E.

Dicrotic notch detection is challenged by the variation in the appearance of the dicrotic notch and the appearance and position of any Pa perturbations that resembles a dicrotic notch. As can be observed in Figure 2-2E, the dicrotic notch is found close to the diastolic pressure. A perturbation in the Pa trace of the canine mongrel, half-way down the fall of the systolic pressure is very similar to the shape of a dicrotic notch. This type of Pa trace signal makes Pa detection extremely difficult[1]. Variation in the appearance of the dicrotic notch can be seen when comparing Figure 2-2D and Figure 2-2E.

Figure 5-1 and Figure 5-2 illustrate the detection of the systolic rise and dicrotic notch. As can be seen from the systolic rise detection in Figure 5-2, once the Pa pressure detection difference criterium is achieved in the detection algorithm logic, the systolic rise detection signal occurs somewhere along the duration of the systolic rise. In comparison to the Pa signal in Figure 2-2E, Figure 5-1 and Figure 5-2 illustrate a Pa trace that is almost ideal for detection. The systolic rise and dicrotic notch are distinct in that their signals have a strong first derivative and second derivative, respectively, which is utilized for detection. In addition, typically no other characteristic within the Pa trace on the fall of systolic pressure rivals in amplitude, the strong second derivative signal of the dicrotic notch.

As an alternative to Pa detection, ECG R-wave detection provides the foundation for CAD control when the ECG signal is utilized as the control signal. Once the modified version of the DD/1 QRS-complex detection algorithm (26)[2] was developed, off-line detection testing was conducted to

---

1. This type of canine mongrel Pa trace in which a dicrotic notch type shape occurs (prior to the dicrotic notch) within the fall of systole is very uncommon but did appear within the Cornell University Medical College Canine Aortic Pressure Database.

2. The DD/1QRS complex algorithm (26) was developed at the Washington University for the purpose of detecting QRS-complexes in the analysis of arrhythmias. The R-wave detector in this dissertation utilizes the same DD/1 algorithm for QRS-complex detection along with an additional software algorithm to prevent the improper detection of the T-wave (false positive).

ensure the algorithm detected the QRS-complex properly for various types of recorded ECG traces with arrhythmetic complexes and ECG signal interference.

The ECG R-wave detection accuracy was calculated using recorded data from the "standard benchmark" for an ECG detection accuracy measurement (42), namely, the MIT/BIH Arrhythmia Database(30). The results of the ECG detection accuracy testing for each of the 48 records are noted in Figure 5-3.

The DD/1 algorithm utilized four basic criteria to detect a QRS complex. The four criteria were height, slope, width and the start and end of the slopes of the QRS-complex which originate and terminate at approximately the same isoelectric potential. The complementary T-wave algorithm developed in this dissertation was designed to prevent the detection of T-waves as a false positive[1].

The general capabilities of the QRS-complex detection algorithm properly detected normal sinus QRS complexes, non-sinus QRS-complexes that resembling normal QRS-complexes (e.g., atrial premature contractions), and ventricular complexes resembling normal QRS-complexes (e.g., premature ventricular contractions).

The small number of QRS complexes that the detection algorithm could not properly detect (due to false negatives) included adjacent QRS complexes with grossly changing heights, e.g., the second of two QRS complexes was less than the one third of the height of the first. Examples of these arrhythmias include ventricular bigeminy, aberrant beats, ventricular couplets, and ventricular tachycardia.

The small number of non-QRS complexes that the detection algorithm improperly detects (due to false positive) included "non-QRS ECG complexes" and artifacts resembling a QRS-complex. Examples of these include noise greater than one-third the height of the average R-wave height, large peaked P-waves and T-waves, artifacts resembling QRS-complexes e.g., pacemaker spikes and double peaked R-waves (i.e., a single R-wave would be detected twice).

Certain records with the MIT/BIH Arrhythmia database had a few dominant arrhythmias or artifacts that caused improper detection (i.e., false positive plus false negatives which was labelled as failed detections in Figure 5-3). The cause of those improper detections typically resulted in a detection accuracy of 98% or less. The dominant causes of false positive R-wave detections within the MIT/ BIH records ranging from 100 to 124 included double QRS-detections for the same dual peaked R-

1. The MIT/BIH database had a considerable number of T-waves that resembled QRS-complexes, therefore, the complementary T-wave algorithm was added to prevent the associated false positives.

wave, noise, peaked P-waves with substantial height, and thin T-waves with substantial height. The dominant causes of false negative R-wave detections within the MIT/BIH records ranging from 100 to 124 included the height of the PVC following the pacemaker spikes was too small in comparison to the height of the pacemaker artifact, and noise. The dominant cause of false positive detections within the MIT/BIH records ranging from 200 to 234 included ventricular tachycardia, atrial fibrillation, noise, and P-waves with substantial height. The dominant cause of false negative detections within the MIT/BIH records ranging from 200 to 234 included ventricular tachycardia, atrial fibrillation, noise, ventricular couplets and triplets, left bundle branch block, and ECG signal amplitude changes, and T-waves with substantial height, and P-waves with substantial height, reduced height R-waves after baseline shifts, and small R-waves due to ventricular bigeminy. The remainder of the records (noted in Figure 5-3), not mentioned specifically in the previous two paragraphs, have a relatively low percentage of failed detections (false positive and false negatives).

The majority of the failed detections are due to artifacts (e.g., noise and pacemaker spikes) and ECG signals (e.g., P-waves and T-waves) that resemble QRS-complexes. In a real-time CAD control application, searching detection patterns back in time to determine an irregularity in R-wave detections to correct an improper detection is not possible[1]. Therefore, due to the inability to review back in time and the finite amount of computational time available, a 96.56% detection accuracy of the QRS-complex detection algorithm (DD/1 algorithm with complementary false positive T-wave detection prevention algorithm) is quite substantial. Specifically, the 96.56% detection accuracy, is among the elite as far as a detection percentage for QRS-complex detection algorithms (i.e., between 95-100%) for the MIT/BIH Arrhythmia database.

The ECG QRS-complex detection accuracy experiments also demonstrate that an R-wave detector can be implemented on a 80386 33 Mhz PC-AT that models the computational power of a single processor within a quad transputer card. The fact that the QRS-complex detection algorithm was computationally efficient enough to run on a single PC-AT 33Mhz 80386 makes the algorithm applicable to operate on a single transputer processor (comparable to the 80386) of multiprocessor CAD control implementation.

On-line detection (i.e., conducted using canine mongrel experimental models) is similar to off-line detection on recorded data except there are no extraneous sources of noise associated with the recording media (i.e., reel-to-reel tape drive). Experiments were conducted to ensure that any

---

1. An example of a QRS-complex detection irregularity may be two R-waves spaced in time within 100 milliseconds from each other.

differences between off-line data and on-line data were not overlooked. An observation was made that the reel-to-reel tape drive was adding some extraneous noise to the off-line recorded data.

On-line CAD control experiments[1] were conducted to demonstrate the detection algorithms could be utilized as a timing foundation for counterpulsation CAD control when control signals were less than ideal due to cardiopathological variation (i.e., arrhythmia) and surgical interference (electrocautery). On-line experiments were utilized for CAD Pa and ECG detection verification because the CAD control triggering signal is derived from the detection of cardiac events.

A factor that make CAD control (and associated detection) during the canine mongrel control experiments very challenging is particularly apparent when using Pa as the control signal because augmentation modifies the shape of the Pa trace. This is a form of positive feedback and makes control very sensitive to late deflation of the CAD[2]. In order to prevent positive feedback from derailing the control phasing with the cardiac cycle, the deflation was increased very slowly to its optimal timing.

A second factors that makes CAD control (and associated detection) during the canine mongrel control experiments very challenging is the inherent delay between the triggering of the electronic control inflation/deflation signal and the augmentation which is observed within the Pa trace. The delay observed within the experiments conducted using the intraaortic balloon was typically 70-80 milliseconds. This delay was accounted for within the CAD inflation and deflation timing of the IAB control algorithm.

The CAD control illustrations captured using the Cornell University Medical Collage Data Acquisition System, Figure 5-6 through Figure 5-19, clearly illustrated the ability of the Pa detection algorithm to be used as the foundation for the CAD control application in less than ideal surgical and physiological conditions including electrocautery and changing heart rates due to arrhythmia.

Figure 5-6, Figure 5-7 and Figure 5-8 illustrate the CAD control algorithm (utilizing the Pa trace for control) providing optimal IAB timing during moderate (140bpm), slow (120 bpm) and fast

---

1. Control experiments in which augmentation is applied can only be conducted when using a canine mongrel experimental model. Off-line data can only be utilized for detection experiments and determining the control signal is properly phased with the cardiac cycle events (e.g., systolic rise and dicrotic notch). The observation of augmentation due to the CAD control signal cannot be observed using off-line data (i.e., previously recorded data).

2. A late deflation can cause the augmentation shape to mask the systolic rise (naturally created by the contraction of the left ventricle), eliminating this timing signal and thus CAD control phasing with the cardiac cycle is lost for at least one beat.

(180bpm) heart rates, respectively. Figure 5-6B, Figure 5-7B, and Figure 5-8B illustrate optimal timing by demonstrating proper augmentation[1] during the constant heart rates. These results illustrate CAD control during constant heart rates which provide an ideal[2] canine mongrel experimental model sinusoid heart rhythm for CAD control timing and detection because inflation and deflation timing relative to the cardiac cycle are identical for each beat. An example of the inflation augmentation delay can be observed in Figure 5-6 when comparing the start of the inflation control signal at exactly 17.2 seconds in Figure 5-6C (CAD control solenoid timing) with the start of augmentation at approximately 17.3 seconds in Figure 5-6B (Pa trace).

A considerably less than ideal Pa trace is provided to the CAD controller when electrocautery is performed on the canine mongrel experimental model during the application of cardiac assistance. The electrocautery utilized for experimentation had two different modes of operation, coagulation[3] and cut[4].

Electrocautery in coagulation mode during cardiac assistance is illustrated in Figure 5-9 through Figure 5-11. The CAD controller is able to maintain cardiac assistance during signal interference due to the noise caused by electrocautery. During electrocautery in coagulation mode contact with the tissue is maintained because the tip of the electrocautery remains in contact with the tissue (i.e., the tissue is not burned away as it is in cut mode).

Electrocautery in cut mode during cardiac assistance is illustrated in Figure 5-12 through Figure 5-14. The CAD controller is able to maintain cardiac assistance during signal interference due to the noise caused by electrocautery. During electrocautery in cut mode contact with the tissue was more difficult to maintain because the tip of the electrocautery quickly burns away the tissue it is in contact with. A comparison of ECG of Figure 5-9A (coagulate mode) and Figure 5-12A (cut mode) demonstrate that the noise generated from coagulation mode is more consistent in appearance than the noise generated from the cut mode because of the different type of function for each mode. The electrocautery CAD control experiment illustrations in Figure 5-9 through Figure 5-14 demonstrated the detection algorithms being utilized as a timing foundation for counterpulsation

---

1. Proper augmentation requires the CAD augmentation to start at the dicrotic notch and the augmentation to stop just prior to the systolic rise.

2. An ideal Pa trace control signal is one in which the canine mongrel experimental model has a constant heart rate and there is no external artifacts (e.g., electrocautery noise) on the Pa signal.

3. An electrocautery in coagulation mode was developed to stop bleeding by searing tissue and blood through the application of high frequency current.

4. An electrocautery in cut mode was developed to burn tissue away to create an incision in the tissue through the application of high frequency current.

CAD control when the Pa control signal was less than ideal due to both coagulation and cut mode of electrocautery.

A physiological phenomenon, arrhythmia, creates a less than ideal Pa control signal. Arrhythmia can cause a quick change in heart rate in the canine mongrel experimental model. The foundation of CAD Pa control, Pa detection, is challenged by changes in heart rate. Changes in heart rate causes the Pa systolic template to change in shape. Also variation in the frequency of appearance of the systolic rise and dicrotic notch must be accounted for in the robustness of the Pa detection algorithm. The two types of arrhythmia demonstrated are bradycardia arrhythmia and tachycardia arrhythmia. Bradycardia causes the heart rate to decrease quickly and tachycardia causes the heart rate to increase quickly.

Experiments were performed to demonstrate that the CAD controller (and underlying Pa detection algorithms) can maintain synchronization with the cardiac cycle during arrhythmia, namely, bradycardia and tachycardia. Figure 5-15 illustrates the CAD controller maintaining synchronization with the cardiac cycle during a decrease in heart rate (bradycardia). The control algorithm is able to maintain synchronization with the cardiac cycle during the sequence of five heart beats at 120 bpm and then six heart beats at 90 bpm as illustrated in Figure 5-15.

Figure 5-16 through Figure 5-18 illustrates the CAD controller maintaining synchronization with the cardiac cycle during an increase in heart rate (tachycardia). The control algorithm is able to maintain synchronization with the cardiac cycle during the sequence of seven heart beats at 120 bpm and then seventeen heart beats at 180 bpm as illustrated in Figure 5-16. The arrhythmia CAD control experiment illustration in Figure 5-15 through Figure 5-18 demonstrated the detection algorithms being utilized as a timing foundation for counterpulsation CAD control when control signals were less than ideal due to both bradycardia and tachycardia.

In order to demonstrate that the CAD Pa control algorithm (and underlying Pa detection algorithm) is capable of controlling a second type of CAD, experiments were performed in which the extra-aortic counterpulsation device (EACD) provided augmentation. Figure 5-19 illustrates augmentation provided by the EACD which is surgically attached to the aorta[1].

Development of Pa detection filters took into consideration different types of less than ideal Pa traces due to external trace interference and cardiopathological variation. From the results of the control research, the development of a computationally efficient robust Pa systolic rise and dicrotic

---

1. This contrasts the IAB which is inserted into the aorta.

notch detector resistant to several forms of Pa trace interference due to cardiothoracic operating environment was demonstrated in a counterpulsation CAD control application. The fact that the algorithm was computationally efficient enough to run on a single PC-AT 33Mhz 80386 makes the algorithm applicable to operate on a single transputer processor (comparable to the 80386) of a multiprocessor CAD control implementation.

ECG detection experiments were conducted to demonstrate the ECG R-wave detection algorithm was capable of functioning properly during CAD experiments on canine mongrel experimental models. The ECG control experiments were conducted to demonstrate the ECG detection algorithm was capable of providing the foundation for proper CAD control on canine mongrel experimental models during various non ideal conditions including baseline wander due to mechanical ventilation and noise due to the cardiothoracic surgery operating room environment.

The fact that the CAD control algorithm (and underlying R-wave detection algorithm) was computationally efficient enough to run on a single PC-AT 33Mhz 80386 makes the algorithm applicable to operate on a single processor within a multiprocessor CAD control implementation with transputer processors comparable to the 80386.

7.1.1.2　Transputer Research

The results of the transputer research demonstrate that a CAD protocol could be developed to allow a quad transputers to route the necessary information through the transputer links (and PC buses and interfaces) to allow appropriate communication for a counterpulsation cardiac assist device controller. Secondly, the results of the transputer research demonstrate that a software methodology to allow the data within the CAD protocol to route through the transputer card and PC-AT host utilizing a small percentage of CPU time (<10%). This allows the remaining CPU time to be utilized for CAD control and detection algorithm computation. A protocol was developed and combined with a developed software communications methodology which exhausted 8.3% of CPU time left 91.7% of the CPU time for CAD control computation. The implementation of a CAD control algorithm protocol and software methodology on a PC-based multiprocessor transputer card, from the standpoint of communications, has been demonstrated.

7.1.1.3 Heart Rate to Systolic Time Interval (STI) Relationship

Section 7.1.1.3 discusses the Heart Rate to STI relationship data illustrated in Figure 5-20 through Figure 5-24 of Section 5.3.2.

7.1.1.3.1 Importance of the Prediction of the STI for Inflation Timing

Prediction of the length of systole[1] (i.e., systolic time interval, STI) is needed for optimal inflation. An inherent delay associated with the activation of the electronic signal of inflation control and the resulting augmentation within the Pa trace requires prediction of the dicrotic notch. During a constant heart rate the systolic time interval (approximately the systolic rise to dicrotic notch time interval) can be used along with the detection of the systolic rise to predict the dicrotic notch. The timing of the dicrotic notch and the inflation delay associated with the CAD (IABP or EACD) is used to optimally time inflation. Optimally timed inflation of the CAD initiates augmentation at the occurrence of the dicrotic notch.

However, when the heart rate is not always constant and an ectopic beat occurs, a prediction method must be used to determine the occurrence of the dicrotic notch. One method investigated within this dissertation to predict the occurrence of the dicrotic notch during ectopic beats is the heart rate to systolic time interval (STI) linear relationship. A heart rate to systolic time method has been demonstrated to be present in humans and can be modelled with a linear regression equation estimate.

7.1.1.3.2 Importance of Inflation Augmentation after Occurrence of Dicrotic Notch

Prediction of the dicrotic notch for optimal inflation must ensure that the cardiac assist device does not in any way hinder the natural contraction of the heart. Particularly with an IAB, Pa augmentation due to inflation prior to the dicrotic notch (i.e., early inflation) indicates that the inflated IAB has obstructed the natural systolic blood flow within the aorta. Precaution to avoid increased resistance in the aorta to an already weakened heart is of primary importance. Thus, any estimate methodology (e.g., HR to STI relationship) to predict the occurrence of the dicrotic notch should ensure that the estimate causes augmentation to initiate during or after (i.e., late inflation[2]) the actual occurrence of the dicrotic notch.

---

1. The length of systole and the detection of the systolic rise provides the timing of the dicrotic notch.

7.1.1.3.3   HR to STI Data

Variation in the data from the HR to STI linear regression equation least squares estimate indicates that the prediction of the dicrotic notch (using the regression equation) provides a poor estimate. For a given heart rate the regression equation will provide STI estimates that are considerably less than the actual STI. This would lead to a dicrotic notch prediction that would occur in time before the actual dicrotic notch. A short STI estimate would cause an early inflation - obstructing blood flow within the aorta during systole.

For example, in the STI to HR graph of Figure 5-24 an actual data point of HR= 130 bpm and STI=200 milliseconds is estimated by the linear regression estimate of STI = 160 milliseconds. If an ectopic beat occurred in which the heart rate was calculated to be 130 bpm, the estimate for the STI would be 160 milliseconds. This estimate would provide a timing inflation that is 40 milliseconds less than the actual optimal timing inflation. As noted previously in Section 7.1.1.3.2, an early inflation hinders the normal pumping function of the heart.

A second reason the heart rate to STI relationship in canine mongrel experimental models is not feasible for the utilization of inflation prediction can be observed by looking at the variation in the slopes of the linear estimates within the graphs of Figure 5-20 through Figure 5-24. It is very apparent that if this type of estimate was utilized for inflation prediction, a separate regression equation would have to be derived for each canine mongrel experimental model. Thus, the stand alone real-time algorithm would have to utilize STI and HR data points acquired during cardiac assistance and derive a regression equation from such data. In addition, the algorithm would be dependent upon the canine model having changes in heart rate so that the linear regression could be derived from two or more heart rates for that particular experimental model[1]. This process would require a computationally demanding algorithm and would not be possible in this real-time CAD control application in which a single processor is utilized for Pa detection and control.

---

2. It must be noted that as the delay of a late inflation increases (as Pa augmentation migrates farther in time from the occurrence of the dicrotic notch) the hemodynamic benefits of the CAD decrease. However, a late deflation does not present additional resistance to the heart, and is therefore not detrimental to the normal pumping action of the heart.

1. A linear regression estimate requires at least two points to establish an linear regression equation.

7.1.2   Pa Simulation Model Results

Section 7.1.2 discusses the results of the Pa trace Modelling and Detection simulations documented in Chapter 6.

7.1.2.1   Stability Simulation

In order to ensure the simulation platform was stable from a software standpoint as well as from a physiological (Pa trace) standpoint, a long term stability simulation was conducted for ten minutes. Figure 6-1 and Figure 6-2 demonstrate the last twenty and five seconds, respectively, of the stability simulation.

From a software reliability standpoint, it was important to demonstrate stable execution of the simulation platform, the Pa model executing within the platform, and the Pa detection algorithm MS Windows DLL imported to the platform. The internal Pa model and external algorithm (i.e., detection algorithm) within the VisSim-based simulation platform was demonstrated to operate properly for ten minutes. This can be seen by the appearance of the Pa trace at the ten minute mark (600 seconds) in Figure 6-2C.

From a physiological standpoint, variation in Pa trace shape or baseline pressure would cause unwanted variation to the "ideal" Pa trace. The "ideal" Pa trace was used as a reference trace for which physiological and cardiothoracic surgery variations were imposed. It was important for the "ideal" Pa trace to be unchanged from beat to beat. The ideal Pa signal remained unchanged throughout the ten minute stability simulation as can be seen in Figure 6-1C and Figure 6-2C. All Pa systolic and diastolic intervals are identical in shape for all cardiac cycles throughout Figure 6-1C and Figure 6-2C.

7.1.2.2   Dicrotic Notch Variation

In several of the canine mongrel experiments, the appearance of the Pa dicrotic notch ranged considerably in appearance. The least pronounced dicrotic notch shapes appeared as only a change in slope within the Pa trace. The most pronounced dicrotic notch shapes appeared as a Pa "notch" located exactly at the change in slope of the Pa trace. In order to model the least and most pronounced types of dicrotic notch shapes within the Pa trace, simulations were conducted for both extremes in the appearance of the dicrotic notch. The first simulation experiments was conducted on a Pa trace in which the a notch was not present and the second was a Pa trace in which the dicrotic

notch was present. Figure 6-4A illustrates detection of the dicrotic notch without a Pa perturbation (i.e., 0 mmHg). Figure 6-6A illustrates the detection of the dicrotic notch with a 3mmHg Pa perturbation. The Pa detection algorithm was able to detect the full range of dicrotic notch perturbation variation, namely 0 to 3 mmHg.

The objective of the simulation was accomplished by demonstrating the single Pa detection algorithm has the universal capability to detect the full range of dicrotic notch shapes that can appear within an Pa trace due to physiological (e.g., model to model) and cardiopathological (e.g., heart rate, systolic and diastolic blood pressure, etc.) variation.

7.1.2.3 Mechanical Ventilation Causing Baseline Wander

Mechanical ventilation is required in a cardiothoracic surgery operating environment. Mechanical ventilation causes variations (wander) in the baseline of the Pa trace. The frequency of the baseline wander is equivalent to the frequency of the mechanical ventilation. Variations in the baseline of the Pa trace can hinder Pa detection of the systolic rise and dicrotic notch which is essential to CAD control when using the Pa trace as the control signal. The simulation illustrations in Figure 6-7A through Figure 6-12A demonstrate proper detection during baseline wander changes in aortic pressure ranging from 10 to 40 mmHg. The objective of the simulation was accomplished by demonstrating the detection of the dicrotic notch during baseline wander due to the effects of mechanical ventilation on the Pa trace. Thus the Pa detection algorithm has a mechanical ventilation baseline artifact immunity up to 40 mmHg.

7.1.2.4 Pa Trace Attenuation

Changes in pressure catheter positioning or blood coagulation on the pressure catheter transducer tip typically causes the Pa trace amplitude to attenuate (i.e., the relative excursion in millivolts representing the systolic to diastolic pressure difference decreases in value). This attenuation can be caused by mechanical ventilation re-orienting the position of the Pa catheter tip (which has a single side that exposes the piezoelectric transducer) which makes contact with the blood within the aorta[1]. The Pa attenuation can also be caused by blood coagulation on the pressure catheter transducer tip.

---

1. A slight rotation of the piezoelectric transducer within the aorta can vary the percentage of contact area exposed to the blood of the aorta causing a change in the relative amplitude deflection difference of the Pa trace.

The attenuation due to mechanical ventilation causes the amplitude to change in the Pa signal at a frequency equal to that of the mechanical ventilator. The Pa attenuation due to blood coagulation typically occurs at a slower rate as the blood forms on the catheter tip. In order to verify the Pa detection algorithm can detect in the most severe form (i.e., fastest rate) of Pa signal attenuation, a model was developed to duplicate the Pa signal attenuation caused by mechanical ventilation.

Variations in the amplitude of the Pa trace can hinder Pa detection of the systolic rise and dicrotic notch which is essential to CAD control when using the Pa trace as the control signal. The simulation illustrations in Figure 6-13A and Figure 6-14A demonstrate proper detection during signal attenuation in aortic pressure ranging from 100% to 50% within 2.5 seconds (this represents a breath rate of 12 breaths/min).

The objective of the simulation was accomplished by demonstrating the detection of the dicrotic notch during signal attenuation due to the effects of mechanical ventilation on the Pa trace. Thus the Pa detection algorithm has a mechanical ventilation attenuation immunity of up to a 50% reduction in amplitude within 2.5 seconds (i.e., 20% reduction in signal amplitude per second up to a 50% reduction).

7.1.2.5   Noise Interference

Noise or unwanted signal appears in all control signals to some extent. Pa traces typically acquired from within a cardiothoracic surgery operating room environment have artifacts of noise. The causes of unwanted noise within the Pa signal include artifacts due to powerline interference, muscle contraction (e.g., due to coughing), baseline drift and amplitude modulation with mechanical ventilation, instrumentation noise generated by electronic devices used in signal processing, and electrosurgical noise(22). A single sinusoid noise source with a constant frequency and amplitude (e.g., powerline interference) was modelled by a uniformly distributed noise source. The contribution of several cardiothoracic surgery noise sources combined was modelled by a Gaussian distributed noise source.

Contributions of noise to the Pa trace can hinder Pa detection of the systolic rise and dicrotic notch which is essential to CAD control when using the Pa trace as the control signal. This is particularly applicable to the CAD detection algorithms developed within this dissertation because the algorithms are derivative based which are sensitive to noise.

The simulations illustrated in Figure 6-15A, Figure 6-16A, Figure 6-18A and Figure 6-19A demonstrate proper detection on an aortic pressure signal with normally distributed noise (Figure 6-15A and Figure 6-16A) and Gaussian distributed noise (Figure 6-18A and Figure 6-19A). The objective of the simulation was accomplished by demonstrating the detection of the dicrotic notch during interference to the Pa trace due to normal and Gaussian distributed noise. The Pa detection algorithm has immunity from normal distribution noise with a mean - 0.5mmHg and a standard deviation - 0.289 mmHg. The Pa detection algorithm also has immunity from Gaussian distributed noise with a mean - 0.0 mmHg and a standard deviation - 0.6 mmHg.

This Pa detection noise immunity is considerable when comparing that amplitude of the noise with the amplitude of the dicrotic notch deflection as seen in Figure 6-17 (normal) and Figure 6-20 (Gaussian). Thus the Pa detection algorithm has a level of immunity to both normal and Gaussian distributed noise.

7.1.2.6   Heart Rate Variability Due to Respiration

A normally occurring physiological phenomenon is a small variation in heart rate due to respiration. The variability in heart rate is taken into account in order to ensure the Pa detection algorithm can handle the effects of this behavior. The change in heart rate is dependent upon the frequency of respiration. For the heart rate variability model, the frequency of respiration was chosen to be 15 breaths /min. In order to ensure the Pa detection algorithm is immune to heart rate variability due to respiration, simulations modelling this physiological occurrence were conducted. Variations in the heart rate of the Pa trace can hinder Pa detection of the systolic rise and dicrotic notch which is essential to CAD control when using the Pa trace as the control signal.

The simulations illustrations in Figure 6-21A through Figure 6-24A demonstrate proper detection during heart rate variation due to respiration in aortic pressure cycling from 60 to 80 beats per minute (bpm) within 2.0 seconds (this represents a breath rate of 15 breaths/min).

The objective of the simulation was accomplished by demonstrating the detection of the dicrotic notch during heart rate variability due to the effects of respiration on the Pa trace. Thus the Pa detection algorithm has a heart rate variability immunity (due to respiration) of 20 bpm in the range of 60 to 80 bpm during a breath rate of 15 breaths/min. This Pa detection immunity of 20 beats per minute (from heart rate variability due to respiration) is considerably more than the maximum variability that can be observed physiologically. Thus the Pa detection algorithm is immune to heart rate variability due to respiration.

7.2   Research Conclusions Based on CAD Control Results

The motivation for Cardiac Assist Device (CAD) Control research is due to the large number of persons with some type of cardiac pathology. In fact, heart attacks are the leading cause of death in the United States claiming over 500,000 people each year (1). In an attempt to reduce the number of fatalities and prolong life, cardiac assistance provides one possible treatment in the fight against heart disease.

In the delicate balance of circulation, if the heart is unable to sustain itself by providing the minimal circulation through the coronary arteries, ischemia will begin to set in and eventually the heart will stop beating. Cardiac assistance can augment circulation to prolong life until surgical intervention can correct the cardiac pathological disorder through heart replacement or other cardiothoracic surgical means. Cardiac assistance methods must be further developed to assist the heart to prolong life (e.g., for patients awaiting heart transplants or corrective cardiothoracic surgery).

In order to assist the heart, timing (i.e., phasing) must be established with the heart so some type of Cardiac Assist Device (CAD) can assist with circulation. Two major timing signals are typically available to the CAD controller, those being ECG and Aortic Pressure (Pa). In general, control is more effective if more than one signal can be used as a reference for control, particularly if both signals are utilized simultaneously. To this date no CAD controller uses both ECG and Pa signals in a fault tolerant system for CAD control. To this date no digital Pa detection algorithm has been developed to detect the Dicrotic Notch under various undesirable physiological and surgical conditions. This dissertation research includes the development of computationally efficient ECG QRS complex and Pa systolic rise and dicrotic notch digital filters for such a purpose. Subsequent analysis is performed through canine mongrel experimental models and through simulation experiments.

The most utilized counterpulsation cardiac assist device controller is the intra-aortic balloon pump (IABP) and is operated in conjunction with the most utilized cardiac assist device, the intra-aortic balloon (IAB). Typically the IABP uses ECG as the "triggering" control signal. However, when electrocautery is utilized during acute cardiothoracic care, the ECG is unusable as a control signal and cardiac assistance is prevented. IABP systems also have aortic pressure (Pa) trigger modes. The current IABP Pa control algorithms detect the systolic rise and use a heart rate to systolic time interval (STI) regression equation to predict the dicrotic notch. During quickly changing heart rates, commercial IABPs in Pa trigger mode will typically stop providing assistance due to the changing heart rate. The Pa detection algorithm devised in this dissertation provides detection of the Pa

dicrotic notch. Detection provides a more accurate timing of the dicrotic notch than prediction. The Pa dicrotic notch detection in this dissertation demonstrates control during arrhythmia and the use of electrocautery on canine mongrel experimental models. The Pa dicrotic notch detection (and associated inflation timing) method is superior because it provides a more accurate detection timing methodology (as oppose to HR to STI prediction). In addition, the Pa dicrotic notch detection algorithm can operate during electrocautery and arrhythmia. The robustness of the Pa detection algorithm developed has the ability to provide counterpulsation cardiac assistance during physiological and cardiothoracic operating conditions in which commercial IABP controllers cannot operate.

Commercial Intra-aortic Balloon Pumps are the most prevalent method utilized for circulatory assistance for patients undergoing open heart surgery. Several studies were performed describing the optimal control criteria using various CADs for different cardiothoracic morphologies. All previous cardiac assist research was developed to optimize the timing of the IAB (and other CAD) based on the assumption that the detection of a cardiac timing event is established (typically the R-wave) and thus control can be derived from that signal. Criteria for optimal timing have been established for the IAB and other CADs. Within a cardiothoracic surgical environment, both physiological (e.g., respiration) and non-physiological (e.g., electrocautery) can interfere with the ideal Pa and ECG trace signals received from the patient. This dissertation research does not assume the establishment of one or more cardiac event signals can be detected without error. This dissertation research addresses the non-ideal Pa and ECG trace signals that can be received from the patient due to physiological and non-physiological interference.

For the purpose of this dissertation research, optimal detection conditions are replaced by non-ideal conditions that can typically exist within a cardiothoracic operating room environment. The non-ideal conditions will be reflected in the reduced quality of both the ECG and Pa traces.

The causes for non-ideal Pa and ECG signal conditions include artifacts due to powerline interference, electrode contact noise, motion artifacts, muscle contraction (electromyographic, EMG), baseline drift and ECG amplitude modulation with respiration, instrumentation noise generated by electronic devices used in signal processing, and electrosurgical noise (22).

As was documented in chapter one, the challenges of CAD detection and control research include inherent biological variation, computational power limitations, limitations in low pass filtering due to real-time control requirements, and inherent positive feedback due to Pa CAD inflation augmentation (specific to the Pa signal). To overcome these challenges, algorithms developed must

have all of the following traits. The algorithms must be independent of biological variation, computationally efficient, maintain a small phase delay, and include robust control algorithms with intelligence to avoid the instabilities of positive feedback. For all these reasons, the research within this area of the dissertation was very challenging.

The developments through the research conducted in this dissertation are significant in the area of CAD control research. The research involved development for experimentation with canine mongrel models as well as development for computer based model simulation. The developments for the canine mongrel experiments included:

1. Robust Computationally Efficient Aortic Pressure Systolic Rise and Dicrotic Notch Detector for Real-time Cardiac Assist Device Control

2. Robust Computationally Efficient ECG R-wave Detector for Real-time Cardiac Assist Device Control,

3. Methodology For Predicting Dicrotic Notch for non-sinus rhythms based on Pa shape in Canine Mongrel Experimental Models

4. Transputer Architecture and Protocol for fault tolerant multiprocessor CAD controller

The development for model (computer based) simulation Pa detection experiments included:

1. A Pa Detection Simulation Platform to Benchmark Detection accuracy during non-ideal conditions

2. An Aortic Pressure (Pa) trace simulation model

3. A Pa artifact models to empirically impair the ideal Pa trace to analyze the limitations of Pa detection algorithms

4. Implementation of an integration methodology that allowed the simulation platform to be interfaced with the Pa detection algorithm

The research conducted has advanced the state of CAD research. The robust Pa detection algorithm developed may be utilized to further optimize CAD control by providing a second reliable means for triggering (i.e., controlling) a cardiac assist device. Also, the modification of an established ECG QRS-complex detector into a computationally efficient R-wave detector for real-time CAD control will also provide another means for control, possibly for an implantable application.

The methodology to predict the dicrotic notch during non-sinus rhythms in canine mongrels will provide a method of more effectively utilizing canine mongrels for research in the area of cardiac assistance during arrhythmias. In addition, the research that has demonstrated that a heart rate to STI interval prevalent in humans is not prevalent in canine mongrel experimental models. This will prevent further use of the canine mongrel experimental model for this type of research. Thus this

regression equation cannot be utilized effectively when investigating CAD control during non-sinus rhythms in canine mongrel experimental models.

The research in the development of a transputer architecture and protocol may be utilized for the advancement of fault tolerant CAD research and provides a path forward in the utilization of multiprocessor hardware for computationally demanding CAD detection and control.

Significant progress was made in the area of counterpulsation CAD Pa detection simulation research. Prior to the completion of the Pa detection simulation research documented in this dissertation, a simulation platform to perform Pa detection analysis did not exist. The simulation platform provides a means for the analysis of Pa detection algorithms to be used in counterpulsation CAD control applications. The Pa detection simulation platform provides an MS Windows 3.1 dynamic link library (DLL) interface to a "C" language based Pa detection algorithm. To provide Pa data to the Pa detection algorithm, a Pa trace model was developed. To challenge the Pa detection algorithm, Pa distortion models were developed that mathematically characterize external disturbances in the Pa trace as well as normal biological variations and phenomena[1]. Lastly, a methodology (simulation experimental procedure) using the simulation platform to benchmark Pa detection algorithms for future research in area of counterpulsation CAD control, was developed and documented in this dissertation.

The Pa detection and control research completed using canine mongrel and simulated models will provide an alternate method to control counterpulsation cardiac assist devices (CADs) during non-ideal conditions (i.e, control using the non-ideal Pa trace). In addition, the research in CAD system architecture (i.e., transputer technology) will provide a means of utilizing both ECG and Pa traces simultaneously for a dual control signal fault tolerant CAD control system. The canine mongrel and simulated developments in Pa detection algorithms for counterpulsation CAD control will provide a new control method in CAD research for the next few years as well as into the twenty-first century.

The results of this dissertation are illustrated in both canine mongrel experimental model traces as well as the Pa detection simulation traces. The canine mongrel experimental model results illustrate proper detection of systolic rise and dicrotic notch Pa and R-wave and P-wave ECG canine mongrel traces. The canine mongrel traces also illustrate optimal control during various ECG and Pa trace interferences and physiological conditions. The non-optimal physiological conditions illustrate

---

1. The distortion models are integrated into the output of the Pa trace model.

control during changing heart rates. The trace interference includes control during electrocautery and mechanical ventilation. Lastly, in an effort to develop a robust R-wave detection algorithm for the canine mongrel experimental models, ECG R-wave detection was demonstrated using the MIT/ BIH Arrhythmia Database.

The results of the Pa detection algorithm analysis using the Pa simulation platform illustrate proper detection of the aortic pressure systolic rise and dicrotic notch. The Pa simulation platform was demonstrated to be stable by performing a long term simulation in which the generation of the ideal Pa model's trace and Pa detection algorithm were displayed for several minutes. In addition, in order to demonstrate the ability of the Pa detection algorithm to handle variation in the dicrotic notch deflection, accurate detection was demonstrated on a Pa trace without and with a dicrotic notch deflection. The results of a Pa detection simulation modelling the effects of mechanical ventilation showed proper Pa detection during baseline wander. A set of simulated experiments demonstrated proper Pa detection during changing amplitude modelling the effects due to changes in transducer positioning or blood coagulation on the pressure catheter transducer tip. To challenge the derivative based Pa detection filters, two different types of noise simulations were conducted, one simulation in which normally distributed noise was combined with the Pa trace and one simulation in which Gaussian distributed noise was combined with the Pa trace. Lastly, a simulation demonstrating proper detection during changing heart rate due to respiration was conducted to address this normal physiological phenomenon.

The Pa detection accuracy analysis was performed visually utilizing the Cornell University Medical College Canine Mongrel Aortic Pressure Database. The dicrotic notch detection accuracy was 99% for 95% of the Canine Mongrel Pa traces stored. The 1 in 20 canine mongrel traces would have Pa perturbation (resembling a Pa dicrotic notch) on the fall of systolic pressure in which the Pa detection algorithm would improperly detect the Pa perturbation and not the dicrotic notch. The overall Pa detection accuracy was 94% (= 0.99 * 0.95).

ECG detection was analyzed using the MIT/BIH Arrhythmia Database and was found to be 96.56%[1] with a maximum 8 millisecond detection delay[2] from the end of the QRS-complex. This R-wave algorithm implemented can be compared with the highest MIT/BIH detection percentage found at 99.77% by Hamilton(42). However, the Hamilton algorithm has Low Pass Filtering (that adds intolerable detection delay) and a search back feature (which is not applicable to real-time

1. Detection accuracy is equal to the 1 - ((False Positive and False Negative Detections)/ (Total Number of Heart Beats))

control applications). Thus the modified version of the DD/1 algorithm(26) implemented in this dissertation provides a comparable MIT/BIH detection accuracy percentage without the unacceptable LPF phase delay and "look back feature."

Pa control experiments were analyzed visually in which the traces demonstrated optimal detection and control during sinusoid[1] heart beats. The Pa detection demonstrated CAD augmentation during changing heart rates and electrocautery.

HR to STI experiments for canine mongrels demonstrated that a linear relationship does not exist (as it does in humans) graphically using least squares fit linear interpolation. Five different experiments showed varying levels of fitting to a linear interpolation. Three of the five experiments demonstrated an estimate error that exceeded 15% for different STI values at the same heart rate.

Transducer architecture and communications throughput demonstrated numerically to show 8.3% processor utilization. This processor utilization was deemed tolerable in that it utilized less than one-tenth of the processor power.

During analysis of the Pa detection algorithm, the variations in the Pa wave were increased in a systematic empirical way to determine the limitations of the Pa detection algorithm. This empirical analysis determined the threshold of the Pa detection algorithm. The simulation platform (Simulation software and interface, ideal-Pa trace and Pa detection algorithm) was demonstrated to be stable for 10 minutes (600 seconds). This was sufficient for the simulation experiments since the Pa detection algorithm would train (be able to detect) within 17 to 35 seconds for all simulations. A Pa trace detection simulation was demonstrated on a Pa wave without dicrotic notch deflection to detect accurately throughout the 10-minute simulation. A Pa trace detection simulation was demonstrated on a Pa wave with dicrotic notch deflection to detect accurately within 17 seconds and subsequently thereafter. A Pa trace detection simulation demonstrated proper detection on a Pa wave with a baseline wander of 40mmHg during a breath rate of 15 breaths/min within 27 seconds and subsequently thereafter. A Pa trace detection simulation demonstrated proper detection on a Pa wave with a variation in amplitude which cycled from 100 to 200% every four seconds within 17

---

2. The detection delay is the worst case time interval from the end of the QRS-complex to when the QRS-complex is detected. In the case of the QRS-complex data preprocessor (AZTEC) and detector (DD/1) implemented in this dissertation, the AZTEC algorithm determines whether ECG data is a slope (e.g., part of the R-wave) or a line (e.g., part of an isoelectric period) within four samples. This allows the algorithm to evaluate the last slope and determine if the detection criteria is met for a QRS-complex. A four sample delay at a 500 Hz sampling rate (2 milliseconds per sample) equates to an 8 millisecond delay.

1. Sinusoid heart beats are the heart beats of a constant heart rate in which the systolic time intervals (STIs) and diastolic time intervals (DTIs) are the same beat to beat.

seconds and subsequently thereafter. A Pa trace detection simulation demonstrated proper detection on a Pa trace with variation due to uniform distributed noise with a mean of 0.5 mmHg and a standard deviation of 0.289 mmHg within 17 seconds and subsequently thereafter. A Pa trace detection simulation demonstrated proper detection on a Pa trace with variation due to Gaussian distributed noise with a mean of zero (0) mmHg and a standard deviation of 0.6 mmHg within 17 seconds and subsequently thereafter. Lastly, a Pa trace detection simulation demonstrated proper detection on a Pa trace with heart rate variability due to respiration from 60 to 80 bpm cycling at a rate of 14 breaths per minute within 15 seconds and subsequently thereafter. This variability due to respiration demonstrates the most severe change that may be encountered physiologically.

Pa detection and control algorithms have been demonstrated using canine mongrel experimental models with two Cardiac Assist Devices. ECG detection for real-time control was demonstrated using the MIT/BIH Arrhythmia Database.

A Pa detection simulation platform was developed that provides an ideal trace, and a trace impaired by surgical operating room interference and physiological variation. This Pa detection platform can be utilized to benchmark future Pa detection algorithms in the advancement of cardiac assist control research.

The research described in this dissertation has advanced CAD control research with improved signal detection and control algorithms for non-sinus rhythms along with non-ideal Pa and ECG conditions typically encountered in a cardiothoracic surgical environment. Furthermore, the simulation research provides a methodology to analyze and demonstrate the advancement of Pa detection algorithms now and in the future. o

Integration of Pa and ECG detection algorithms into a fault tolerant control system for cardiac assistance would be the next step in the advancement of cardiac assist device control research. Further, P-wave detection, which could provide advance warning of when deflation should occur (prior to R-wave and opening of the aortic valve) should be investigated. However, it must be noted that considerable computational power will be necessary to address such a complex investigation in the realm of cardiac assistance control detection research.

In closing, the future ideal CAD will be an implantable cardiac assist device in which the patient may be ambulatory shortly after implantation. This device will require considerable control to ensure the CAD is assisting in proper phasing with the heart through the various physiological changes associated with normal daily activities. The current state of research in the development of the ideal CAD is still in its infancy. An ideal CAD would be one which is surgically implanted and

the patient become completely independent of cardiothoracic and cardiovascular care shortly thereafter (e.g., much like pacemakers of today).

On a positive note, the research in this dissertation advances the control research toward the ideal CAD, particularly in the area of Pa detection by providing an alternate means of control. In addition, the simulation research also facilitates the advancement of further refinements in Pa detection by providing a foundation for development and basis of comparison through simulation.

7.3   Direction for Future Research

The ongoing development of more advanced software and hardware provides a means of faster processing for real-time digital filters. If the sampling frequency (and thus the interval between samples) remains the same, additional processing power is available in the development of robust Pa detection filters for real-time counterpulsation CADs. For the continuation of this research in the future, additional processing power may allow for the low pass filter (LPF) to have more poles for better attenuation of noise at unwanted frequencies. Also, the implementation of the LPF may use real numbers, such that integer overrun will no longer be a filtering consideration. A second detection advancement may include more precise fitting of the matched filter. The approximated matched filters in this dissertation may be used to detect the systolic rise and dicrotic notch. Subsequently thereafter, a more exact replica of the matched filter may be derived from the actual data and used for filtering. If several matched filter "snapshots" of the detected cardiac event demonstrate a considerable amount of variation, several may be collected. The detection could then be determined utilizing an "OR"ing function of a select set of the matched filters. If additional processing power is still available, a search-back feature could be used to learn about suspected false negative and false positive detections. Overall, more advanced hardware provides a means to execute more advanced detection algorithms and thus continuously provides an avenue for future counterpulsation CAD research.

The research and development of a robust aortic pressure (Pa) detection filter for counterpulsation cardiac assist device control was the main focus of this dissertation. The robust Pa detection filters were developed to properly detect the systolic rise and dicrotic notch during both ideal and non-ideal conditions (e.g., physiological variation and external cardiothoracic surgery interference) of detection. The foundation of detection was a matched filter approach which modeled the systolic rise and dicrotic notch with polynomial fit derivative filters that approximately match the shape of the respective event to be detected. The presumption is that no information would have been

available about the characteristic shape of the Pa trace signal or the associated disease of the patient. However, if this information were available, the filter parameters could be tailored to the specific patient and/or type of disease. For example, if the Pa signal of a patient had been previously recorded, the parameters of the matched filter could be tuned to more accurately match the associated cardiac event (e.g., systolic rise). This approach provides a path for future research.

However, it should be considered that tuning the filtering to a specific Pa signal at a particular time may make the detection vulnerable to changes in the Pa signal at a future time (e.g., during the occurrence of a previously undiagnosed arrhythmic heart beat). If a patient developed an additional cardiovascular complication, it may cause a variation in their Pa signal waveshape. The variation of the Pa waveshape. The variation in the Pa waveshape, in combination with the previous tuning of the parameters of the detection filter, could reduce the statistical accuracy of detection.

In the same way detection filters could be tuned to specific Pa signal waveshapes, the filters may be tuned to maximize detection during the appearance of a specific external cardiothoracic operating room interference. Dials on the CAD controller may provide a means for the cardiothoracic care professional to help tune out the effects of certain interference to the Pa detection filter. Again, as noted in the previous paragraph, caution must be noted with respect to ensuring that filter tuning doesn't prevent robust detection (e.g., in the event a second form of interference is generated or the current interference has a different effect on the Pa signal).

One method to perform automatic Pa detection filter tuning may be provided through the use of neural networks. Neural networks adaptively change their detection parameters to provide a form of artificial intelligence. However, neural networks are typically based on the recognition of a known signal. The Pa detection filters described in this dissertation could provide the automated detection and potential delineation of the Pa events as a pre-filtering process for the neural network Pa detection solution. Neural networks have been applied to the detection of ECG signals. However, their implementation typically utilized a search-back feature. In real-time control, a search-back feature is not feasible, since the current event has already passed at that time. However, the search-back feature may provide a means for learning from improper detections (e.g., false negative detections).

The detection/delineation of the Pa event template for a neural network may be performed by the cardiothoracic care professional using a graphical user interface. However, in acute cardiothoracic care, time is of the essence. Thus, the graphical user interface solution to determine the neural

network event characteristics to be detected, may not be feasible in all cases. In any event, this approach also provides a path for future research.

The Pa detection simulation research in this dissertation focuses on assessing the robustness of the Pa detection in the algorithm's ability to detect the Pa events during several non-ideal Pa trace conditions. The research rigorously addresses each condition separately to empirically assess the Pa detection immunity for the various forms of non-ideal Pa traces. Conditions may arise where a combination of several non-ideal conditions may be present. For example, in diabetic patients the dicrotic notch shape typically is missing. Detection of the dicrotic notch during noisy conditions will be more difficult due to the reduced detection signal strength (i.e., second and third derivative amplitudes). Future investigation into the different combinations of interference would provide additional insight into the effects of non-ideal Pa signals.

Externally imposed interference and the randomness of cardiovascular signals (e.g., ECG and Pa) will always provide a challenge to detection of the associated events within those signals. In order to prevent the dependence of detection (for control timing) on a single cardiovascular signal (e.g., Pa), other signals may be utilized to provide additional detection fault tolerance (e.g., missed beats). Previous investigators utilized the ECG Atrial P-wave for IABP deflation timing. The investigation of the robust real-time surface P-wave and T-wave detection/delineation for CAD control would increase the number of signals with which the controller could make inflation and deflation decisions. Robust real-time P-wave and T-wave detection for CAD control would provide further advances in the optimal control of counterpulsation cardiac assistance.

If P-wave and T-wave detection and delineation could be developed, some arrhythmias could be detected in real time. Utilizing that information, the counterpulsation CAD real-time controller could modify inflation and deflation decisions based on the particular arrhythmias detected. For example, if premature ventricular contractions (PVCs) were present, the control algorithm could take special precautions for deflation. The precautions would help ensure that the CAD would not deflate too late in the event the next beat was a PVC (generating a relatively premature systolic rise relative to timing of a sinusoid rhythm).

Lastly, research could be performed regarding the concept of an implantable chronic care (i.e., semi-permanent) counterpulsation cardiac assist device. The detection filters developed in this dissertation are digital algorithms that may be implemented in a compact microprocessor design. The compact multiprocessor CAD controller may be paired with the development of a compact inflation device (e.g., balloon) that may be positioned in the chest cavity adjacent to the aorta. The

chest cavity could be utilized to provide back pressure when the balloon inflates. Unlike the IAB which displaces fluid within the aorta by using the enclosure of the aorta for back pressure, this implantable inflatable CAD would provide assistance by compressing the aorta using the chest cavity for back pressure. The ideal device to perform the compression of the aorta would be a toroid. If a toroid-type CAD device were used, no back pressure would be needed from the chest cavity. The sleeve of sphygmomanometer with a Velcro fastener, (the device to used to measure blood pressure around the upper arm) would provide that type of functionality. However, the implantation of the device would most likely require a mid-line incision and entry through the rib cage. If a balloon with the shape of a IAB (a long tubular shape) could be positioned next to the aorta, it is possible that it could be implanted through orthoscopic surgery, thus preventing the need for open heart surgery. Several other factors must be considered including the amount of stress the aorta can endure over a period of time. In conclusion, the research and development of the robust digital Pa detection filters described within this dissertation make possible future research in implantable counterpulsation CADs. The potential for a compact microprocessor design make the implantation of a counterpulsation CAD controller utilizing robust Pa detection filters feasible.

Appendix A: Cardiac Assist Device Glossary

Table A-1. Cardiac Assist Device Control Glossary and Abbreviations (55)

CAD Control Term	Definition
Arrhythmia	"Any deviation from the normal rhythm (sinus rhythm) of the heart." (55)
Aorta	"The main artery of the body, from which all others emanate. It arises from the left ventricle (ascending aorta) arches over the top of the heart (aortic arch) and descends in front of the backbone (descending aorta) giving off large and small branches and finally dividing to form the right and left iliac arteries. the part of the descending aorta from the aortic arch to the diaphragm is called the thoracic aorta, the part below the diaphragm is called the abdominal aorta." (55)
Aortic Pressure (PA,Pa)	The blood pressure in the ascending aorta just outside the aortic valve.
Cardiac Assist Device (CAD)	An apparatus used to assist the circulation of the failing heart (i.e., left ventricle) for example the intra-aortic balloon (IAB).
Cardiac Assist Device (CAD) Controller	An electronic controller used to activate (typically inflate) and de-activate (typically deflate) a cardiac assist device (CAD) using a synchronized timing methodology with the heart to optimize cardiac hemodynamic benefits to the patient while simultaneously not hindering normal circulation.
Catheter	"A tubular instrument to allow passage of fluid from or into a body cavity." (55)
Counterpulsation	"A means of assisting the failing heart by automatically removing arterial blood just before and during ventricular ejection and returning it to circulation during diastole; for IABP cardiac assistance, a balloon catheter is inserted into the aorta and activated by an automatic mechanism triggered by the ECG or aortic pressure." (55)
Diastole	"The period between two contractions of the heart, when the muscle of the heart relaxes and allows the chambers to fill with blood. The term usually refers to ventricular diastole which lasts about 0.5 seconds in a normal heart rate of about 70 beats / minute. During exertion the period shortens, allowing the heart rate to increase." (55)
Ectopic Beat (Extrasystole)	"A heart beat generated somewhere in the heart outside the sinoatrial node. Ectopic beats are generally premature in timing; they are classified as supraventricular if they originate in the atria and ventricular if they arise from a focus in the ventricles." (55)

Table A-1. Cardiac Assist Device Control Glossary and Abbreviations (55)

CAD Control Term	Definition
Electrocardiogram (ECG)	"A recording of the electrical activity of the heart on a moving paper strip or through electronic means. The ECG tracing is recorded by means of an apparatus called an electrocardiograph. It aids in the diagnosis of heart disease which may produce characteristic changes in the ECG." (55)
Electrocardiography	"A technique for recording the electrical activity of the heart. Electrodes connected to the recording apparatus (electrocardiograph) are placed on the skin of the four limbs and chest wall; the record itself is called an electrocardiogram (ECG). In conventional scalar electrocardiography 12 leads (see Lead2) are recorded, but more may be employed in special circumstances (for example an esophageal electrode within the gullet may be used on the analysis of arrhythmias). Vectorcardiography is less commonly used, but may be employed to obtain a 3-D impression of electrical activities of the heart." (55)
Electrocautery (Electric Cautery)	"An instrument for directing a high frequency current through a local area of tissue or a metal cauterizing instrument heated by an electric current." (55)
Femoral Artery	"An artery arising from the external iliac artery at the inguinal ligament. It is situated superficially, running down the front medial aspect of the thigh. Two thirds of the way down it passes into the back of the thigh, continuing downward behind the knee as the popliteal artery." (55)
Hypertensive	"Elevation of the arterial blood pressure above the normal range expected in a particular age group." (55)
Hypotensive	"A condition in which the arterial blood pressure is abnormally low." (55)
Iliac Artery	"The arteries that supply most of the blood to lower limbs and pelvic region. The right and left common iliac arteries from the terminal branches of the abdominal arteries form the terminal branches of the abdominal aorta. Each branches into the external iliac artery and the smaller internal iliac artery." (55)
Intra-aortic Balloon (IAB)	A percutaneous counterpulsation cardiac assist device used in the event of left ventricular power failure (cardiogenic shock) or weakness. The IAB is inserted percutaneously into the femoral artery up to the aorta.
Percutaneous	"Through the skin, often applied to the route administration of drugs in ointment, etc. which are absorbed through the skin." (55)
P-wave	"The minor ECG deflection generated by electrical activity of the atrial contraction." (55)

Table A-1. Cardiac Assist Device Control Glossary and Abbreviations (55)

CAD Control Term	Definition
QRS complex (R-wave)	"The major ECG deflection generated by electrical activity of the ventricular contraction." (55)
Systole	"The period of the cardiac cycle during which the heart contracts. The term usually refers to ventricular systole, which lasts about 0.3 seconds. Atrial systole lasts about 0.1 seconds." (55)
Ventricle	"Either of two chambers of the heart which have thick muscular walls. The left ventricle, which is thicker than the right, receives blood from the pulmonary vein via the left atrium and pumps it into the aorta. The right ventricle pumps blood received from the venae cava (via the right atrium) into the pulmonary artery." (55)

REFERENCES

1. J. E. Tsitlik, "Guest Editorial: Circulatory Support Systems Entering the 1990's," IEEE BME-37, No. 2. February, 1990, pp. 117-120.

2. 1988 Research Facts, American Heart Association, Dallas, TX, 1988

3. 1988 Heart Facts, American Heart Association, Dallas, TX, 1988.

4. S. Scheidt, M. Collins, J. Goldstein, J. Fisher, "Mechanical Circulatory Assistance with the Intraaortic Balloon Pump and Other Counterpulsation Devices", Progress in Cardiovascular Diseases, Vol. XXV, No. 1 (July/August) 1982, pp. 55-76.

5. B. Min, W. Welkowitz, S. Fich, D. Jaron, A. Kantrowitz, "Dynamic Optimization of In-Series Cardiac Assistance by means of Intra-Aortic Balloon Pumping," Bulletin of Mathematical Biology, Vol. 37, 1975, pp. 19-35.

6. William R. Milnor, Cardiovascular Physiology, Oxford University Press, 200 Madison Ave., New York, NY 10016, 1990, pp. 12, 38.

7. M. J. Williams, Jr., J. W. Rubin, R. G. Ellison, "Experimental Determination of Optimum Performance of Counterpulsation Assist Pumping Under Computer Control," Comp. Biomed. Res., 10:545-59, 1977.

8. John Angelo Zelano, "The Computer Control of Intra-Aortic Balloon Pumping," Rutgers University, The State University of NJ (New Brunswick) 1986.

9. Webster's II, New Riverside University Dictionary, The Riverside Publishing Company, Houghton Miflin Company, New York, NY 1984.

10. K. T. Weber, J. S. Janicki, "Intraaortic Balloon Counterpulsation," The Annals of Thoracic Surgery, Vol. 17, No. 6, June 1974, pp. 602-36.

11. J. A. Zelano, J. K.-J. Li, W. Welkowitz, "A Closed-Loop Control Scheme for Intraaortic Balloon Pumping," IEEE BME-37, No. 2, February 1990, pp. 182-192.

12. W. Welkowitz, Engineering Hemodynamics: Applications to Cardiac Assist Devices. Lexington, MA: Heath, 1977

13. D. Jaron, T. W. Moore, P. He, "Theoretical Considerations Regarding the Optimization of Cardiac Assistance by Intraaortic Balloon Pumping," IEEE BME-30, No. 3, March 1983, pp. 177-85.

14. E. Phillippe, J. W. Clark, A. Lande, J. R. Ellis, "Microprocessor Control of Intra-Aortic Balloon Pumping," Annals of Biomedical Engineering, Vol. 8, 1980 pp. 209-24.

15. S. Sasayama, G. Oskada, M. Takahashi et al., "Effects of Intraaortic Balloon Counterpulsation on Regional Myocardial Function during Acute Coronary Occlusion in the Dog," Amer. J. Cardiol., Vol. 43, p. 59, 1979.

16. W. L. Sugg, W. R. Webb, and R. R. Ecker, "Reduction of Extent of Myocardial Infarction By Counterpulsation," An. Thorac. Surg., Vol. 7, p. 311, 1969.

17. E. A. Amsterdam, N.A. Awan, G. Lee, R. Low, J. A. Joye et al., "Intraaortic Balloon Counterpulsation: Rationale, Application, and Results," in Critical Care Cardiology, C. E. Rackley and A. N. Brest, Eds. Philadelphia. PA, Davis, 1981, pg. 79.

18. D. Jaron, "Left Ventricular Afterload and Systemic Hydraulic Power During In-Series Cardiac Assistance: Studies using Intraaortic Balloon Pumping in Dogs," Ann. Biomed Eng., Vol. 5, p. 95, 1977.

19. J. W. Clark Jr., G. R. Kane, H. M. Bourland, "On the Feasibility of Closed-Loop Control of Intra-Aortic Balloon Pumping," IEEE BME-20, No. 6., November 1973, pp. 404-12.

20. D. W. Benson Jr." An Algorithm for Defining the Cardiac Cycle using Ascending Aortic Blood Flow," Computers and Biomedical Research 4, 216-223 (1971).

21. C. F. Starmer, P. A. McHale, J. C. Greenfield Jr., "Processing Arterial Pressure Waves with a Digital Computer," Computers and Biomedical Research 6, 90-96 (1973).

22. G. M. Friesen, T, C, Jannett, M. A. Jadallah, S. L. Yates, S. R. Quint, H. T. Nagle, "A Comparison of the Noise Sensitivity of Nine QRS Detection Algorithms," IEEE BME-37, No. 1, Jan 1990, pp. 85-98.

23. J. Fraden and M. R. Neuman, "QRS-wave Detection," Med. Biol. Eng. Comput., Vol. 18, pp. 125-132, 1980.

24. W. A. H. Englese and C. Zeelenberg, "A Single Scan Algorithm for QRS-detection and Feature Extraction," IEEE Comput. Card., Long Beach: IEEE Computer Society, 1979, pp. 37-42.

25. J. R. Cox, F. M. Nolle, H. A. Fozzard, G. C. Oliver Jr., "AZTEC, A Preprocessing Program for Real-Time ECG Rhythm Analysis," IEEE BME-15, No. 2. April 1968. pp. 128-9.

26. C. N. Mead, K. W. Clark, S. J. Potter, S. M. Moore, L. J. Thomas Jr., "Development and Evaluation of a New QRS Detector/Delineator," IEEE Computers in Cardiology, Sept 1979, pp. 251-4.

27. J. A. Zelano, W. Ko. R. Lazzaro, W. D. Lazenby, S. Topaz, W. J. Kollf, O. W. Isom, K H. Krieger, "Comparison of an Extraaortic Counterpulsation Device versus Intraaortic Balloon Pumping in Severe Cardiac Failure," Trans. Am. Soc. Artif. Intern. Organs, Vol. 37, No. 3. July-September 1991.

28. M.-E. Nygards, J. Tranesjo, J.-H. Atterhog, P. Blomqvist, L.-G. Ekelhund and O. Wigertz, "On-Line Computer Processing of Pressure Data from Cardiac Catherizations," Computer Programs in Biomedicine 5 (1976) 272-282, North Holland Publishing Company.

29. A. M. Weissler, W.S. Harris and C.D. Schoenfeld, "Systolic Time Intervals in Heart Failure in Man," Circulation, 37 (1968) 149.

30. "MIT/BIH Arrhythmia Database - Tape Directory and Format Specification," Document BMEC TR00, Mass. Inst. Technolo., Cambridge 1980. Database is available from Bioengineering Division KB-26, Beth Israel Hospital, 330 Brookline Avenue, Boston, MA 02215.

31. A. M. Weissler, R. G. Peeler, W. H Roehll Jr., "Relationship Between Left Ventricular Ejection Time, Stroke Volume, and Heart Rate in the Normal Individuals and Patients with Cardiovascular Disease," American Heart Journal, Vol. 62, No. 3, Sept 1961 pp. 367-78.

32. A. M. Weissler, W. S. Harris, c. D. Schoenfeld, "Bedside Techniques for the Evaluation of Ventricular Function in Man," The American Journal of Cardiology, Vol. 23, April 1969 pp. 577-83.

33. A. M. Weissler, R. P. Lewis, S. E. Rittgers, W. F. Forester, H. Boudoulas, "Review of Contemporary Laboratory Methods: A Critical Review of the Systolic Time Intervals," Circulation, Vol. 56, No. 2, Aug. 1977 pp. 146-58.

34. A. M. Weissler, R. P. Lewis, H. Boudoulas, "Key References: Systolic Time Intervals," Circulation Vol. 64, No. 4, 1981 pp. 862-7.

35. J. W. Remington, W. F. Hamilton, R. P. Alquist, "Interrelation Between the Length of Systole, Stroke Volume and Left Ventricular Work in the Dog," American Journal of Physiology, Volume 154, July 1948. pp. 6-15.

36. M. L. Murphy, J. E. Doherty, N. DeSoyza, J. J. Kane, K. D. Straub, "Systolic Time Intervals in the Experimental Animal with Aortic Outflow Obstruction", Cardiology Vol. 68: 19-29 (1981).

37. F. S. Pipers, R. L. Hamlin, A. Weissler, R. Smith, "Computer Measurement of Durations of Phases of Systole in Dogs," Am. J. Vet. Res. Vol. 31, No. 2., Feb. 1970, pp.315-20.

38. N. El-Sherif, R. Mehra, M. Restivo, G. Kelen, "A Low Noise P-Wave Discriminating Electrocardiogram in the Diagnosis of Complex Cardiographic Arrhythmias," The American Journal of Cardiology, Vol. 59, January 1987, pp. 173-5.

39. D. E. Gustafson, J.-Y. Wang, S. Gelfand, "P-wave Detection and Identification using Statistical Signal Analysis," IEEE 1979 JACC pp.420-5.

40. D. E. Gustafson, I. C. Schick, "Surface Lead P-wave Detection using Statistical Signal Analysis," 33rd ACEMB, Washington Hilton Hotel, Washington D.C. Sept. 30 - Oct 3, 1980. p. 20.

41. J. Pan, W. J. Tompkins, "A Real-Time QRS Detection Algorithm," IEEE BME-32, No. 3, March 1985, pp.230-6.

42. P. S. Hamilton, W. J. Tompkins, "Quantitative Investigation of the QRS Detection Rules Using the MIT/BIH Arrhythmia Database," IEEE BME-33, No. 12, Dec 1986 pp. 1157-65.

43. Datascope Model 870 and 871, Portable Physiological Monitors Service Manual, Paramus NJ, May 1983.

44. Brian W. Kernighan, Dennis M, Ritchie, The C Programming Language, Second Edition. PRT, Prentice Hall, Englewood Cliffs, NJ 07632, 1988.

45. Borland C++, Programmer Guide, Version 3.1, Borland International, Inc., 1800 Green Hills Road, P.O. Box 660001, Scotts Valley CA 95067-0001, 1992.

46. William D. Stanley, Gary R. Dougherty, Ray Dougherty, Digital Signal Processing, Second Edition, Reston Publishing Company, Inc. Reston, VA, 22090, 1984, pp. 141, 171.

47. Willis J. Tompkins, John G. Webster, Design of Microcomputer-Based Medical Instrumentation, Prentice Hall, Inc., Englewood Cliffs, NJ 07632, pp. 132-7.

48. Arthur J. Vander, James H. Sherman, Dorothy S. Luciano, Human Physiology, Fourth Edition, McGraw Hill Book Company, New York, NY 1985, p. G-35.

49. VisSim User's Guide, Visual Solutions Inc., USA 1/94, 1-2640, Version 1.5, 1994, 487 Groton Road, Westford, MA 01886.

50. Willis J. Tompkins and John G. Webster, Editors, Interfacing Sensors to the IBM PC, Prentice Hall, Englewood Cliffs, NJ 07632, 1988.

51. Anthanasios Papoulis, Probability, Random Variables, and Stochastic Processes, Second Edition, McGraw-Hill, New York, NY,1984, pp. 73, 74, 104 and 108.

52. Allan V. Oppenheimer and Ronald W. Schafer, Digital Signal Processing, Prentice-Hall, Inc., Englewood Cliffs, NJ, 1975.

53. James W. Nilsson, Electric Circuits, Addisson-Wesley Publishing Company, Reading, MA, 1983.

54. Norman Lewis, The New Roget's Thesaurus in Dictionary Form, A Berkeley Medallion Book, Published by G. P. Putnam's Sons, Inc., Distributed by Berkeley Publishing Corporation New York, NY 1985.

55. The Bantam Medical Dictionary, Revised Edition, Bantam Books, New York, NY,1990.

56. New World Dictionary, Second College Edition of the American Language, William Collins + World Publishing Co., Inc. New York, NY, 1974.

57. Dick K. Blanford, The Digital Filter Analyzer, Addison-Wesley Publishing Company, New York, NY, 1988.

58. John G. Webster, Editor, Medical Instrumentation, Applications and Design, Houghton Mifflin Company, Boston MA, 1978.

59. M. Morris Mano, Digital Logic and Computer Design, Prentice-Hall, Inc., Englewood Cliffs, NJ, 1979.

60. Transputer Toolset, Computer Systems Architects (CSA), Version 89.1, January 15, 1990.

61. Transputer 'C' Library Description, Computer Systems Architects, Version 89.1, January 15, 1990.

62. Computer Systems Architects: Technical Note, "User-Written Servers for Logical Systems C", Provo, UT, 1993.

63. Estrin, Herman A. and Timothy E. Roche, "Guidelines for Writing Theses and Dissertations," Kendall/Hunt Publishing Company, Dubuque, IO 52004-0539, 1992.

64. Xue, Qiuzhen, Yu Hen Hu, Willis J. Tompkins, "Neural-Network-Based Adaptive Matched Filtering for QRS Detection," IEEE BME Vol. 39, No. 4, April 1992.